EVALUATING THE POTENTIAL OF USING SATELLITE EARTH OBSERVATION DATA TO QUANTIFY THE CONTRIBUTION OF RIPARIAN TOTAL EVAPORATION TO STREAMFLOW TRANSMISSION LOSSES

SHAEDEN GOKOOL

Submitted in fulfilment of the requirement
for the degree of Doctor of Philosophy in Hydrology

Centre for Water Resources Research
School of Agriculture, Earth and Environmental Sciences
University of KwaZulu-Natal
Pietermaritzburg
South Africa

November 2017

Supervisor: Doctor ES Riddell
Co-supervisor: Miss KT Chetty
Co-supervisor: Doctor C Jarmain

EXECUTIVE SUMMARY

Numerous perennial rivers which flow through arid and semi-arid environments in South Africa, have become severely constrained as water resources abstractions are close to exceeding, or have exceeded the available supply and ecosystem resilience. This is a common phenomenon, as river basins are increasingly developed and often over allocated, in order to maximize socio-economic benefits through consumptive water use, often at the expense of the environment. Thus, managing and maintaining environmental water requirement (EWR) flow allocations in these circumstances becomes increasingly important but all the more challenging, especially during periods of water scarcity.

The Letaba River situated in the semi-arid north-eastern region of South Africa is a typical example of a river system in which water governance challenges and infrastructural development have resulted in flows within the river no longer resembling the natural flow regime. This situation has improved to some extent after the establishment of river operating rules and an adaptive operational water resources management system. However, one of the major challenges with successfully implementing and managing EWR flows to date has been the uncertainty regarding the magnitude and influence of streamflow transmission losses (TL's) on flows within the river system. TL's along the Letaba are thought to be a significant proportion of streamflow during dry periods and this therefore constrains the ability to meet target EWR flows, as it is often the case that specified EWR releases from the Tzaneen dam are not adequately met further downstream at EWR target gauges.

To ensure that water provisions and in particular EWR flows can be managed more effectively and efficiently in the future, it is imperative that the hydrological processes contributing to TL's are quantified at various spatial and temporal scales. Considering this statement as a point of departure, the overall objective of this thesis was to reduce the uncertainty associated with TL's by attempting to acquire an improved hydrological process understanding of the natural drivers of loss in this system, so that TL's along the Letaba River can be more accurately quantified. This research involved, conducting detailed characterizations of hydrological processes along a 14 km reach of the Groot Letaba River which has similar land use activities and hydrological characteristics to the broader river system.

Particular emphasis was placed upon establishing the influence of riparian total evaporation (inclusive of open water evaporation) on TL's, as this process is a major contributing factor to the water balance of arid and semi-arid environments, yet has seldom been incorporated or adequately represented into TL's estimation procedures. These investigations were centred on evaluating the potential of using a satellite-based approach to acquire spatially explicit estimates of evapotranspiration (ET) during the low flow period in this river system (May to October), which typically represents a critical period with regards to water shortages. For this purpose, the satellite-based surface energy balance (SEBS) model and satellite earth observation data acquired from Landsat and Moderate-resolution imaging spectroradiometer (MODIS) were used to estimate ET. However, the trade-off between the spatial and temporal resolution associated with these data sets can limit the reliability of satellite-based ET modelling (except where occasionally correct).

Consequently, the SEBS ET estimates from these data sets were used as inputs to two relatively simplistic approaches (actual crop coefficient or Kc_{act} and output downscaling with linear regression or ODLR) to quantify ET at a moderate spatial resolution (30 m) on a daily time step. These ET estimates were compared against *in-situ* ET estimates using a one sensor Eddy Covariance system to quantify any uncertainties associated with the satellite-derived estimates. To further investigate spatial and seasonal variations in source contributions to plant water uptake during the investigation period, stable isotope analysis (of ^{18}O and ^{2}H) and a Bayesian mixing model were coupled with the satellite derived ET estimates. The insights acquired from these investigations, were then used to derive baseline estimates of TL's. This involved using the satellite-derived daily ET time series in conjunction with data obtained from a parallel investigation focusing on quantifying the rapport between surface and sub-surface water storage processes.

Initial comparisons of ET estimates acquired using the Kc_{act} and ODLR approaches against EC_{ET} were fairly poor yielding RMSE values of; 1.88 and 2.57 mm d^{-1} and 1.10 and 2.39 mm d^{-1} (for two replicate transects), respectively. The poor performance of these techniques was largely attributed to the SEBS ET estimates used as inputs to these techniques, as SEBS may overestimate evapotranspiration during conditions of water stress.

This limitation was overcome using an evaporative calibration factor (termed the environmental stress factor or *ESF*) into the original SEBS formulation ($SEBS_0$), to correct for the overestimation of the latent heat flux (*LE*) and the evaporative fraction (*EF*). The *ESF* calibration factor was empirically derived and then integrated into $SEBS_0$, so as to better represent the influence of water stress on the *EF* and consequently *LE*. The implementation of the modified version of SEBS ($SEBS_{ESF}$) was shown to significantly improve the estimation of energy fluxes, which in turn resulted in an improved correlation and an increase in the percentage of modelled ET estimates within an acceptable accuracy range (± 15 to 30 %) when compared against *in-situ* observations.

Through the application of this modified version of SEBS ($SEBS_{ESF}$), the ability of the ODLR and Kc_{act} approaches to develop a time-series of daily moderate spatial resolution ET estimates could now be demonstrated. The use of $SEBS_{ESF}$ ET estimates as inputs to the Kc_{act} approach was shown to compare most favourably to EC_{ET}, yielding correlation coefficient and Nash-Sutcliffe efficiency values of 0.79 and 0.60, respectively. With the ability of this satellite-based approach to adequately represent ET within this environment now confirmed. Stable isotope analysis (of ^{18}O and ^{2}H) and a Bayesian mixing model were coupled with the Kc_{act} derived ET estimates, to further investigate spatial and seasonal variations in plant water uptake dynamics.

The results of these investigations showed that soil water was the main contributing source to ET. While stream and groundwater use during transpiration was also prevalent within the study area and increased with aridity, the magnitude of the contribution of these sources to transpiration was fairly minimal and not as significant as generally reported in literature. The insights gained from these investigations, as well as those obtained from the quantification of surface and sub-surface water storage processes, assisted in deriving baseline estimates of TL's along the length of river reach studied.

In general, it was found that during the latter stages of the dry season (August to October) TL's accounted for approximately 5 to 15 % of the flow in the river system, with riparian total evaporation and in particular transpiration the dominant contributing processes to this loss. Through linkages with the recent gazetting of the Letaba Management Class (resource objective setting) and the mandatory implementation of EWR flows, it was shown that flows within the river system were unable to meet low flow targets and are required to be increased in order to fulfil this requirement, whilst simultaneously accounting for TL's.

It should be noted that while the various investigations undertaken in this study enabled the estimation of TL's and the contribution of processes *viz.* riparian ET to TL's, the estimates provided could not be verified due to the lack of reliable upstream (inflow) flow gauge data. Although the investigations and observations detailed in this study provide an understanding of the system for a limited period in time, they would substantially benefit from longer-term monitoring, so that the assumptions and related uncertainties that had to be factored into the analysis could be reduced. Overall the study has detailed key hydrological processes influencing TL's along the Groot Letaba River, providing invaluable insights on existing knowledge gaps and contributing new knowledge to this research area. It is envisaged that this will enable the establishment of an improved conceptual understanding of the system, which may prove to be beneficial for future hydrological modelling applications in this region.

DECLARATION 1 - PLAGIARISM

I, Shaeden Gokool declare that

(i) The research reported in this thesis, except where otherwise indicated, is my original work.

(ii) This thesis has not been submitted for any degree or examination at any other university.

(iii) This thesis does not contain other persons' data, pictures, graphs or other information, unless specifically acknowledged as being sourced from other persons.

(iv) This thesis does not contain other persons' writing, unless specifically acknowledged as being sourced from other researchers. Where other written sources have been quoted, then:

(a) their words have been re-written but the general information attributed to them has been referenced;

(b) where their exact words have been used, their writing has been placed inside quotation marks, and referenced.

(v) Where I have reproduced a publication of which I am an author, co-author or editor, I have indicated in detail which part of the publication was actually written by myself alone and have fully referenced such publications.

(vi) This thesis does not contain text, graphics or tables copied and pasted from the Internet, unless specifically acknowledged, and the source being detailed in the thesis and in the references sections.

Signed: ……..

Shaeden Gokool

Supervisor: ……..

Dr ES Riddell

Co-supervisor: ……

Ms KT Chetty

Co-supervisor: ……

Dr C Jarmain

DECLARATION 2 - PUBLICATIONS

DETAILS OF CONTRIBUTION TO PUBLICATIONS that form part of and/or include research presented in this thesis (including publications submitted and published, giving details of the contributions of each author to the research and writing of each publication):

The * in each paper, indicates my role as the corresponding author

Publication 1 (chapter 2 of this thesis): Gokool, S*, Jarmain, C, Riddell, E, Swemmer, Lerm, R and Chetty, KT. 2017. Quantifying riparian total evaporation along the Groot Letaba river: A comparison between infilled and spatially downscaled satellite derived total evaporation estimates. *Journal of Arid Environments* 147: 114-124. http://dx.doi.org/10.1016/j.jaridenv.2017.07.014 0140-1963/© 2017.

The data reported are based on *in-situ* field measurements acquired during a window period field campaign in 2015. This field campaign required a team of researchers, to select appropriate sites, setup instrumentation required for monitoring and maintenance of this equipment. Consequently, the team members are co-authors or have been acknowledged in the text. S Gokool was actively involved in the collection of data and was assisted by R Lerm, who was responsible for the maintenance of the instrumentation due to its remote locality. C Jarmain wrote the data logger programs and setup the instrumentation during the initial stages of the field campaigns. Advice regarding the interpretation of the data and structuring of the research presented within the paper, was provided by Riddell, E, Jarmain, C, Swemmer, A and Chetty, KT. The review of relevant literature, methodological design and data analysis for this paper was undertaken by S Gokool. The publication was written in its entirety by S Gokool and all results, figures, tables and graphs were produced by the same, unless otherwise stated within the text of the paper.

Publication 2 (chapter 3 of this thesis): Gokool, S*, Riddell, ES, Jarmain, C and Chetty, KT. 2017. Integration of an environmental stress factor in SEBS for improving the estimation of evapotranspiration in environments during conditions of water stress. Oral presentation to 2017 IAHS Scientific Assembly (Port Elizabeth, South Africa, 10th to 14th July) and *In preparation for submission to Water SA Journal*.

The data reported on are based on *in-situ* field measurements acquired during two window period field campaigns in 2015 and 2016. These field campaigns required a team of researchers to setup instrumentation required for monitoring and maintenance of this equipment. Furthermore, ancillary data was provided by the Council for Scientific and Industrial Research for the Malopeni Flux Tower. Consequently, the team members are co-authors or have been acknowledged in the text. The logger program previously written by C Jarmain was used during each of the field campaigns. S Gokool was actively involved in the collection of data and was assisted by R Lerm. Advice regarding the interpretation of the data and structuring of the research presented within the paper, was provided by Riddell, E, Jarmain, C and Chetty, KT. The review of relevant literature, methodological design and data analysis for this paper was undertaken by S Gokool. The publication was written in its entirety by S Gokool and all results, figures, tables and graphs were produced by the same, unless otherwise stated within the text of the paper.

Publication 3 (chapter 4 of this thesis) was under review when this thesis was submitted for examination. It has subsequently been accepted for publication in the Journal of Arid Environments, with amendments as: Gokool, S*, Riddell, ES, Swemmer, A, Nippert, J, Raubenheimer, R and Chetty, KT. 2017. Estimating groundwater contribution to transpiration using satellite-derived evapotranspiration estimates coupled with stable isotope analysis. The data reported on are based on *in-situ* field measurements acquired during a window period field campaign in 2016. This field campaign required a team of researchers to collect and analyse water samples acquired from multiple sources for stable isotope analysis. S Gokool was actively involved in the collection of data and was assisted by R Raubenheimer. Preparation and processing of the samples for stable isotope analysis was undertaken by the Centre for Water Resources Research laboratory team at University of KwaZulu-Natal, as well as the laboratory team at the Physiological Ecology Lab at Kansas State University. Advice regarding the interpretation of the data and structuring of the research presented within the paper, was provided by Riddell, E, Swemmer, A, Nippert, J and Chetty, KT. The review of relevant literature, methodological design and data analysis for this paper was undertaken by S Gokool. The publication was written in its entirety by S Gokool and all results, figures, tables and graphs were produced by the same, unless otherwise stated within the text of the paper.

Publication 4 (chapter 5 of this thesis): Gokool, S*, Riddell, ES, Nel, JM, Swemmer, A, Raubenheimer, R, Strydom, T and Chetty, KT. 2017. Quantifying the contribution of riparian total evaporation to streamflow transmission losses: Preliminary investigations along the Groot Letaba River. *In preparation for submission to Journal of Hydrology: Regional studies*.

The data reported on are based on *in-situ* field measurements acquired during window period field campaigns in 2015 and 2016. These field campaigns required a team of researchers to collect and analyse data on various hydrological processes. S Gokool was actively involved in the collection and analysis of evapotranspiration data. Supplementary data used in this study pertaining to surface and subsurface water storage processes were obtained from parallel investigations which involved the monitoring and analysis of groundwater and surface water interactions, this was undertaken by R Raubenheimer, JM Nel and T Strydom. Advice regarding the interpretation of the data and structuring of the research presented within the paper, was provided by Riddell, E, Swemmer, A and Chetty, KT. The review of relevant literature, methodological design and data analysis for this paper was undertaken by S Gokool. The publication was written in its entirety by S Gokool and all results, figures, tables and graphs were produced by the same, unless otherwise stated within the text of the paper.

PREFACE

The work described in this thesis was carried out in the Centre for Water Resources Research, School of Agriculture, Earth and Environmental Sciences, University of KwaZulu-Natal, Pietermaritzburg and the South African Environmental Observation Network (SAEON), Ndlovu node, Phalaborwa, under the supervision of Dr Edward Riddell, Ms Kershani Tinisha Chetty and Dr Caren Jarmain. The research represents original work by the author and has not otherwise been submitted in any form for any degree or diploma to any tertiary institution. Where use has been made of the work of others it is duly acknowledged in the text

ACKNOWLEDGEMENTS

The research presented in this paper emanates from a Water Research Commission (WRC) project entitled: Quantification of Transmission Losses along the Letaba River for Improved Delivery of Environmental Water Requirements (ecological reserve), WRC Project No K5/2338. I would like to extend my gratitude to the Water Research Commission (WRC) and the South African Environmental Observation Network (SAEON) for the funding required to successfully complete this research.

Foremost I am grateful to the Almighty for the opportunity to further my studies and for the guidance and blessing which I received throughout the duration of this project. I would also like to acknowledge the following people and extend my gratitude for the invaluable contributions they have made to successfully completing the research presented in this thesis:

My supervisor Dr Eddie Riddell, it has been a truly rewarding experience to have been on the receiving end of your tutelage throughout the duration of this study. The advice and guidance you have provided me with, as well as the freedom to further explore my own research ideas has markedly improved my abilities as a researcher and has given me the confidence to present my research to both the local and international scientific community.

My co-supervisor Miss Kershani Chetty, you have been my supervisor and mentor since the beginning of my postgraduate endeavours, your guidance, advice and words of encouragement has been invaluable. You have been an ever-present source of wisdom throughout my academic career. I consider myself extremely fortunate that I have been on the receiving end of your unwavering support throughout this journey.

My co-supervisor Dr Caren Jarmain, I have learned a great deal from you both from an academic standpoint as well as from your extensive knowledge in the field. Thank you for imparting some of this knowledge onto me.

Dr Anthony Swemmer, many thanks for your advice and assistance with various aspects of this study, most notably improving my understanding of the use of stable isotopes for hydrological applications which has in no doubt added an extra dimension to my capabilities as a researcher. While this was fairly new to me, it proved to be one of the most enjoyable aspects I undertook in this study.

Mr Rion Lerm, Mr Reinhard Raubenheimer and Tercia Strydom, thank you for your invaluable assistance during the various field campaigns, it was the hours that were expended in the field that have laid the foundations for this study to be completed.

Thank you to the anonymous reviewers who commented on the published manuscripts (chapters 2 and 4), as well as the remaining manuscripts that are in review. These suggestions have significantly improved the work that has been undertaken in this study.

Mrs Martie van der Westhuizen, thank you for always timeously taking care of my stay and travel requirements as well as the great filter coffee. You have played a key role in making my stays away from home pleasurable. Many thanks to the SAEON staff who assisted in the field with special mention to Desmond, Elijah, Mightyman, Patrick, Lassie and Queen.

Many thanks to; the Council for Scientific and Industrial Research (CSIR) and UKZN for the provision of equipment required for in-situ monitoring and gauging. Further thanks are extended to the CSIR for the provision of data required for the Malopeni study site. To the laboratory team at the Physiological Ecology Lab at Kansas State University, as well as the Centre for Water Resources Research laboratory team at University of KwaZulu-Natal with special mention to Professor Simon Lorentz, Dr Goitom Adhanom, Mr Vivek Naiken and Miss Ntombiyenkosi Nxumalo. Thank you for assisting me with the numerous samples that were required for the stable isotope analysis.To the staff at the Centre for Water Resources Research and my fellow colleagues. Thank you for the various roles that you have played during this study.

To all my family members, especially my father Mr Praveen Gokool and my mother Mrs Nisha Cassim. Thank you for all the support and love throughout my life and allowing me to pursue this dream, none of this would have been possible without you. These acknowledgements would not be completed without expressing my love and gratitude to my fiancé Rebecca Banell Solomon. Thank you firstly, for your patience throughout my academic endeavors, this was a lengthy journey that you must have thought would never end. All that I have achieved thus far is largely due to you being an ever-present source of motivation, love, and support. You have truly been amazing and I am grateful to have had you there by my side to share it all with.

To my daughter Laylah Anya, I hope that one day all my dreams will become your reality. This one is for you!

TABLE OF CONTENTS

Page

LIST OF FIGURES

Page

LIST OF TABLES

Page

LIST OF SYMBOLS

‰:	Permil
^{0}C:	Degrees Celcius
Cd:	Drag coefficient of foliage elements (dimensionless and assumed to be = 0.2)
C_p:	Heat capacity of dry air (Jkg^{-1})
C_{t*}:	Heat transfer coefficient of the soil
C_t:	Heat transfer coefficient of the leaf and bounded between $0.005N \leq C_t \leq 0.075N$ (*N* is the number of sides of the leaf which participates in heat transfer process) for most canopies and environmental conditions
d_o:	Zero plane displacement height (m)
e_a:	Actual vapour pressure (hPa)
E_{daily}:	Actual daily total evaporation (mm)
e_s:	Saturation vapour pressure (hPa)
ET_0/ET_{ref}:	FAO Penman-Monteith reference evaporation (mm d^{-1})
ET_a:	Actual evapotranspiration (mm d^{-1})
f_c:	Fractional vegetation coverage
g:	Acceleration due to gravity (m s^{-2})
G_0:	Soil Heat Flux (W m^{-2})
H:	Sensible Heat Flux (W m^{-2})
H_{dry}:	*H* at the dry limit (W m^{-2})
H_{wet}:	*H* at the wet limit (W m^{-2})
k:	von Karman's constant (= 0.4)
K:	Kelvin
kB^{-1}:	Extra resistance parameter dependent upon the soil and fractional vegetation coverage.
Kc_{act}:	Actual Crop Coefficient (dimensionless)
L:	Obukhov length (m)
LE:	Latent Heat Flux (W m^{-2})
N_{ec}:	Within-canopy profile extinction coefficient
Pr:	Prandtl number
R_{e*}:	Roughness Reynold number
r_e:	Aerodynamic resistance (s m^{-1})
r_i:	Bulk surface internal resistance (s m^{-1})

R_{lwd}: Downward longwave radiation (W m^{-2})

R_n: Net Radiation (W m^{-2})

R_{swd}: Downward solar radiation (W m^{-2}),

T_o Surface temperature (K)

Tr: Radiometric Temperature (K)

$u(h)$: Horizontal wind speed at the top of the canopy (m s^{-1})

u_*: Friction velocity (m s^{-1})

z: Reference meteorological height (m)

z_{oh}: Scalar roughness height for heat transfer

z_{om}: Roughness height for momentum transfer (m)

α: Albedo or Surface reflectance (dimensionless)

γ: Psychometric constant (hPa K^{-1})

Δ: Rate of change of the saturation vapour pressure with temperature (hPa K^{-1})

δ: Represents change in the ratio of the uncommon to common isotopes ($^2H/^1H$ or $^{18}O/^{16}O$) for the sample and standard, represented in ‰ notation

ε: Emissivity of the surface (dimensionless)

θ_a: Potential air temperature (K) at height (z)

θ_o: Potential surface temperature (K)

θ_v: Potential virtual temperature (K)

Λ: Evaporative Fraction (dimensionless)

Λ^{24}: Daily average *EF*.

λE: Latent Heat Flux (W m^{-2})

Λr: Relative evaporation (dimensionless)

ρ: Density of air (kg m^{-3})

σ: Stefan-Boltzman constant (W m^{-2} K^{-4})

ψ_h: Stability correction factor for heat transfer

ψ_m: Stability correction factor for momentum

Γ_c: Assumed to be 0.05 (dimensionless) for a fully vegetated canopy

Γ_s: Assumed to be 0.315 for a bare soil surface (dimensionless)

LIST OF ABBREVIATIONS

^{18}O:	Oxygen-18
^{2}H:	Deuterium
AAR:	Acceptable Accuracy Range
ANOVA:	Analysis of Variance
CSR:	Coarse Spatial Resolution
EC:	Eddy Covariance
EC_{ET}:	Eddy Covariance ET Measurements
EF:	Evaporative Fraction
EF_{new}:	Modified Evaporative Fraction integrated into $SEBS_0$
EF_{old}:	Original Evaporative Fraction derived in $SEBS_0$
ESF:	Environmental Stress Factor
ET:	Evapotranspiration
ET_g:	Contribution of Groundwater to Transpiration (mm d^{-1})
EWR:	Environmental Water Requirement
GMWL:	Global Meteoric Water Line
GW:	Groundwater
HTR:	High Temporal Resolution
ILWIS:	Integrated Land and Water Information System
L1:	Landsat ET image for day one
L2:	Landsat ET image for day two
L3:	Landsat ET image for day three
LMWL:	Local Meteoric Water Line
LST:	Land Surface Temperature
M1:	MODIS ET image for day one
M2:	MODIS ET image for day two
M3:	MODIS ET image for day three
MAD:	Mean Absolute Difference
MCMC:	Markov Chain Monte Carlo
METRIC:	Mapping Evapotranspiration at High Resolution with Internalized Calibration
MODIS:	Moderate Resolution Imaging Spectroradiometer
MOST:	Monin-Obukhov Similarity Theory
MSR:	Moderate Spatial Resolution

NDVI: Normalized Difference Vegetation Index

NIR: Near Infra-Red

NWA: National Water Act

ODLR: Output Downscaling with Linear Regression

RMSE: Root Mean Square Error

R_{sample}: Ratio of uncommon to common isotopes ($^{2}H/^{1}H$ or $^{18}O/^{16}O$) for the sample

$R_{standard}$: Ratio of uncommon to common isotopes ($^{2}H/^{1}H$ or $^{18}O/^{16}O$) for the standard

RVE: Relative Volume Error

SEBAL: Surface Energy Balance Algorithm for Land

SEBI: Simplified Surface Energy Balance Index

SEBS: Surface Energy Balance System

$SEBS_0$: Original SEBS model formulation

$SEBS_{ESF}$: A modified version of SEBS which integrates a scaling factor representing the influence of environmental stress factor into the original model formulation

$SEBS_{NDVI}$: A modified version of SEBS which integrates a scaling factor representing the influence of vegetation and temperature into the original model formulation

$SEBS_{SM}$: A modified version of SEBS which integrates a scaling factor representing the influence of soil moisture into the original model formulation

SEL: Fitting line of the soil water $\delta^{2}H$ and $\delta^{18}O$ relationship/Soil water evaporation line

SEO: Satellite Earth Observation

Simmr: Stable Isotope Mixing Model package in R

SM: Soil Moisture

SW: Stream Water

T: Temperature

TL's: Streamflow Transmission Losses

VWC: Volumetric Water Content

1. INTRODUCTION

Globally, water scarcity has been exacerbated by the effects of increasing population growth, socio-economic development and climate change (Molle *et al*, 2010; Pittock and Lankford, 2010). As a result, the availability of water to sustain the natural functioning of riverine ecosystems and the provision of ecosystem goods and services has fallen under threat (Pittock and Lankford, 2010). This situation has escalated river basin closure (Falkenmark and Molden, 2008; Molle *et al*, 2010), which Molle *et al*. (2010) defines as the situation in which the available supply of water is unable to fulfil the water quality and quantity demands within a river or basin, for a period of time.

The deterioration in the health of riverine ecosystems has been largely accredited to alterations in the natural flow regime of river systems, resulting from significant land-use changes and poor water governance (Pollard and du Toit, 2011b). Consequently, it has become increasingly difficult to implement Environmental Water Requirement (EWR) flows. In order to remedy this situation, it is of critical importance to efficiently manage and monitor abstractions of water from the riverine ecosystem and dam outflows, whilst simultaneously ensuring that all water users receive an acceptable quantity and quality of water which can be supplied and sustained at an acceptable assurance level without impeding the ability to maintain the natural functioning of the riverine ecosystem. The following sub-sections (1.1 to 1.4) provide a detailed discussion from a South African perspective on the current state of EWR flow management and some of the challenges faced to date with implementing these flows.

1.1 Maintaining and Managing Environmental Water Requirements

South African environmental laws are internationally recognised and acclaimed, particularly the laws relating to the governance of water i.e. the National Water Act (NWA), Act 36 of 1998. The NWA promotes the fair and equitable use of water to all water users, whilst ensuring that this valuable resource is protected and managed in a sustainable manner. This is achieved through a holistic approach that involves the integrated management of catchments (The NWA, 1998). The NWA is responsible for the fortification of water resources through the allocation of a pre-established quantity of water present in a system, to preserve the natural functioning of the riverine ecosystem and surrounding environments and the provision of ecosystem goods and services to society (Brown *et al*., 2010).

EWR flows are centred on some predefined condition, which has been established from reserve determination and water resources classification studies (Brown *et al*., 2010). To satisfy the aforementioned requirement, the water resource must be made available at an appropriate volume and quality for relevant periods. This is known locally as the Ecological Reserve (Brown *et al*., 2010) but more generally in the scientific literature as Environmental Flows or EWR flows (Pittock and Lankford, 2010; Smakhtin *et al*., 2004; Swirepik *et al*., 2015).

In a South African context, numerous perennial rivers which flow through arid and semi-arid regions are close to being fully allocated (all available water in the system has or is close to being fully used up), with options for additional water users in the system being 'closed'. Consequently, catchments within these regions have been adversely affected, as the ecological functioning and resilience of riverine ecosystems as well as surrounding environments begin to steadily decline, due to the minimum amount of water that is required to sustain environmental processes within these catchments being unavailable (Falkenmark and Molden, 2008; Pollard and Du Toit, 2011a; Adams *et al*., 2016).

This is a common phenomenon, as river basins are generally overdeveloped to maximize socio-economic benefits through consumptive water use, at the expense of the environment (Wester *et al*., 2005; Venot *et al*., 2007; Falkenmark and Molden, 2008; Molle *et al*, 2010; Pittock and Lankford, 2010). Thus, managing and maintaining EWR flow allocations in these circumstances becomes more challenging, especially during periods of water scarcity (Pittock and Lankford, 2010; Adams *et al*., 2016).

According to Pollard and Du Toit (2011a) during the latter periods of the 20th century, the EWR flows in various catchments of the South African Lowveld (a region that lies between 150 and 600 m above mean sea level, dominated by a mixture of savanna grasses and woodland; Mucina and Rutherford, 2006), have been on the decline. This has been attributed to the compounded effects of land-use change, as well as the constrained management of water resources within these catchments (Pollard and Du Toit, 2011a). Consequently, these catchments have been adversely affected, as the ecological functioning of these riverine ecosystems and surrounding environments begin to steadily decline, due to the minimum amount of water that is required to sustain environmental processes within these catchments being unavailable (Pollard and Du Toit, 2011a).

The hydrological characteristics of South African catchments display a high degree of variability, which is largely due to its climatic zones which range from the tropical to hyper-arid. The inter and intra-annual variability in hydrological processes such as streamflow and runoff is notably high in the semi-arid zones (McMahon, 1979). The efficient management of limited water resources in these environments is therefore dependent on comprehensively quantifying all hydrological processes, to understand and account for how these processes impact the flows within these river systems (van Dijk and Renzullo, 2011).

Presently, knowledge regarding precipitation inputs to a river system, releases from dams and permitted water abstractions from river systems, which are relatively easy to quantify, have been used to manage the flows for river operations within these environments (Riddell *et al*., 2017). However, the lack of an adequate quantitative understanding of channel water losses or streamflow transmission losses (TL's) remains a constraint to the effective management of flows especially in the arid and semi-arid environments (Lange *et al*., 2005; Hughes, 2008; Costa *et al*., 2013; Villeneuve *et al*., 2015).

1.2 Streamflow Transmission Losses

The loss of water from the stream is termed TL's, which can be defined as a reduction in the volume of flow in a river system between upstream and downstream points (Lane *et al*., 1990; Walters, 1990; Hughes and Sami, 1992; Cataldo *et al*., 2010; Costa *et al*., 2013; Shanafield and Cook, 2014; Huang *et al*., 2015). TL's have been identified as a significant contributing process to the water balance of river systems, particularly in arid and semi-arid environments (Hughes and Sami, 1992; Lange, 2005; Costelloe *et al*., 2003; Cataldo *et al*., 2010; Shanafield and Cook, 2014; Huang *et al*., 2015). They influence the recharge of ground water resources, attenuation and storage of flood waters and supports the ecological functioning of the riparian ecosystem (Renard, 1970; Walters, 1990, De Vries and Simmers, 2002; Morin *et al*., 2009; Costa *et al*., 2013; Huang *et al*., 2015).

Depending on the interaction between the river and the hydrogeological template the river traverses, a river or stream segment may be described as losing or gaining; i) if water is lost to total evaporation or the underlying aquifer and ii) water is gained from the discharge of ground-water, respectively (Heath, 1983; Winter *et al*., 1998; Ivkovic, 2009).

This loss of water from the river or stream is largely regulated by three natural processes; (i) riparian evapotranspiration (ET), (ii) open-water evaporation or infiltration of flood waters stored in channel depressions or the flood plain and (iii) the recharge of ground water as water infiltrates the stream channel or open-water evaporation directly from the stream channel (Cataldo *et al*., 2004; 2010; Shannafield and Cook, 2014). These processes ultimately influence the hydraulic gradient between the surface water and the groundwater level, resulting in the loss of water from the stream to the underlying aquifer (Figure 1.1).

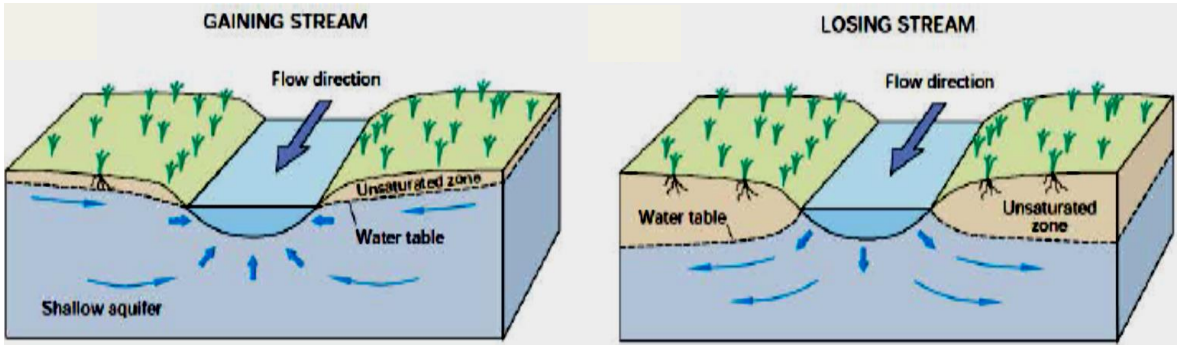

Figure 1.1 An illustrated example of gaining stream and losing stream reaches (Winter *et al*., 1998)

TL's may occur in any climatic region, with the most frequent occurrences taking place in arid and semi-arid climatic regimes, where their effects are enhanced due to deep water tables which are predominantly lower than the level of water in the river channel (Cataldo *et al*., 2010). As the loss of water from the river is largely controlled by the hydraulic gradient, groundwater recharge by the stream occurs when the surface water level is higher than the groundwater level (Winter *et al*., 1998).

In South Africa, these TL's generally occur along rivers within two distinct environments; i) deep fractured hard rock landscapes and ii) alluvial systems (Smakhtin, 2001; Hughes, 2008). Rivers which traverse channels characterized by surface fracturing and structural weakness in hard rock environments or unconsolidated material in alluvial environments, offers the ideal opportunity for substantial TL's to occur during both the initial phases of flood events, as well as for low flow periods (Smakhtin, 2001).

It should also be noted that the processes driving TL's may be more significant and vary depending on type of flow within the system (high or low flow). For example, Lange (2005) and Morin et al. (2009) showed that there was a higher contribution to aquifer recharge during single high magnitude flood events, as compared to small and medium flow events. This was largely attributed to the flooding of overbank areas, which enhanced recharge.

1.3 Estimation of Streamflow Transmission Losses in South Africa

TL's have been well documented internationally for arid and semi-arid environments, with Cataldo *et al*. (2004) and Shanafield and Cook (2014) providing comprehensive discussions on the various approaches which have been implemented to understand and quantify this process. However, there remains a paucity of studies of this process in southern Africa (Hughes, 2008; Tanner and Hughes, 2015a, 2015b).

Although, TL's have not been adequately quantified for any South African river system, the magnitude of these losses is estimated to be high, especially for perennial river systems flowing through arid and semi-arid environments (Everson, 1999; Everson et al., 2001; Riddell *et al*., 2017). Boroto and Gorgens (2003) predicted that up to 30 % of the Limpopo rivers mass balance may be allocated to TL's, as a result of riparian ET and aquifer storage. More recently, the Letaba River Reserve Determination study (DWAF, 2006) estimated that TL's may account for between 8 to 50 % of channel inflows. A 10 % loss of channel inflows to TL's is currently used for flow management within the Olifants River (DWA, 2011).

In order to reduce the uncertainty associated with implementing EWR flows, it is imperative that the hydrological processes contributing to TL's are quantified at various spatial and temporal scales. The use of conceptual models and time series analysis is one method for the reliable prediction of TL's for regions possessing long time series of streamflow data (Sharma and Murthy, 1994a; Costa *et al*., 2012).

However, in arid and semi-arid environments the routine monitoring of streamflow is generally limited (Lange *et al*., 2005). In such circumstances, the use of process-orientated models, which are parameterized using representative measurements of hydrological parameters, represent the most suitable tool to quantify TL's. This in turn may facilitate the improved management of EWR flows (El-Hames and Richard, 1998; Gheith and Sultan, 2002).

1.4 Understanding and Quantifying the Contribution of Riparian Total Evaporation to Streamflow Transmission Losses

According to Gu and Deutschman (2001) the proficient management of EWR flows and water provisions in arid and semi-arid regions is dependent on understanding and accurately quantifying the hydrological processes contributing to TL's in these environments. Sharp and Saxton (1962) describe various key factors which have been identified to have an influence on the TL's process, however only a select few parameters have been successfully incorporated into TL estimation techniques (Hacker, 2005). Runoff volume and velocity, the river channel geometry and characteristics of the channel bed material are amongst the most commonly utilized factors in these procedures (Hacker, 2005). Ultimately, the choice of factors used during the estimation of TL's is largely controlled by the characteristics of the study-site and the availability of data (Cataldo *et al*., 2004).

However, it is often the case that riparian ET is ignored or inadequately represented in the TL's estimation procedures, even though it has been identified as a contributing process to TL's (Hacker, 2005; Cataldo *et al*., 2010; Shanafield and Cook, 2014). Research and TL's estimation techniques have tended to focus more on the flow reduction in relation to infiltration (Hacker, 2005; Cataldo *et al*., 2010; Shanafield and Cook, 2014), as TL's in most rivers generally occur as a result of infiltration-based losses and open-water evaporation losses (Everson et al., 2001; Cataldo *et al*., 2010). While these infiltration-based losses may generally possess a relatively larger contribution to TL's, the absolute losses resulting from riparian ET cannot be discounted.

This is particularly pertinent, to environments where total evaporation (inclusive of open water evaporation) is a considerably large component of the water budget (McKenzie, 2001; Hacker, 2005; Shanafield and Cook, 2014). Everson et al. (2001) showed that losses due to riparian ET between two gauged sites on the Sabie River was approximately 0.32 $m^3 s^{-1}$, during low flow periods. This was a fairly significant proportion of total available flow, considering that low flow rates during this period were approximately 0.35 $m^3 s^{-1}$. This finding reaffirms the need to acknowledge and quantify the influence of riparian total evaporation, to successfully model TL's accurately in arid and semi-arid environments.

While riparian ET may significantly contribute to TL's in arid and semi-arid environments. The transpiration component of this process, may ultimately influence the magnitude of these losses, especially during arid periods (Cadol *et al*., 2012). Daily transpiration demands are generally met by available soil moisture. However, during arid conditions, riparian vegetation generally become increasingly reliant on stream and groundwater to fulfil a portion of their water requirements (Gribovski *et al*., 2008; Cadol *et al*., 2012; Lin *et al*., 2016; Qian *et al*., 2017).

While ET of waters stored within the river banks may enhance TL's during high flow periods when flood waters exceed the bank full storage. During low flow periods, TL's may be largely due to the proportion of water transpired directly from stream and groundwater. Consequently, the increased dependency on stream and groundwater by riparian vegetation may increase the magnitude of TL's during arid conditions.

Groundwater used during transpiration is typically replenished by subsurface flows further away from the stream channel or flow maybe redirected from the stream channel into the adjacent aquifer due to an inverse in the hydraulic gradient, ultimately resulting in a loss of streamflow (Winter et al., 1998; Gribovski *et al*., 2008; Tanner and Hughes, 2015a). According to Cadol et al. (2012) the volume of water lost from stream and groundwater to transpiration, should equal the volume of water transpired over an area of influence within and adjacent to the stream.

1.4.1 Estimating Riparian Evapotranspiration

In order to adequately quantify the influence of riparian ET and particularly transpiration on TL's, it is essential to develop techniques or approaches which can be used to better understand and accurately quantify how this process influences the rapport between subsurface water storage processes, streamflow and TL's. Conventional or traditional approaches used for the estimation of total evaporation (for example eddy covariance, scintillometry, surface renewal), have been invaluable in improving our understanding of the role which total evaporation plays in various environmental processes (Jarmain *et al.*, 2009b).

However, these techniques are only able to provide point or line averaged estimates of total evaporation (Lu *et al*., 2013; Liou and Kar, 2014; Mengistu *et al*., 2014; Zhuo *et al*., 2014). Consequently, the estimates which are obtained are only representative of localised conditions and cannot be easily extended to provide estimates of total evaporation over larger areas (Bastiaansen *et al.*, 2012; Teixera and Batsiaansen, 2012; Mengistu *et al*., 2014; Jassas *et al*., 2015).

This can essentially be attributed to the land surface heterogeneity, which becomes more distinct over larger geographic areas, as well as the dynamic nature of heat transfer processes at larger spatial scales (Li *et al.*, 2009; Bastiaansen *et al.*, 2012). Furthermore, it would prove to be impractical and relatively costly to create a network of *in-situ* measurements which can be used to provide representative large-scale total evaporation estimates (Elhaddad and Garcia, 2008; Bastiaansen *et al.*, 2012). In such situations, the use of satellite earth-observation (SEO) data represents the most suitable and efficient alternative to obtain spatial hydrological process information, preferably in combination with in-situ measurements for verification purposes.

In the last decade, ET estimation, has substantially benefited from advancements in SEO (Nourhi *et al*., 2013). SEO can be used to overcome spatial limitations generally associated with conventional approaches (Fernández-Prieto *et al*., 2012). Furthermore, SEO can be used to acquire data in remote and data scarce regions, as well as making allowance for seasonal and inter-annual comparisons of hydro-meteorological variables due to the periodic updating of information (Gokool *et al*., 2016).

Consequently, the use of SEO data makes allowance for the relatively timeous and inexpensive quantification of ET, which can prove to be invaluable towards improving decision making with regards to water resources management. Numerous satellite-based methods have been formulated for the estimation of ET, with techniques predicated on semi-physical and physical approaches being most extensively applied for both scientific research and operational purposes (Bastiaanssen., *et al*.,1998; Senay *et al*., 2007; Gokmen *et al*., 2012). Some of the most commonly applied models include; Surface Energy Balance System (SEBS) (Su, 2002); Surface Energy Balance Algorithm for Land (SEBAL) (Bastiaanssen et al., 1998) and Mapping Evapotranspiration at High Resolution with Internalized Calibration (METRIC) (Allen et al, 2007).

According to Li *et al*. (2009) the aforementioned ET models are derivatives of the Surface Energy Balance Index SEBI, detailed in (Menenti and Choudhury, 1993). The distinguishing characteristic between these ET models, as well as other frequently applied single-source models, is the way in which the sensible heat flux is derived. More specifically this relates, to defining the wet and dry limits, as well as upper and lower limits, in order to derive the sensible heat flux for particular boundary layer conditions, after which the latent heat flux (LE) is derived by subtraction (for example closure of the energy balance equation) (Li *et al*., 2009). A brief narrative of these models is given as follows:

i. The conceptualization of the SEBAL Model is discussed in detail by Bastiaansen *et al*. (1998). SEBAL uses Thermal infrared (TIR), Visible and Near-infrared radiation data acquired from SEO, in conjunction with physical modules and empirical relationships, to derive the instantaneous and 24-hr integrated surface heat flux for each pixel within a satellite image (Bastiaansen *et al*., 1998). The SEBAL algorithm computes key hydro-meteorological fluxes, using minimal *in-situ* information, to derive the instantaneous terms of the shortened energy balance (Bastiaansen *et al*., 1998). The latent heat flux can be determined, as a residual of the shortened energy balance equation (Bastiaansen *et al*., 1998). Once the instantaneous latent heat flux has been derived, the *EF* (ratio of latent heat to the energy available at the land surface) for each pixel can then be calculated (Bastiaansen, 2000). The *EF* is then assumed to be constant throughout the day, which facilitates the estimation of the daily total evaporation (Bastiaansen *et al*., 1998a; Bastiaansen, 2000; Jarmain *et al.*, 2009; Mengistu *et al*., 2014).

ii. SEBAL is used as the basis, for the conceptualization of the METRIC Model described in Allen *et al*. (2007). According to Li *et al*. (2009) the model was formulated, to overcome limitations associated with SEBAL, for the mapping of regional total evaporation over complex environments. The distinguishing features between SEBAL and METRIC is the manner in which the cold pixel value is determined and the upscaling of instantaneous total evaporation to daily total evaporation (Allen *et al*., 2007; Li *et al*., 2009; Liou and Kar, 2014).

The energy balance conditions for the cold pixel are determined, using the alfalfa reference evaporation (Allen *et al.*, 2007). The cold pixels are selected for an agricultural setting, whereby the biophysical characteristics ought to be akin to an alfalfa reference crop (Allen *et al.*, 2007). The daily total evaporation is computed, using the ratio of instantaneous total evaporation and the reference crop evaporation, acquired from *in-situ* meteorological measurements at the time of satellite overpass (Allen *et al.*, 2007). According to Li *et al*. (2009), determining the daily total evaporation in this way instead of assuming a constant *EF* for the day, allows for the effects of advection and changes in climatic variables during the day, to be better accounted for.

iii. The conceptualization of the SEBS Model is discussed in Su (2002). SEBS estimates atmospheric turbulent fluxes using both SEO and meteorological data (Su, 2002; Mengistu *et al*., 2014; Liou and Kar, 2014; Pardo *et al.*, 2014). The model consists of a suite of tools used for the determination of land surface physical parameters from spectral reflectance and radiance (Su *et al*., 1999), a comprehensive model for the approximation of the roughness length of heat transfer (Su et al., 2001) and an innovative procedure for the estimation of the *EF* on the basis of the energy balance at limiting cases (Su, 2002). The model applies the shortened surface energy balance equation to partition the available energy into sensible and latent heat flux density. Similar to the approach used in SEBAL, the daily total evaporation is estimated, assuming the *EF* remains constant throughout the day (Su, 2002).

A summary of the recent applications, as well as the relative strengths and weaknesses associated with the aforementioned models, which are discussed in further detail in Bastiaanssen *et al*. (1998), Su (2002), Allen *et al*. (2007), Jarmain *et al.* (2009) and Li *et al*., (2009) is given in Table 1.1. Considering the advantages and disadvantages associated with these models, the SEBS Model was chosen for application in this study. This decision was based largely on the accessibility of the model, as it is open-source. Furthermore, SEBS has been extensively applied for the estimation of regional fluxes and total evaporation and has been shown, to provide relatively high precision estimates of total evaporation and terrestrial heat fluxes (Jarmain *et al*., 2009; Yang *et al*., 2010; Zhuo *et al*., 2014).

Table 1.1 A summary of recent applications, advantages and disadvantages associated with the commonly applied satellite based ET models

Technique	Recent Operational and Research Applications	Advantages	Disadvantages
SEBAL	• ET estimation for improved water resources planning and management (Allen *et al*., 2011; Sun *et al*., 2011; Papadavid *et al*., 2012, 2017; Kamble *et al*., 2013; Kiptala *et al*., 2013; Jana *et al*., 2016)	• Minimal *in-situ* data requirements • Physically based • Land use data not required • Multiple-sensor approach • Automatic internalized calibration • Atmospheric corrections not required	• User defined hot and cold pixels • Generally applicable to flat terrain • *EF* is assumed to be constant for the estimation of daily total evaporation • Not open source
METRIC	• ET estimation for improved water resources planning and management (Allen *et al*., 2011; Hankerson *et al*., 2012; Trezza *et al*., 2013; Spiliotopoulos *et al*., 2017)	• Conceptualization of the model similar to SEBAL but surface slope and aspect can be considered • The method used to determine total evaporation allows for the effects of advection and changes in climatic variables during the day, to be better accounted for.	• Uncertainty, can be introduced in the determination of hot and cold pixels • Not open source
SEBS	• ET estimation for improved water resources planning and management (Ma *et al*., 2012, 2014; Szporak-Wasilewska *et al*., 2013; Matinfar and Soorghali, 2014; Shoko *et al*., 2014; Yang *et al*., 2015; Abdelrady *et al*., 2016; Ferreira et al., 2016; Gokool *et al*., 2016; Mohammadian *et al*., 2017)	• *Apriori* knowledge of actual turbulent fluxes is not required • Explicitly computes roughness length of heat transfer • Open source software available in ILWIS • Application of the model is fairly user-friendly • Less assumptions are made then in other techniques • The shortened energy balance is solved with more physical parameterizations	• Dry and wetland requirement to determine the sensible heat flux, • Solution to determine turbulent heat flux is fairly complex • *EF* is assumed to be constant for the estimation of daily total evaporation • Pre-packaged version of the model in ILWIS has been parameterized for agricultural crops

1.4.2 Satellite-based Total Evaporation Estimation using the SEBS Model

Su (2002) provides a detailed conceptualization of the SEBS model, which is described as a single-source surface energy balance model, which can be used to estimate atmospheric turbulent fluxes, as well as the *EF*, using both SEO and meteorological data. A suite of tools is available within the model, which facilitates the determination of land surface physical parameters from spectral reflectance and radiance (Su *et al*., 1999), a comprehensive model for the approximation of the roughness length of heat transfer (Su *et al*., 2001) and an innovative procedure for the estimation of the *EF* on the basis of the energy balance at limiting cases (Su, 2002).

Su (2002) states that there are three primary sets of information or data are required by the model for the estimation of daily total evaporation. The first set of data comprises the land surface physical parameters *viz.* albedo, emissivity, temperature, fractional vegetation cover, leaf area index (LAI) and vegetation height. The normalized vegetation difference index (NDVI) is used as surrogate when vegetation information is unavailable. Information, relating to the land surface physical parameters can be derived from a combination of SEO data and ancillary information regarding the surface of interest (Su, 2002).

The second set, relates to data which can be acquired from meteorological stations, this includes measurements of air temperature and pressure, humidity and wind speed at a reference height. The reference height is used, as the measurement height, as well as the height of the planetary boundary layer (PBL) for point application and regional application, respectively. Large scale meteorological models can be used for the estimation of this data set (Su, 2002; Jarmain *et al*., 2009; Mengistu *et al*., 2014).

The third data set includes both the downward shortwave radiation and downward longwave radiation, which can be obtained through measurements or estimated through parameterization of the model (Su *et al.*, 2001; Su, 2002). The various sets of input information are incorporated into three sub-models, which is then used for the computation of the components of the shortened energy balance, the roughness length of heat transfer and the *EF* on the basis of the energy balance at limiting cases (Su, 2002).

The use of SEO data within the SEBS Model allows for an improved spatial representation of total evaporation estimates. Furthermore, the open source nature of the model, its strong physical conceptualization and relatively user-friendly operability, make it an attractive tool, for the provision of spatially representative total evaporation data.

1.4.2.1 *Determination of total evaporation within the SEBS Model*

Satellite earth observation data and meteorological data are used, to derive the various input parameters required for the estimation of total evaporation within the SEBS Model. The formulation of SEBS (Su, 2002) is given as follows:

Derivation of surface energy balance terms

The SEBS Model employs the shortened surface energy balance equation (Equation 1.1) and partitions the available energy into sensible and latent heat fluxes.

$$R_n = G_o + H + \lambda E \quad (1.1)$$

Where Rn is net radiation (W m^{-2}), G_0 is soil heat flux (W m^{-2}), H is sensible heat flux (W m^{-2}) and λE is the latent heat flux (W m^{-2}).

The equation to determine the net radiation term in Equation 1.1 is given as:

$$R_n = (1 - \alpha)R_{swd} + \varepsilon R_{lwd} - \varepsilon\sigma T_o^4 \quad (1.2)$$

Where α is the albedo (surface reflectance), R_{swd} is the downward solar radiation (W m^{-2}), R_{lwd} is the downward longwave radiation (W m^{-2}), ε is the emissivity of the surface, σ is the Stefan-Boltzman constant and T_o is the surface temperature (K).

The soil heat flux equation is parameterised as:

$$G_o = R_n[\Gamma + (1 - f_c)(\Gamma_s - \Gamma_c)] \quad (1.3)$$

Where the ratio of soil heat flux to net radiation Γ_c is assumed to be 0.05 for a fully vegetated canopy (Monteith, 1973) and Γ_s is assumed to be 0.315 for a bare soil surface (Kustas and Daughtry, 1989). The fractional vegetation coverage f_c is used to perform an interpolation between the aforementioned limiting cases, to separate land surfaces into non-vegetated, partially vegetated and densely vegetated surfaces.

SEBS makes use of the Monin-Oukhov similarity theory (MOST) for the estimation of the sensible and latent heat fluxes. MOST relates surface variables and variables in the atmospheric surface layer (ASL) to surface fluxes (Su *et al*., 2001). Su (2002) states that the similarity relationships for profiles of the mean wind speed and mean temperature difference (θ_o - θ_a) in the ASL, are usually written in integral form as:

$$u = \frac{u_*}{k}\left[\ln\left(\frac{z-d_o}{z_{oh}}\right) - \psi_m\left(\frac{z-d_o}{L}\right) + \psi_m\left(\frac{z_{om}}{L}\right)\right] \quad (1.4)$$

$$\theta_o - \theta_a = \frac{H}{ku_*\rho C_p}\left[\ln\left(\frac{z-d_o}{z_{oh}}\right) - \psi_h\left(\frac{z-d_o}{L}\right) + \psi_h\left(\frac{z_{oh}}{L}\right)\right] \quad (1.5)$$

Where z is the reference meteorological height (m), u_* is the friction velocity (m s^{-1}), ρ is the density of air (kg m^{-3}), C_p is the heat capacity of dry air (Jkg^{-1}), k = 0.4 is von Karman's constant, d_o is the zero plane displacement height (m), z_{om} is the roughness height for momentum transfer (m), θ_o and θ_a are the potential surface temperature and potential air temperature at height (z) respectively (K), z_{oh} is the scalar roughness height for heat transfer, ψ_m and ψ_h are the stability correction factors for momentum and heat transfer respectively and L is the Obukhov length (m), which is given as:

$$L = \frac{pC_p u_*^3 \theta_v}{kgH} \quad (1.6)$$

Where g is the acceleration due to gravity (m s^{-2}) and θ_v is the potential virtual temperature near the surface (K). The stability length L is a function of the sensible heat flux H, which in turn is dependent on u_* and is calculated in equation 1.6 as a function of θ and u_*. Consequently, iterative procedures are required for the estimation of H and u_* (Jarmain *et al*., 2009).

Derivation of the roughness length for heat transfer

The above derivations require the aerodynamic (d_o and z_{om}) and thermal dynamic roughness parameters (z_{oh}) to be known (Su, 2002). The turbulence model proposed by Massman (1997) can be used, to estimate the aforementioned aerodynamic parameters when near surface wind speed and vegetation parameters (LAI and wind speed) are available. However, when information with regards to the abovementioned vegetation parameters are unavailable, the aerodynamic parameters can be related to satellite-derived vegetation indices (Su, 2002).

According to Su and Jacobs (2001) z_{om} can be estimated, using empirical relationships with NDVI. Empirical relationships are also used for the estimation of vegetation height (h) and d_o (Brutsaert, 1982). The estimation of these parameters is given as:

$$Z_{om} = 0.005 + 0.5\left(\frac{NDVI}{NDVI_{max}}\right)^{2.5} \quad (1.7)$$

$$h = \left(\frac{z_{om}}{0.316}\right) \quad (1.8)$$

$$d_o = \frac{2}{3}h \quad (1.9)$$

The scalar roughness height for heat transfer can be derived as:

$$z_{oh} = \frac{z_{om}}{\exp(kB^{-1})} \quad (1.10)$$

Where B^{-1} is the inverse Stanton number, a dimensionless heat transfer coefficient

The kB^{-1} value can be determined using the extended physical model proposed by Su *et al*. (2001), which is given as:

$$kB^{-1} = \left(\frac{kC_d}{4C_t\frac{u_*}{u(h)}1-e^{\frac{nec}{2}}}\right)f_c^2 + 2f_cf_s\frac{k\frac{u_*}{u(h)}\text{x}\frac{z_{om}}{h}}{C_t^*} + kB^{-1}f_s^2 \quad (1.11)$$

Where Cd is the drag coefficient of foliage elements assumed to possess a value of 0.2, N_{ec} is the within-canopy profile extinction coefficient, $u(h)$ is the horizontal wind speed at the top of the canopy, f_c is the fractional vegetation cover and f_s is its complement, C_t is the heat transfer coefficient of the leaf and bounded between $0.005N \leq C_t \leq 0.075N$ (N is the number of sides of the leaf which participates in heat transfer process) for most canopies and environmental conditions.

C_{t*} is the heat transfer coefficient of the soil which is given as $C_{t*} = P_r^{\frac{-2}{3}}$ x $R_{e*}^{\frac{-1}{2}}$, where Pr is the Prandtl number and R_{e*} is the roughness Reynold number. According to Brutsaert (1982) the kB^{-1} for a bare soil surface can be estimated as:

$$kB_s^{-1} = 2.46(R_{e*})^{\frac{1}{4}} - \ln(7.4) \quad (1.12)$$

Determination of the evaporative fraction on the basis of the energy balance at limiting cases

Su (2002) discusses the derivation of the *EF* on the basis of the energy balance at limiting cases. In SEBS, the actual sensible heat flux (*H*) is constrained in the range set by the sensible heat flux at the wet limit (H_{wet}) and the sensible heat flux at the dry limit (H_{dry}) (Su, 2002).

Due to the limitation of soil moisture, the latent heat flux (or the evaporation) becomes zero, at the dry limit, and the sensible heat flux attains its maximum value (Su, 2002). The sensible heat flux at the dry limit is given as:

$$\lambda E_{dry} = R_n - G_o - H_{dry} = 0, \text{ or} \quad (1.13)$$

$$H_{dry} = R_n - G_o$$

The sensible heat flux attains its minimum value, at the wet limit, as evaporation can take place at potential rates (evaporation is constrained, only by the energy available for given surface and atmospheric conditions). The sensible heat flux at the wet limit (H_{wet}) is given as:

$$H_{wet} = R_n - G_o - \lambda E_{wet} \quad (1.14)$$

Su (2002) combines Equation 1.14 with an equation similar to the Penman-Monteith combination equation, in order to derive H_{wet}. Menenti (1984) grouped the bulk internal and external resistances to express the combination equation as:

$$\lambda E = \frac{\Delta r_e (R_n - G_o) + P C_p (e_s - e_a)}{r_e (\gamma + \Delta) + \gamma r_i} \quad (1.15)$$

Where Δ is the rate of change of the saturation vapour pressure with temperature (hPa K^{-1}), γ is the psychometric constant (hPa K^{-1}), e_s and e_a are the saturation vapour pressure (hPa) and actual vapour pressure (hPa) respectively, r_e is the aerodynamic resistance (s m^{-1}) and r_i is bulk surface internal resistance (s m^{-1}). The roughness length for heat transfer and vapour transfer are assumed to be equal, in Equation 1.15 (Brutsaert, 1982). The Penman-Monteith equation is only valid for a vegetated canopy, whereas by definition Equation 1.15 is also valid for a soil surface with defined bulk internal resistance (Su, 2002). Su (2002) states that it may prove difficult to estimate the latent heat flux, using Equation 1.15. This is largely due to the difficulty in determining the bulk internal resistance (r_i), which is regulated by water availability (Su, 2002).

An alternative is proposed by Su (2002), to circumvent the direct use of r_i for the estimation of λE. By definition, the internal resistance under the wet limit is equal to zero. Su (2002) applied this property to Equation 1.15 and altered the parameters accordingly to reflect wet limit conditions, so that the sensible heat flux at the wet limit can be given as:

$$H_{wet} = \frac{(R-G)-(\frac{pC_p}{r_{ew}})(\frac{e_s-e_a}{\gamma})}{1+\frac{\Delta}{\gamma}} \quad (1.16)$$

The external resistance is also dependent on the Obukhov Length L, which is a function of the sensible heat flux H and friction velocity u_* (Equations 1.4-1.6). As the Obukhov Length has been previously determined, the external resistance r_{ew} can be estimated from Equation 1.5 as:

$$r_{ew} = \frac{1}{k_{u*}}[\ln\left(\frac{z-d_o}{z_{oh}}\right) - \psi_h\left(\frac{z-d_o}{L_w}\right) + \psi(\frac{z_{oh}}{L_w}) \quad (1.17)$$

The stability length at the wet limit can be given as:

$$L_w = \frac{\rho u_*^3}{0.61kg\frac{R_n-G_o}{\lambda}} \quad (1.18)$$

The relative evaporation can then be given as:

$$\Lambda r = \frac{\lambda E}{\lambda E_{wet}} \quad (1.19)$$

$$= 1-(\frac{\lambda E_{wet}-\lambda E}{\lambda E_{wet}})$$

Substitution of Equations 1.1, 1.13 and 1.14, into Equation 1.19 and after some algebra yields:

$$\Lambda r = 1-\frac{H-H_{wet}}{H_{dry}-H_{wet}} \quad (1.20)$$

The evaporative fraction is given as:

$$\Lambda = \frac{\lambda E}{R_n-G_o}$$

$$= \frac{\Lambda_r \lambda E_{wet}}{R_n-G_o} \quad (1.21)$$

Determination of the actual total evaporation

The actual latent heat flux can be determined by inverting Equation 1.21. The daily soil heat flux is assumed to be close to zero, because the diurnal downward flux and the nocturnal upward flux, approximately balance each other (Jarmain *et al*., 2009). Subsequently, the actual total evaporation can be computed by assuming the *EF* is constant throughout the day. The actual total evaporation is estimated as:

$$E_{daily} = \frac{8.64\text{x}10^{7}\Lambda 24(R_n - G_o)}{\lambda \rho_w} \quad (1.22)$$

Where E_{daily} is the actual daily total evaporation (mm), Λ^{24} is the daily average *EF*.

1.4.2.2 *Limitations associated with satellite earth observation data and the pre-packaged version of the SEBS Model*

Despite the fact that, there are several advantages associated with the use of SEO data for the estimation of total evaporation there does exist a number of general, as well as technique specific constraints which can limit the effectiveness of these technologies. Cloud contamination within an image, satellite revisit and repeat cycles and lack of trained personnel to process and analyse imagery, are general limitations which can significantly impede the application of satellite based technologies and data, for the estimation of total evaporation (McCabe and Wood, 2006; Li *et al.*, 2008; Jarmain *et al*., 2009).

It has also been shown that, satellite-based ET estimation approaches often overestimate ET in areas of arid and semi-arid climatic regimes in which the availability of water is limiting ET (Seneviratne et al., 2010). Studies undertaken by Timmermans and Meijerink (1999), Lubczynski and Gurwin (2005) and van der Kwast et al. (2009) in these environments, have shown that satellite-based ET estimation models may overestimate ET in the magnitude of 0.50 to 3.00 mm d^{-1}, as a result of an under-estimation of the sensible heat flux (*H*).

The abovementioned challenges generally relate to satellite-based approaches for the estimation of ET, however, there are technique specific limitations which also need to be considered. The pre-packaged version of SEBS in the Integrated Land and Water Information System (ILWIS) has been found to be extremely sensitive to particular model parameters. Consequently, any uncertainty associated with these parameters will be further exacerbated in the model output.

These parameters include; (i) the land surface temperature and air temperature gradient (Su, 2002), (ii) the selection of the fractional vegetation cover formula (Lin, 2006; Badola, 2009), (iii) the height of wind speed measurements and the displacement height (Timmermans *et al.*, 2005; van de Kwast *et al.*, 2009) and (iv) the spatial heterogeneity of the area of interest (McCabe and Wood, 2006; Li *et al.*, 2008). Gibson *et al*. (2011) provides a detailed discussion of these parameters and the potential uncertainties which may be introduced to the model output.

In addition to the aforementioned limitations, the daily ET is computed in SEBS by assuming that the evaporative fraction remains constant throughout the day (Su, 2002). The findings of research embarked upon by Stewart (1996), Lhomme and Elguerro (1998), Gentine *et al.* (2007); (2011) and Mkhwanazi and Chavez (2013), have shown that this assumption can lead to inaccuracies in the daily actual total evaporation estimate, especially when advective conditions are prevalent (Gentine *et al.*, 2007; Mkhwanazi and Chavez, 2013).

1.4.2.3 *SEBS Modifications*

Surface energy balance ET estimation models such as SEBS do not explicitly account for the influence of soil moisture dependency and biophysical factors during the derivation of fluxes and ET (Gokmen et al., 2012; Pardo et al., 2014). The individual influence of soil water evaporation, transpiration, soil moisture and interception storage are all implicitly encompassed in input variables, such as the land surface temperature *LST*, ignoring their direct impact on fluxes and ET (Gokmen et al., 2012; Wu et al., 2014; Li et al., 2015). While, the aforementioned approach may be suitable for environmental settings in which the available energy is limiting ET such as in the high latitude regions, it may prove to be inadequate where water availability is the principle limiting factor to ET, such as in arid and semi-arid environments (Seneviratne et al., 2010).

Hence, satellite-based ET modelling necessitates an improvement for the estimation of fluxes for different land covers experiencing conditions of water stress (Gokmen et al., 2012; Wu et al., 2014). Due to this limitation in implementing satellite-based surface energy balance ET estimation models during conditions of water stress, Gokmen et al. (2012) and Pardo et al. (2014) proposed the implementation of modified versions of SEBS, which involves the integration of a scaling factor into the original SEBS formulation ($SEBS_0$). While studies by Wu et al. (2014) and Li et al. (2015) discuss alternative approaches in deriving scaling factors that can be integrated with $SEBS_0$, these approaches are essentially based on the procedure described in Gokmen et al. (2012).

Gokmen et al. (2012) proposed a scaling factor which considers the influence of soil moisture (SM) on ET estimates ($SEBS_{SM}$), where SM estimates can be acquired from *in-situ* data or satellite based approaches. The rationale for introducing this scaling factor into $SEBS_0$ was to correct the underestimation of *H*, so that an overestimation of *EF* and *LE* can be avoided (Gokmen et al., 2012). This scaling factor can be integrated in $SEBS_0$ during the computation of the Kb^{-1} parameter, which is used in the estimation of z_{oh} and is given as follows:

$$Scale_{factor} = a + \frac{1}{1+\exp(b-c*SM_{rel})} \quad (1.23)$$

$$SM_{rel} = \frac{SM-SM_{min}}{SM_{max}-SM_{min}} \quad (1.24)$$

$$New\_Kb^{-1} = Kb^{-1} * Scale_{factor} \quad (1.25)$$

Where *a*, *b* and *c* are coefficients of a sigmoid function, which can be determined by performing an optimization, which involves reducing the error between observed and modeled *H* values for a particular area of interest. Gokmen et al. (2012) states that a sigmoid function was chosen to derive $Scale_{factor}$ values, as it significantly lowers the Kb^{-1} value for relatively dry conditions, while the influence of soil moisture on Kb^{-1} is not significant for wet conditions. Therefore, this approach allows for an improved representation of fluxes and ET for water limited environments, as well as enabling the distinct behavior of irrigated fields surrounded by extremely dry landscapes to be captured (Gokmen et al., 2012).

The second approach detailed by Pardo et al. (2014) ($SEBS_{NDVI}$) involves the application of a scale factor which considers the influence of temperature and vegetation over fluxes and is given as:

$$EF_{scalefactor} = \left(scale\_T_{surf}^{a}\right)[\exp(b * NDVI)] \quad (1.26)$$

$$scale\_T_{surf} = \frac{LST_{max} - T_{surf}}{LST_{max}} \quad (1.27)$$

Where LST is the land surface temperature (K) and LST_{max} is fixed at 320.15 K. The parameters in $EF_{scalefactor}$ can be fitted using a Marquardt algorithm. Once $EF_{scalefactor}$ has been determined it is then applied to the EF calculated in $SEBS_0$ prior to the computation of LE (Pardo et al., 2014).

$$EF_{new} = EF_{old} * EF_{scalefactor} \quad (1.28)$$

In order to ensure closure in Equation 1.1, H should also be recalculated using EF_{new} as follows (Pardo et al., 2014):

$$H_{new} = (1 - EF_{new})(R_n - G_0) \quad (1.29)$$

Pardo et al. (2014) evaluated the $SEBS_0$ algorithm, as well as the aforementioned modifications. The results of the study indicated that while the application of both the $SEBS_{SM}$ and $SEBS_{NDVI}$ approaches resulted in an improved agreement between the observed and modelled H. Only the $SEBS_{NDVI}$, was shown to have significantly improved modelled LE and EF when compared with observed values.

1.4.3 Determining Source Contribution to Evapotranspiration

Previous research has demonstrated how conventional and SEO techniques can provide fairly accurate estimates of riparian ET. However, these estimates often represent the total water used by vegetation from multiple sources, such as; soil, stream and groundwater. According to Tanner and Hughes (2015) there remains a fair degree of uncertainty regarding the contribution of groundwater to riparian ET. Consequently, identifying source contribution to ET can prove to be of added benefit to improving our understanding of the role which riparian ET plays in the TL's process.

Since the uptake of water during transpiration does not result in the fractionation of oxygen-18 (^{18}O) and deuterium (^{2}H) within suberized tissue (non-photosynthesising tissue) (White *et al*., 1985; Dawson, 1993; Dawson and Ehlringer, 1993; Evaristo *et al*., 2017)., the isotopic composition of ^{18}O and ^{2}H of xylem water should represent the sources present within the root zone (Evaristo *et al*., 2017). Consequently, stable isotope analysis can be used to determine the proportion of source contribution to ET (February *et al*., 2007; Eamus *et al*., 2015; Lin *et al*., 2106; Ma and Song; 2016).

According to Craig (1961), there exists a linear relationship between ^{2}H and ^{18}O within freshwater that can be explained by the global meteoric water line (GMWL), which can be described as:

$$\delta^{2}H = 8\delta\,^{18}O + 10 \qquad (1.30)$$

According to Gat (2005) the relationship described in Equation 1.30 can be affected by meteorological conditions, such as temperature and relative humidity, as well as by processes such as evaporation, condensation and mixing). Therefore, the linear relationship between ^{2}H and ^{18}O at a particular site may differ from the GMWL and may be better described using a Local Meteoric Water Line (LMWL).

The GMWL or LMWL provides a reference point by which localized differences in water can be characterized, subsequently facilitating the source of the water to be determined. For example, free evaporative processes may typically result in a line with a slope and intercept that is less than 8 and 10, respectively. The shallower slope can be attributed to the non-equilibrium kinetic effects that occur during evaporation, resulting in the fractionation of Hydrogen and Oxygen isotopes (Kendall and McDonnell 1998; February *et al*., 2007). Subsequently, fractionation may result in waters exhibiting distinct isotopic compositions indicative of the source of water or the processes that formed them (Kendall and McDonnell 1998).

Stable isotope techniques have been extensively used to provide a qualitative understanding of the source of water uptake by vegetation, as well as to quantify the amount of water which is used from a particular source (Zencich *et al*., 2002; Holland *et al*., 2006; Feikema *et al*. 2010; Goedhart and Pataki 2011; Ma and Song; 2016; Lin *et al*., 2106; Qian *et al*., 2017).

Kendall and McDonell (1998) define stable isotopes, as atoms which do not decay over time to form other isotopes, however they can be fashioned by the decay of other radioactive isotopes. The concentration of ^{18}O and ^{2}H in the plant xylem water provides an indication of the isotopic concentration at the source, this is due to fractionation not taking place during plant water uptake (White *et al*., 1985). The isotopic composition of water (^{2}H and ^{18}O) is expressed in delta notation relative to the Vienna Standard Mean Oceanic Water (VSMOW), as:

$$\delta = \left(\frac{R_{sample}}{R_{standard}} - 1\right)*1000 \quad (1.31)$$

Where δ (expressed in ‰ notation) represents changes in the ratio of the uncommon to common isotopes ($^{2}H/^{1}H$ and $^{18}O/^{16}O$) for the sample (R_{sample}) and standard ($R_{standard}$). The value of δ (‰) can be positive or negative, contingent to the isotopic concentration of the water sample being enriched or depleted relative to the VSMOW.

According to Orrelana *et al*. (2012) the general isotopic concentration of xylem water originates from a mixture of multiple sources with each one potentially, being isotopically different. Therefore, isotopic analyses can also be used to quantify the quantity of water acquired from a particular source through the application of a mixing model (Orrelana *et al*., 2012). The mixing model is predicated on a mass balance approach, whereby the concentration of isotopes in the plant xylem water is representative of the weighted average of isotopic concentrations from the various sources of water (Orrelana *et al*., 2012).

Several studies have quantified the proportion of source contribution to ET using mixing models, some of which include Snyder and Williams (2000), Zencich *et al*. (2002) and Feikema *et al*. (2010), Ma and Song (2016) and Qian *et al*. (2017). The advantage of conducting investigations using stable isotope techniques is the non-destructive nature of the sampling procedures and the ability to clearly differentiate between different sources of water use (Ehlringer and Dawson, 1992; Yang *et al*., 2010). However, the successful application of the technique can be limited by data interpretation and the restricted number of possible water sources represented within the mixing model (Yang *et al*., 2010; Orrelana *et al*., 2012).

1.5 Research Aims, Objectives and outline of thesis structure

As mentioned previously, it is imperative that all hydrological processes contributing to TL's are understood and accurately quantified, so that water provisions and in particular EWR flows can be managed competently.

Considering this statement as a point of departure, the overall aim of this thesis was to improve the hydrological process understanding of TL's by attempting to understand and quantify the key hydrological processes which contribute to TL's along the Letaba River. The Letaba River is a typical example of a river system in which EWR flow management has been adversely impacted by the lack of a quantitative understanding of TL's (DWA, 2014) and therefore provides an ideal study site to perform the research necessary to fulfil the objective of this thesis. This research involved, conducting detailed characterizations of hydrological processes along a 14 km reach of the Groot Letaba River.

Particular emphasis was placed upon establishing the influence of riparian ET on TL's. This was centred around evaluating the potential of using a satellite-based approach to estimate ET along the length of river reach studied; assessing both the strengths and limitations associated with the implementation of a satellite-based ET model and requisite SEO data sets, to determine the most suitable and pragmatic approach which can be adopted for water resources management purposes.

Furthermore, these investigations were supplemented by a parallel study which focused on the continuous monitoring of the groundwater phreatic surface and hydraulic characterisation of aquifer properties, to determine baseline estimates of losses and gains along the river (Riddell *et al*., 2017). It was envisaged that the improved hydrological understanding gained from this integrated analysis along the portion of river reach studied, would enable the comprehensive and quantitative conceptual representation of the system, which can then be integrated into future hydrological modelling applications. Figure 1.2 illustrates the approach adopted to fulfil the aim and objectives of this particular study.

Considering the overall aim of the study, the thesis is divided into two parts which progressively documents existing and innovative approaches which are intended to fulfil the following specific objectives;

i. Development of a satellite based approach and time-series to adequately represent ET within the study area.
ii. Employ a multi-disciplinary approach, using stable isotope analysis, hydrological and geohydrological data in conjunction with the satellite-derived ET time-series to quantify TL's within the study area.

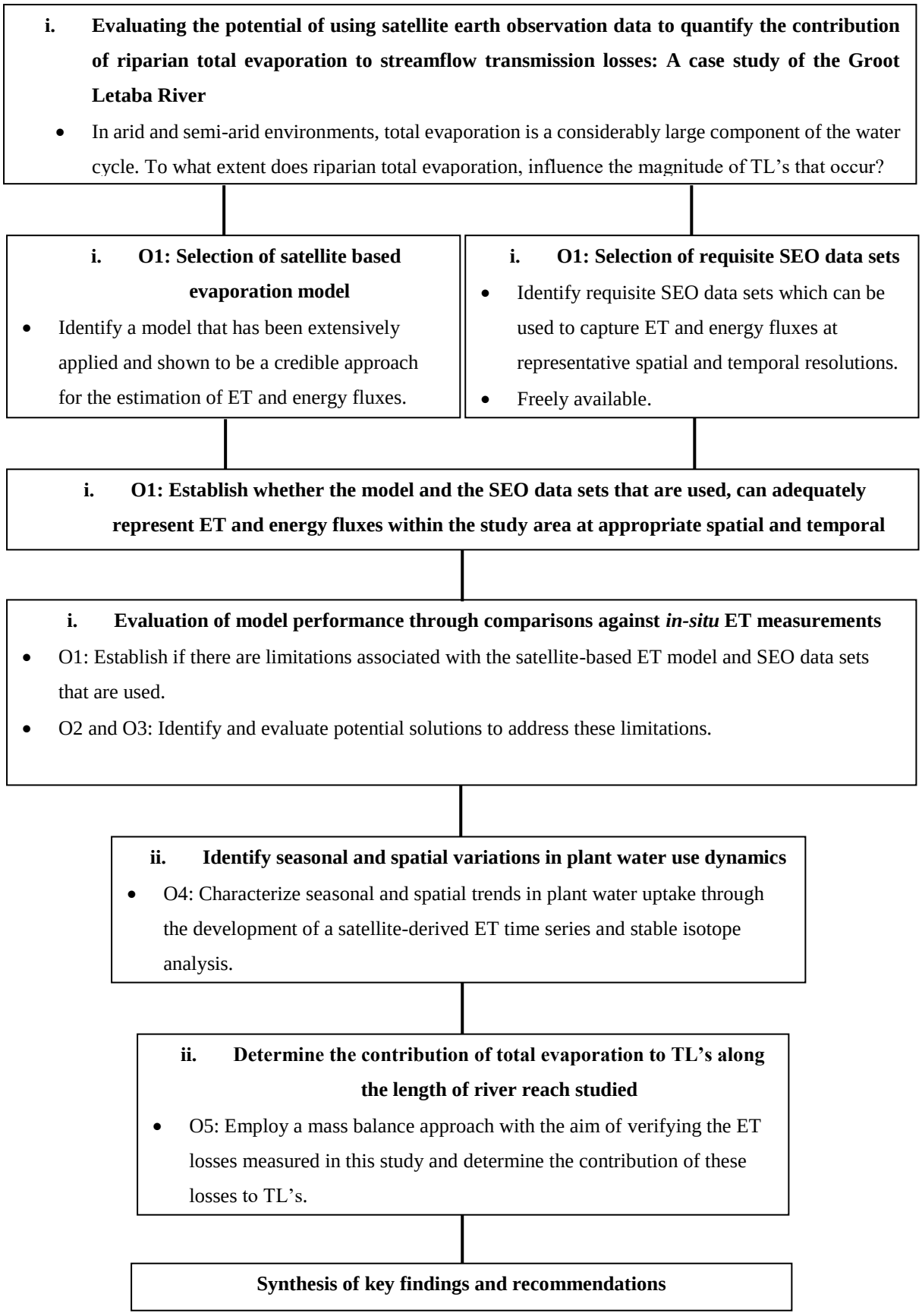

Figure 1.2 The conceptual framework of the study

Considering the significant role total ET plays in the water balance of river systems flowing through arid and semi-arid environments, it is essential to develop techniques or approaches which can be used to accurately quantify riparian ET at varying spatial and temporal scales, to better understand and quantify how this process influences the magnitude of TL's in these environments.

While the use of satellite-based ET models and SEO data provide an opportunity to acquire such information. The trade-off between the spatial and temporal resolution of available imagery (Gokool *et al*., 2016), may restrict the feasibility of using SEO data for operational water resources management. Previous studies *inter alia* by; Hong *et al*. (2011), Spiliotopolous *et al*. (2013) and Bhattarai *et al*. (2015) have reported potential solutions to address spatio-temporal limitations, through the application of downscaling/disaggregation procedures. However, the success of these techniques is ultimately dependent on the ability of the satellite-based ET model to capture ET for a particular area of interest, within an acceptable accuracy range (AAR) (± 15 to 30 %) when compared to *in-situ* observations (Kalma *et al*., 2008; Seneviratne *et al*., 2010; Gibson, 2013).

Given these limitations, an evaluation study was undertaken by selecting an appropriate satellite-based ET model and the requisite SEO data sets, to model ET within the study area. The following hypothesis and sub-objectives were tested in chapters 2 and 3 respectively.

H_0: The selected satellite-based ET model and associated data sets are able to adequately represent spatio-temporal dynamics in ET within the study area

O1: Evaluate the performance of the selected satellite-based ET model and associated data sets through comparisons against in-situ measurements of ET (chapter 2).

O2: Identify limitations associated with the SEO data sets and evaluate potential solutions to address these limitations (chapter 2).

O3: Identify limitations associated with the satellite based ET model and evaluate potential solutions to address these limitations (chapter 3).

Once the aforementioned objectives were achieved and the ability of the model to adequately represent ET within the study area confirmed, seasonal and spatial variations in plant water use dynamics could then be investigated. As previously mentioned, there remains a fair degree of uncertainty regarding the contribution of groundwater to riparian ET. Consequently, the following hypothesis and sub-objective were tested in chapter 4.

H_0: Riparian vegetation within the study area become increasingly reliant on groundwater to fulfil a portion of their daily water use requirements during arid conditions.

O4: Quantify spatial and seasonal variations in the proportional and volumetric contribution of sources to ET by developing a daily moderate spatial resolution satellite-derived ET time series and coupling this data with stable isotope analysis.

Once spatial and seasonal variations in the contribution of sources to ET was determined, the following hypothesis and sub-objective were tested in chapter 5.

H_0: Riparian ET is a key contributing process to TL's within the study area.

O5: Employ a mass balance approach with the aim of verifying the ET losses measured in this study and determine the contribution of these losses to TL's.

A synthesis of the key findings relating to the various methodologies that were adopted to fulfil the aim and objectives of this thesis, as well as recommendations for future studies are presented in chapter 6. A brief introduction, as well as Figure 1.2 (with the relevant parts being highlighted) is presented before the beginning of each chapter, to provide an indication of the research that is to be discussed.

It should also be noted that chapters 2 to 5 of this thesis will be presented as a series of research papers which have been submitted for publication in ISI rated peer-reviewed journals, following the approach that has been accepted by the University of KwaZulu-Natal. While every attempt was made to present each chapter as an independent investigation, some overlap was inevitable due to the structure adopted in this thesis.

This overlap, primarily relates to the description of the study area and the satellite-based ET model that was selected. A traditional literature review is not provided in this thesis, instead a review of relevant literature relating to the objective and implemented methodology is presented in each research paper. The referencing style for each of the research papers conforms to the journal in which the paper has been published or submitted to, in accordance with University of KwaZulu-Natal thesis guidelines.

1.6 References

Adams, J, Cowie, M and Van Niekerk, L. 2016. Assessment of completed ecological water requirement studies for South African estuaries and responses to changes in freshwater inflow. WRC Project No K8/1073.

Allen, R, Irmak, A, Trezza, R, Hendrickx, JMH, Bastiaanssen, W and Kjaersgaard, J. 2011. Satellite-based ET estimation in agriculture using SEBAL and METRIC. *Hydrological Processes* 25(26): 4011–4027.

Badola, A. 2009. Validation of Surface Energy Balance System (SEBS) over forest land cover and sensitivity analysis of the model, Unpublished Msc Thesis, International Institute for Geo-Information Science and Earth Observation, Enschede, The Netherlands.

Bastiaansen, WGM, Menenti, M, Feddes, RA and Holtslag, AAM. 1998. A remote sensing surface energy budget algorithm for land (SEBAL). 1. Formulation. *Journal of Hydrology* 212-213(1-4): 213.

Bastiaanssen, WGM, Cheema, MJM, Immerzeel, WW, Miltenberg, IJ and Pelgrum, H. 2012. Surface energy balance and actual evapotranspiration of the transboundary Indus Basin estimated from satellite measurements and the ET Look model. *Water Resources Research*, 48. Issue 11, Article first published online 21 November 2012, W11512. DOI:10.1029/2011WR010482.

Bhattarai, N, Quackenbush, LJ, Dougherty, M and Marzen, LJ 2015. A simple Landsat–MODIS fusion approach for monitoring seasonal evapotranspiration at 30 m spatial resolution. International Journal of Remote Sensing 36(1): 115-143.

Boroto, J and Gorgens, AHM. 2003. Limpopo River: an overview of alternative methods for estimating transmission losses. *Hydrology of Mediterranean and Semiarid regions. Proc. Montpellier Conference. IAHS Publ. 278*.

Brown, CA, van Der Berg, E, Sparks, A and Magoba, RN. 2010. Options for meeting the ecological Reserve for a raised Clanwilliam Dam, *Water SA* 36 (4).

Brutsaert, W. 1982. Evaporation into the atmosphere. D. Reidel, Dordrecht, Holland.

Cadol, D, Kampf, S and Wohl, E. 2012. Effects of evapotranspiration on baseflow in a tropical headwater catchment. *Journal of Hydrology* 462–463: 4–14.

Cataldo, J, Behr, C, Montalto, F and Pierce, RJ. 2010. Prediction of Transmission Losses in Ephemeral Streams, Western U.S.A. *The Open Hydrology Journal* 4: 19-34.

Costa, AC, Bronstert, A and de Araujo, JC. 2012. A channel transmission losses model for different dryland rivers. *Hydrology Earth System Science* 16: 1111–1135.

Costa, AC, Foerster, S, de Araujo, JC and Bronstert, A. 2013. Analysis of channel transmission losses in a dryland river reach in north-eastern Brazil using streamflow series, groundwater level series and multi-temporal satellite data. *Hydrological Process*es 27: 1046–1060.

Costelloe, JF, Grayson, RB, Argent, RM, and McMahon, TA. 2003. Modelling the flow regime of an arid zone floodplain river, Diamantina River, Australia. *Environmental Modelling and Software* 18: 693–703.

Craig, H. 1961. Isotopic variations in meteoric waters. *Science* 133: 1702–1703.

Dawson, T. 1993. Water sources of plants as determined from xylem-water isotopic composition: perspectives on plant competition, distribution, and water relations. In: Ehleringer J R, Hall A E, Farquhar G D. *Stable Isotopes and Plant Carbon-water Relations*. San Diego: Academic Press Inc, 465–496.

Dawson, TE and Ehleringer JR. 1993. Isotopic enrichment of water in the "woody" tissues of plants: implications for plant water source, water uptake, and other studies which use the stable isotopic composition of cellulose. *Geochimica et Cosmochimica Acta* 57(14): 3487–3492.

De Vries, JJ and Simmers, I. 2002. Groundwater recharge: an overview of processes and challenges. *Hydrogeology Journal* 10: 5–17.

Department of water Affairs (DWA). 2011. Development of Operating Rules for the Integration of the Blyde and Olifants River Systems DWA Report No: P WMA O4/B60/00/8510

Department of Water Affairs (DWA). 2014. Development of a reconciliation strategy for the Luvuvhu and Letaba water supply system: reconciliation strategy. Report No. P WMA 02/B810/00/1412/10

Department of Water Affairs and Forestry (DWAF). 2006. Letaba River System Annual Operating Analysis. DWAF Report No: WMA 02/000/00/0406.

Eamus, D, Zolfaghar, S, Villalobos-Vega, R, Cleverly, J and Huete, A. 2015. Groundwater-dependent ecosystems: recent insights from satellite and field-based studies. *Hydrol Earth Syst Sci* 19: 4229–4256.

Ehleringer, JR and Dawson, TE. 1992. Water uptake by plants: Perspectives from stable isotope composition. *Plant Cell Environ* 15(9): 1073–1082.

Elhaddad, A, and Garcia, L.A. 2008. Surface energy balance-based model for estimating evapotranspiration taking into account spatial variability in weather, *J. Irrig. Drain. Eng ASCE* 134(6): 681–689.

El-Hames, AS, and Richards, SK. 1998. An integrated, physically based model for arid region flash flood prediction capable of simulating dynamic transmission loss. *Hydrol Process* 12, 1219-1233.

Evaristo, J and McDonnell, JJ. 2017. Prevalence and magnitude of groundwater use by vegetation: a global stable isotope meta-analysis. *Scientific Reports* 7: 44110. http://dx.doi.org/10.1038/srep44110.

Everson, C. 1999. Quantifying open water resources. *WRC Report No.* 683/1/99, ISBN 1 86845 520 3.

Everson, CS, Burger, C, Olbrich, BW, Gush, M. 2001. Verification of estimates of Water use from riverine vegetation on the Sabie River in the Kruger National park. WRC Report No 877/1/01.

Falkenmark, M and Molden, D. 2008. Wake up to the realities of river basin closure. *Water Resour Dev* 24(2): 201–215.

February, EC, Higgins, SI, Netwon, R and West, AG. 2007. Tree distribution on a steep environmental gradient in an arid savanna. *Journal of Biogeography* 34: 270–278.

Feikema, PM, Morris, JD and Connell, LD. 2010. The water balance and water sources of a eucalyptus plantation over shallow saline groundwater. *Plant Soil* 332(1–2): 429–449.

Fernández-Prieto, D, van Oevelen, P, Su, Z and Wagner, W. 2012. Advances in Earth observation for water cycle science. *Hydrology and Earth System Science* 16: 543–549.

Ferreira, E, Mannaerts, CM, Dantas, AA and Maathius, BH. 2016. Surface Energy Balance System (SEBS) and satellite data for monitoring water consumption of irrigated sugarcane. 36(6): *Journal of the Brazilian Association of Agricultural Engineering* 1176-1185.Gat J. 2005. In Isotope Hydrology: A Study of the Water Cycle, Gat J (ed). Imperial College Press: 57 Shelton Street, Covent Garden, London.

Gheith, H and Sultan, M. 2002. Construction of a hydrology model for estimating wadi runoff and groundwater recharge in the Eastern Desert, Egypt. *Journal of Hydrology* 263: 36-55.

Gibson, LA, M¨unch, Z and Engelbrecht, J. 2011. Particular uncertainties encountered in using a pre-packaged SEBS model to derive evapotranspiration in a heterogeneous study area in South Africa. *Hydrol Earth Syst Sci* 15: 295–310.

Gibson, LA. 2013. The application of the Surface Energy Balance System model to estimate evapotranspiration in South Africa. Unpublished PhD Thesis, Department of Environmental and Geographical Science, Faculty of Science, University of Cape Town, South Africa.

Gentine, P, Entekhabi, D, Chehbouni, A, Boulet, G and Duchemin, B. 2007. Analysis of evaporative fraction diurnal behavior. *Agricultural and Forest Meteorology* 143: 13-19.

Gentine, P, Entekhabi, D and Polcher, J. 2011. The Diurnal Behavior of Evaporative Fraction in the Soil-Vegetation-Atmospheric Boundary Layer Continuum. *Journal of Hydrometeorology* 12:1530-1546.

Goedhart, CM and Pataki, DE. 2011. Ecosystem effects of groundwater depth in Owens Valley, California. *Ecohydrology* 4(3): 458–468.

Gokmen, M., Vekerdy, Z., Verhoef, A., Verhoef, W., Batelaan, O., Tol, C., 2012. Integration of soil moisture in SEBS for improving evapotranspiration estimation under water stress conditions. *Remote Sens Environ* 121: 261–274. DOI: 10.1016/j.rse.2012.02.003.

Gokool, S, Chetty, KT, Jewitt, GPW and Heeralal, A. 2016. Estimating total evaporation at the field scale using the SEBS model and data infilling procedures. *Water SA* 42(4): 673-683.

Gribovski, Z, Kalicz, P, Szilagyi, J and Kucsara, M. 2007. Riparian zone evapotranspiration estimation from diurnal groundwater level fluctuations. *Journal of Hydrology* 349: 6.

Gu, R and Deutschman, M. 2001. Hydrologic Assessment of Water Losses in River. *Journal of Water Resources Planning and Management* 127 (1): 6-12.

Hacker, F. 2005. Model for Water Availability in Semi-Arid Environments (WASA): Estimation of transmission losses by infiltration at rivers in the semi-arid Federal State of Ceara (Brazil). MSc Thesis, University of Potsdam, Germany.

Hankerson, B, Kjaersgaard, J and Hay, C. 2012. Estimation of Evapotranspiration from Fields with and without Cover Crops Using Remote Sensing and in situ Methods. *Remote Sensing* 4: 3796-3812. doi:10.3390/rs4123796.

Heath, RC. 1983. Basic ground-water hydrology. U.S. Geological Survey. *Water-Supply Paper* 2220, Washington, D.C.

Hervé-Fernández, P, Oyarzún, C, Brumbt, C, Huygens, D, Bodé, S, Verhoest, NEC and Boeckx, P. 2016. Assessing the 'two water worlds' hypothesis and water sources for native and exotic evergreen species in south-central Chile. *Hydrol Process* Published online in Wiley Online Library (wileyonlinelibrary.com) DOI: 10.1002/hyp.10984

Holland, KL, Tyerman, SD, Mensforth, LJ and Walker, GR. 2006. Tree water sources over shallow, saline groundwater in the lower River Murray, South-Eastern Australia: Implications for groundwater recharge mechanisms. *Aust J Bot* 54(2): 193–205.

Hong, S. Hendrickx. JMH and Borchers. B. 2011. Down-scaling of SEBAL derived evapotranspiration maps from MODIS (250 m) to Landsat (30 m) scales. International Journal of Remote Sensing 32(21): 6457–6477.

Huang, Y, Chen, X, Chen X and Ou, G. 2015. Transmission losses during two flood events in the Platte River, south-central Nebraska. *Journal of Hydrology* 520: 244–253.

Hughes, DA and Sami, K. 1992. Transmission losses to alluvium and associated moisture dynamics in a semi-arid ephemeral channel system in southern Africa. *Hydrological Processes* 6: 45-53.

Hughes, DA, Mallory, SJL and Louw D. 2008. Methods and software for the real-time implementation of the ecological reserve-explanations and user manual. *WRC Report 1582/1/08*.

Ivkovic, KM. 2009. A top-down approach to characterize aquifer-river interaction processes, *Journal of Hydrology* 365: 145–155.

Jana, C, Rawat, M, Sena, DR and Mishra, PK. 2016. Application of SEBAL model to estimate Evapotranspiration in Doon Valley, India. *Journal of Soil and Water Conservation* 44(2):191-197.

Jarmain, C, Bastiaansen, W, Mengistu, MG and Kongo, V. 2009. A Methodology for Near-Real Time Spatial Estimation of Evaporation. *WRC Report No. 1751/1/09*, ISBN 978-1-77005-725-8.

Jassas, H, Kanoua, W and Merkel, B. 2015. Actual evapotranspiration in the Al-Khazir Gomal Basin (Northern Iraq) using the Surface Energy Balance Algorithm for Land (SEBAL) and water balance. *Geosciences* 5: 141-159.

Kalma, JD, McVicar TR, and McCabe MF. 2008. Estimating Land Surface Evaporation: A Review of Methods Using Remotely Sensed Surface Temperature Data. Surveys in Geophysics 29(4-5): 421-469.

Kamble, B, Irmak, A, Hubbard, K and Gowda, P. 2013. Irrigation Scheduling Using Remote Sensing Data Assimilation Approach. *Advances in Remote Sensing* 2: 258-268.

Kendall, C and McDonnell, J. 1998. Isotope tracers in catchment hydrology. Elsevier, Oxford. United Kingdom.

Kiptala, JK, Mohamed, Y, Mul, ML and van der Zaag, P. 2013. Mapping evapotranspiration trends using MODIS and SEBAL model in a data scarce and heterogeneous landscape in Eastern Africa. *Water Resources Res*earch 49: 8495–8510. doi:10.1002/2013WR014240.

Kustas, WP and Daughtry, CST. 1989. Estimation of the soil heat flux/net radiation ratio from spectral data. *Agricultural Forest Meteorology* 49: 205–223.

Lane, LJ. 1990. Transmission losses, flood peaks and groundwater recharge. Hydraulics/hydrology of arid lands (H2AL): proceedings of the International Society of Civil Engineers, Hydraulics Division 1990.

Lange, J. 2005. Dynamics of transmission losses in a large arid stream channel. *Journal of Hydrology* 306: 112–126.

Lhomme, JP and Elguero, E. 1998. Examination of evaporative fraction diurnal behaviour using a soil-vegetation model coupled with a mixed-layer model. *Hydrology and Earth System Sciences* 3(2): 259- 270.

Li, F, Kustas, WP, Anderson, MC, Prueger, JH and Scott, R.L. 2008. Effect of remote sensing spatial resolution on interpreting tower-based flux observations. *Remote Sensing of the Environment* 112: 337–349.

Li, Z, Tang, R, Wan, Z, Bi, Y, Zhou, C, Tang, B, Yan, G and Zhang, X. 2009. A Review of Current Methodologies for Regional Evapotranspiration Estimation from Remotely Sensed Data. *Sensors* 9(5): 3801-3853.

Li, Y, Zhou, J, Wang, H, Li, D, Jin, R, Zhou, Y and Zhou, Q. 2015. Integrating soil moisture retrieved from L-band microwave radiation into an energy balance model to improve evapotranspiration estimation on the irrigated oases of arid regions in northwest China. *Agricultural and Forest Meteorology* 214-215: 306–318.

Lin, W. 2006. Satellite based regional scale evapotranspiration in the Hebei Plain, Northeastern China, Msc Thesis, International Institute for Geo-Information Science and Earth Observation, The Netherlands.

Lin, Z, Huili, Z, Xue, G, Yashu, QI and Xing, XU. 2016. Seasonal patterns in water uptake for *Medicago sativa* grown along an elevation gradient with shallow groundwater table in Yanchi county of Ningxia, Northwest China. *Journal of Arid Lands* 8(6): 921-934.

Liou, Y and Kar, SK. 2014. Evapotranspiration Estimation with Remote Sensing and Various Surface Energy Balance Algorithm: A Review. *Energies* 7: 2821-2849.

Lu, J, Li, Z, Tang, R, Tang, B, Wu, H, Yang, F, Labed, J and Zhou, G. 2013. Evaluating the SEBS-estimated evaporative fraction from MODIS data for a complex underlying surface. *Hydrological Processes* 27(22): 3139-3149.

Lubczynski MW and Gurwin J. 2005. Integration of various data sources for transient groundwater modeling with spatio-temporally variable fluxes: Sardon study case, Spain. *Journal of Hydrology* 306(1-4): 71-96.

Ma, W, Hafeez, M, Ishikawa, H and Ma, Y. 2012. Evaluation of SEBS for estimation of actual evapotranspiration using ASTER satellite data for irrigation areas of Australia. *Theoretical and Applied Climatology* 112(3-4).

Ma, W, Ma, Y and Ishikawa, H. 2014. Evaluation of the SEBS for upscaling the evapotranspiration based on in-situ observations over the Tibetan Plateau. *Atmospheric Research* 138: 91-97.

Ma, Y and Song, X. 2016. Using stable isotopes to determine seasonal variations in water uptake of summer maize under different fertilization treatments. *Science of the Total Environment* 550: 471–483.

Massman, WJ. 1997. An analytical one-dimensional model of momentum transfer by vegetation of arbitrary structure. *Bound-Lay Meteorology* 83: 407–421.

Matinfar, HR and Soorghali, M. 2014. Estimate evapotranspiration (ET) using SEBS Model based on Landsat 5 (TM) thermal data and GIS. *Indian Journal of Fundamental and Applied Life Sciences* 4 (3): 30-34.

McCabe, MF and Wood, EF. 2006. Scale influences on the remote estimation of evapotranspiration using multiple satellite sensors. *Remote Sensing of the Environ* 105: 271–285.

McKenzie, RS and Craig, AR. 2001. Evaluation of river losses from the Orange River using hydraulic modelling. *Journal of Hydrology* 241: 62–69.

McMahon, TA. 1979. Hydrological characteristics of arid zones. Symposium on the hydrology of areas of low precipitation, IAHS Publ. No 128. Proc. Canberra Symposium, Dec. 1979: 105-123.

Menenti, M. 1984. Physical aspects of and determination of evaporation in deserts applying remote sensing techniques. Report 10 (special issue), Institute for Land and Water Management Research (ICW), The Netherlands, 202pp.

Menenti, M and Choudhury, B. 1993. Parameterization of land surface evaporation by means of location dependent potential evaporation and surface temperature range. Proceedings of IAHS conference on Land Surface Processes. *IAHS Publ* 212: 561-568.

Mengistu, MG, Everson, CS, Moyo, NC and Savage, MJ. 2014. The validation of the variables (evaporation and soil moisture) in hydrometeorological models. *WRC Report No. 2066/1/13*, ISBN 978-1-4312-0514-1.

Mkhwanazi, MM and Chavez, JL. 2013. Mapping evapotranspiration with the remote sensing Et algorithms METRIC and SEBAL under advective and non-advective conditions: accuracy determination with weighing lysimeters. *Hydrology Days 2013.*

Mohammadian, M, Arfania, R and Sahour, H. 2017. Evaluation of SEBS Algorithm for Estimation of Daily Evapotranspiration Using Landsat-8 Dataset in a Semi-Arid Region of Central Iran. *Open Journal of Geology* 7: 335-347.

Molle, F, Wester, P and Hirsch, P. 2010. River basin closure: Processes, implications and responses. Agricultural Water Management 97: 569-577.

Monteith, JL. 1973. *Principles of environmental physics*. Edward Arnold Press. 241 pp.

Morin, E, Grodek, T, Dahan, O, Benito, G, Kulls, C, Jacoby, Y, Langenhove, GV, Seely, M and Enzel, Y. 2009. Flood routing and alluvial aquifer recharge along the ephemeral arid Kuiseb River, Namibia. *Journal of Hydrology* 368: 262–275.

Mucina, L and Rutherford, MC. 2006. The Vegetation of South Africa, Lesotho and Swaziland. *Strelitzia* 19. South African National Botanical Institute, Pretoria.

Nourhi, H, Beecham, S, Kazemi, F, Hassanli, AM and Anderson, S. 2013. Remote sensing techniques for predicting evapotranspiration from mixed vegetated surfaces. *HESS Discuss* 10: 3897–3925.

Orellana, F, Verma, P, Loheide II, SP and Daly, E. 2012. Monitoring and modeling water-vegetation interactions in groundwater-dependent ecosystems. *Reviews of Geophysics* 50 Paper number 2011RG000383.

Papadavid, G, Neocleous, D, Kountios, G, Markou, M, Michailidis, A, Ragkos, A and Hadjimitsis, D. 2017. *Journal of Imaging* 3(30). doi:10.3390/jimaging3030030.

Papadavid, G, Perdikou, S, Hadjmitsis, M and Hadjmitsis, D. 2012. Remote Sensing Applications for Planning Irrigation Management. The Use of SEBAL Methodology for Estimating Crop Evapotranspiration in Cyprus. *Environmental and Climate Technologies*. doi: 10.2478/v10145-012-0012-z.

Pardo, N., Sanchez, L.M., Timmermans, J., Su, Z., Perez, I.A., and Garcia, M.A., 2014. SEBS validation in a Spanish rotating crop. Agricultural and Forest Meteorology 195-196: 132-142.

Pittock, J and Lankford, BJ. 2010. Environmental water requirements: demand management in an era of water scarcity. *Journal of Integrative Environmental Sciences* 7(1): 75–93.

Pollard, S and du Toit D. 2011a. Towards Adaptive Integrated Water Resources Management in Southern Africa: The Role of Self-organisation and Multi-scale Feedbacks for Learning and Responsiveness in the Letaba and Crocodile Catchments. *Water resources management* 25 (15): 4019-4035.

Pollard, S and du Toit, D. 2011b. Towards the sustainability of freshwater systems in South Africa: An exploration of factors that enable and constrain meeting the ecological Reserve within the context of Integrated Water Resources Management in the catchments of the lowveld. *WRC Report No* K8/1711.

Qian, J, Zheng, H, Wang, P, Liao, X, Wang, C, Hou, J, Ao, Y, Shen, M, Liu, J and Li K. 2017. Assessing the ecohydrological separation hypothesis and seasonal variations in water use by *Ginkgo biloba* L. in a subtropical riparian area. *Journal of Hydrology* 553:486-500.

Renard, KG. 1970. The hydrology of semiarid rangeland watersheds. ARS 41-162, USDA, ARS, Washington, DC, 26 pp.

Riddell, E.S., Nel, J.M., Gokool, S., Jarmain, C., Raubenheimer, R., Strydom, T., Swemmer, A., 2017. Quantification of transmission losses along the Letaba River for improved delivery of environmental water requirements (ecological reserve). Water Research Commission Report, Project Number K5/2338.

Senay, GB, Budde, M, Verdin, JP and Melesse, AM. 2007. A coupled remote sensing and simplified surface energy balance approach to estimate actual evapotranspiration from irrigated fields. *Sensors* 7(6): 979–1000.

Seneviratne, SI, Corti, T., Davin, EL, Hirschi, M, Jaeger, EB, Lehner, I, Orlowsky, B and Teuling, AJ. 2010. Investigating soil moisture–climate interactions in achanging climate: a review. Earth Sci. Rev. 99, 125–161.

Shanafield, M and Cook, PG. 2014. Transmission losses, infiltration and groundwater recharge through ephemeral and intermittent streambeds: A review of applied methods. *Journal of Hydrology* 511: 518–529.

Sharma KD and Murthy JSR. 1994. Estimating transmission losses in an arid region. *Journal of Arid Environments* 26: 209-219.

Sharp, AL and Saxton KE. 1962. Transmission losses in natural streamflow valleys. *Journal of Hydraulic Division ASCE 88*(HY5): 121-142.

Shoko, C, Dube, T, Sibanda, M and Adelabu, S. 2014. Applying the Surface Energy Balance System (SEBS) remote sensing model to estimate spatial variations in evapotranspiration in Southern Zimbabwe. Transactions of the Roya Society of South Africa 70(1).

Smakhtin, V, Revenga, C and Döll, P. 2004. Taking into Account Environmental Water Requirements in Global-scale Water Resources Assessments. *Comprehensive Assessment Research Report 2*. Colombo, Sri Lanka: Comprehensive Assessment Secretariat.

Smakhtin, VY. 2001. Estimating continuous monthly baseflow time series and their possible applications in the context of the ecological reserve. *Water SA* 27: 213-217.

Snyder, KA and Williams, DG. 2000. Water sources used by riparian trees varies among stream types on the San Pedro River, Arizona. *Agricultural Forest Meteorology* 105(1–3): 227–240.

Spiliotopolous, M, Adaktylou, N, Loukas, A, Michalopoulou, H, Mylopoulos, N and Toulios, L. 2013. A spatial downscaling procedure of MODIS derived actual evapotranspiration using Landsat images at central Greece. Proceedings of SPIE - The International Society for Optical Engineering - August 2013. DOI: 10.1117/12.2027536.Abdelrady, A, Timmermans, J, Vekerdy, Z and Salama, MS. 2016. Surface Energy Balance of Fresh and Saline Waters: AquaSEBS. *Remote Sensing* 8(583). doi:10.3390/rs8070583.

Spiliotopoulos, M, Holden, NM and Loukas, A. 2017. Mapping Evapotranspiration Coefficients in a Temperate Maritime Climate Using the METRIC Model and Landsat TM. *Water* 9(23). doi:10.3390/w9010023.

Su, Z., Pelgrum, H. and Menenti, M. (1999). Aggregation effects of surface heterogeneity in land surface processes. *Hydrology Earth System Sci*ence 3(4): 549-563.

Su, Z and Jacobs, C. 2001. Advanced Earth Observation– Land Surface Climate. *Report USP-2, 01-02*, Publications of the National Remote Sensing Board (BCRS). 184pp.

Su, Z. 2002. The Surface Balance Energy System (SEBS) for estimating turbulent heat fluxes. *Hydrology and Earth System Sciences*, 6(1): 85-99.

Sun, Z, Wei, B, Su, W, Shen, W, Wang, C, You, D and Liu, Z. 2011. Evapotranspiration estimation based on the SEBAL model in the Nansi Lake Wetland of China. *Mathematical and Computer Modelling* 54(3-4): 1086-1092.

Stewart, JB. 1996. Extrapolation of evaporation at time of satellite overpass to daily totals, In: J.B. Stewart *et al.* (editors) *Scaling up in Hydrology using Remote Sensing*. Wiley, Chichester, UK.

Swirepik, JL, Burns, IP, Dyre, FJ, Neave, IA, O'Brien, MG, Pryde, GM and Thompson, RM. 2015. Establishing environmental water requirements for the Murray–Darling basin, Australia's largest developed river system. *River Research and Applications*. DOI: 10.1002/rra.2975.

Szporak-Wasilewska, S, Szatyłowicz, J, Okruszko, T and Stefan Ignar. 2013. Application of the Surface Energy Balance System Model (SEBS) for mapping evapotranspiration of extensively used river valley with wetland vegetation. Towards Horizon 2020, 33rd EARSeL Symposium, At Matera, Italy.

Tanner, JL and Hughes, DA. 2015a. Understanding and modelling surface water-groundwater interactions. WRC Report No. 2056/2/14. ISBN 978-1-4312-0630-8.

Tanner, JL and Hughes, DA. 2015b. Surface water–groundwater interactions in catchment scale water resources assessments: Understanding and hypothesis testing with a hydrological model. *Hydrological Sciences Journal* 60 (11). http://dx.doi.org/10.1080/02626667.2015.1052453

Teixera, DCA and Bastiaansen, WGM. 2012. Five methods to interpret field measurements of energy fluxes over a micro-sprinkler irrigated mango orchard. *Irrig Sci* 30(1): 13–28.

Timmermans, WJ and Meijerink AMJ. 1999. Remotely sensed actual evapotranspiration: Implications for groundwater management in Botswana. *International Journal of Applied Earth Observation and Geoinformation* 1: 222–233.

The National Water Act (NWA). 1998. Act No. 36 of 1998. Republic of South Africa. *Government Gazette No. 19182.* Government Printers. Pretoria.

Trezza, R, Allen, RG and Tasumi, M. 2013. Estimation of Actual Evapotranspiration along the Middle Rio Grande of New Mexico Using MODIS and Landsat Imagery with the METRIC Model. *Remote Sensing* 5: 5397-5423. doi:10.3390/rs5105397.

Van der Kwast, J, Timmermans, W, Gieske, A, Su, Z, Olioso, A, Jia, L, Elbers, J, Karssenberg, D and de Jong, S. 2009. Evaluation of the Surface Energy Balance System (SEBS) applied to Aster imagery with flux-measurements at the SPARC 2004 site (Barrax, Spain). *Hydrology and Earth System Sciences* 13(7): 1337-1347.

Van Dijk, AI and Renzullo, LJ. 2011. Water resource monitoring systems and the role of satellite observations. *Hydrology and Earth System Science* 15: 39–55.

Venot, JP, Turral, H, Samad, M and Molle, F. 2007. *Shifting waterscapes: Explaining basin closure in the Lower Krishna Basin, South India*. Colombo, Sri Lanka: International Water Management Institute. IWMI Research Report 121.

Villeneuve, S, Cook, PG, Shanafield, M, Wood, C and White, N. 2015. Groundwater recharge via infiltration through an ephemeral riverbed, central Australia. *Journal of Arid Environments* 117: 47-58.

Walters, MO 1990. Transmission losses in arid regions. *Journal of Hydraulic Engineering ASCE* 116:129-38.

Wester, P, Scott, CA and Burton, M. 2005. *Irrigation and River Basin Management*, Chapter 8, 119-138.

White, WC, Cook, ER, Lawrence, JR and Broecker, WS. 1985. The D/H ratios of sap in trees: Implications for water sources and tree ring D/H ratios. *Geochimica et Cosmochimica Acta* 49: 237–246.

Winter, TC, Harvey, JW, Frank, OL and Alley, WM. 1998. Groundwater and surface water a single resource. *U.S. Geological Survey Circular 1139*.

Wu, X, Zhou, J, Wang, H, Li, Y and Zhong, B. 2014. Evaluation of irrigation water use efficiency using remote sensing in the middle reach of the Heihe river, in the semi-arid Northwestern China. *Hydrol Process* (2014) DOI: 10.1002/hyp.10365.

Yang, H, Luo, P, Wang, J, Mou, C, Mo, L, Wang, Z, Fu, Y, Lin, H, Yang, Y and Bhatta, LD. 2015. Ecosystem Evapotranspiration as a Response to Climate and Vegetation Coverage Changes in Northwest Yunnan, China. *PLoS ONE* 10(8): e0134795. https://doi.org/10.1371/journal.pone.0134795.

Yang, Q, Xiao, H, Zhao, L, Zhou, M, Li, C and Cao, S. 2010. Stable isotope techniques in plant water sources: A review. *Sci. Cold Arid Reg* 2(2): 112–122.

Zencich, SJ, Froend, RH, Turner, JV and Gailitis, V. 2002. Influence of groundwater depth on the seasonal sources of water accessed by banksia tree species on a shallow, sandy coastal aquifer. *Oecologia* 131(1): 8–19.

Zhuo, G, Ba, L, Ciren, P and Bu, L. 2014. Study on daily surface evapotranspiration with SEBS in Tibet Autonomous Region. *Journal of Geographical Sciences* 24(1): 113-128.

*****

Lead into chapter 2: While the use of SEO data provides an opportunity to acquire spatially explicit hydrological process information, the trade-off between the spatial and temporal resolution of available imagery and the ability of the associated models to accurately estimate fluxes and ET in different environmental settings, may restrict the feasibility of using SEO data for operational water resources management. The objective of chapter 2 was to evaluate an appropriate satellite-based ET model and the requisite SEO data sets, through comparisons against *in-situ* measurements of ET. This was done to identify potential limitations to possible solutions for improving the mapping of ET within the study area. Supplementary information and/or data which was used during the various analyses undertaken in this chapter but not presented herein, are provided in Appendix A.

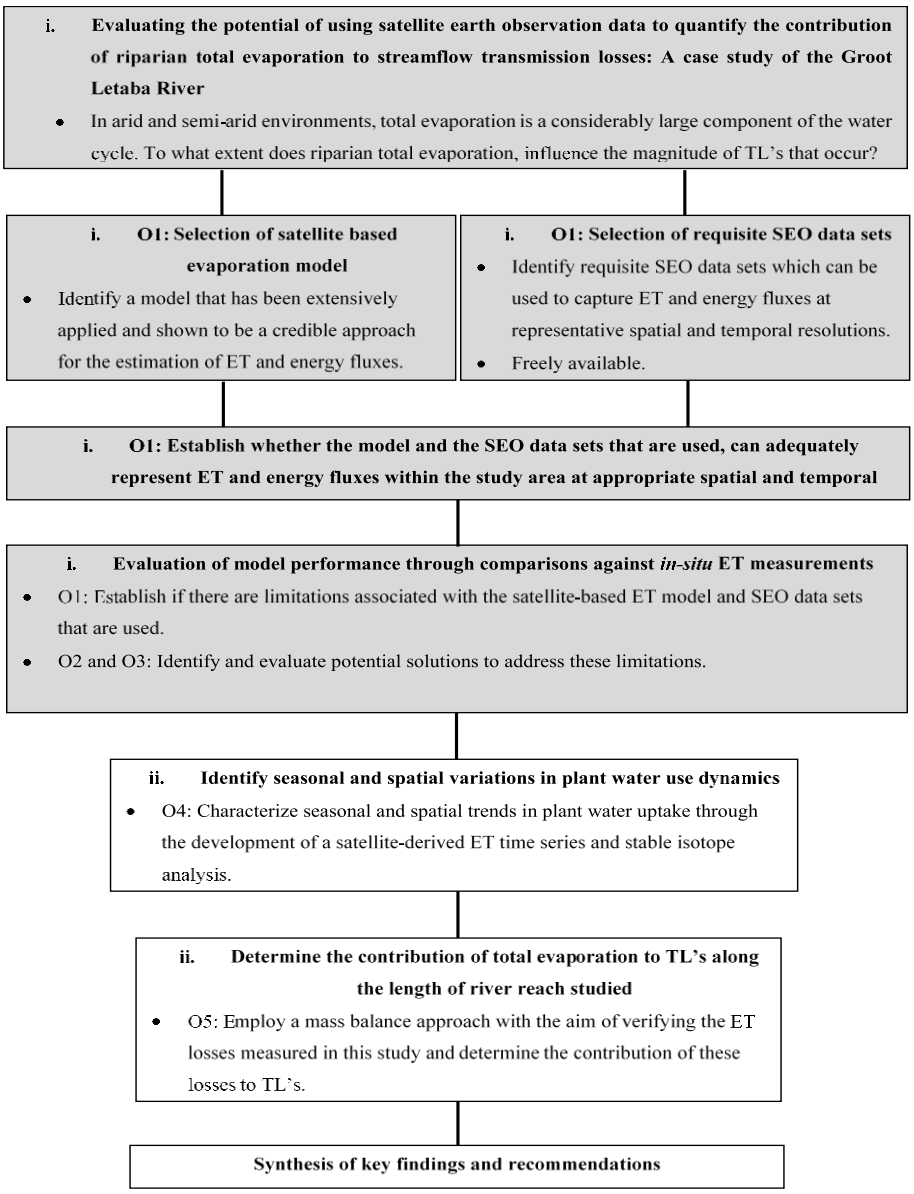

2. QUANTIFYING RIPARIAN TOTAL EVAPORATION ALONG THE GROOT LETABA RIVER: A COMPARISON BETWEEN INFILLED AND SPATIALLY DOWNSCALED SATELLITE DERIVED TOTAL EVAPORATION ESTIMATES[1]

S Gokool[a], C Jarmain[b], E Riddell[a&c], A Swemmer[d], R Lerm Jr[d] and KT Chetty[a]

[a]Centre for Water Resources Research, University of KwaZulu-Natal, Pietermaritzburg, South Africa
[b]Independent Researcher, University of Stellenbosch, Stellenbosch, South Africa
[c]Conservation Management, South African National Parks, Skukuza, South Africa
[d]South African Environmental Observation Network (SAEON), Ndlovu Node, Phalaborwa, South Africa

Corresponding Author: Shaeden Gokool, shaedengokool@gmail.com, University of KwaZulu-Natal, Pietermaritzburg, South Africa, 3201

ABSTRACT

The use of satellite earth observation data for the estimation of evapotranspiration has been well documented and represents a viable approach for the quantification of riparian water use at landscape to regional scales. However, the trade-off between the spatial and temporal resolution associated with imagery can limit the reliability of satellite-based evapotranspiration modelling. This study investigated two approaches to quantify evapotranspiration at a moderate spatial resolution (30 m) on a daily time step, for a perennial river flowing through a semi-arid, savanna landscape. The Surface Energy Balance System (SEBS) Model was used to derive daily evapotranspiration from satellite imagery.

1S Gokool, C Jarmain, ES Riddell, A Swemmer, R Lerm and KT Chetty. 2017. Quantifying riparian total evaporation along the Groot Letaba river: A comparison between infilled and spatially downscaled satellite derived total evaporation estimates. *Journal of Arid Environments In Press*, http://dx.doi.org/10.1016/j.jaridenv.2017.07.014 0140-1963/© 2017.

* Referencing conforms to format of *Journal of Arid Environments.*

*It should be noted that minor variations in the text may exist between the published version of the manuscript and the version presented herein, due to recommendations put forward by the examiners of the thesis.

The actual crop coefficient (Kc_{act}) and output downscaling with linear regression (ODLR) approaches were then evaluated by comparing their respective estimates against Eddy covariance (EC_{ET}) measurements at two locations. Comparisons of ET estimates acquired using the Kc_{act} and ODLR approaches against EC_{ET}, yielded RMSE values of; 1.88 and 2.57 mm d^{-1} and 1.10 and 2.39 mm d^{-1} (for two replicate transects), respectively. The poor performance of these techniques was largely attributed to the SEBS ET estimates used as inputs to these techniques, as SEBS may overestimate evapotranspiration during conditions of water stress.

Keywords: Total evaporation; Satellite imagery; SEBS; Infilling; Downscaling

2.1 Introduction

Riparian vegetation plays a significant role in the interaction between surface water and ground water systems, by reducing the recharge of aquifers, as a result of water uptake and/or alteration of the flow path of precipitation to the water table in recharge zones (LeMaitre et al., 1999).While, the significance of riparian vegetation water use has been acknowledged, there remains a paucity of research on the water use requirements of riparian species in South Africa (Le Maitre et al., 1999; Schachtshneider, 2010). According to Hughes (2008), one such area which necessitates the need for our current knowledge to be expanded upon, is the relationship between streamflow transmission losses (TL) and riparian evapotranspiration (ET).

Numerous studies have been published regarding the estimation of TL's for different environmental settings and have successfully demonstrated the effects of several factors which influence the TL process (Cataldo et al., 2010). However, the influence of riparian ET on TL has rarely been included or sufficiently represented in these estimation procedures (Hacker, 2005; Martinet et al., 2009; Cataldo et al., 2010; Shanafield and Cook, 2014).

Previous research has shown that, riparian ET can significantly influence the water balance of alluvial aquifers and its effects may be further accentuated in river systems flowing through arid and semi-arid regions (Everson, 2001; McKenzie, 2001; Smakhtin, 2001; Tanner, 2013 and Shanafield and Cook, 2014). Therefore, it is essential to develop techniques or approaches which can be used to accurately quantify riparian ET, to better understand and quantify how this process influences the rapport between subsurface water storage processes, streamflow and TL.

Conventional ET estimation approaches, have been extensively applied and proven to be invaluable in furthering our understanding of the role which ET plays in various environmental processes (Jarmain et al. 2009b). However, these techniques are only able to provide point or line averaged estimates of ET, which are representative of localised conditions only and cannot be easily extended to provide estimates of ET over larger areas (Lu et al., 2013; Liou and Kar, 2014; Zhuo et al., 2014; Jassas et al., 2015).

Furthermore, gauging and monitoring in arid and semi-arid environments remains fairly limited due to lower populations, remote location of hydrological gauging stations and financial constraints (Lange et al., 2005, Costa et al., 2013). Consequently, this has hindered the ability for expansive hydrological research to be undertaken (Lange et al., 2005). In such situations, the use of satellite earth-observation (SEO) data represents the most suitable and efficient alternative to obtain spatial hydrological process information.

The use of SEO data enables representative information to be captured for large geographic scales, as well as data scarce regions, at near real time. Moreover, the periodic updating of information, allows for invaluable time series compilations of data (van Dijk and Renzullo, 2011; Fernández-Prieto et al., 2012; Xu et al., 2014). However, one of the major challenges facing ET modelling using SEO data, is the trade-off between the spatial and temporal resolution associated with imagery (Singh et al., 2014b). Coarse spatial resolution (CSR) imagery, such as MODIS Level 1 B Geotiff imagery (250 m, 500 m and 1 km), are ideally suited for the routine monitoring and estimation of ET due to their high temporal resolution (HTR) (available daily) (Hong et al., 2011; Ha et al., 2013).

However, it is often the case that CSR pixel sizes generally exceed the size of the area under observation. Consequently, CSR imagery may prove to be inadequate in providing useful information for field scale hydrological applications (Spiliotopolous et al., 2013; Singh et al. 2014b; Bhattarai et al., 2015). Conversely, moderate spatial resolution (MSR) imagery, such as Landsat Level 1 Geotiff imagery (30 m), are ideally suited for the estimation of ET at the field scale to local levels (Anderson et al. 2012; Ha et al. 2013). However, their limited temporal resolution (available every 16 days) may prove to be inadequate for the operational monitoring of ET (Singh et al., 2014b).

The continuous advancement in SEO technologies and capabilities has seen an increase in the demand for MSR ET products for field and catchment scale applications (Bhattarai et al. 2015). Consequently, recent studies *inter alia* by Hong et al. (2011) and Spiliotopolous et al. (2013) have attempted to overcome the spatial and temporal scaling issues associated with satellite imagery, through the application of relatively simplistic downscaling procedures, in order to facilitate the quantification of ET at both a MSR and HTR.

While the findings of Hong et al. (2011) and Spiliotopolous et al. (2013) highlight the potential of these procedures to facilitate the estimation of ET at both a MSR and HTR, Bhattarai (2015) notes that these procedures have not yet been applied to obtain seasonal continuous MSR ET estimates. Consequently, the suitability of applying such approaches to generate daily ET at a MSR remains relatively unknown.

The objective of this paper was to address this knowledge gap through the evaluation of; relatively simplistic satellite-based approaches used to quantify ET at a MSR on a daily time step, within the riparian zone along a portion of the Groot Letaba River. Two techniques, a simple output downscaling with linear regression (ODLR) procedure and an infilling approach, were evaluated. The performance of these techniques was assessed, by comparing their respective ET estimates against (i) modelled ET estimates derived from Landsat Level 1 Geotiff imagery and (ii) measured ET obtained from a one-sensor Eddy Covariance system (EC_{ET}).

2.2 Materials and methodology

2.2.1 Study site and data sets

The study area is situated along a portion of the Groot Letaba River, located in the Letaba catchment in north-eastern South Africa, as depicted in Figure 2.1. The Groot Letaba River frequently experiences water shortages and curtailments (Pollard and du Toit, 2011a). Consequently, the system has a high incidence of non-compliance with environmental flow requirements (Pollard and du Toit, 2011a). This is particularly concerning, as the river flows through various conservation areas, most notably the Kruger National Park. The acquisition of accurate hydrological process information is therefore crucial for water resources managers in this region, to maintain the natural functioning of this environment.

The catchment experiences a semi-arid climate and receives seasonal rainfall, with majority of the rainfall occurring in the summer months (October to March) (Katambara and Ndiritu, 2010; Pollard and du Toit, 2011a). According to Katambara and Ndiritu (2010) approximately 40 to 50% of the rainfall generally occurs during January and February. The mean annual precipitation and the mean annual potential evaporation (as measured by A-pan) are approximately 417.5 mm and 2097.93 mm, respectively (Schulze et al., 2008). Mean annual temperatures range from 18 ^{0}C in the mountainous regions to 28 ^{0}C in the eastern regions. The elevation of the riparian zone within the study area is approximately 332 m above mean sea level.

Heritage et al. (2001) state that approximately three quarters of the catchment is underlain by gneiss and granite. The varied distribution of sediment along the Letaba River has given rise to a variety of morphological units, which has resulted in the formation of various channel types, each displaying a particular morphology and vegetative nature. The river system within the study area is largely dominated by alluvial channel types (Heritage et al., 2001).

The study site is characterized by savanna vegetation with *Phragmites mauritianus*, *Ficus sycomorus* (Fig), *Philenoptera violacea* (Apple leaf) and *Diospyros mespiliformis* (Jackalberry) predominantly found within and along the riparian zone. Additionally, numerous agricultural fields, predominantly planted with *Cucurbita moschata* (Butternut) and *Medicago sativa* (Lucerne) are situated adjacent to the riparian zone.

A one sensor eddy covariance (EC) system (excludes Infrared Gas Analyzer) was installed within a portion of the Groot Letaba River channel and was used to determine the latent heat flux as a residual of the shortened energy balance equation, which is given as:

$$R_n = G_o + H + \lambda E \quad (2.1)$$

Where Rn is net radiation (W m^{-2}), G_0 is soil heat flux (W m^{-2}), H is sensible heat flux (W m^{-2}) and λE is the latent heat flux (W m^{-2}). The EC system was installed at two separate locations along the Groot Letaba River between Letaba Ranch (23.658^0 S; 31.047^0 E) and Mahale weirs (23.669^0 S; 30.991^0 E) during the drier low flow periods of the study (May to October). The EC system was first installed within the river channel (Figure 2.2) within the vicinity of an irrigated farm and measurements were acquired from the 17th June to 13th August 2015.

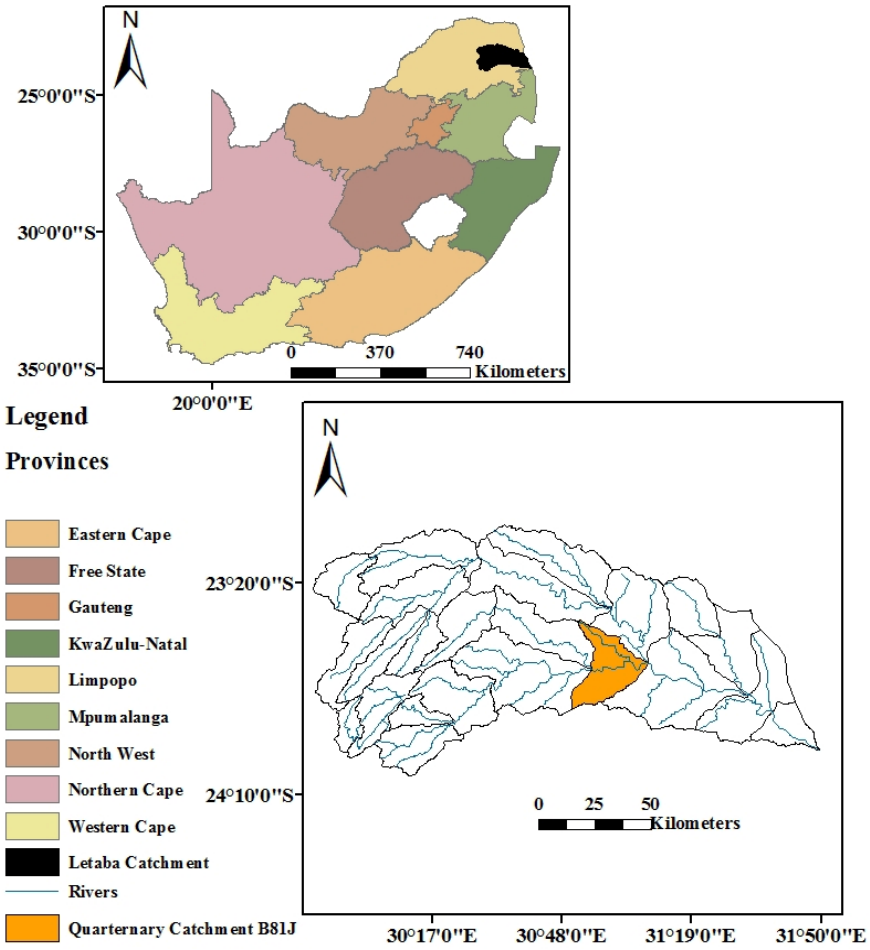

Figure 2.1 Location of the study area within the quaternary B81J (Schulze et al., 2008), situated in the Letaba Catchment, South Africa

The system was then moved to a pristine protected area (transect 2) approximately 1.2 km further downstream within the river channel and measurements were acquired from the 21st August to 22nd October 2015. The width of the riparian corridor studied at each of these locations is approximately 60 m (only inclusive of river channel width). As the channel morphology, does not change within this 1.2 km reach the EC_{ET} estimates at these locations were representative of the morphological reach.

The EC system, was equipped with a CSAT 3-D sonic anemometer that measures the sonic air temperature, wind speed and direction. The anemometer was connected to a CR3000 datalogger and measurements were taken with a sampling frequency of 10 Hz. The averages of these high frequency measurements (from instantaneous data) were then used to compute a half-hourly sensible heat flux (Riddell et al., 2017).

The sonic anemometer was installed at a placement height of 2.0 m above the soil surface and approximately 1.0 m above the average vegetation (*Phragmites mauritianus*) height within the river channel.

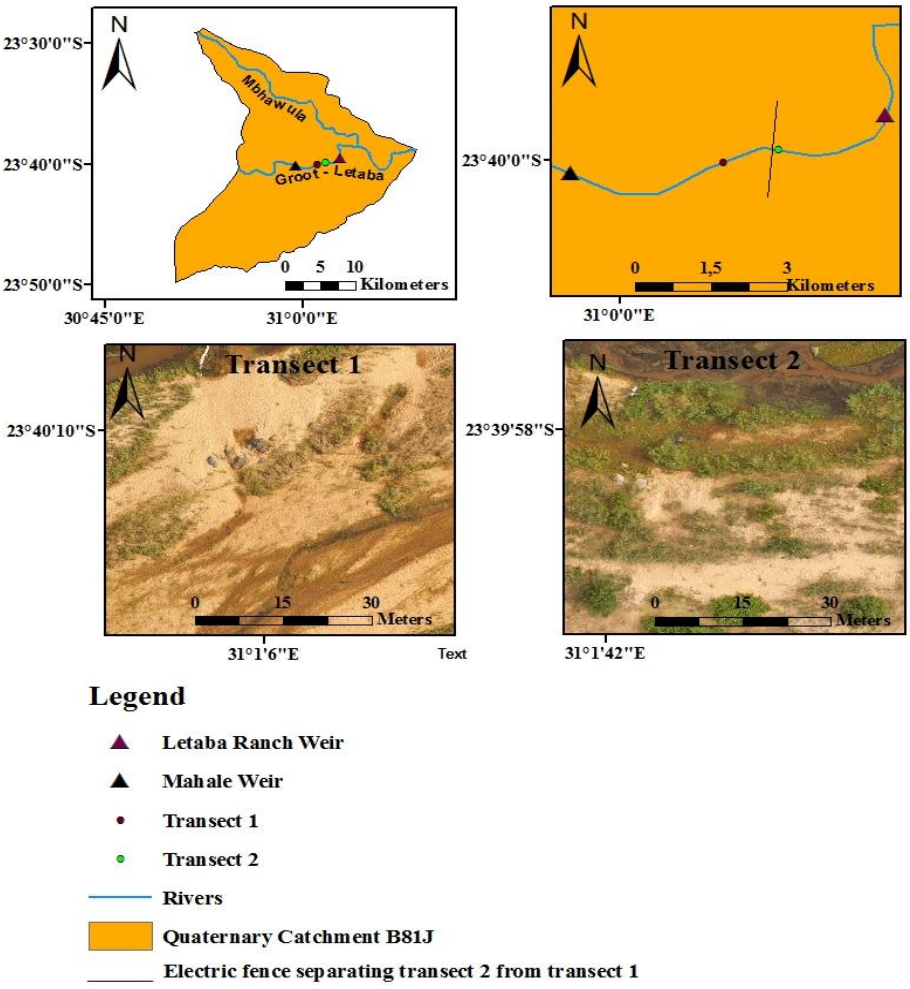

Figure 2.2 Location of the EC system and the general land cover distribution for transects 1 and 2

Meteorological instrumentation and energy balance sensors were used to provide measurements of; net radiation, a computed soil heat flux density, soil temperature, relative humidity, horizontal wind speed and wind direction, solar radiation, air temperature and rainfall. Observations were made every 10 seconds and the appropriate statistical outputs were stored on a data logger (CR23 X, Campbell Scientific Inc., Logan, UT, USA) at 10-minute intervals.

These values were then used to compute the daily estimates. The instrumentation consisted of; two Kipp and Zonen NR Lite-2 net radiometers installed at approximately 1.0 m above the bare soil surface and vegetation, respectively, in order to provide representative and integrated estimates of *Rn* above these surfaces, Licor LI200X Pyranometer, RM Young wind sentry, HMP60 temperature and relative humidity sensor and a Texas Tipping bucket raingauge (0.1 mm), six HFP01 HukseFlux soil heat flux plates (installed approximately 0.08 m below the soil surface), three pairs of soil temperature averaging probes (installed at 0.02 and 0.06 m below the surface) and two CS616 soil water reflectometers (approximately 0.08 m below the soil surface). The soil heat flux was determined as the weighted average of the computed soil heat flux for bare soil, vegetation and open water heat flux (Riddell et al., 2017).

EC_{ET} values were estimated by weighting the contribution of the components of the energy balance, according to the percentage coverage of landcover classes across the area in which the system was situated. The average net radiation measured over bare soil and vegetation and the weighted soil heat flux density were used as inputs to Equation 2.1. The soil heat flux density was weighted according to the percentage composition of the dominant landcover classes present in this riparian environment, which are *P. mauritianus*, bare soils and open water. Table 2.1 provides an approximation of the percentage cover for each of the aforementioned classes within each of the transects, with the value for *P. mauritianus* representing the percentage of basal cover.

Table 2.1 Percentage cover of the dominant landcover classes within each of the sites in which the EC system was situated

Land Cover class	**Transect 1**	**Transect 2**
P. mauritianus	40 %	60 %
Bare Soils	40 %	20 %
Open Water	20 %	20 %

The percentage contributions shown in Table 1 were determined from a visual assessment of the study site through a field survey and using imagery captured from a DJI Phantom 3 Advanced Unmanned Aerial Vehicle (UAV). These images were captured at a 5 cm resolution, by an on-board 12 megapixel DJI camera at an altitude of 120 m above ground level. An orthophoto was then created using the Open Drone Map Software (https://github.com/OpenDroneMap/OpenDroneMap).

A sensitivity analysis was performed to assess, the influence which the weighting of the soil heat flux density may have on the EC_{ET}. For the sensitivity analysis, the weighting of the contributions for bare soil, as well as vegetation were incrementally increased and decreased respectively. While the contribution of the open water heat flux density was kept constant, as there was no difference in the percentage area of open water between transects 1 and 2. The results of the sensitivity analysis indicated that changes in the weighting of the contributions for bare soil and vegetation did not significantly impact the EC_{ET}.

The rationale for moving the EC system from transect 1 to transect 2, was to capture the ET associated with distinctive land cover compositions and environmental conditions in a riparian environment. From Table 2.1, it can be seen that there is a higher percentage of basal cover for *P. mauritianus* at transect 2. Livestock (cattle) are allowed to graze within the river channel at transect 1, whereas transect 2 is situated within a pristine protected area where livestock are prevented from grazing. Although buffalo and elephant graze this region their densities are significantly lower than the cattle.

Consequently, both the percentage of basal cover and canopy cover associated with *P. mauritianus* were different at both these locations. Changes in environmental conditions during the period of measurement, such as seasonal and climatic changes from winter to summer which influence environmental stress conditions may have also contributed to the higher percentage of basal cover at location 2.

Furthermore, the timing of this study coincided with a large El Nino induced drought period (Kogan and Guo, 2016). While the measuring tower was installed within a riparian environment, it should be noted that soil water availability is quite variable along the portion of river that was studied and has been further exacerbated by the drought. Therefore, while the two locations are situated within the same morphological reach, their respective evaporative surfaces are different in both their basal and canopy cover, as well as soil moisture status.

EC_{ET} measurements taken during the period 17th June to 22nd October 2015, were used to validate ET estimates derived from SEO data. Thirteen Clear sky Landsat (7 and 8) Level 1 Geotiff products (16-day temporal resolution), as well as 114 MODIS Level 1 B Terra images (Daily temporal resolution) for the corresponding period, were selected to estimate ET using the SEBS Model. The pre-processing of images was conducted, using the Integrated Land and Water Information System (ILWIS) and the MODIS Swath Tool.

The procedures outlined in Su and Wang (2013), Singh et al. (2014a) and USGS (2015), were used to derive the necessary land surface parameters required as inputs to SEBS for the estimation of ET.

2.2.2 The Simplified Surface Energy Balance System (SEBS)

The SEBS Model was selected for application in this study, as it has been extensively applied for the estimation of regional fluxes and ET and has been shown, to provide accurate estimates of ET and terrestrial heat fluxes (Jarmain et al., 2009a; Yang et al., 2010; Zhuo et al., 2014). Whilst the conceptualization of SEBS is discussed in Su (2002), the principle is that SEBS estimates atmospheric turbulent fluxes using both SEO and spatially representative meteorological data (Su, 2002).

The model consists of a suite of tools to estimate; land surface physical parameters from spectral reflectance and radiance (Su et al., 1999), a comprehensive model for the approximation of the roughness length of heat transfer (Su et al., 2001) and an innovative procedure for the estimation of the evaporative fraction (*EF*) on the basis of the energy balance at limiting cases (Su, 2002). The model applies Equation 2.1 to partition the available energy into sensible (*H*) and latent heat flux density (*LE*). The daily ET is estimated, assuming the *EF* remains constant throughout the day (Su, 2002).

SEBS was therefore applied in this study, using SEO data acquired from open access imagery derived from Landsat (7&8) and MODIS, to estimate ET for the riparian zone along the Letaba River. The spatial resolution of the SEBS ET estimate is dependent on the spatial resolution of the thermal band (Su, 2002; Alidoost et al., 2015) and therefore the study was limited to the spatial resolution of these open access products.

MSR imagery acquired by Landsat (7&8) provides thermal bands at a spatial resolution of 60m and 100 m, respectively, which are resampled to 30 m and possess a temporal resolution of 16-days (USGS, 2015), however; data can be obtained with an 8-day gap between consecutive data acquisitions, if data from both Landsat 7 and 8 is available and used (USGS, 2015). CSR imagery acquired by MODIS provides thermal bands at a spatial resolution of 1 km at a daily temporal resolution.

In order to, obtain a complete daily MSR ET record for the riparian zone along the Letaba River for the study period; a combination of two approaches were followed: (a) the ODLR approach (Hong et al., 2011) and (b) an infilling approach using an actual crop coefficient (Kc_{act}) (Santos et al., 2008).

2.2.3 Spatial Downscaling of Satellite Derived ET

Bierkens et al. (2000) and Liang (2004) define downscaling as the increase in spatial resolution resulting from the disaggregation of the original dataset. Downscaling procedures attempt to restore spatial variations at a particular scale, by assuming the values at the larger scale represent the average of the values at the smaller scale (Bierkens et al. 2000). The procedure results in an increase of the number of pixels within an image, with the output of each pixel representing a smaller area (Hong et al. 2011).

According to Ha et al. (2013) and Spiliotopolous et al. (2013) downscaling procedures can be broadly classified into two categories; (i) scale based traditional downscaling and (ii) pan sharpening or data fusion techniques. In this study, a relatively simplistic ODLR approach (Hong et al., 2011) was tested, as it has been shown by Hong et al. (2011) and Spiliotopolous et al. (2013) to produce credible results.

The aforementioned approach disaggregates CSR imagery, by applying a linear regression between two CSR images to a preceding or subsequent MSR image covering the same area of interest (Hong et al., 2011). The technique is predicated on the assumption that the linear relationship between CSR imagery remains valid between MSR imagery (Hong et al., 2011). In order, to create a daily MSR ET dataset for the period of investigation in this study, a linear regression was initially applied between two consecutive MODIS ET estimates (*M1* and *M2*) generated using SEBS, to obtain regression coefficients. These coefficients were then applied to the Landsat ET image (*L1*) generated using SEBS for the same date as the first MODIS ET image (*M1*), in order to generate an ET image (*L2*) at the Landsat spatial resolution, for the same date as the subsequent MODIS ET image (*M2*).

This procedure was repeated, however; the linear regression was then performed between the MODIS ET image for day one (*M1*) and the MODIS ET image for day three (*M3*) to obtain regression coefficients. These coefficients were then applied to the Landsat ET image (*L1*) obtained for the same date as the first MODIS ET image (*M1*), in order to generate an ET image (L3) at the Landsat spatial resolution, for the same date as the subsequent MODIS ET image (*M3*).

This procedure was systematically repeated, until a new Landsat Level 1 Geotiff product was available. Once this product was available, the abovementioned procedure was repeated. Figures 2.3 and 2.4 provide a schematic representation of the abovementioned process to better understand how the daily continuous MSR ET dataset was generated and an example of a downscaled ET map generated for this study, respectively.

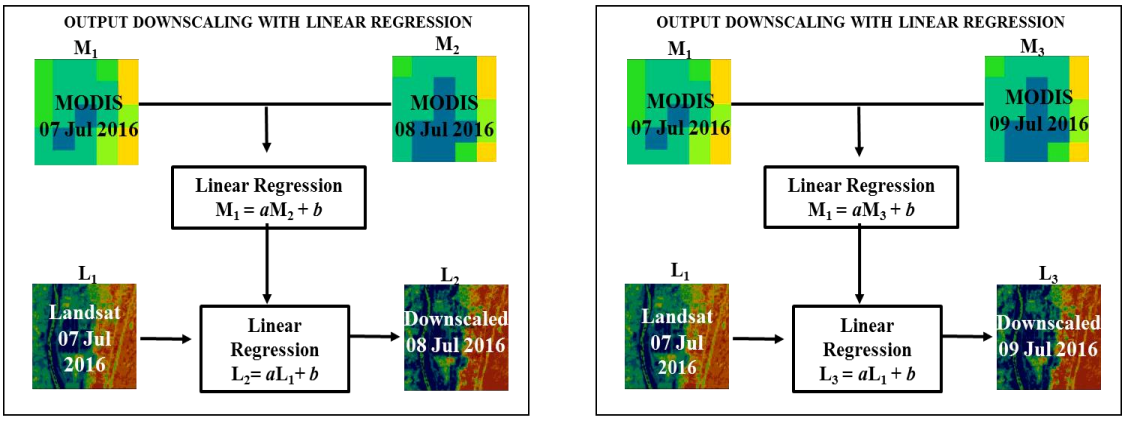

Figure 2.3 Schematic of the output downscaling with linear regression methodology, where *a* and *b* are the linear regression coefficients and *L2* and *L3* are the subsequent spatially downscaled ET maps at the Landsat resolution (adapted from Hong et al., 2011)

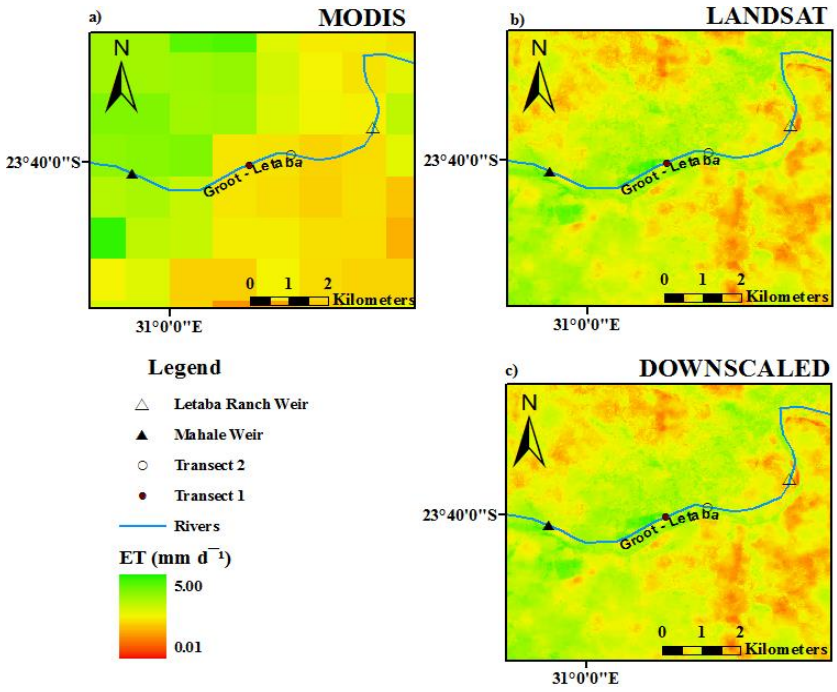

Figure 2.4 An illustration of SEBS ET at varying spatial resolutions for the 24th August 2015; a) MODIS (1 km), b) Landsat (30 m) and c) Downscaled (30 m)

2.2.4 The Kc_{act} infilling approach

The Kc_{act} approach discussed in Santos et al. (2008), was applied to generate a daily MSR ET time series. The actual ET and reference evaporation required for the application of this technique were acquired, respectively, from SEBS ET estimates derived using Landsat and FAO Penman-Monteith reference evaporation derived from meteorological data collected for the study area. The calculation of Kc_{act} is given as:

$$Kc_{act} = \frac{ET_a}{ET_{ref}} \quad (2.2)$$

Where Kc_{act} can be defined as the actual crop coefficient which accounts for the effects of environmental stress (Allen et al., 2005), ET_a is the ET (mm d^{-1}) and ET_{ref} is the grass reference evaporation determined using the FAO Penman-Monteith reference evaporation approach (mm d^{-1}). The advantage of utilising the Kc_{act} approach is that; (i) it is relatively simplistic to apply with fairly short processing times and (ii) ET estimates extending from only one satellite earth observation data set is required. The successful application of the Kc_{act} approach is predicated on the assumption that the conditions which are used to derive Kc_{act} remain the same for the period in which it is applied. Furthermore, spatially representative meteorological data is required for the determination of ET_{ref}, in order to estimate spatially representative ET_a.

Thirteen useable Landsat (7&8) Level 1 Geotiff products were available during the study period. These values were then used to develop a Kc_{act} curve as shown in Figure 2.5. An exponential curve was generated, to interpolate values between images so that the temporal progression of Kc_{act} can be accounted for (Santos et al., 2008). The Kc_{act} values were used in conjunction with ET_{ref} to estimate the SEBS ET at Landsat resolution for the study period.

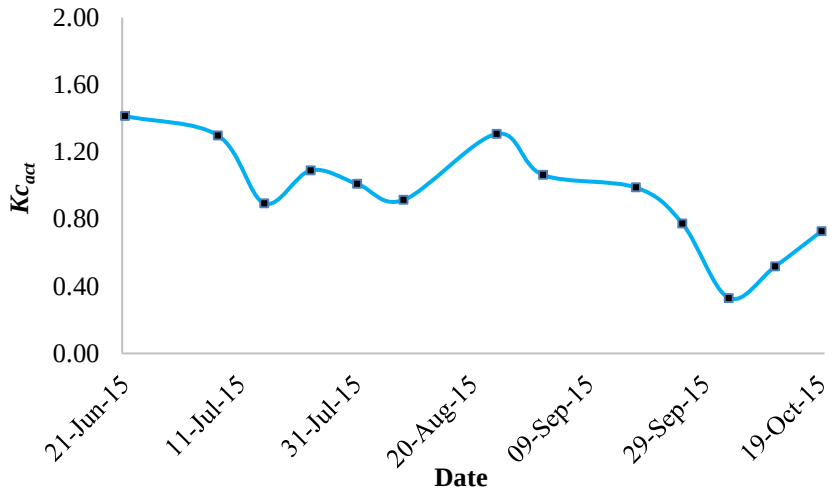

Figure 2.5 Kc_{act} curve generated for the study area using SEBS estimates of ET, derived from Landsat imagery. The black dots represent the Kc_{act} values calculated from the thirteen available Landsat images, which were then used to quantify the temporal progression of Kc_{act}

The downscaled ET estimates and the ET estimated using the Kc_{act} approach were compared to the original SEBS ET estimates derived using Landsat (7 and 8), as well as against the EC_{ET}. The satellite pixel/s located in close proximity to the EC system was selected as areas of interest and only the data within these pixels were used for data comparisons.

2.3 Results

2.3.1 A comparison of SEBS ET derived using Landsat against infilled ET and downscaled ET

Descriptive statistics of the comparisons between the Kc_{act} and downscaled ET against the original SEBS ET derived using Landsat are presented in Table 2.2. The relative volume error (RVE) indicates that on average the Kc_{act} approach over-estimated ET by approximately 3% compared to the original SEBS ET. The Mean Absolute Difference (MAD) and RMSE values are 0.68 and 0.69 mm d^{-1}, respectively. While, the results of the ANOVA test at the 95% confidence level, indicate that there is no significant difference between the Kc_{act} ET and the original SEBS ET derived using Landsat.

The RVE indicates that on average the ODLR approach under-estimated ET by approximately 5% compared to the original SEBS ET. The MAD and RMSE values are 1.21 and 1.41 mm d^{-1}, respectively. While, the results of the ANOVA test at the 95% confidence level, indicate that the differences between the downscaled ET and the original SEBS ET derived using Landsat are not significant. The original SEBS ET estimates derived using Landsat, the Kc_{act} ET estimates and the downscaled ET estimates were accumulated for the 13 days in which useable Landsat Level 1 Geotiff imagery was available and are illustrated in Figure 2.6. Both the Kc_{act} and the downscaled ET estimates appear to follow the cumulative trend of the original SEBS ET estimates derived using Landsat.

Table 2.2 A comparison of SEBS ET estimates derived using Landsat, Kc_{act} ET and downscaled ET for the 13 days in which useable Landsat Level 1 Geotiff imagery was available

	Original SEBS ET derived using Landsat (7 and 8) (mm)	Kc_{act} ET(mm)	Downscaled ET (mm)
Total	39.30	37.73	35.23
Daily Average	3.02	2.90	2.71
Median	3.32	2.90	2.37
Variance	0.61	0.03	2.06
Std Dev	0.80	0.19	1.39
RVE		-2.56	5.36
MAD		0.68	1.21
RMSE		0.69	1.41
ANOVA (p value)		0.55	0.45
Pearson correlation		0.48	0.27

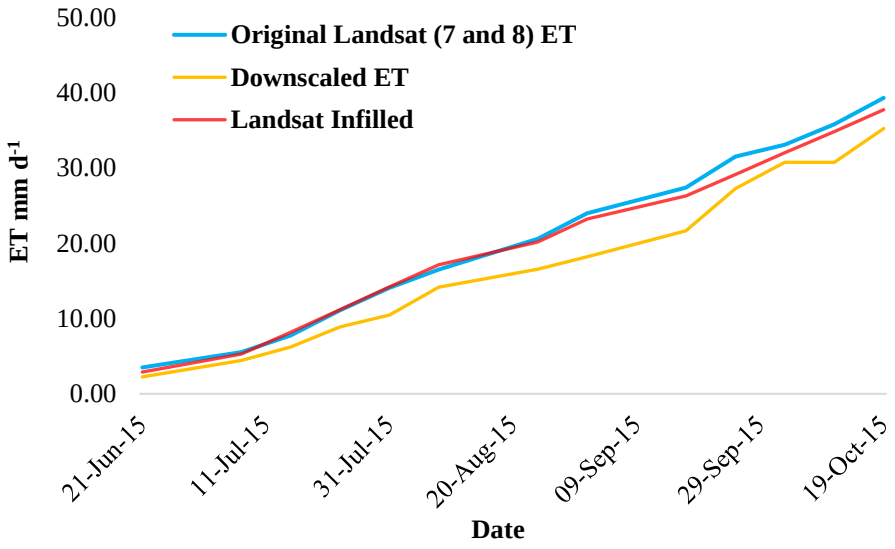

Figure 2.6 Comparison of accumulated SEBS ET estimates derived using Landsat, Kc_{act} ET and downscaled ET

2.3.2 A comparison of satellite derived ET against ET measured *in-situ* for the period 17th June to 22nd October 2015

The Kc_{act} and the ODLR approach was used to derive daily ET estimates during the period 17th June to 22nd October 2015. These estimates were then compared to the EC_{ET}. SEBS ET estimates derived using MODIS and Landsat imagery, which were required as inputs to the abovementioned techniques are illustrated in Figure 2.7. A statistical comparison between the original SEBS ET derived using MODIS and Landsat imagery, against the EC_{ET} for the days in which clear sky imagery was available, is provided in Table 2.3.

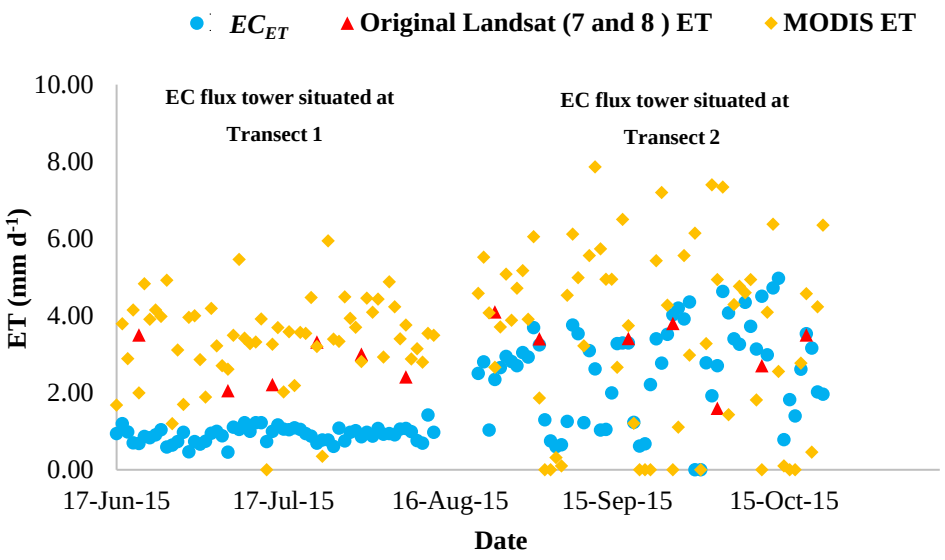

Figure 2.7 A comparison of SEBS ET derived using Landsat and MODIS imagery against EC_{ET} for the period 17th June to 22nd October

Table 2.3 Comparison of SEBS ET estimates derived using Landsat and MODIS against EC_{ET}

	EC_{ET} (mm)	SEBS Landsat ET(mm)		EC_{ET} (mm)	SEBS MODIS ET(mm)
Total	28.40	29.30	**Total**	217.72	418.74
Daily Average	2.18	3.02	**Daily Average**	1.80	3.67
Median	2.34	3.32	**Median**	1.08	3.75
Variance	2.09	0.61	**Variance**	1.57	2.89
Std Dev	1.45	0.80	**Std Dev**	1.25	1.70
ANOVA (p value)		0.05	**ANOVA (p value)**		0.00
Pearson correlation		0.32	**Pearson correlation**		0.30

Statistical comparisons between the Kc_{act} and downscaled ET estimates against the EC_{ET} for transects 1 and 2 are presented in Tables 2.4 and 2.5, respectively. In general, the comparisons between the satellite derived ET estimates and the measured EC_{ET} was fairly poor, as illustrated in Figure 2.8. The comparisons between Kc_{act} ET against the EC_{ET} were in better agreement for transect 2 as compared to transect 1. The MAD and RMSE values for transect 1 were 1.82 and 1.88 mm d^{-1}, respectively. While, the MAD and RMSE values for transect 2 were 0.89 and 1.10 mm d^{-1}, respectively.

Overall, the comparison between the downscaled ET and the EC_{ET} was fairly poor, as illustrated in Figure 2.8. The MAD and RMSE values for transect 1 were 2.33 and 2.57 mm d^{-1}, respectively. While, the MAD and RMSE values for transect 2 were 1.87 and 2.39 mm d^{-1}, respectively.

Table 2.4 A comparison of EC_{ET}, Kc_{act} ET and downscaled ET for the period 17th June to 13th August 2015 (Transect 1)

	EC ET (mm)	Kc_{act} ET(mm)	Downscaled ET (mm)
Total	52.92	151.08	183.96
Average	0.91	2.80	3.23
Median	0.94	2.89	3.44
Variance	0.04	0.14	1.43
Std Dev	0.20	0.37	1.20
RVE		-199.74	-260.40
MAD		1.82	2.33
RMSE		1.88	2.57
ANOVA (p-value)		0.00	0.00
Pearson correlation		0.14	0.19

Table 2.5 Comparison of EC_{ET}, Kc_{act} ET and downscaled ET for the period 21st August to 22nd October 2015 (Transect 2)

	EC ET (mm)	Kc_{act} ET(mm)	Downscaled ET (mm)
Total	164.80	177.78	229.57
Average	2.62	2.82	3.64
Median	2.02	2.95	3.80
Variance	0.45	0.01	2.15
Std Dev	0.67	0.10	1.47
RVE		-29.43	-94.88
MAD		0.89	1.87
RMSE		1.10	2.39
ANOVA (p-value)		0.14	0.00
Pearson correlation		0.50	0.36

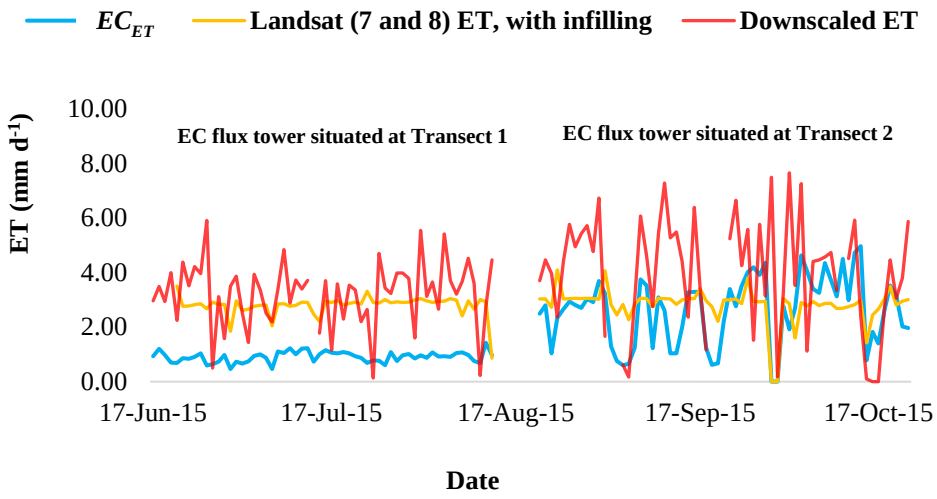

Figure 2.8 A comparison of EC_{ET}, Kc_{act} ET and the downscaled ET for the period 17th June to 22nd October 2015

2.4 Discussion

The Kc_{act} and ODLR provided credible approaches for the estimation of ET at a MSR. Both techniques were able to produce estimates which were of similar magnitude to the original SEBS ET derived using Landsat. The results of this investigation further support the proposed application of these techniques for the estimation of daily ET at a MSR. While statistical comparisons of the downscaled ET estimates and the original SEBS ET estimates, derived using Landsat, showed no significant differences, there were noticeable differences in the spatial distribution of ET (Figure 2.4). This can be attributed to the spatial characteristics of the Landsat image used as an input for the downscaling procedure. According to Hong et al. (2011) the overall spatial distribution of ET in the downscaled image should resemble the original SEBS ET map derived using Landsat.

The comparisons between ET estimates acquired from the application of the Kc_{act} and ODLR approaches against EC_{ET} were generally found to be poor. The poor performance of these techniques can be attributed to the original SEBS ET estimates derived using Landsat and MODIS imagery. SEBS does not explicitly account for the influence of soil moisture and biophysical parameters during the derivation of surface fluxes, instead their influence is implicitly encompassed in input variables, ignoring their direct impact on ET estimates (Gokmen et al., 2012; Pardo et al., 2014; Huang et al., 2015).

While this assumption may hold true for environments in which the available energy is the limiting factor for ET, SEBS may overestimate the *EF* and *LE* for environments in which the availability of water is the limiting factor for ET (Huang et al., 2015). This in turn may result in the over estimation of ET. As both the Kc_{act} and the downscaled ET estimates were generated from the original SEBS ET estimates, it can therefore be expected that uncertainties associated with these estimates, will be introduced to the downscaled/infilled ET.

It has been shown that the Kc_{act} and downscaled ET estimates are generally higher than the EC_{ET}. However, the results presented in Figure 2.8 as well as in Tables 2.4 and 2.5, indicate that the discrepancies between the satellite derived ET estimates and the EC_{ET} were higher for transect 1. The apportionment of the net radiation to the soil heat flux is noticeably higher for transect 1 compared to transect 2, as illustrated in Figure 2.9.

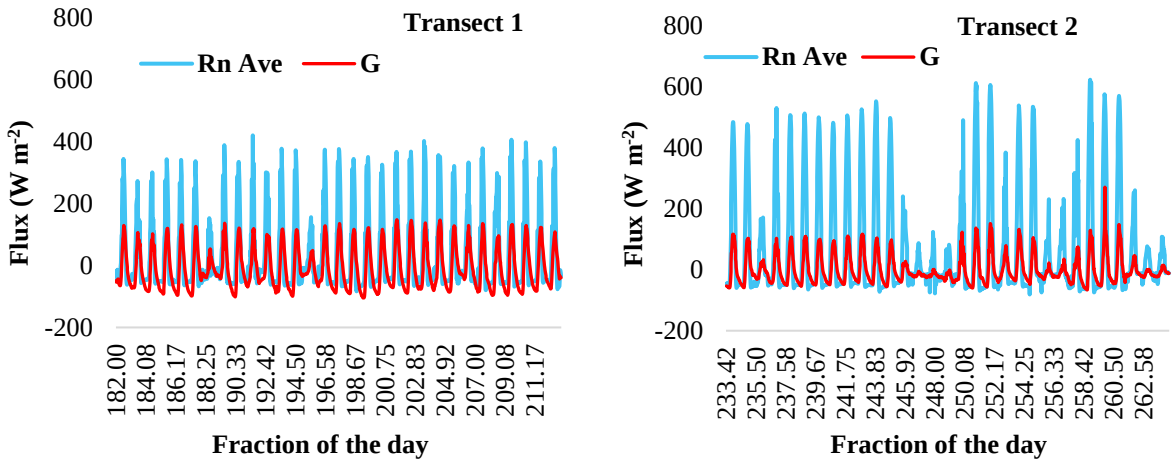

Figure 2.9 An illustration of the apportionment of net radiation to the soil heat flux for transects 1 and 2, where fraction of the day on the x-axis represents a combination of the Julian day and time

The proportion of bare soil in each transect significantly influences the energy available for sensible and latent heat transfer (Huang et al., 2015). Transect 1 possesses a greater bare soil fraction compared to transect 2, as illustrated in Figure 2.9. Furthermore, the soil's in transect 1 are relatively drier (Riddell et al., 2017). Consequently, the associated soil heat flux density measured at transect 1 was higher (Sauer and Horton, 2005).

As there was a greater apportionment of net radiation to the soil heat flux for transect 1, the energy available for sensible and latent heat transfer was lower, hence the lower EC_{ET} measured at transect 1. While Huang et al. (2015) acknowledges that SEBS may overestimate ET for water limited environments, Gokmen et al. (2012) and Pardo et al. (2014) note that the overestimation of *EF* and *LE* in SEBS may be markedly higher when the soil is dry and lacks vegetation coverage. Consequently, the general degree of over-estimation associated with the comparisons between the satellite derived ET estimates and the EC_{ET}, was further exacerbated for the period in which the EC_{ET} measurements were taken at transect 1.

The results obtained for comparisons between the Kc_{act} ET estimates and EC_{ET} are noticeably different, with the Kc_{act} ET estimates showing fairly limited variability. While, the limited variability in the Kc_{act} ET estimates may be due to relatively stable conditions experienced during each of the investigation periods, the poor correlations between the Kc_{act} ET estimates and EC_{ET} can be largely attributed to the original SEBS ET derived using Landsat. As shown in Figure 2.8 Kc_{act} ET estimates were in better agreement with the EC_{ET} for transect 2 as compared to transect 1. Hence, the Kc_{act} ET estimates and EC_{ET} were generally found to be in better agreement for transect 2. The successful application of the Kc_{act} approach is contingent to the settings in which the Kc_{act} values were derived, remaining stable for the period in which it is applied.

For transect 1 this assumption was generally not upheld. The original SEBS ET derived using Landsat was generally higher than the ET_{ref} for this period. However, for the thirteen selected days in which K_{Cact} values were derived for the study, the original SEBS ET estimates derived using Landsat were generally lower than the ET_{ref}. Consequently, the values obtained from the Kc_{act} curves, which were used to generate daily MSR ET for transect 1, were not representative of the conditions for the period in which it was applied.

For transect 2, the abovementioned assumption for which the successful application of the Kc_{act} approach is predicated upon, was upheld. The original SEBS ET derived using Landsat was generally lower than the ET_{ref} for this period. Consequently, the values acquired from the Kc_{act} curves, which were used to generate daily MSR ET for transect 2, were representative of the conditions for the period in which it was applied. Consequently, the Kc_{act} ET estimates were found to be in better agreement with the EC_{ET} for this period, although these estimates are still substantially higher than the observed values.

The results obtained for comparisons between the downscaled ET estimates and EC_{ET} are noticeably different. The original SEBS ET derived using MODIS was in better agreement with the EC_{ET} for transect 2 as compared to transect 1, as shown in Figure 2.8. Hence, the downscaled ET estimates and EC_{ET} were generally found to be in better agreement for transect 2.

Although the downscaling approach performed better for transect 2, the technique generally performed poorly for the period of study. This poor performance can be largely attributed to the original SEBS ET estimates derived using MODIS. As the spatial resolution of MODIS is 1 km, there is potentially a greater contribution of other land covers being encompassed within the ET estimate. The downscaled ET estimate is dependent on the regression and slope of the two SEBS ET images derived using MODIS (Hong *et al*. 2011). Consequently, the downscaled ET estimate is largely influenced by the ET captured at the MODIS spatial resolution.

Furthermore, the ET contribution of riparian vegetation and irrigated agriculture situated outside the footprint of the EC system, which are captured within the original SEBS ET derived using MODIS, may have also further exacerbated the degree of overestimation for the downscaling approach at transect 1. Hong et al. (2011) acknowledges that while the ODLR approach may provide credible estimates of ET for riparian and desert environments which experience less dynamic changes in their climates and plant phenology, he technique may prove to be inadequate for regions experiencing dynamic temporal changes over a short period, such as irrigated agricultural fields (Hong et al., 2011).

2.5 Conclusion

Both the Kc_{act} infilling and ODLR approaches were found to perform well, as these approaches were able to produce ET estimates, which were consistent with the original SEBS ET estimate derived using Landsat. The results presented in this investigation indicated that, these methods could be applied to estimate the ET at a MSR for the riparian zone. The comparison between the ET estimates acquired from the abovementioned techniques against daily EC_{ET} measurements were less than satisfactory. Both techniques were shown to perform poorly when compared to the daily EC_{ET}. This poor correlation was largely attributed to the inability of SEBS to explicitly account for the influence of soil moisture and biophysical parameters during the derivation of surface fluxes. Consequently, SEBS may overestimate the *EF* and *LE* for environments experiencing water stress, which in turn results in an overestimation of ET.

Recent studies have highlighted potential solutions to address this limitation. While the testing and validation of these procedures could not be undertaken during the duration of this study, it is highly recommended that future investigations should attempt to incorporate these procedures when applying the SEBS model in conjunction with downscaling/infilling procedures in semi-arid and arid environments. This may facilitate more meaningful comparisons to be drawn between the techniques used to estimate daily ET at a MSR and *in-situ* ET measurements.

Furthering our knowledge in this regard, provides a prospective opportunity to broaden our existing knowledge base and exploit the potential of using satellite EO data to better understand and quantify the temporal progression of ET at a MSR. The coupling of existing knowledge with data captured by practical alternatives, such as those presented in this study assist in improving our understanding of hydrological processes, which in turn can facilitate improved water resources management for arid and semi-arid environments.

Acknowledgements

The research presented in this paper emanates from a Water Research Commission (WRC) project entitled: Quantification of transmission losses along the Letaba River for improved delivery of environmental water requirements (ecological reserve), WRC Project No K5/2338. The authors would like to extend their gratitude to the WRC and the South African Environmental Observation Network (SAEON) for the funding required to successfully complete this research. We would also like to extend our appreciation to the anonymous reviewers for their invaluable comments on the previous version of this manuscript.

REFERENCES

Alidoost, F., Sharifi, M.A., Stein, A., 2015. Region and pixel-based image fusion for disaggregation of actual evapotranspiration. International Journal of Image and Data Fusion. DOI: 10.1080/19479832.2015.1055834.

Allen, R.G., Pereira, L.S., Smith, M., Raes, D., Wright, J.L., 2005. FAO-56 dual crop coefficient method for estimating evaporation form soil and application extensions. Journal of Irrigation and Drainage Engineering ASCE 131(1) 2–13.

Anderson, M.C., Allen, R.G., Morse, A., Kustas, W.P., 2012. Use of Landsat Thermal Imagery in Monitoring Evapotranspiration and Managing Water Resources. Remote Sensing of Environment 122: 50–65.

Bhattarai, N., Quackenbush, L.J., Dougherty, M., Marzen, L.J., 2015. A simple Landsat–MODIS fusion approach for monitoring seasonal evapotranspiration at 30 m spatial resolution. International Journal of Remote Sensing 36(1): 115-143.

Bierkens, M.F.P., Finke, P.A., Willigen, D.E., 2000. Upscaling and Downscaling Methods for Environmental Research. Dordrecht: Wageningen University and Research Centre. Kluwer Academic.

Cataldo, J., Behr, C., Montalto, F., Pierce, R.J., 2010. Prediction of Transmission Losses in Ephemeral Streams. Western U.S.A. The Open Hydrology Journal 4: 19-34.

Costa, A.C., Foerster, S., de Araujo, J.C., Bronstert, A., 2013. Analysis of channel transmission losses in a dryland river reach in north-eastern Brazil using streamflow series, groundwater level series and multi-temporal satellite data. Hydrological Processes 27: 1046–1060.

Elhaddad, A., and Garcia, L.A., 2008. Surface energy balance-based model for estimating evapotranspiration taking into account spatial variability in weather. J. Irrig. Drain. Eng ASCE 134(6): 681–689.

Everson C.S., 2001. The water balance of a first order catchment in the montane grasslands of South Africa. Journal of Hydrology 241: 110-123.

Fernández-Prieto, D., van Oevelen, P., Su, Z., Wagner, W., 2012. Advances in Earth observation for water cycle science. Hydrology and Earth System Science 16: 543–549.

Gokmen, M., Vekerdy, Z., Verhoef, A., Verhoef, W., Batelaan, O., Tol, C., 2012. Integration of soil moisture in SEBS for improving evapotranspiration estimation under water stress conditions. Remote Sens Environ 121: 261–274. DOI: 10.1016/j.rse.2012.02.003

Ha, W., Gowda, P.H., Howell, T.A., 2013. A review of downscaling methods for remote sensing-based irrigation management: Part I. Irrigation Science 31: 831–850.

Hacker, F., 2005. Model for Water Availability in Semi-Arid Environments (WASA): Estimation of transmission losses by infiltration at rivers in the semi-arid Federal State of Ceara (Brazil). MSc Thesis, University of Potsdam, Germany.

Heritage, G.L., Moon, B.P., Large, ARG., 2001. The February 2000 floods on the Letaba River, South Africa: an examination of magnitude and frequency. Koedoe 44 (2): 1-6.

Hong, S., Hendrickx, J.M.H., Borchers. B., 2011. Down-scaling of SEBAL derived evapotranspiration maps from MODIS (250 m) to Landsat (30 m) scales. International Journal of Remote Sensing 32(21): 6457–6477.

Hueng, C., Li, Y., Gu, J., Lu, J., Li, X., 2015. Improving Estimation of Evapotranspiration under Water-Limited Conditions Based on SEBS and MODIS Data in Arid Regions. Remote Sens 7:16795–16814. DOI:10.3390/rs71215854.

Hughes, D.A., 2008. Modelling semi-arid and arid hydrology and water resources the Southern African experience. gwadi.org/sites/gwadi.org/files/hughes_L5.pdfand#8206; Hughes. DA. Mallory. SJL and Louw D. 2008. Methods and software for the real-time implementation of the ecological reserve-explanations and user manual. WRC Report 1582/1/08.

Jarmain, C., Everson, C.S., Savage, M.J., Mengistu, M.G., Clulow, A.D., Walker, S., Gush, M.B., 2009a. Refining tools for evaporation monitoring in support of water resources management. WRC Report No 1567/1/08. ISBN 978-1-77005-798-2.

Jarmain, C., Bastiaansen, W., Mengistu, M.G., Kongo, V., 2009b. A Methodology for Near-Real Time Spatial Estimation of Evaporation. WRC Report No. 1751/1/09. ISBN 978-1-77005-725-8.

Jassas, H., Kanoua, W., Merkel., B., 2015. Actual evapotranspiration in the Al-Khazir Gomal Basin (Northern Iraq) using the Surface Energy Balance Algorithm for Land (SEBAL) and water balance. Geosciences 5: 141-159.

Katambara, Z., and Ndiritu, J.G., 2010. A hybrid conceptual-fuzzy inference streamflow modelling for the Letaba River system in South Africa. Physics and Chemistry of the Earth 35(13-14): 582-595.

Kogan, F., and Guo W., 2016. Strong 2015–2016 El Niño and implication to global ecosystems from space data. International Journal of Remote Sensing 38(1): 161-178.

Lange, J., 2005. Dynamics of transmission losses in a large arid stream channel. Journal of Hydrology 306: 112–126.

LeMaitre, D.C., Scott, D.F., Colvin C., 1999. A review of information on interactions between vegetation and groundwater. Water SA 25(2).

Liang, S., 2004. Quantitative Remote Sensing of Land Surfaces. New York: JohnWiley and Sons.

Liou, Y., and Kar, S.K., 2014. Evapotranspiration Estimation with Remote Sensing and Various Surface Energy Balance Algorithm: A Review. Energies 7: 2821-2849.

Lu, J., Li, Z., Tang, R., Tang, B., Wu, H., Yang, F., Labed, J., Zhou, G., 2013. Evaluating the SEBS-estimated evaporative fraction from MODIS data for a complex underlying surface. Hydrological Processes 27(22): 3139-3149.

McKenzie, R.S., and Craig. A.R., 2001. Evaluation of river losses from the Orange River using hydraulic modelling. Journal of Hydrology 241: 62–69.

Martinet, M.C., Vivoni, E.R., Cleverly, J.R., Thibault, J.R., Schuetz, J.F., and Dahm, C.N., 2009. On Groundwater Fluctuations, Evapotranspiration and Understory Removal in Riparian Corridors. *Water Resources Research* 45: W05425, doi:10.1029/2008WR007152.

Pardo, N., Sanchez, L.M., Timmermans, J., Su, Z., Perez, I.A., and Garcia, M.A., 2014. SEBS validation in a Spanish rotating crop. Agricultural and Forest Meteorology 195-196: 132-142.

Pollard, S., and du Toit, D., 2011b. Towards the sustainability of freshwater systems in South Africa: An exploration of factors that enable and constrain meeting the ecological Reserve within the context of Integrated Water Resources Management in the catchments of the lowveld. WRC Report No K8/1711.

Riddell, E.S., Nel, J.M., Gokool, S., Jarmain, C., Raubenheimer, R., Strydom, T., Swemmer, A., 2017. Quantification of transmission losses along the Letaba River for improved delivery of environmental water requirements (ecological reserve). Water Research Commission Report, Project Number K5/2338.

Santos, C., Lorite, I.J., Tasumi, M., Allen, R.G., Fereres, E., 2008. Integrating satellite-based evapotranspiration with simulation models for irrigation management at the scheme level. *Irrigation Science* 26(3): 277-288.

Sauer, J.T., and Horton, R., 2005. Soil Heat Flux. *Micrometeorology in Agricultural Systems Agronomy Monograph* 47: 131-154.

Schulze, R.E., 2008. Electronic version of the South African atlas of climatology and agrohydrology. South African Atlas of Climatology and Agrohydrology. RE Schulze. Water Research Commission, Pretoria, South Africa, WRC Report 1489/1/06, Section 1.1.

Shanafield, M., and Cook, P.G., 2014. Transmission losses. infiltration and groundwater recharge through ephemeral and intermittent streambeds: A review of applied methods. Journal of Hydrology 511: 518–529.

Singh, R.K., Senay, G.B., Velpuri, N.M., Bohms, S., Scott, R.L., and Verdin, J.P., 2014a. Actual Evapotranspiration (Water Use) Assessment of the Colorado River Basin at the Landsat Resolution Using the Operational Simplified Surface Energy Balance Model. Remote Sensing 6: 233-256.

Singh, R.K., Senay, G.B., Velpuri, N.M., Bohms, S., and Verdin, J.P., 2014b. On the Downscaling of Actual Evapotranspiration Maps Based on Combination of MODIS and Landsat-Based Actual Evapotranspiration Estimates. Remote Sensing 6: 10483-10509.

Smakhtin, V., Revenga, C., and Döll, P., 2004. Taking into Account Environmental Water Requirements in Global-scale Water Resources Assessments. *Comprehensive Assessment Research Report 2*. Colombo, Sri Lanka: Comprehensive Assessment Secretariat

Spiliotopolous, M.., Adaktylou, N, Loukas, A., Michalopoulou, H., Mylopoulos, N., and Toulios, L., 2013. A spatial downscaling procedure of MODIS derived actual evapotranspiration using Landsat images at central Greece. Proceedings of SPIE - The International Society for Optical Engineering - August 2013. DOI: 10.1117/12.2027536.

Su, Z., Pelgrum, H., and Menenti, M., (1999). Aggregation effects of surface heterogeneity in land surface processes. Hydrology Earth System Science 3(4): 549-563.

Su, Z., Schmugge, T., Kustas, W.P., Massman, W.J., 2001. An evaluation of two models for estimation of the roughness height for heat transfer between the land surface and the atmosphere. Journal of Applied Meteorology 40(10): 1933-1951.

Su, Z., 2002. The Surface Balance Energy System (SEBS) for estimating turbulent heat fluxes. Hydrology and Earth System Sciences. 6(1): 85-99.

Su, Z., and Wang, L., 2013. Earth Observation of Water Resources (SEBS). Practical Session Instructions (July 2013). ITC. University of Twente. The Netherlands.

United States Geological Survey (USGS)., 2015. Landsat 8 (l8) Data Users Handbook. Version 1.0. June 2015.

Van Dijk, A.I., and Renzullo, L.J., 2011. Water resource monitoring systems and the role of satellite observations. Hydrology and Earth System Science 15: 39–55.

Xu, X., Li, J., Tolson, B.A., 2014. Progress in integrating remote sensing data and hydrologic modelling. Progress in Physical Geography 38(4): 464–498.

Yang, D., Chen, H., Lei, H., 2010. Estimation of evapotranspiration using a remote sensing model over agricultural land in the North China Plain. International Journal of Remote Sensing 31(14): 3783–3798.

Zhuo, G., Ba, L., Ciren, P., and Bu, L., 2014. Study on daily surface evapotranspiration with SEBS in Tibet Autonomous Region. Journal of Geographical Sciences 24(1): 113-128.

*****

Lead into chapter 3: The findings of the previous chapter have demonstrated potential solutions to address the trade-off between the spatial and temporal resolution associated with the SEO data sets (MODIS and Landsat) used as inputs to SEBS to derive daily ET. However, it was noted that the inability of the model to adequately represent ET during water stressed conditions, ultimately influenced the successful application of these approaches. Consequently, the objective of chapter 3 was to establish and implement an approach which could be integrated within SEBS to more adequately represent ET within the study area during water stressed conditions. Supplementary information and/or data which was used during the various analyses undertaken in this chapter but not presented herein, are provided in Appendix A.

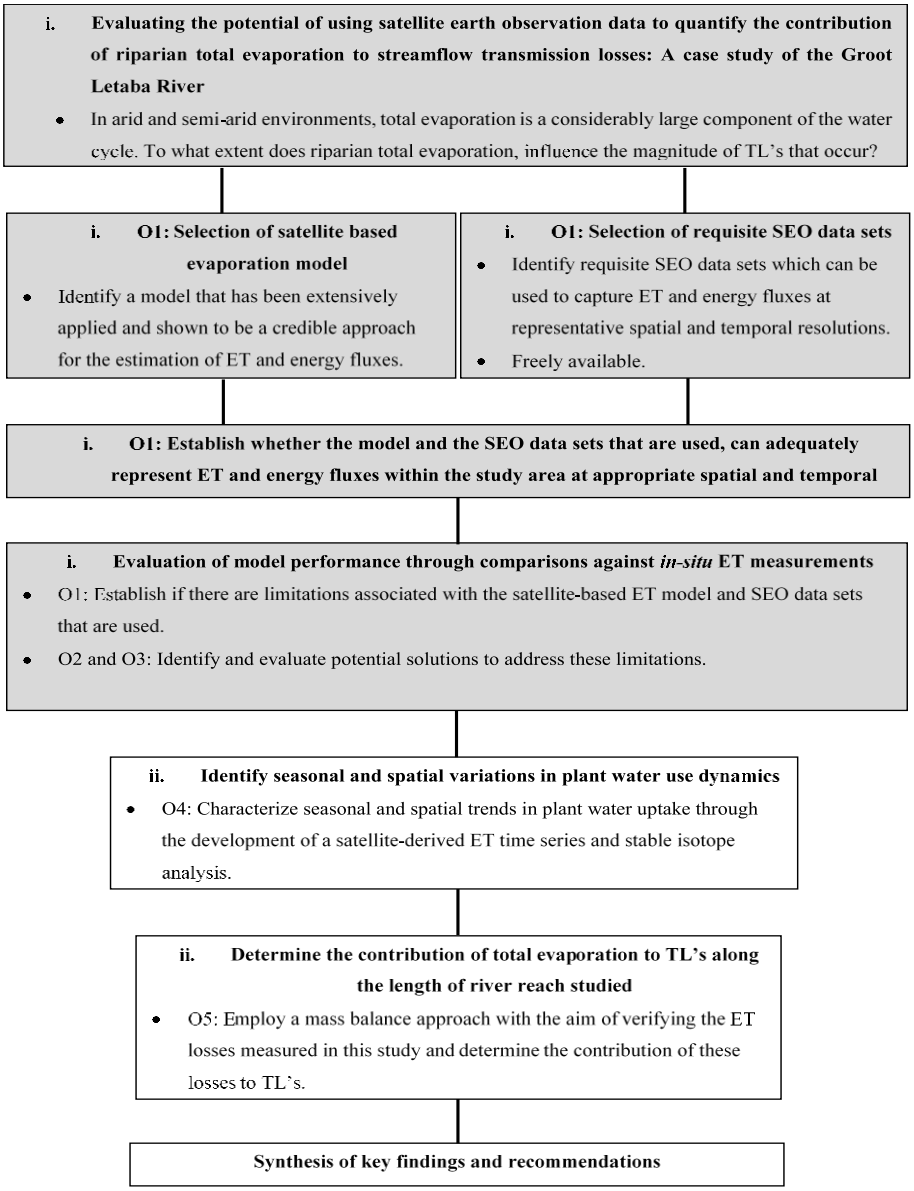

3. INTEGRATION OF AN ENVIRONMENTAL STRESS FACTOR IN SEBS FOR IMPROVING THE ESTIMATION OF EVAPOTRANSPIRATION IN ARID AND SEMI-ARID ENVIRONMENTS[2]

S Gokool[1], ES Riddell[1&2], C Jarmain[3] and KT Chetty[1]

[1]School of Agriculture, Earth and Environmental Sciences, Centre for Water Resources Research, University of KwaZulu-Natal, Pietermaritzburg, South Africa

[2]Conservation Management, South African National Parks, Skukuza, South Africa

[3]Independent Researcher, University of Stellenbosch, Stellenbosch, South Africa

Corresponding Author: Shaeden Gokool, shaedengokool@gmail.com, University of KwaZulu-Natal, Pietermaritzburg, South Africa, 3201

ABSTRACT

Surface energy balance models such as the surface energy balance system (SEBS) assume that the influence of soil moisture and biophysical parameters on evapotranspiration, are implicitly encompassed in model input variables such as the land surface temperature. This simplification may generally be suitable for environments in which the available energy constrains ET, but may prove to be inadequate during conditions of water stress. To address this limitation, a modified version of SEBS ($SEBS_{ESF}$) was applied, using a calibration factor that considers the combined influence of soil moisture, vegetation characteristics and temperature on fluxes. $SEBS_{ESF}$ was evaluated by comparing the modelled ET estimates against Eddy covariance ET measurements (EC_{ET}) at two sites, with contrasting environmental conditions. Comparisons between EC_{ET} and modelled ET indicated that the implementation of $SEBS_{ESF}$ resulted in an improved correlation between EC_{ET} and modelled ET estimates, as well as an increase in the percentage of modelled ET estimates within an acceptable accuracy range (± 15 to 30 %).

2S Gokool, ES Riddell, C Jarmain and KT Chetty. 2017. Integration of an environmental stress factor in SEBS for improving the estimation of evapotranspiration in environments during conditions of water stress. *Submitted to Water SA*

*Referencing conforms to format of Water SA

The potential improvements in mapping of ET by $SEBS_{ESF}$ provides an opportunity to better understand and quantify localized energy and water fluxes, in arid and semi-arid environments for varying landcover conditions.

Keywords: Total evaporation; SEBS; water stress; Evaporative fraction; Calibration Factor

3.1 Introduction

Monitoring and gauging of hydro-meteorological fluxes in arid and semi-arid environments remains fairly constrained due to limitations, such as *inter alia*; lower populations, financial limitations and the remote locality of hydrological gauging stations (Lange et al., 2005). Consequently, this has generally restricted the ability for extensive hydrological research to be undertaken in these environments (Lange et al., 2005). In such circumstances, the use of satellite earth observation (SEO) technologies represents the most suitable and efficient method to acquire hydrological process information (Gokool et al., 2017).

In recent times satellite-based approaches are being utilized more frequently to determine the parameters of the shortened surface energy balance, with an emphasis being placed upon assessing the spatio-temporal distribution of evapotranspiration (ET) (Gokmen et al., 2012). While numerous satellite-based methods have been formulated for the estimation of ET, techniques predicated on semi-physical and physical approaches have been most extensively applied for both scientific research and operational purposes (Bastiaanssen., et al 1998; Senay et al., 2007; Gokmen et al., 2012).

Some of the most commonly applied models include; the Simplified Surface Energy Balance Index (S-SEBI) (Roerink et al., 2000), Surface Energy Balance System (SEBS) (Su, 2002); Surface Energy Balance Algorithm for Land (SEBAL) (Bastiaanssen et al., 1998) and Mapping Evapotranspiration at High Resolution with Internalized Calibration (METRIC) (Allen et al, 2007). The implementation of the aforementioned models makes allowance for the relatively timeous and inexpensive quantification of ET, which can prove to be invaluable for operational water resources management. However, two of the major challenges which are limiting factors to the modelling of ET, using these technologies is; i) the trade-off between the spatial and temporal resolution of available imagery (Gokool et al., 2017) and ii) the accuracy of the models and the requisite data used to capture hydrological processes (Seneviratne et al., 2010).

Previous studies *inter alia* by; Hong et al. (2011), Spiliotopolous et al. (2013) and Bhattarai et al. (2015) have reported potential solutions to address spatio-temporal limitations, through the application of downscaling/disaggregation procedures. However, the success of these techniques is ultimately dependent on the ability of the satellite-based ET model to capture the ET for a particular area of interest, within an acceptable accuracy range (AAR) (± 15 to 30 %) when compared to *in-situ* observations (Kalma et al., 2008; Gibson, 2013).

According to Seneviratne et al. (2010), satellite-based ET estimation approaches often overestimate ET in areas of arid and semi-arid climatic regimes in which the availability of water is limiting ET. Studies undertaken by Timmermans and Meijerink (1999), Lubczynski and Gurwin (2005) and van der Kwast et al. (2009) in these environments, have shown that satellite-based ET estimation models may overestimate ET in the magnitude of 0.50 to 3.00 mm d^{-1}, as a result of an under-estimation of the sensible heat flux (*H*).

The poor performance of these models can largely be attributed to their inability to adequately account for the influence of soil moisture availability, land surface temperature (LST) and physical characteristics of vegetation during the estimation of fluxes (Gokmen et al., 2012; Pardo et al., 2014; Long et al., 2014; Li et al., 2015; Huang et al., 2015). The influence of soil moisture and vegetation on fluxes, are implicitly encompassed in input variables, ignoring their direct impact on ET estimates (Gokmen et al., 2012; Huang et al., 2015; Li et al., 2015).

While, the aforementioned approach may be suitable for environmental settings in which the available energy is limiting ET such as in the high latitude regions, it may prove to be inadequate where water availability is the principle limiting factor to ET (Seneviratne et al., 2010). Hence, satellite-based ET modelling necessitates an improvement for the estimation of fluxes for different land covers experiencing conditions of water stress (Wagle et al., 2017).

In this study the pre-packaged version of the single-source SEBS model available in the Integrated Land and Water Information System (ILWIS), was implemented to determine the ET within a semi-arid, savanna landscape in the north-eastern region of South Africa. SEBS has been extensively applied for the estimation of regional fluxes and ET and has been shown, to generally provide accurate estimates of ET and terrestrial heat fluxes (Yang et al., 2010; Zhuo et al., 2014).

However, previous studies have reported uncertainties in flux and ET estimates acquired from the implementation of SEBS over arid and semi-arid environments (Timmermans and Meijerink, 1999; Lubczynski and Gurwin, 2005; van der Kwast et al., 2009). Furthermore, Pardo et al. (2014) and Gokool et al. (2017) reported that the general degree of overestimation of the daily ET was significantly higher for an environmental setting dominated by sparse vegetation coverage and drier soils.

Recent studies by Gokmen et al. (2012), Pardo et al. (2014) and Huang et al. (2015) have discussed the application of a modified version of SEBS to improve the estimation of the evaporative fraction (*EF*), latent heat (*LE*) and *H* fluxes through the integration of a scaling factor in SEBS to better represent the influence of soil moisture availability and vegetation characteristics during the estimation of ET.

In this particular study, we propose the use of an empirically derived calibration factor that considers the combined influence of soil moisture, temperature and vegetation characteristics on fluxes, which can be integrated into the original SEBS formulation following the approach adopted in Pardo et al. (2014). The integration of this factor in SEBS is proposed as an alternative approach to improve upon the localized estimation of ET for water limited environments, using the SEBS model. The aim of this study was to implement the modified version of SEBS to improve the local mapping of ET within the study area, as Gokool et al. (2017) showed that the implementation of the original SEBS formulation within this region resulted in the over-estimation of ET. The performance of the original SEBS ($SEBS_0$) and Modified SEBS formulation ($SEBS_{ESF}$) were evaluated by comparing the estimated fluxes *(H* and *LE*), as well as daily ET estimates against *in situ* observations.

3.2 Measuring site

Flux tower data records were acquired from two sites (Malopeni, Kruger National Park and within the riparian zone along a portion of the Groot Letaba river) within the Letaba catchment and the northern region of the Kruger National Park, both of which are situated in the semi-arid north-eastern half of South Africa, as illustrated in Figure 3.1.

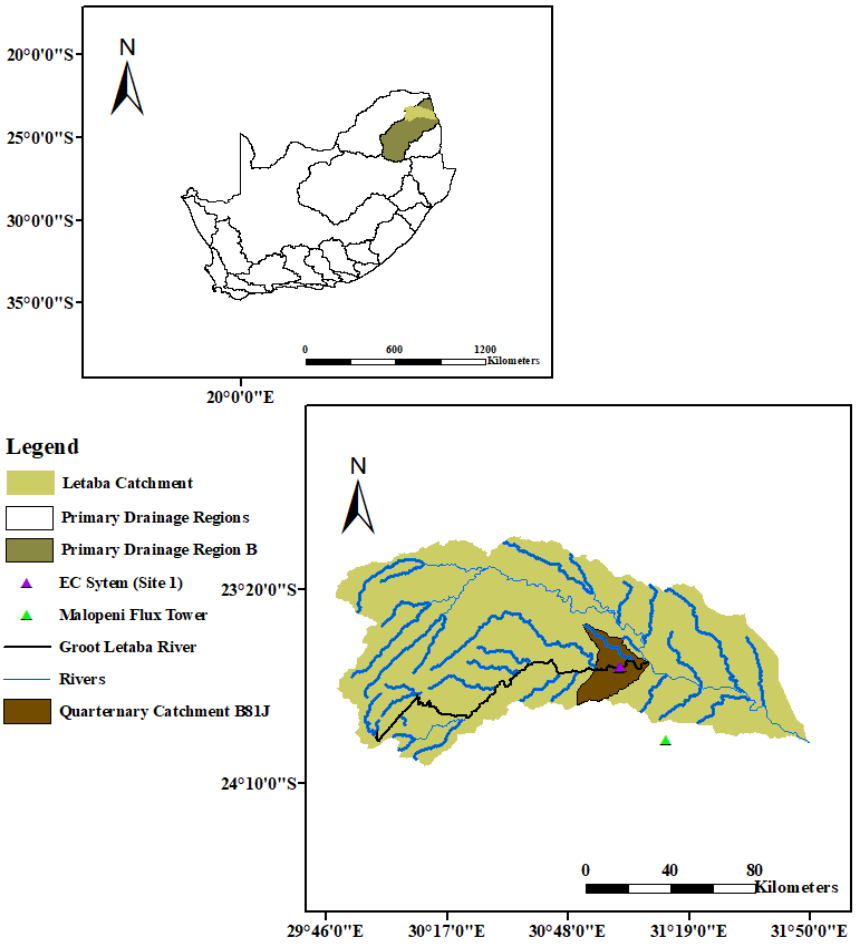

Figure 3.1 Geographical location of the measuring sites within the Letaba Catchment in South Africa (adapted from Schulze et al., 2008)

The Groot Letaba River which flows through this catchment, often experiences water scarcities due to high water demands in its upper reaches for commercial agriculture, this has consequently given rise to frequent occurrences of non-compliance with environmental flow requirements (Pollard and du Toit, 2011b). This situation is particularly concerning, as the river flows through numerous conservation areas, including the Kruger National Park.

The measurement sites are situated in a semi-arid region, which experiences seasonal rainfall. A vast majority of this rainfall is received during the summer months between October and March (Katambara and Ndiritu, 2010; Pollard and du Toit, 2011a), with 40 to 50 %, occurring during January and February (Katambara and Ndiritu, 2010). Mean annual potential evaporation (2097.3 mm as measured by A-pan) exceeds the mean annual precipitation (417.5 mm) (Schulze et al., 2008).

Temperatures across the catchment vary from warm conditions in the eastern region (mean annual temperature approximately 28˚C) to cooler conditions in the mountainous regions (mean annual temperature approximately 18˚C). The vast majority of the catchment is underlain by gneiss and granite, with a varied distribution of sediment along the river channel (Heritage et al., 2001). This has given rise to the formation of numerous channel types, characterized by distinct morphologies and vegetative composition.

The Malopeni study site is situated in the ephemeral Malopeni catchment of the Letaba, and the area is pristine savanna dominated by broad-leafed *Colophosopermum mopane* (Ramoelo et al., 2014). Savanna vegetation such as *Diospyros mespiliformis*, *Philenoptera violacea*, *Ficus sycomorus* and *Phragmites mauritianus* (Lowveld Reed) is predominantly found within and along the riparian zone of the perennial Groot Letaba River. Furthermore, numerous irrigated agricultural fields can be found situated adjacent to the riparian zone at the Groot Letaba site.

3.3 Instrumentation and data

3.3.1 Micrometeorological and energy flux measurements

A measuring tower was installed within a selected portion of the Groot Letaba River channel (Site 1) to measure energy fluxes, as well as all meteorological variables required to describe the ecosystem of the site in detail. The system was alternated between two positions within the river channel during the drier low flow periods of the study (May to October) between Mahale (23.669° S; 30.991° E) and Letaba Ranch Weirs (23.658° S; 31.047° E). The width of the riparian corridor studied at each of these locations is approximately 60 m (only inclusive of river channel width) (Gokool et al., 2017).

The measuring tower was first installed at a point upstream of Mahale weir within the river channel (Location 1) from 17th June to 13th August 2015. The measuring tower was then moved approximately 1.2 km further upstream (Location 2) and measurements were acquired from 21st August to 22nd October 2015 (Gokool et al., 2017). The same procedure was repeated for 2016. The measuring tower was first installed at Location 1 from 18th May to 25th July 2016. The measuring tower was then moved approximately 2.0 km further upstream from the 2015 Location 2 position and measurements were acquired from 27th July to 11th November 2016. The situation of the measuring tower further upstream from the position of the 2015 location 2, was due to the removal of an electric fence which previously separated Location 2 from Location 1.

Consequently, this area no longer represented a pristine protected area, as livestock were no longer prevented from grazing in this region (Riddell et al., 2017). Therefore, the system was moved to the 2016 location 2, which had similar characteristics to the 2015 Site 2. The channel morphology remained unchanged within this 3.2 km reach, therefore the EC_{ET} estimates acquired at these locations were considered to be characteristic of the morphological river reach (Gokool et al., 2017).

The measuring tower which incorporated a one sensor EC system (excluding Infra-Red Gas Analyzer) was equipped with a CSAT 3-D sonic anemometer, which was situated at a placement height of 2.0 m above the soil surface and 1.0 m above the average vegetation (*Phragmites mauritianus*) height, a HMP60 temperature and relative humidity sensor and energy balance sensors consisting of two Kipp and Zonen NR Lite-2 net radiometers (situated approximately 1.0 m above the bare soil and vegetation, respectively), six soil heat flux plates (inserted at a depth of 0.08 m), three pairs of soil temperature averaging probes (inserted at a depth of 0.02 and 0.06 m), two CS616 soil water reflectometers (inserted at a depth of 0.06 m), a Licor LI200X Pyranometer, RM Young wind sentry, HMP60 temperature and relative humidity sensor and a Texas Tipping bucket raingauge (0.1 mm) (Gokool et al., 2017).

The system measures net radiation, a computed soil heat flux density, a computed sensible heat flux, temperature, relative humidity, horizontal wind speed and wind direction, solar radiation, air temperature and rainfall (Gokool et al., 2017). Further details regarding the site characteristics and instrumentation setup are provided in Gokool et al. (2017). The average integrated estimates of net radiation (R_n), the computed H and the weighted average of the computed soil heat flux (G_0) were then used to determine the LE as a residual of the shortened energy balance equation, which is given as:

$$R_n = G_0 + H + LE \quad (3.1)$$

In addition to the data collected from the measuring tower installed in this particular study, energy-flux and meteorological data were also acquired from the Malopeni flux tower (Site 2) (23.833°S; 31.215°E). The Malopeni flux tower was established in 2009 as part of the CARBOAFRICA network. The tower is situated in a hot and dry savanna region, approximately 12 km from the town of Phalaborwa (Ramoelo et al., 2014). Further details regarding the Malopeni flux tower study area and instrumentation specifications are provided in Ramoelo et al. (2014) and available at www.csir.co.za/eddy-covariance-flux-towers.

The differences in environmental characteristics associated at the two study sites provided the ideal platform to assess the performance of implementing the $SEBS_0$ and $SEBS_{ESF}$ formulations for environments characterized by distinctive land cover compositions and meteorological conditions, in a semi-arid region.

3.3.2 Satellite earth observation data collection and processing

215 clear sky MODIS Level 1 B Terra images (MOD21 and MOD 03 data products) were collected and analysed for 2015 and 2016 (17th June to 22nd October), respectively. 26 clear sky Landsat (7 & 8) Level 1 GeoTiff products were collected for the corresponding periods. According to Alidoost et al. (2015) the spatial resolution of the daily ET map output by SEBS is dependent upon the spatial resolution of the thermal band used to derive LST. MODIS thermal bands are provided daily at a 1 km spatial resolution. Whereas Landsat 7 and 8 thermal bands are provided every 16 days at a spatial resolution of 60 m and 100 m, respectively, which are then resampled to 30 m.

The Modis Swath Tool and ILWIS, were used for the pre-processing and processing of the abovementioned images, based on the procedures detailed in Su and Wang (2013), Singh et al. (2014a) and USGS (2015), in order to derive the requisite land surface parameters (such as Albedo, LST, Emissivity and *NDVI*) which are required in conjunction with meteorological data as inputs to SEBS for the estimation of ET.

3.4 Methodology

3.4.1 SEBS Methodology

The SEBS Model computes all surface energy balance components, as well as the evaporative fraction (*EF*) using meteorological data and land surface parameters, which are acquired from meteorological and SEO sources, respectively. A brief description of the model methodology is presented below. A detailed discussion of the model formulation is presented in Su (2002). SEBS employs the shortened surface energy balance equation (Equation 3.1) and partitions the available energy into *H* and *LE* fluxes.

The equation to determine the net radiation term in Equation 3.1 is given as (Su, 2002):

$$R_n = (1 - \alpha)R_{swd} + \varepsilon R_{lwd} - \varepsilon\sigma T_o^4 \quad (3.2)$$

Where α is the albedo (surface reflectance), R_{swd} is the downward solar radiation (W m^{-2}), R_{lwd} is the downward longwave radiation (W m^{-2}), ε is the emissivity of the surface, σ is the Stefan-Boltzman constant and T_o is the surface temperature (K).

The soil heat flux equation is parameterised as (Su, 2002):

$$G_o = R_n[\Gamma + (1 - f_c)(\Gamma_s - \Gamma_c)] \quad (3.3)$$

Where the ratio of soil heat flux to net radiation Γ_c is assumed to be 0.05 for a fully vegetated canopy (Monteith, 1973) and Γ_s is assumed to be 0.315 for a bare soil surface (Kustas and Daughtry, 1989). The fractional vegetation coverage f_c is used to perform an interpolation between the aforementioned limiting cases, to separate land surfaces into non-vegetated, partially vegetated and densely vegetated surfaces.

SEBS makes use of the Monin-Obukhov similarity theory (MOST) for the estimation of the *H* and *LE*. MOST relates surface variables and variables in the atmospheric surface layer to surface fluxes (Su et al., 2001).

Su (2002) states that the similarity relationships for profiles of the mean wind speed and mean temperature difference (θ_o - θ_a) in the ASL, are usually written in integral form as:

$$u = \frac{u_*}{k}\left[\ln\left(\frac{z-d_o}{z_{oh}}\right) - \psi_m\left(\frac{z-d_o}{L}\right) + \psi_m\left(\frac{z_{om}}{L}\right)\right] \quad (3.4)$$

$$\theta_o - \theta_a = \frac{H}{k u_* \rho C_p}\left[\ln\left(\frac{z-d_o}{z_{oh}}\right) - \psi_h\left(\frac{z-d_o}{L}\right) + \psi_h\left(\frac{z_{oh}}{L}\right)\right] \quad (3.5)$$

Where z is the reference meteorological height (m), u_* is the friction velocity (m s^{-1}), ρ is the density of air (kg m^{-3}), C_p is the heat capacity of dry air (Jkg^{-1}), k = 0.4 is von Karman's constant, d_o is the zero plane displacement height (m), z_{om} is the roughness height for momentum transfer (m), θ_o and θ_a are the potential surface temperature and potential air temperature at height (z) respectively (K), z_{oh} is the scalar roughness height for heat transfer, ψ_m and ψ_h are the stability correction factors for momentum and heat transfer respectively and L is the Obukhov length (m)

The scalar roughness height for heat transfer can be derived as:

$$z_{oh} = \frac{z_{om}}{\exp(kB^{-1})} \quad (3.6)$$

Where the parameter kB^{-1} value is dependent upon the soil and fractional vegetation coverage. The estimation of this parameter can be determined using the extended physical model proposed by Su et al. (2001). *H* is recalculated iteratively in SEBS using the MOST parameters until the lowest possible error is obtained (Su, 2002). Su (2002) discusses the derivation of a formulation for the estimation of *EF* on the basis of the energy balance at limiting cases.

In SEBS, *H* is constrained in the range set by the *H* at the wet limit (H_{wet}) and *H* at the dry limit (H_{dry}) (Su, 2002). Due to the limitation of soil moisture, *LE* (or the evaporation) becomes zero, at the dry limit, and *H* attains its maximum value (Su, 2002). *H* attains its minimum value, at the wet limit, as evaporation can take place at potential rates (evaporation is constrained, only by the energy available for given surface and atmospheric conditions). Therefore, the relative evaporation can be calculated as:

$$\Lambda r = 1 - \frac{H - H_{wet}}{H_{dry} - H_{wet}} \quad (3.7)$$

The *EF* can then be derived as follows:

$$\Lambda = \Lambda_r \frac{R_n - G_o - H_{wet}}{R_n - G_o} \quad (3.8)$$

Consequently, the ET can be computed by assuming the *EF* is constant throughout the day.

3.4.2 SEBS modifications

Gokmen et al. (2012) and Pardo et al. (2014) discuss two separate approaches involving the integration of scaling factors into $SEBS_0$ to improve the estimation of *H*, *LE* and *EF* during conditions of water stress. The poor performance of $SEBS_0$ during conditions of water stress can be ascribed to the inability of the model, to explicitly account for biophysical feedbacks between aerodynamic conductance, surface conductance and vapor pressure deficit. Instead an extra resistance parameter (kB^{-1}) is used to overcome the difference between aerodynamic and radiometric temperature (*Tr*).

However, this may lead to uncertainties during the estimation of ET during conditions of water stress, such as the underestimation of *H*. In order to address this limitation and correct the underestimation of *H*, so that an overestimation of *EF* and *LE* can be avoided, Gokmen et al. (2012) integrated a soil moisture scaling factor ($SEBS_{SM}$) to adjust kB^{-1}. Alternatively,Pardo et al. (2014) used LST and the normalized difference vegetation index (*NDVI*) to scale ($SEBS_{NDVI}$) *EF*.

Pardo et al. (2014) evaluated the $SEBS_0$ algorithm, as well as the aforementioned modifications in order to determine whether these approaches resulted in the improved estimation of fluxes and ET during water stressed conditions. The results of the study indicated that while the application of both the $SEBS_{SM}$ and $SEBS_{NDVI}$ approaches resulted in an improved agreement between the observed and modelled *H*. Only $SEBS_{NDVI}$, was shown to have significantly improved modelled *LE* and *EF* when compared with observed values. According to Pardo et al. (2014) other factors in addition to soil moisture, *viz.* biophysical parameters associated with different vegetation types, may have a significant influence on the $SEBS_0$ algorithm, as these parameters influence the roughness heights for momentum transfer.

While the $SEBS_{NDVI}$ approach accounts for these factors, the $SEBS_{SM}$ approach does not adequately do so. Consequently, the application of the $SEBS_{SM}$ approach may not be suitable for application in environmental settings in which there are great differences in the biophysical parameters characterizing the vegetation in a particular area of interest (Pardo et al., 2014). Considering the findings of Pardo et al. (2014) and the characteristics of our study site (site 1), a similar approach to $SEBS_{NDVI}$ was implemented in this study.

Previous studies have shown that as environmental stress increases, the *EF* and ET consequently decrease. In order to better represent this influence of stress on the *EF* and *LE* derived in $SEBS_0$, calibration factors were empirically derived as indicators of stress, to better represent the influence of environmental stress on fluxes within the study areas. To derive the aforementioned factors, we first computed the ratio of actual ET(ET_a) to ET_o (FAO Penman-Monteith reference evaporation) during the 2015 measurement period at site 1, to represent the influence of environmental stress on ET. This is given as

$$Kc_{act} = \frac{ET_a}{ET_o} \tag{3.9}$$

Where Kc_{act} (dimensionless), hereafter referred to as the environmental stress factor (*ESF*), can be defined as the actual crop coefficient which accounts for the influence of environmental stress (Allen et al., 2005), ET_a is the ET measured *in-situ* (mm d^{-1}) and ET_o is the FAO Penman-Monteith reference evaporation (mm d^{-1}).

Thereafter we quantified the dependence of the *ESF* on soil moisture (*SM*), temperature (*T*) and *NDVI* by performing a simplistic multi-variable ordinary least squares regression. *SM* (m^3 m^{-3}) and *T* (^{0}C) were obtained from *in-situ* meteorological measurements. Although, *SM* data can be retrieved using satellite-earth observation, point based *in-situ* measurements were the preferred option, as data available through satellite-earth observation sources were too course to fulfil the objectives outlined in this study. *NDVI* was derived from Landsat data, as:

$$NDVI = \frac{(NIR-Red)}{(NIR+Red} \quad (3.10)$$

Where *NIR* is the Near-Infra Red band (W m^{-2} μm^{-1}) and Red is the red band (W m^{-2} μm^{-1}).

As Landsat data was only available every 8 days (using both Landsat 7 and 8), only measurements of *SM* and *T* which coincided with these days were used during the regression analysis. The results of this analysis showed the there is a strong correlation between the *ESF* and these variables ($R^2 = 0.81$) within our study site. Consequently, *ESF* can alternatively be determined as:

$$ESF = 0.2NDVI + 0.03SM - 0.01T + 0.25 \quad (3.11)$$

Using Equation 3.11 daily *ESF* was estimated, using daily measurements of *SM* and *T*, whereas we assumed that *NDVI* values remained unchanged between Landsat image acquisitions. *ESF* was then incorporated into Equations 3.12 and 3.13, to obtain EF_{new} and H_{new}, respectively (Pardo et al., 2014).

$$EF_{new} = EF_{old} * ESF \quad (3.12)$$

$$H_{new} = (1 - ESF)(R_n - G_0) \quad (3.13)$$

Once the EF_{new} has been determined, it could be applied in conjunction with the R_n and G_0 previously determined in $SEBS_0$, to estimate the daily ET.

To assess if the implementation of $SEBS_{ESF}$ improves the estimation of ET in this semi-arid region; daily ET, *H* and *LE* flux estimates acquired using the $SEBS_0$ and $SEBS_{ESF}$, were compared against EC measurements obtained at Site 1 during the 2015 measurement period. In general, the footprint of EC measurements can extend to hundreds of meters depending on the instrument heights of the system (Huang et al., 2015). In this study, we did not derive the flux tower footprint. Instead we adopted the approach described in Huang et al. (2015), comparing estimations of the pixel/s covering the location of the EC flux tower with measurements from the EC system.

Furthermore, to test if the *ESF* approach was robust and applicable to other environmental settings and for changing climatic conditions, we used the relationship described in Equation 3.11, to derive *ESF* values during the 2016 measurement period at site 1, as well as for the 2015 and 2016 measurement period at site 2. These values were then used to estimate daily ET using the $SEBS_{ESF}$ approach.

3.5 Results

3.5.1 Comparison of satellite derived fluxes and ET against *EC* measurements at Site 1 during the 2015 measurement period

In general, our results show that the modelled values of *H* from $SEBS_0$ are clearly underestimated when compared against observed values, as illustrated in Figure 3.2, whereas *LE* is overestimated when compared against observed values. To assess the effect of integrating *ESF* values in $SEBS_0$, bias and root mean square error (RMSE) values for $SEBS_0$ and $SEBS_{ESF}$ were compared against observed *H* and *LE* fluxes.

The implementation of $SEBS_{ESF}$, resulted in a significant improvement in the correlation between modelled and observed values of *H* and *LE* (Table 3.1). Furthermore, there is a 29.30 and 28.37W m^{-2} reduction in the bias and RMSE for modelled *H*, respectively. Whereas the bias and RMSE for modelled *LE* was reduced by 19.67 and 44.03 W m^{-2}, respectively, when *ESF* is integrated into $SEBS_0$.

Table 3.1 Error evaluation of the estimated *H* and *LE* derived from implementing $SEBS_0$ and $SEBS_{ESF}$ during the 2015 measurement period at site 1

	H		***LE***	
	$SEBS_0$	$SEBS_{ESF}$	$SEBS_0$	$SEBS_{ESF}$
RMSE	66.48	37.18	48.11	28.43
Bias	56.23	28.25	66.59	22.55
Correlation coefficient	0.20	0.40	0.54	0.73
T test *p* value	0.00	0.99	0.00	0.27

EC_{ET} was then compared with modelled ET estimates acquired from using MODIS data as inputs to $SEBS_0$ and $SEBS_{ESF}$, during the 2015 field campaign. The implementation of $SEBS_{ESF}$ resulted in an improved estimation of the ET derived at the MODIS spatial resolution, as shown in Table 3.2 and Figure 3.3. Bias and RMSE values for ET estimates derived using $SEBS_{ESF}$, decreased by 1.41 and 1.48 mm d^{-1}. Furthermore, increases in the Nash-Sutcliffe efficiency values, as well as the percentage of values within an AAR, indicated that there was a significant improvement in the association between the EC_{ET} and the ET estimates derived from implementing $SEBS_{ESF}$.

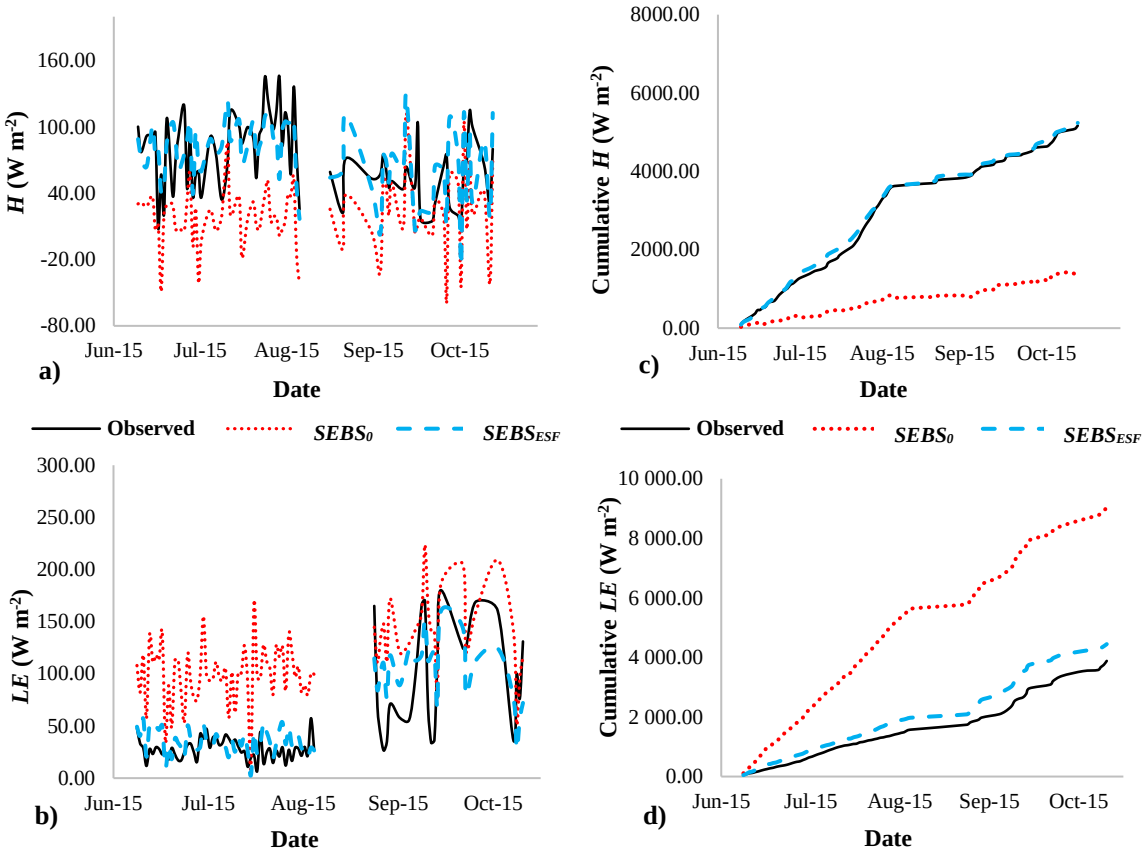

Figure 3.2 Comparison of observed and modelled fluxes at site 1 during the 2015 measurement period; a) and b) show a time series comparison of *H* and *LE* values, respectively. Whereas c) and d) show cumulative plots of *H* and *LE* values, respectively

3.5.2 Comparison of observed and satellite derived ET estimates using MODIS data, at site 1 during the 2016 measurement period

Comparisons between observed and modelled daily ET (Table 3.3 and Figure 3.4), show that the implementation of $SEBS_{ESF}$ resulted in the improved estimation of modelled ET derived at the MODIS spatial resolution within the study site during the 2016 measurement period. Bias and RMSE values for ET estimates derived using $SEBS_{ESF}$ decreased by 0.35 and 0.28 mm d^{-1}. Moreover, there was an increase in the Nash-Sutcliffe efficiency values, as well as the percentage of values within an AAR, further indicating that there was a significant improvement in the association between the EC_{ET} and the ET estimates derived from implementing $SEBS_{ESF}$.

Table 3.2 Statistical comparison of $SEBS_0$ and $SEBS_{ESF}$ ET estimates derived at the MODIS spatial resolution, against EC_{ET} at Site 1 during the 2015 measurement period

	$SEBS_0$	$SEBS_{ESF}$
Relative volume error (RVE)	-181.40	-22.84
Bias	2.17	0.71
RMSE	2.51	1.13
Kruskal-Wallis (*p* value)	0.00	0.07
Correlation coefficient	0.30	0.64
Nash-Sutcliffe	-2.77	0.24
AAR (± 15 %)	17 %	41 %
AAR (± 30 %)	24 %	57 %

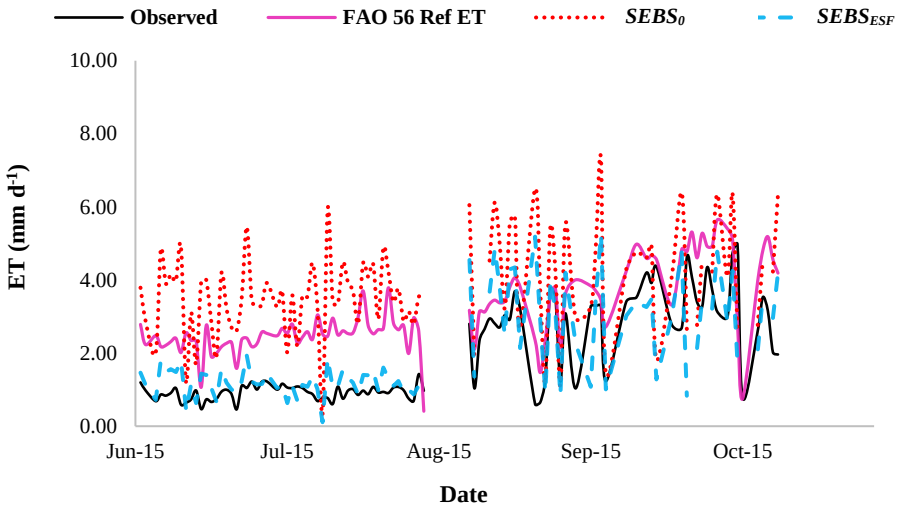

Figure 3.3 A time-series comparison of $SEBS_0$ and $SEBS_{ESF}$ ET estimates derived at the MODIS spatial resolution, against EC_{ET} during the 2015 measurement period

Table 3.3 Statistical comparison of $SEBS_0$ and $SEBS_{ESF}$ ET estimates derived at the MODIS spatial resolution, against EC_{ET} at Site 1 during the 2016 measurement period

	$SEBS_0$	$SEBS_{ESF}$
RVE	-29.86	1.56
Bias	1.18	0.83
RMSE	1.48	1.17
Kruskal-Wallis (*p* value)	0.03	0.14
Correlation coefficient	0.12	0.47
Nash-Sutcliffe	-0.83	-0.14
AAR (± 15 %)	24 %	38 %
AAR (± 30 %)	40 %	61 %

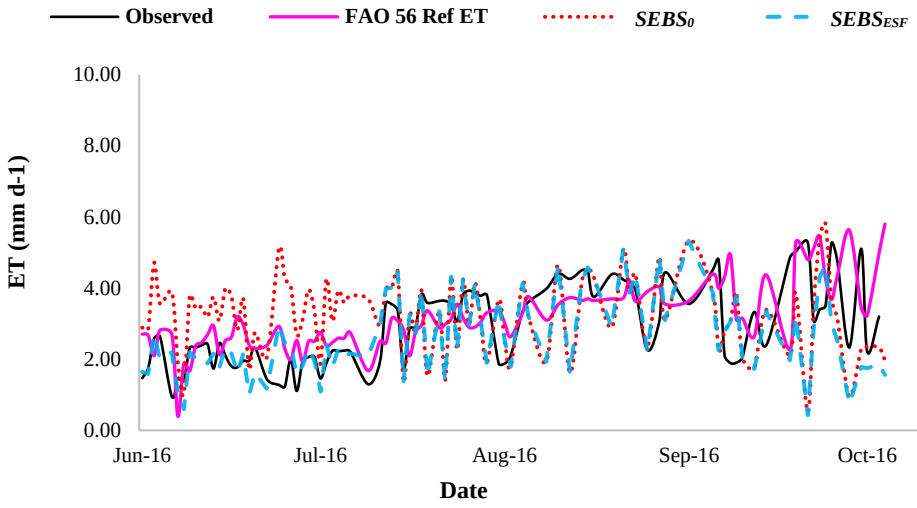

Figure 3.4 A time-series comparison of $SEBS_0$ and $SEBS_{ESF}$ ET estimates derived at the MODIS spatial resolution, against EC_{ET} during the 2016 measurement period

3.5.3 Comparison of observed and satellite derived ET estimates using Landsat data, at site 1 during the 2015 and 2016 measurement period

Due to the limited number of Landsat images acquired during the investigation period we combined our results for 2015 and 2016 at site 1. This was done to increase the population size used during the statistical analysis, so that a more meaningful assessment of integrating *ESF* values in $SEBS_0$ could be ascertained. Similar to our previous observations for site 1, the implementation of $SEBS_{ESF}$ resulted in the improved estimation of ET at the Landsat resolution, when compared against EC_{ET} (Table 3.4 and Figure 3.5).

Table 3.4 Statistical comparison of $SEBS_0$ and $SEBS_{ESF}$ ET estimates derived at the Landsat spatial resolution, against EC_{ET} at Site 1 during the 2015 and 2016 measurement period

	$SEBS_0$	$SEBS_{ESF}$
RVE	-72.34	12.12
Bias	1.19	0.69
RMSE	1.43	0.94
Kruskal-Wallis (*p* value)	0.33	0.24
Correlation coefficient	0.33	0.79
Nash-Sutcliffe	-0.14	0.51
AAR (± 15 %)	22 %	35 %
AAR (± 30 %)	35 %	65 %

Bias and RMSE values for ET estimates derived using $SEBS_{ESF}$ decreased from 1.19 to 0.69 mm d^{-1} and 1.43 to 0.94 mm d^{-1}, respectively, while there were significant increases in the Nash-Sutcliffe efficiency and the percentage of values within an AAR.

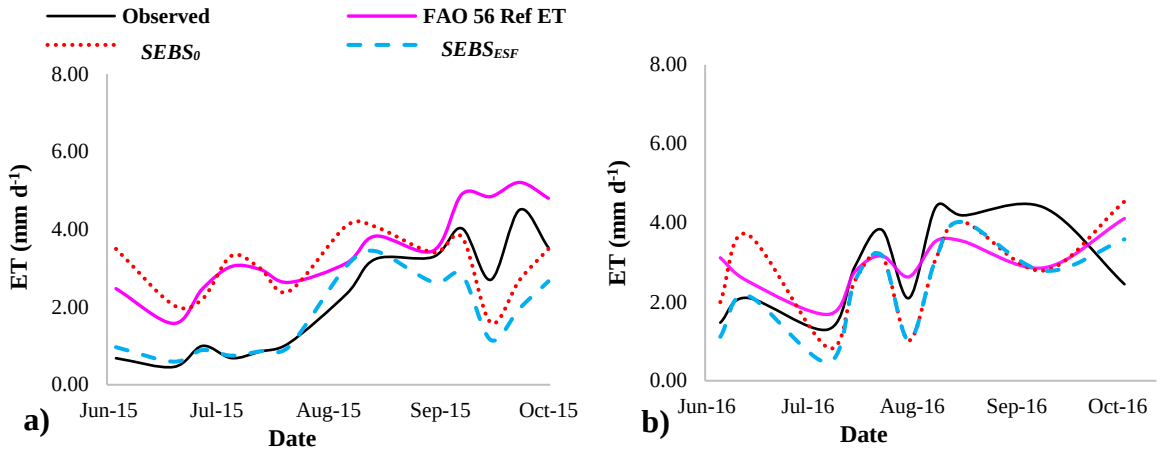

Figure 3.5 A time-series comparison of $SEBS_0$ and $SEBS_{ESF}$ ET estimates derived at the Landsat spatial resolution, against EC_{ET} during the; a) 2015 and b) 2016 measurement period

3.5.4 Comparison of observed and satellite derived ET estimates using MODIS data, at site 2 during the 2015 and 2016 measurement period

As mentioned previously, there were only a limited number of Landsat images available during the investigation period which restricted our statistical analysis to a relatively small sample size. However, we attempted to overcome this limitation by combining our results for 2015 and 2016. While this approach was successful for analyses at site 1, we were unable to adopt a similar approach at site 2. This was largely attributed to frequent occurrences of insufficient measurements (less than 40 thirty-minute ET measurements per day) in the observed ET data record (Ramoelo et al., 2014). Consequently, the results discussed herein (Table 3.5 and Figure 3.6) are limited, to comparisons between observed and modelled daily ET derived at the MODIS spatial resolution during the 2015 and 2016 measurement periods.

It should be noted that the observed ET data used during these data comparisons seldom fit the aforementioned criteria discussed in Ramoelo et al. (2014). Therefore, to increase the number of observed ET data records which could be used for data comparisons, we limited this selection criteria to a minimum of 17 thirty-minute diurnal (6:00 to 18:00) ET measurements per day, assuming that ET only occurs between sunrise and sunset (Gribovski et al., 2010).

The integration of *ESF* in $SEBS_0$ significantly reduced the degree of overestimation in the modelled ET estimates derived at the MODIS spatial resolution. Bias and RMSE values for ET estimates derived using $SEBS_{ESF}$ decreased by 2.21 and 2.66 mm d^{-1} and 1.38 to 1.70 mm d^{-1}, for 2015 and 2016 respectively. Furthermore, there were increases in Nash-Sutcliffe efficiency values indicating that there is an improvement in the model performance when compared against observed ET. While these results indicate that the modelled ET estimates improved through the integration of *ESF* in $SEBS_0$, this approach was only able to marginally increase the percentage of estimates within an AAR.

Table 3.5 Statistical comparison of $SEBS_0$ and $SEBS_{ESF}$ ET estimates derived at the MODIS spatial resolution, against EC_{ET} at Site 2 during the 2015 and 2016 measurement period

	2015		2016	
	$SEBS_0$	$SEBS_{ESF}$	$SEBS_0$	$SEBS_{ESF}$
RVE	-359.80	-26.61	-274.36	-37.27
Bias	2.69	0.48	1.81	0.43
RMSE	2.96	0.30	2.20	0.50
Kruskal-Wallis (*p* value)	0.00	0.22	0.00	0.07
Correlation coefficient	0.33	0.57	0.56	0.65
Nash-Sutcliffe	-20.91	0.45	-13.67	0.23
AAR (± 15 %)	0.00 %	0.00 %	6.00 %	6.00 %
AAR (± 30 %)	0.00 %	30.40 %	12.00 %	18.00 %

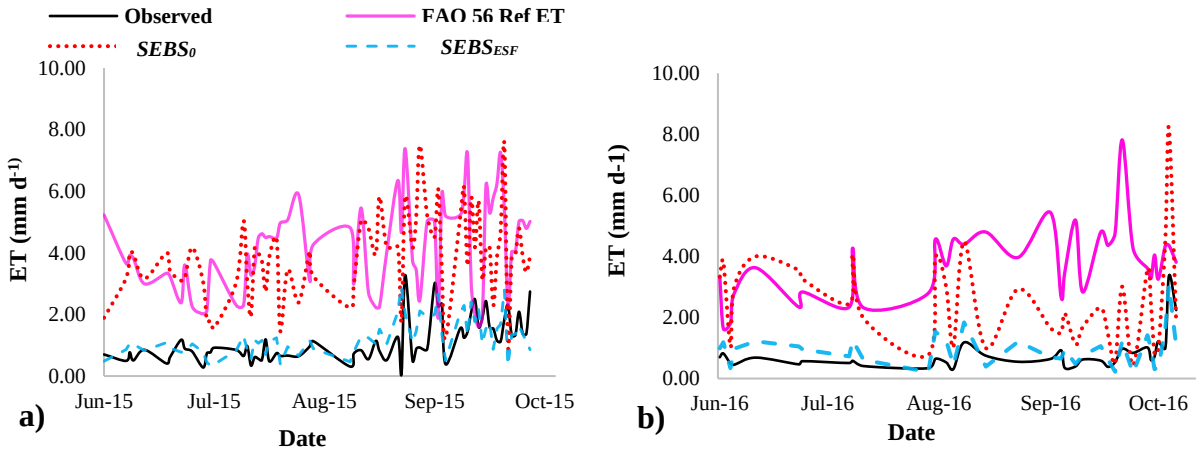

Figure 3.6 A time-series comparison of $SEBS_0$ and $SEBS_{ESF}$ ET estimates derived at the MODIS spatial resolution, against EC_{ET} during the; a) 2015 and b) 2016 measurement period

3.6 Discussion

Overall our results have shown that the implementation of $SEBS_{ESF}$ was able to significantly improve the estimation of ET under conditions of water stress within the study sites. This observation is reaffirmed in Figures 3.7 and 3.8, which provides an illustration of the differences in ET derived using $SEBS_0$ and $SEBS_{ESF}$ at sites 1 and 2. Using 21st June 2015 as an example, it is evident that $SEBS_0$ ET estimates derived at the Landsat and MODIS spatial resolutions, are generally greater than 2.50 mm d^{-1} at sites 1 and 2.

These values are significantly higher than EC_{ET} which was less than 1.00 mm d^{-1} at sites 1 and 2. However, after *ESF* is integrated into $SEBS_0$ the overestimation of ET is significantly reduced and is typically less than 1.20 mm d^{-1} at sites 1 and 2.

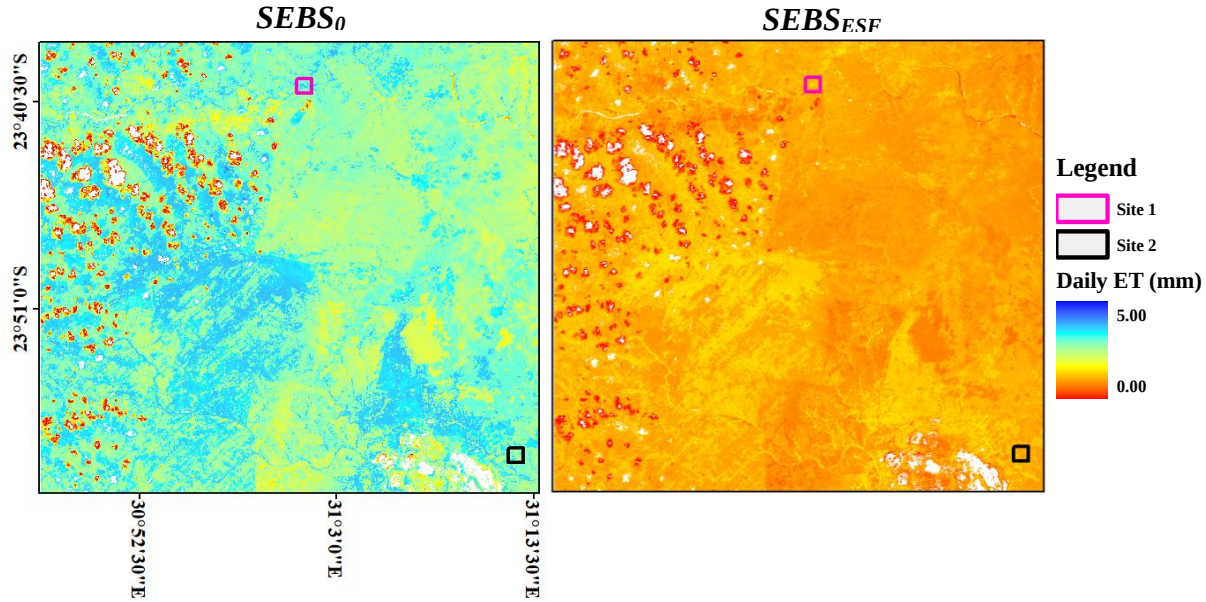

Figure 3.7 Daily ET maps of the study area derived at the Landsat spatial resolution for the 21st June 2015

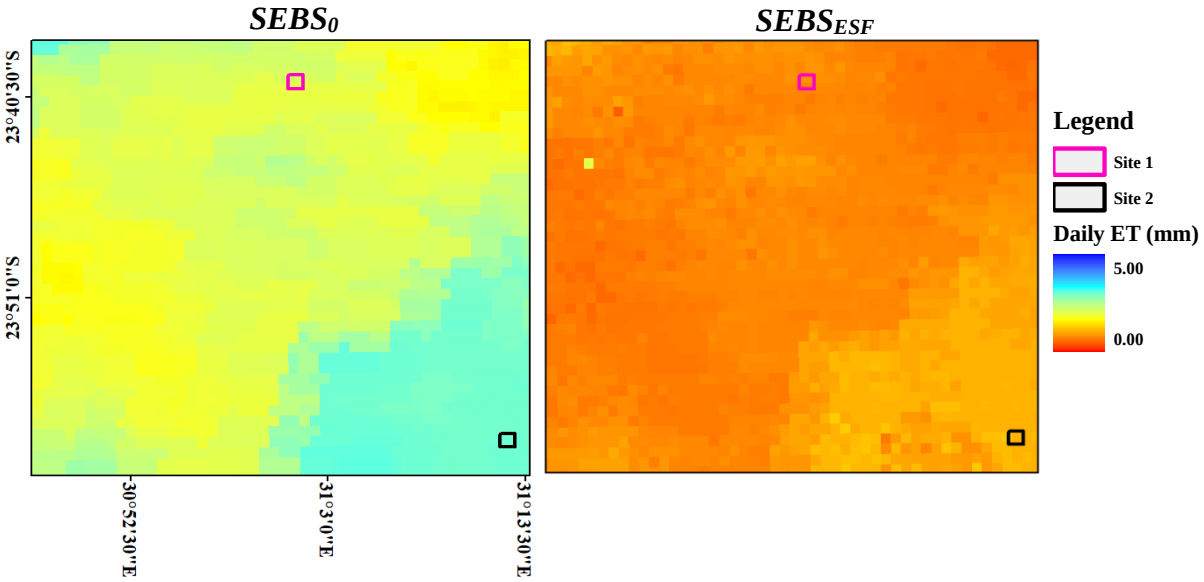

Figure 3.8 Daily ET maps of the study area derived at the MODIS spatial resolution for the 21st June 2015

While the implementation of $SEBS_{ESF}$ was generally shown to improve ET estimation, there were discernable trends identified during our analysis which indicated poor performance of the approach. These are given as follows; i) ET estimates derived at the Landsat spatial resolution were generally in better agreement with EC_{ET} ii) inter-annual comparisons at site 1 showed that the $SEBS_{ESF}$ approach generally perfomed better during 2015 and iii) only a marginal increase in the percentage of ET estimates within an AAR at site 2 was obtained using the $SEBS_{ESF}$ approach.

The correlation coefficient and Nash-Sutcliffe efficiency values were relatively higher for ET estimates derived at the Landsat resolution. The larger discrepancies between the MODIS derived ET estimates and EC_{ET} can essentially be attributed to the mixed pixel effect (Gibson et al., 2013) associated with the single MODIS pixel. Due to the spatial resolution of MODIS pixels, ET contribution of land-uses outside the footprint of the EC system were captured (Gokool et al., 2017). Whereas for Landsat there are several pixels which fall within the footprint of the EC system. Furthermore, the higher correlations achieved for Landsat may also be a consequence of the population size used during statistical analysis, *viz.* 26 days for Landsat and 215 days for MODIS.

The poorer correlation between $SEBS_{ESF}$ ET estimates and EC_{ET} during 2016 can be explained by the *ESF* values derived during each of the measurement periods, as *ESF* values ultimately influences the degree to which the overestimation of the modelled ET is reduced by. During the 2015 measurement period *ESF* values were lower than 2016 and did not approach 1. Whereas for 2016 there were numerous instances in which *ESF* values were equal to 1. This variation in the *ESF* can be attributed to inter-annual changes in the factors *NDVI*, temperature and soil moisture. However, since variations in the *NDVI* and temperature were relatively similar and of comparable magnitude for 2015 and 2016 (Figure 3.9), these factors would have presumably had a marginal influence on the observed differences in the 2015 and 2016 *ESF* values (Figure 3.10).

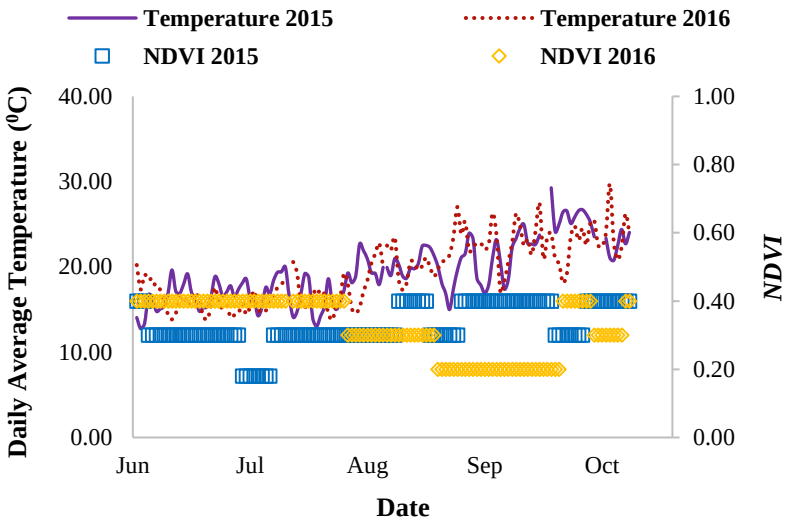

Figure 3.9 Inter-annual comparison of *NDVI* and temperature values at site 1

Ultimately, the differences in *ESF* values were largely attributed to changes in the soil moisture content in the root zone. During the initial stages of the investigation periods when volumetric water content (VWC) in the root zone was less than 0.14 m^3 m^{-3}, the integration of *ESF* into $SEBS_0$ was able to significantly reduce the overestimation in the modelled ET estimates. However, when VWC in the root zone increased above 0.22 m^3 m^{-3}, $SEBS_{ESF}$ ET estimates were similar to those of $SEBS_0$. It is presumable that during these periods there was minimal water stress within the study area. Consequently, ET was regulated by the available energy rather than soil moisture, hence $SEBS_0$ and $SEBS_{ESF}$ ET estimates were of similar magnitude.

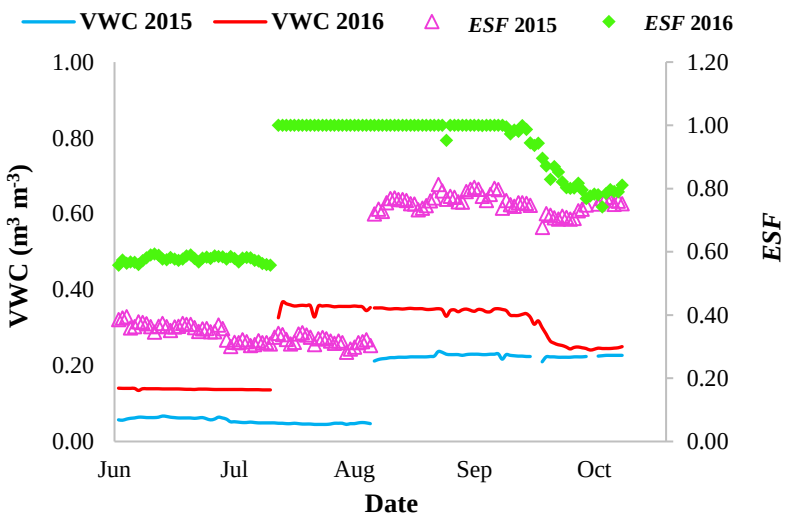

Figure 3.10 Inter-annual comparison of VWC and *ESF* values at site 1

Although the integration of *ESF* in $SEBS_0$ significantly improved the correlation between EC_{ET} and modelled ET at site 2, this approach was only able to marginally increase the percentage of estimates within an AAR. This occurrence can be ascribed to uncertainties associated with the flux tower measurement record.

During the 2015 and 2016 investigation periods, only 42 and 14 % of the observed ET values that were captured accounted for the maximum number (24) of thirty-minute diurnal ET measurements per day. Consequently, the daily ET for this region is presumably higher than the values used during validation. Therefore, the degree of overestimation in our modelled ET estimates may have been exaggerated, due to the underrepresentation of ET captured within the observed record.

Furthermore, it should be noted that the poorer performance of $SEBS_{ESF}$ approach during 2016, as well as at site 2 may also be partially due to the effect of the calibration effort required to derive *ESF* values.

3.7 Conclusions

Physically-based surface energy balance such as SEBS are generally found to perform well for a variety of crop types and moderate/dense land covers. However, these models may overestimate the ET for regions experiencing conditions of water stress, especially those characterized by drier soils with sparse vegetation coverage.

The integration of scaling factors, dependent on soil moisture or biophysical parameters into $SEBS_0$ has been proposed as a potential solution to address these limitations. In this study, we evaluated the performance of $SEBS_{ESF}$ which integrates a calibration factor that considers the influence of environmental stress on energy fluxes and daily ET. $SEBS_{ESF}$ was first evaluated by comparing the modelled daily ET, *H* and *LE* flux estimates against EC measurements obtained at Site 1 during the 2015 measurement period.

Integrating the *ESF* into $SEBS_0$ resulted in the *EF* decreasing as water stress increases. This in turn resulted in a decrease in the modelled *LE*, while there was an increase in the modelled *H*. The results also showed significant improvements in the correlation, as well as the percentage of values within an AAR between EC_{ET} and modelled ET estimates. Furthermore, to test if the *ESF* approach is robust and applicable to other environmental settings and for changing climatic conditions. *ESF* values were derived during the 2016 measurement period at site 1, as well as for the 2015 and 2016 measurement period at site 2.

Thereafter we implemented $SEBS_{ESF}$ and evaluated the modelled daily ET estimates against EC_{ET}. Significant improvements in the correlation, as well as the percentage of values within an AAR between the modelled ET and EC_{ET} were attained through the integration of the *ESF* into $SEBS_0$ for each of these scenarios. Overall the proposed integration of *ESF* into $SEBS_0$ was shown to be a credible approach for estimating ET during conditions of water stress. Only a limited number of observed ET measurements are required, thereafter the factors; *NDVI*, soil moisture and LST can be used to derive the *ESF* scaling factors. However, the feasibility of utilizing this approach in data scarce regions may be limited by the need for observed ET measurements to initially derive the *ESF* calibration equation.

The *ESF* scaling factors were derived using *in-situ* measurements of soil moisture and temperature, as the aim of this study was to improve the localized mapping of ET within the study area. Nevertheless, the $SEBS_{ESF}$ approach may potentially be applicable for regional applications, by acquiring estimates of the aforementioned meteorological variables from satellite-earth observation data products. However, this may only be possible if the environmental conditions within the greater study area are similar to the region in which the *ESF* calibration values are derived. Furthermore, the implementation of the $SEBS_{ESF}$ approach negates the advantage that SEBS has over other satellite-based ET estimation models, *viz*. that it is a purely physical process of the model and consequently provides credible results irrespective of season or location.

Although it was beyond the scope of this study, we recommend that future investigations regarding the application of the $SEBS_{ESF}$ approach are also compared against other modified versions of SEBS in additional environmental settings, to truly gauge if the proposed method offers any significant improvement to the localized mapping of ET in arid and semi-arid environments. Additionally, future research efforts could be focused on improving the modelling of the kB^{-1} parameter or extra (stomatal) resistance terms when deriving H, during conditions of water stress.

Notwithstanding the aforementioned limitations, the results presented in this study highlight the potential of implementing $SEBS_{ESF}$ for the mapping of ET in this region. This can prove to be extremely beneficial in furthering our understanding of the rapport between hydro-meteorological fluxes and the natural functioning of ecosystems, at varying spatial scales. This provides an opportunity to facilitate the improved management of our limited water resources, through the relatively timeous and cost-effective quantification of ET.

Acknowledgements

The research presented in this paper emanates from a Water Research Commission (WRC) project entitled: Quantification of transmission losses along the Letaba River for improved delivery of environmental water requirements (ecological reserve), WRC Project No K5/2338. The authors would like to extend their gratitude to the WRC and the South African Environmental Observation Network (SAEON) for the funding required to successfully complete this research. The authors would also like to extend their gratitude to the Council for Scientific and Industrial Research (CSIR), with special mention to Mr A. Mdau and Miss H.Thenga, for the provision of meteorological and ET flux data for the Malopeni study site. We would also like to extend our gratitude to the anonymous reviewers who commented on the previous version of this manuscript.

References

ALIDOOST F, SHARIFI MA and STEIN A (2015) Region and pixel-based image fusion for disaggregation of actual evapotranspiration. *International Journal of Image and Data Fusion*. DOI: 10.1080/19479832.2015.1055834.

ALLEN RG, PEREIRA LS, SMITH M, RAES D and WRIGHT JL (2005) FAO-56 dual crop coefficient method for estimating evaporation form soil and application extensions. *Journal of Irrigation and Drainage Engineering ASCE* **131**(1) 2–13.

ALLEN R, TASUMI M, MORSE A, TREZZA R, WRIGHT J, BASTIAANSSEN W, KRAMBER W, LORITE I and ROBISON C (2007) Satellite-Based Energy Balance for Mapping Evapotranspiration with Internalized Calibration (METRIC)—Applications. *Journal of Irrigation and Drainage Engineering* **133**(4): 395–406.

BASTIAANSSEN WGM, MENENTI M, FEDDES RA and HOLTSLAG AAM (1998) A remote sensing surface energy budget algorithm for land (SEBAL). 1. Formulation. *Journal of Hydrology* **212-213**(1-4): 213.

BHATTARAI N, QUACKENBUSH LJ, DOUGHERTY M and MARZEN LJ (2015) A simple Landsat–MODIS fusion approach for monitoring seasonal evapotranspiration at 30 m spatial resolution. *International Journal of Remote Sensing* **36**(1): 115-143.

GIBSON LA (2013) The application of the Surface Energy Balance System model to estimate evapotranspiration in South Africa. Unpublished PhD Thesis, Department of Environmental and Geographical Science, Faculty of Science, University of Cape Town, South Africa.

GOKMEN M, VEKERDY Z, VERHOEF A, VERHOEF W, BATELAAN O and TOL C (2012) Integration of soil moisture in SEBS for improving evapotranspiration estimation under water stress conditions. *Remote Sens Environ* **121**: 261–274. DOI: 10.1016/j.rse.2012.02.003.

GOKOOL S, JARMAIN C, RIDDELL E, SWEMMER A, LERM R and CHETTY KT (2017) Quantifying riparian total evaporation along the Groot Letaba River: A comparison between infilled and spatially downscaled satellite derived total evaporation estimates. *Journal of Arid Environments* **147**: 114-124.

HERITAGE GL, MOON BP and LARGE ARG (2001) The February 2000 floods on the Letaba River, South Africa: an examination of magnitude and frequency. *Koedoe* **44** (2): 1-6.

HONG S, HENDRICKX JMH and BORCHERS B (2011) Down-scaling of SEBAL derived evapotranspiration maps from MODIS (250 m) to Landsat (30 m) scales. *International Journal of Remote Sensing* **32**(21): 6457–6477.

HUANG C, LI Y, GU J, LU L and LI X (2015) Improving Estimation of Evapotranspiration under Water-Limited Conditions Based on SEBS and MODIS Data in Arid Regions. *Remote Sens*ing **7**: 16795–16814.

KALMA JD, MCVICAR TR and MCCABE MF (2008) Estimating Land Surface Evaporation: A Review of Methods Using Remotely Sensed Surface Temperature Data. *Surveys in Geophysics* **29**(4-5): 421-469.

KATAMBARA Z and NDIRITU JG (2010) A hybrid conceptual-fuzzy inference streamflow modelling for the Letaba River system in South Africa. *Physics and Chemistry of the Earth* **35**(13-14): 582-595.

LANGE J (2005) Dynamics of transmission losses in a large arid stream channel. *Journal of Hydrology* **306**: 112–126.

LI Y, ZHOU J, WANG H, LI D, JIN R, ZHOU Y and ZHOU Q (2015) Integrating soil moisture retrieved from L-band microwave radiation into an energy balance model to improve evapotranspiration estimation on the irrigated oases of arid regions in northwest China. *Agricultural and Forest Meteorology* **214-215**: 306–318.

LONG D, LONGUEVERGNE L and SCANLON BR (2014) Uncertainty in evapotranspiration from land surface modeling, remote sensing, and GRACE satellites. *Water Resources Research* **50**: 1131-1151.

LUBCZYNSKI MW and GURWIN J (2005) Integration of various data sources for transient groundwater modeling with spatio-temporally variable fluxes: Sardon study case, Spain. *Journal of Hydrology* **306**(1-4): 71-96.

PARDO N, SANCHEZ LM, TIMMERMANS J, SU Z, PEREZ IA and GARCIA MA (2014) SEBS validation in a Spanish rotating crop. *Agricultural and Forest Meteorology* **195-196**: 132-142.

POLLARD S AND DU TOIT D (2011a) Towards Adaptive Integrated Water Resources Management in Southern Africa: The Role of Self-organisation and Multi-scale Feedbacks for Learning and Responsiveness in the Letaba and Crocodile Catchments. *Water resources management* 25 (15): 4019-4035.

POLLARD S and DU TOIT D (2011b) Towards the sustainability of freshwater systems in South Africa: An exploration of factors that enable and constrain meeting the ecological Reserve within the context of Integrated Water Resources Management in the catchments of the lowveld. WRC Report No K8/1711.

RAMOELO A, MAJOZI N, MATHIEU R, JOVANOVIC N, NICKLESS A and DZIKITI S (2104) Validation of Global Evapotranspiration Product (MOD16) using Flux Tower Data in the African Savanna, South Africa. *Remote Sensing* **6**: 7406-7423.

RIDDELL, ES, NEL, JM, GOKOOL, S, JARMAIN, C, RAUBENHEIMER, R, STRYDOM, T and SWEMMER, A. 2017. Quantification of transmission losses along the Letaba River for improved delivery of environmental water requirements (ecological reserve). Water Research Commission Report, Project Number K5/2338.

ROERINK GJ, SU Z and MENENTI M (2000) S-SEBI: a simple remote sensing algorithm to estimate the surface energy balance. *Phys Chem Earth* **25**(2): 147–157.

SCHULZE RE (2008) Electronic version of the South African atlas of climatology and agrohydrology. South African Atlas of Climatology and Agrohydrology. RE Schulze. Water Research Commission, Pretoria, South Africa, WRC Report 1489/1/06, Section 1.1.

SENAY GB, BUDDE M, VERDIN JP and MELESSE AM (2007) A coupled remote sensing and simplified surface energy balance approach to estimate actual evapotranspiration from irrigated fields. *Sensors* **7**(6): 979–1000.

SENEVIRATNE SI, CORTI T, DAVIN EL, HIRSCHI M, JAEGER EB, LEHNER I, ORLOWSKY B and TEULING AJ (2010) Investigating soil moisture–climate interactions in a changing climate: a review. *Earth Sci. Rev* **99**: 125–161.

SINGH RK, SENAY GB, VELPURI NM, BOHMS S, SCOTT RL and VERDIN JP (2014a) Actual Evapotranspiration (Water Use) Assessment of the Colorado River Basin at the Landsat Resolution Using the Operational Simplified Surface Energy Balance Model. *Remote Sensing* **6**: 233-256.

SPILIOTOPOLOUS M, ADAKTYLOU N, LOUKAS A, MICHALOPOULOU H, MYLOPOULOS N and TOULIOS L (2013) A spatial downscaling procedure of MODIS derived actual evapotranspiration using Landsat images at central Greece. Proceedings of SPIE - *The International Society for Optical Engineering* - August 2013. DOI: 10.1117/12.2027536.

SU Z and JACOBS C (2001) Advanced Earth Observation– Land Surface Climate. Report USP-2, 01-02, *Publications of the National Remote Sensing Board* (BCRS). 184pp.

SU Z (2002) The Surface Balance Energy System (SEBS) for estimating turbulent heat fluxes. *Hydrology and Earth System Sciences*. **6**(1): 85-99.

SU Z and WANG L (2013) Earth Observation of Water Resources (SEBS). Practical Session Instructions (July 2013). ITC. University of Twente. The Netherlands.

TIMMERMANS WJ AND MEIJERINK AMJ (1999) Remotely sensed actual evapotranspiration: Implications for groundwater management in Botswana. *International Journal of Applied Earth Observation and Geoinformation* **1**: 222–233.

UNITED STATES GEOLOGICAL SURVEY (USGS) (2015) Landsat 8 (l8) Data Users Handbook. Version 1.0. June 2015.

VAN DER KWAST J, TIMMERMANS W, GIESKE A, SU Z, OLIOSO A, JIA L, ELBERS J, KARSSENBERG D AND DE JONG S (2009) Evaluation of the Surface Energy Balance System (SEBS) applied to Aster imagery with flux-measurements at the SPARC 2004 site (Barrax, Spain). *Hydrology and Earth System Sciences* **13**(7): 1337-1347.

WAGLE P, BHATTARAI N, GOWDA PH and KAKANI VJ (2017) Performance of five surface energy balance models for estimating daily evapotranspiration in high biomass sorghum. *ISPRS Journal of Photogrammetry and Remote Sensing* **128**: 192–203.

YANG D, CHEN H and LEI H (2010) Estimation of evapotranspiration using a remote sensing model over agricultural land in the North China Plain. *International Journal of Remote Sensing* **31**(14): 3783–3798.

ZHUO G, BA L, CIREN P AND BU L (2014) Study on daily surface evapotranspiration with SEBS in Tibet Autonomous Region. *Journal of Geographical Sciences* **24**(1): 113-128.

*****

Lead into chapter 4: The integration of the *ESF* values into $SEBS_0$ was shown to considerably improve the representation of modelled ET estimates within the study area. With the ability of the modified version of SEBS, to more adequately represent ET within the study area confirmed (chapter 3), the objective of chapter 4 was to quantify seasonal and spatial variations in plant water use dynamics through the development of a satellite-derived ET time series and stable isotope analysis. Supplementary information and/or data which was used during the various analyses undertaken in this chapter but not presented herein, are provided in Appendices A and B.

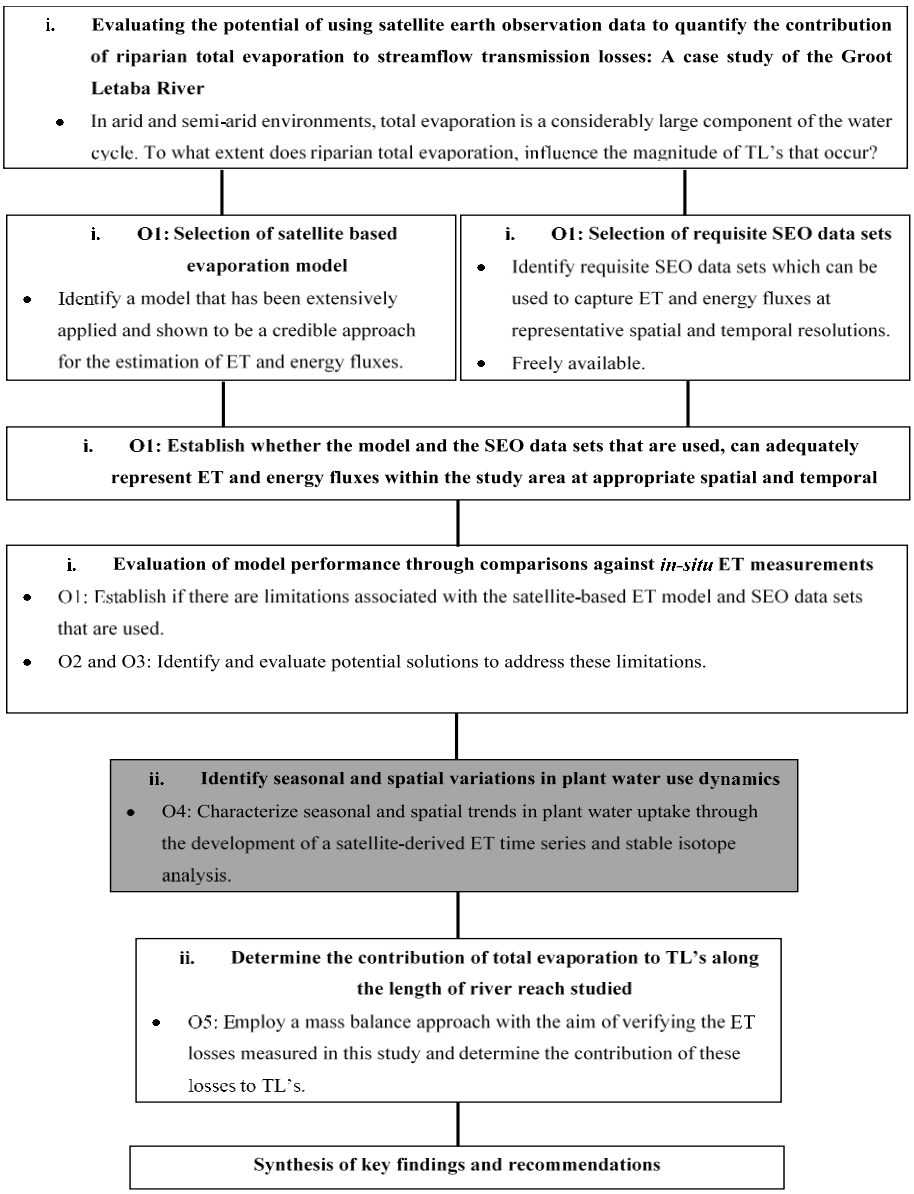

4. ESTIMATING GROUNDWATER CONTRIBUTION TO TRANSPIRATION USING SATELLITE-DERIVED EVAPOTRANSPIRATION ESTIMATES COUPLED WITH STABLE ISOTOPE ANALYSIS[3]

S Gokool[1], ES Riddell[1&2], A Swemmer[3], JB Nippert[4], R Raubenheimer[5] and KT Chetty[1]

[1]School of Agriculture, Earth and Environmental Sciences, Centre for Water Resources Research, University of KwaZulu-Natal, Pietermaritzburg, South Africa

[2]Conservation Management, South African National Parks, Skukuza, South Africa

[3]South African Environmental Observation Network (SAEON), Ndlovu Node, Phalaborwa, South Africa

[4]Division of Biology, Kansas State University, Manhattan, USA

[5] GCS Consulting, Pretoria

Corresponding Author: Shaeden Gokool, shaedengokool@gmail.com, University of KwaZulu-Natal, Pietermaritzburg, South Africa, 3201

ABSTRACT

The relative importance of groundwater (GW) to sustain terrestrial vegetation has been well documented. However, quantifying GW use by riparian vegetation in data scarce regions may prove to be challenging. For this purpose, we coupled evapotranspiration (ET) estimates from the satellite-based surface energy balance system (SEBS) model with stable isotope analysis, to map and quantify the contribution of GW to transpiration (ET_g), along the lower reaches of a perennial river system, in the semi-arid north-eastern region of South Africa. Plant stem, soil, stream and GW samples were collected on 3 sampling occasions during the 2016 dry season. δ^2H and $\delta^{18}O$ values of the respective samples were measured and analysed.

3S Gokool, ES Riddell, A Swemmer, JB Nippert, R Raubenheimer and KT Chetty. 2017. Estimating groundwater contribution to transpiration using satellite-derived evapotranspiration estimates coupled with stable isotope analysis. *Accepted for publication in Journal of Arid Environments*

*Referencing conforms to format of Journal of Arid Environments

*It should be noted that minor variations in the text may exist between the published version of the manuscript and the version presented herein, due to recommendations put forward by the examiners of the thesis.

We found that while GW use was prevalent and increased with aridity, overall ET_g was fairly minimal. During the initial stages of the dry season ET_g for the study area was extremely low, approximately 0.10 % of daily ET or 0.01 mm d^{-1}. However, as aridity increased, ET_g increased to approximately 10 % of daily ET or 0.30 mm d^{-1}. The results of these various investigations undertaken demonstrates the potential of coupling satellite-based ET approaches with stable isotope analysis, to quantify spatial and seasonal dynamics in ET_g.

Keywords: **SEBS, Satellite-based ET, Stable isotopes, Riparian vegetation, Groundwater dependency**

4.1 Introduction

In arid and semi-arid environments groundwater (GW) is often the most important source of freshwater for human consumption and vegetation and makes a significant contribution to streamflow (Lange et al., 2005). Therefore, balancing the amount of GW that is used for basic human needs with environmental water requirements (EWR) is crucial for successful water resource management in these regions (Tanner and Hughes, 2015). According to Eamus et al. (2015), quantifying seasonal and spatial variations GW consumption by vegetation is one of the key areas which can facilitate the sustainable management of GW resources, especially the EWR flow allocations of this resource.

In the last decade, ET estimation, has substantially benefited from advancements in satellite earth observation techniques (SEO) (Nourhi et al., 2013). SEO techniques can be used to quantify the water use of riparian vegetation and are often utilized to overcome spatial limitations generally associated with conventional approaches, such as *inter alia*; FAO 56 Penman Monteith reference evaporation, eddy covariance, scintillometry (Allen et al., 1998; Savage et al., 2004; Fernández-Prieto et al., 2012; Jassas et al., 2015). Furthermore, SEO can be used to acquire data in remote and data scarce regions, as well as allowing for seasonal and inter-annual comparisons of hydro-meteorological variables due to the periodic updating of information (Gokool et al., 2017).

Despite these advantages, the trade-off between the spatial and temporal resolution of available imagery and the ability of the models to accurately estimate fluxes and ET in different environmental settings, may limit the use of SEO technologies to guide water resources management decisions (Gokool et al., 2017).

While there exist approaches to address these limitations and improve upon the accuracy of ET estimates (Hong et al., 2011; Pardo et al., 2014; Gokool et al., 2017), the ET estimate provided is often the total water used from multiple sources such as; soil water, GW or stream water. Therefore, the ET estimate acquired by these techniques requires further disaggregation to determine ET_g (Eamus et al., 2015).

Several studies have identified approaches to quantify subsurface moisture dynamics at varying spatial and temporal scales, because the movement of water in the soil-root system plays a significant role in regulating ecohydrological processes at the surface (Kumar et al., 2014; Daly et al., 2017). These techniques include; conventional approaches (time-domain reflectometry, gravimetric methods and neutron probes), isotope hydrology, geophysical techniques (electrical resistivity imaging), the cosmic ray probe, SEO data and root water uptake models (Robinson et al., 2012; Villarreyes et al., 2013; Kumar et al., 2014; Mares et al., 2016; Daly et al., 2017; Zhang et al., 2017).

Isotope hydrology and in particular environmental isotopes (stable and radioactive) techniques are amongst the most effective and frequently used tools to understand and quantify soil-plant-water dynamics (Yang et al., 2010; Penna et al., 2013). While both radioactive and stable isotopes have been extensively applied for ecohydrological investigations (Marwick et al., 2015; Thaw et al., 2016; Zhang et al., 2017; Evaristo and McDonnell, 2017), the use of stable isotope techniques has generally been applied more frequently for quantifying the depth and sources of water uptake for transpiration (Penna et al., 2013; Thaw et al., 2016).

For most species and locations, the uptake of water during transpiration does not generally result in the fractionation of oxygen-18 (^{18}O) and deuterium (^{2}H) within non-photosynthesising tissue (Evaristo and McDonnell, 2017). The isotopic composition of ^{18}O and ^{2}H of xylem water should represent the sources present within the root zone (Evaristo and McDonnell, 2017). Although this assumption has been supported and well documented in various soil-plant-water interaction studies (Zimmerman et al., 1966, White et al., 1985; Walker and Richardson, 1991; Dawson et al., 2002), it should be noted that certain plant species within particular environmental settings may fractionate ^{2}H during root water uptake (see: Lin and Sternberg, 1993; Ellsworth and Williams, 2007; Zhao et al., 2016; Evaristo et al., 2017).

In this study, we aimed to quantify ET_g along the riparian zone situated in the lower reaches of a perennial river system in the semi-arid north-eastern region of South Africa, employing a relatively simplistic approach that required two independent types of data; (i) daily estimates of ET and (ii) the stable isotopic composition of ^{18}O and ^{2}H of xylem water from all possible sources. Once the proportional contribution of these sources to the xylem water has been established, ET_g could be derived as the product of the GW proportion and ET (Eamus et al., 2015).

Based on the aforementioned approach, we implemented the satellite-based Surface Energy Balance System (SEBS) Model and two approaches, to quantify daily ET at a moderate spatial resolution (MSR) (Gokool et al., 2017). ET estimates acquired from these approaches were evaluated against *in-situ* measurements of ET acquired from a one-sensor (excludes Infra-Red Gas Analyzer) Eddy Covariance system (EC_{ET}), in order to determine which approach most adequately represented the ET for the portion of river reach studied. During a separate investigation, we coupled isotope analysis of ^{18}O and ^{2}H with a Bayesian mixing model to determine the proportional contribution of water sources to transpiration.

The results from these investigations were then used to provide insights on spatial and seasonal dynamics in ET_g within the study area. Furthermore, the timing of this study also coincided with a large El Nino induced drought period (Kogan and Guo, 2016), providing further insights into plant water use dynamics during extreme drought conditions.

4.2 Methodology

4.2.1 Study Area

The study site is situated in the Limpopo Province in the north-eastern region of South Africa, along the lower reaches of the Groot Letaba River between Letaba Ranch (B8H007; 23.658^0 S; 31.047^0 E) and Mahale (B8H007; 23.669^0 S; 30.991^0 E) weirs, as depicted in Figure 4.1. According to Pollard and du Toit (2011), the Letaba River system often experiences water shortages and restrictions and has frequently been unable to meet its EWR. Therefore, understanding and accurately quantifying the dynamics of vegetation water use requirements in this region, is essential to maintain the natural functioning of this environment. A semi-arid climate, characterized by hot wet summers and mild dry winters is experienced across the region. Mean annual temperatures vary across the region ranging from 18 ^{0}C in the mountainous areas to 28 ^{0}C in the eastern regions (Katambara and Ndiritu, 2010).

A majority of the rainfall occurs in the summer months (October to March) and is predominantly characterized by thundershowers occurring from the north and north-east, as well as from tropical cyclones originating over the Indian Ocean (Katambara and Ndiritu, 2010; February et al., 2007). According to Heritage et al. (2001) approximately three quarters of the catchment is underlain by granite and gneiss. There exists a variety of morphological units within the study area which is due to the varied distribution of sediment along the river.

The portion of the Groot Letaba River flowing through the study area is largely characterized by alluvial channel types (Heritage et al., 2001). The study area was categorized into three separate geomorphological zones during sampling. These were; i) the near stream northern and ii) southern banks which includes the alluvial terrace situated adjacent to the active stream channel, as well as iii) within the active river channel.

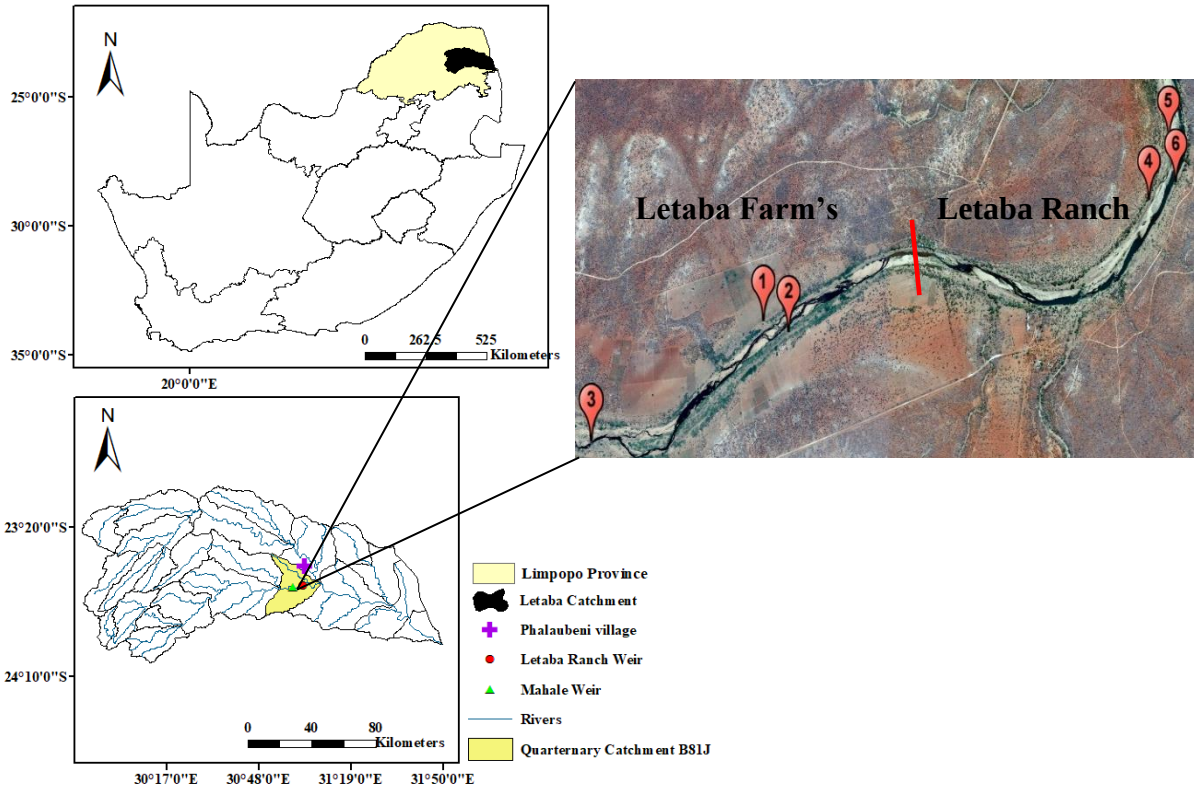

Figure 4.1 Location of the study area and stable isotope sampling points (Google Earth ™ image), situated along the lower reach of the Groot Letaba River within the Quaternary catchment B81J (adapted from Schulze et al., 1997)

The total area of the river channel and riparian zone contributing to ET was estimated to be approximately 1.96 km^2. This was calculated by summing up the width of the river channel (approximately 60 m and constitutes 50 % vegetation, 30 % bare soil and 20 % open water) and riparian zone (40 m on either side of the channel and complete vegetation coverage) and multiplying it by the longitudinal distance of the portion of river reach studied between the two weirs (~14 000 m) (Gokool et al., 2017; Riddell et al., 2017).

A variety of woody plant species were situated along geomorphological zones i and ii. The common species included; *Ficus sycomorus, Philenoptera violacea, Diospyros mespiliformis, Colophosphermum mopane, Combretum microphyllum, Gymnosporia senegalensis, Cassia abbreviata and Ziziphus mucronata*. While the predominant plant species situated within geomorphological zone iii is *Phragmites mauritianus*. Additionally, numerous agricultural fields, predominantly planted with *Cucurbita moschata* and *Medicago sativa* are situated further away from the active river channel. These were however not considered during sampling. Although the abundance of the trees within the study area (given as a percentage of total land cover) was not provided, the trees that were sampled are the predominant vegetation found within the study area.

43 individual trees from the abovementioned species; 9 *F. sycomorus*, 8 *P. violacea*, 10 *D. mespiliformis*, 3 *C. mopane*, 3 *C. microphyllum*, 5 *G. senegalensis* and 5 *Z. mucronata* distributed among the six sampling regions, were randomly selected and sampled for subsequent stable isotope analysis (Lin et al., 2016). These sampling regions were categorized, according to their respective locations with regards to Letaba Farm (20 trees) and Letaba Ranch (26 trees). Figure 4.1 provides a Google Earth™ illustration of the sampling regions distributed between the farming areas and Letaba Ranch.

4.2.2 Estimation of daily ET using satellite earth observation data

SEBS was applied in this study to estimate daily ET. Su (2002) provides a detailed conceptualization of the model. However, the underlying principle of SEBS, is to compute all components of the shortened surface energy balance (Equation 4.1), as well as the evaporative fraction (*EF*), using land surface parameters which are derived from meteorological and SEO sources, respectively (Su, 2002).

$$R_n = G_0 + H + \lambda E \quad (4.1)$$

Where Rn is net radiation (W m^{-2}), G_0 is soil heat flux (W m^{-2}), H is sensible heat flux (W m^{-2}) and λE is the latent heat flux (W m^{-2}).

The original SEBS formulation ($SEBS_0$) has been widely implemented and shown to be a credible approach for the estimation of regional fluxes and ET. However, studies have shown, that the model may over-estimate the *EF* and consequently the ET during conditions of water stress, as it is unable to adequately account for the influence of soil moisture availability and biophysical characteristics during the estimation of ET (Pardo et al., 2014; Gokool et al., 2017). Consequently, a modified version of SEBS ($SEBS_{ESF}$), which was proposed as a means to improve upon ET estimation for water limited environments, was applied in this study. The $SEBS_{ESF}$ approach detailed in Riddell et al. (2017) attempts to improve upon the estimation of the *EF* and daily ET, through the integration of a calibration factor in $SEBS_0$, so that the influence of environmental stress is more adequately represented during the estimation of ET.

Daily ET estimates were derived in $SEBS_{ESF}$ using SEO data acquired from both Landsat and MODIS, as well as meteorological data measured *in situ* (Riddell et al., 2017). 215 clear sky MODIS Level 1 B Terra images (MOD21 and MOD 03 data products, available daily at a 1 km spatial resolution), as well as 26 clear sky Landsat (7 and 8) Level 1 GeoTiff images (available every 16 days at a 30 m spatial resolution) were acquired, during 2015 and 2016 (18^{th} June to 31^{st} October). Pre-processing and processing of these images were undertaken based on the procedures detailed in Su and Wang (2013), Singh et al. (2014) and USGS (2015).

Although the use of Landsat and MODIS data in SEBS facilitates the relatively timeous and inexpensive quantification of ET. The spatial and temporal resolutions associated with these data sets may limit their feasibility to estimate ET for operational water resources management (Gokool et al., 2017). In order to, overcome these limitations; two techniques *viz.* a simple output downscaling with linear regression (ODLR) and the actual crop coefficient (Kc_{act}) approach as described in Gokool et al. (2017) were applied and evaluated.

The daily ET estimates derived from implementing $SEBS_{ESF}$ were used as inputs to these approaches to produce a time-series of daily ET at a MSR. The ODLR and Kc_{act} derived ET estimates were then evaluated through statistical comparisons with EC_{ET}. Only the values from satellite-pixels covering the location of the EC system were used during data comparisons.

The results from these investigations were then used to determine which approach most adequately represented the riparian ET within the study area. A detailed description of the instrumentation setup, study site and data collection for ET and meteorological variables is given in Gokool et al. (2017) and Riddell et al. (2017).

4.2.3 Water sampling and isotope analyses

Plant stem/s, soil, stream and GW samples were collected on 3 sampling occasions during the 2016 dry season (in May, August and October) which were representative of the late autumn, late winter and mid spring seasons, respectively in the study area.

During this period (from May to October) the study area usually experiences drier conditions and low flows, a critical period with regards to water shortages. From the 43 individual trees, twig samples of mature wood approximately 0.30 to 1.00 cm in diameter and 4.00 to 7.00 cm in length were collected. These samples were collected from randomized locations from each tree and the epidermis was removed immediately, before being transferred into small airtight glass vials (Lin et al., 2016). Soil samples at depths of 30, 60, 100 and 140 cm were collected concurrently with the twig samples. The soil samples were obtained using a hand auger and then transferred and sealed into airtight 500 ml plastic bottles.

Stream samples were collected at sampling points 1, 3 and 6 and stored in airtight 500 ml plastic bottles. Each sample bottle was rinsed three times with the sample water before the actual sample was taken. GW samples were collected from 5 boreholes situated adjacent to the active river channel at sampling points 1, 3, 4 and 5, as well as from a borehole situated within the active river channel at sampling point 6. The boreholes were purged, ensuring steady state chemical conditions (stable electrical conductivity and pH) were reached, so that a GW sample representative of the surrounding aquifer could be collected.

These samples were then stored in airtight 500 ml plastic bottles. In order to ensure that an unevaporated sample was collected from the borehole, the pump was left to run continuously while the representative sample was being collected (Riddell et al., 2016). The various samples collected in field were stored in a cooler bag and then stored in a fridge prior to transportation to the laboratory for analysis in the following days. Rainfall data for the study area was collected from a Davis^{TM} Vantage Pro2 station situated in Phalaubeni, approximately 6 km north of the study site.

However, there were very few rain events experienced on site due to the drought. Consequently, only a limited number of samples were available for analysis. 10 rainfall samples from 15th November 2015 to 19th May 2016 were collected and analysed. The δ^2H and $\delta^{18}O$ values for these precipitation events were then used to construct a local meteoric water line (LMWL) for the study site. The δ^2H and $\delta^{18}O$ values for all samples were then plotted and compared relative to this LMWL.

^2H and ^{18}O contents of rainfall, stream and GW samples were measured using a Los Gatos Research (LGR) DLT-100 Liquid Water Isotope Analyser. Plant stem and soil waters were extracted using a 2-step cryogenic open manifold system that facilitated the removal of non-condensable gases and potential organic contaminants (Nippert and Knapp, 2007). This extraction procedure minimizes the likelihood of organic molecules influencing the isotopic signature of the water extracted from plants and soils. Furthermore, the "ChemCorrect" software offered by Picarro, was used to screen the samples post-analysis (West et al., 2011), to identify samples that should be excluded from further analysis.

^2H and ^{18}O contents of the xylem water and soil water were measured using a Picarro L1102-i CRDS analyser (Picarro, Santa Clara, California, USA). The overall analytical precision of both the spectrometers was less than 2 permil ($0.002^{‰}$) for ^2H and less than 0.3 permil ($0.0003^{‰}$) for ^{18}O.

The ^2H and ^{18}O of the various samples (^2H and ^{18}O) were expressed in delta notation relative to the Vienna Standard Mean Oceanic Water (VSMOW), as:

$$\delta = \left(\frac{R_{sample}}{R_{standard}} - 1\right)*1000 \quad (4.2)$$

Where δ (expressed in ‰ notation) represents changes in the ratio of the uncommon to common isotopes ($^2H/^1H$ and $^{18}O/^{16}O$) for the sample (R_{sample}) and standard ($R_{standard}$).

The freely available stable isotope mixing model package in R (Simmr), which has been designed to solve mixing equations for stable isotope data using a Bayesian statistical framework (Parnell and Inger, 2016), was used to identify proportional contributions of sources to transpiration. Bayesian mixing models such as Simmr possess several advantages over conventional linear mixing models, such as their ability to quantify; i) the proportional contribution of water sources to transpiration, ii) account for uncertainties associated with the sources and iii) allow for the input of isotope data from multiple sources (Ma and Song, 2016).

The Simmr package requires three sets of input data as a minimum, to determine the proportions of water used from a particular source, this includes; i) δ^2H and $\delta^{18}O$ of the xylem water, ii) mean δ^2H and $\delta^{18}O$ for the various sources and iii) standard deviations of δ^2H and $\delta^{18}O$ for the various sources (Parnell and Inger, 2016). The isotopic composition of GW and stream water was found to be statistically different (non-parametric Mann-Whitney test $p < 0.05$).

Similarly, soil δ^2H and $\delta^{18}O$ values at each of the depth regions that were sampled were found to be statistically different from each other (Mann-Whitney test $p < 0.05$). Consequently, the potential sources of water used during transpiration were considered to be soil water (at each depth region sampled), GW and stream water (Penna et al., 2013; Phillips et al., 2014; Zhang et al., 2017). Simmr was implemented with 100 000 iterations (discarding the first 10 000), no prior information was used to guide the model, thus all sources had an equal likelihood of contribution (Zhang et al., 2017). Trophic enrichment factors and concentration dependence values were set to zero.

The estimated proportions of source contribution to the xylem mixture were Consequently determined using a Markov Chain Monte Carlo function to repeatedly estimate the proportions of the various sources in the mixture and determine the values which best fit the mixture data (Parnell and Inger, 2016). The median (50 % quantile) source contribution value determined for each of the sources was then used during analytical comparisons and subsequent investigations.

4.3 Results

4.3.1 Estimation of daily ET using satellite earth observation data

Statistical comparisons between the Kc_{act} and ODLR ET estimates against the EC_{ET} are presented in Table 4.1. The implementation of $SEBS_{ESF}$ resulted in an improved estimation of the daily ET derived at a MSR for both the Kc_{act} and ODLR approaches, as illustrated in Figure 4.2. The correlation between modelled and observed ET, improved from 0.48 to 0.79 and 0.30 to 0.74, respectively for Kc_{act} and ODLR ET estimates. Furthermore, there was a significant increase in Nash-Sutcliffe efficiency values. While the use of $SEBS_{ESF}$ ET estimates as inputs to the Kc_{act} and ODLR approaches, resulted in an improved estimation of the daily ET at a MSR. The Kc_{act} approach was selected to quantify daily ET, due to the reduced bias and higher correlations achieved between the modelled and observed ET.

Table 4.1 Statistical comparison of Kc_{act} and ODLR ET estimates derived from implementing $SEBS_0$ and $SEBS_{ESF}$, against EC_{ET} during the 2015 and 2016 period of investigation

	Kc_{act} ET derived from $SEBS_0$	Kc_{act} ET derived from $SEBS_{ESF}$	ODLR ET derived from $SEBS_0$	ODLR ET derived from $SEBS_{ESF}$
RVE	-72.24	-5.82	-100.25	8.40
Bias	1.10	0.62	1.68	0.76
RMSE	1.35	0.87	2.03	1.04
Kruskal-Wallis (p value)	0.00	0.60	0.00	0.05
Correlation Coefficient	0.48	0.79	0.30	0.74
Nash-Sutcliffe	0.03	0.60	-1.21	0.42

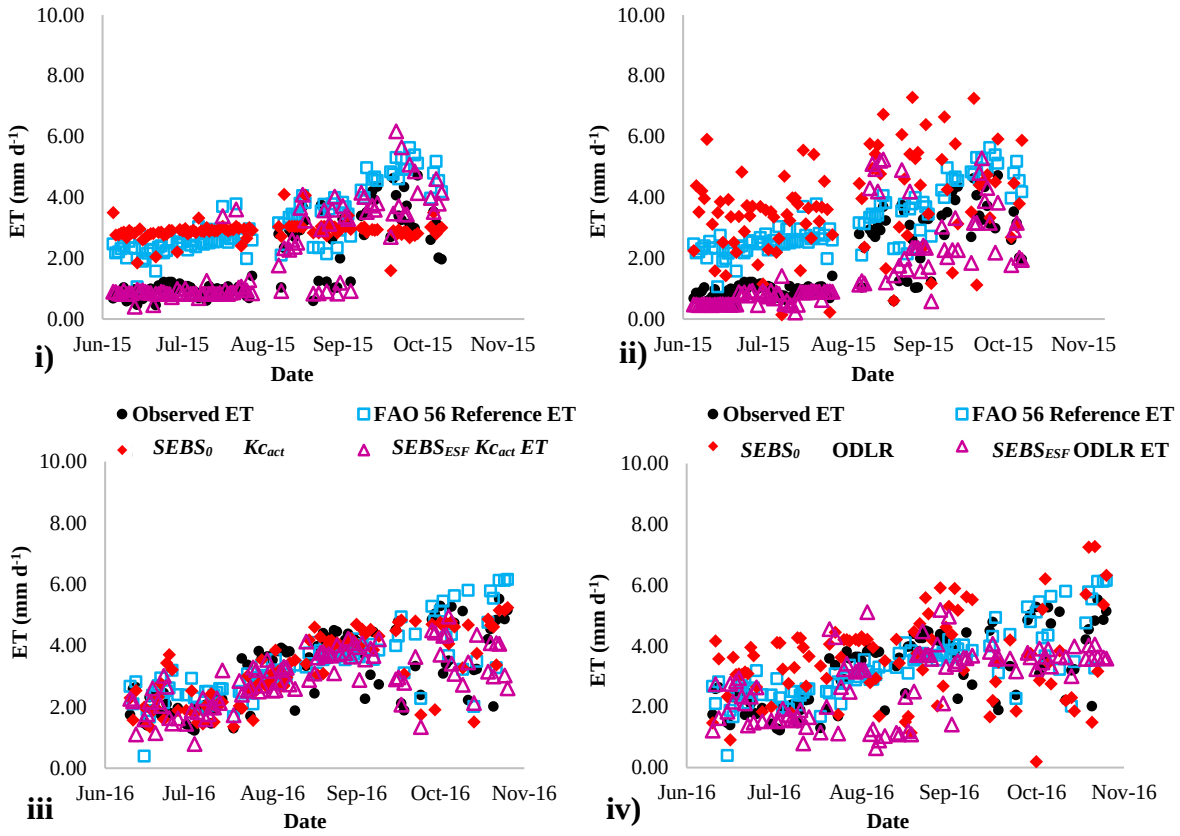

Figure 4.2 A comparison of observed and modelled ET derived using the Kc_{act} and ODLR approaches during the 2015 (i and ii) and 2016 (iii and iv) period of investigation

4.3.2 Isotopic composition of water

δ^2H in rainfall ranged from -22.9 to 15.30 ‰, with a mean value of 0.20 ‰ (± 11.60 ‰), whereas $\delta^{18}O$ in rainfall ranged from -4.30 to 0.90 ‰, with a mean value of -1.70 ‰ (± 1.60 ‰). The LMWL for our study site, as shown in Figure 4.3, was established as $\delta^2H = 7.06\delta^{18}O + 12.13$, with a R^2 value of 0.89.

The slope of the LMWL is lower than the slope of the global meteoric water line, described respectively in Craig (1961) and Liu et al. (2014), as $\delta^2H = 8\delta^{18}O + 10$ and $\delta^2H = 7.94\delta^{18}O + 3.92$. This can be attributed to rapid evaporation of falling raindrops (Ma and Song, 2016), which would be expected in this semi-arid region. Due to the limited number of rainfall samples collected, the LMWL that was generated may not be representative of the conditions experienced during the collection of the other isotope samples.

Consequently, we also plotted the Pretoria meteoric water line described in Mekiso et al. (2015), as $\delta^2H = 7.05\delta\ ^{18}O + 7.60$ (Figure 4.3), for a site approximately 400 km away and based on a far longer time series, so that any regional climatic differences in the rainfall received within our study site could also be determined. Rainfall during the study period was generally dominated by convective rainfall with lighter isotopes, the exception being the rain during March and a single event in May 2016 which had a much more depleted signature.

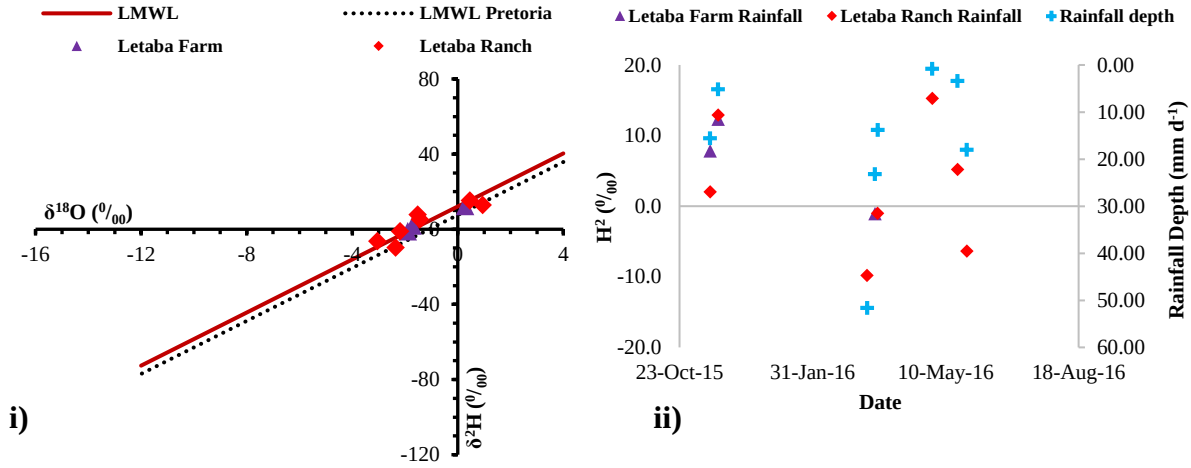

Figure 4.3 i) Stable isotopes of rainfall during the study period against LMWL and ii) time-series comparison

The δ^2H and $\delta^{18}O$ of stream water, soil water and xylem water plot below the LMWL, showing evaporative enrichment in these samples relative to rainfall (Figure 4.4). δ^2H and $\delta^{18}O$ values for GW plot closest to the LMWL providing evidence that precipitation is one of the principal sources to GW. δ^2H in surface water ranged from -9.16 to 9.48 ‰, with a mean value of -1.32 ‰ (± 6.78 ‰). Whereas $\delta^{18}O$ in surface water ranged from -1.85 to 2.75 ‰, with a mean value of 0.19 (± 1.79 ‰).

δ^2H in soil water (30, 60, 100 and 140cm) ranged from -53.00 to 7.00 ‰, with a mean value of -23.95 ‰ (± 14.89 ‰). Whereas $\delta^{18}O$ in soil water (30, 60, 100 and 140 cm) ranged from -6.90 to 7.90 ‰, with a mean value of -1.06 (± 3.25 ‰). δ^2H and $\delta^{18}O$ in soil water were enriched in the top soil layers and generally depleted with depth. The higher levels of enrichment associated with the δ^2H and $\delta^{18}O$ values of soil water in the upper soil layers are due to the effects of evaporation at the surface.

This observation is reaffirmed by the lower slope of the fitting line of the soil water δ^2H and $\delta^{18}O$ (SEL) relationship in comparison to the LMWL (Figure 4.4), being indicative of the strong evaporation effect on soil moisture which is characteristically associated with semi-arid regions. The higher levels of depletion generally associated with soil water deeper down the profile could presumably be attributed to deep preferential infiltration of heavy rainfall events.

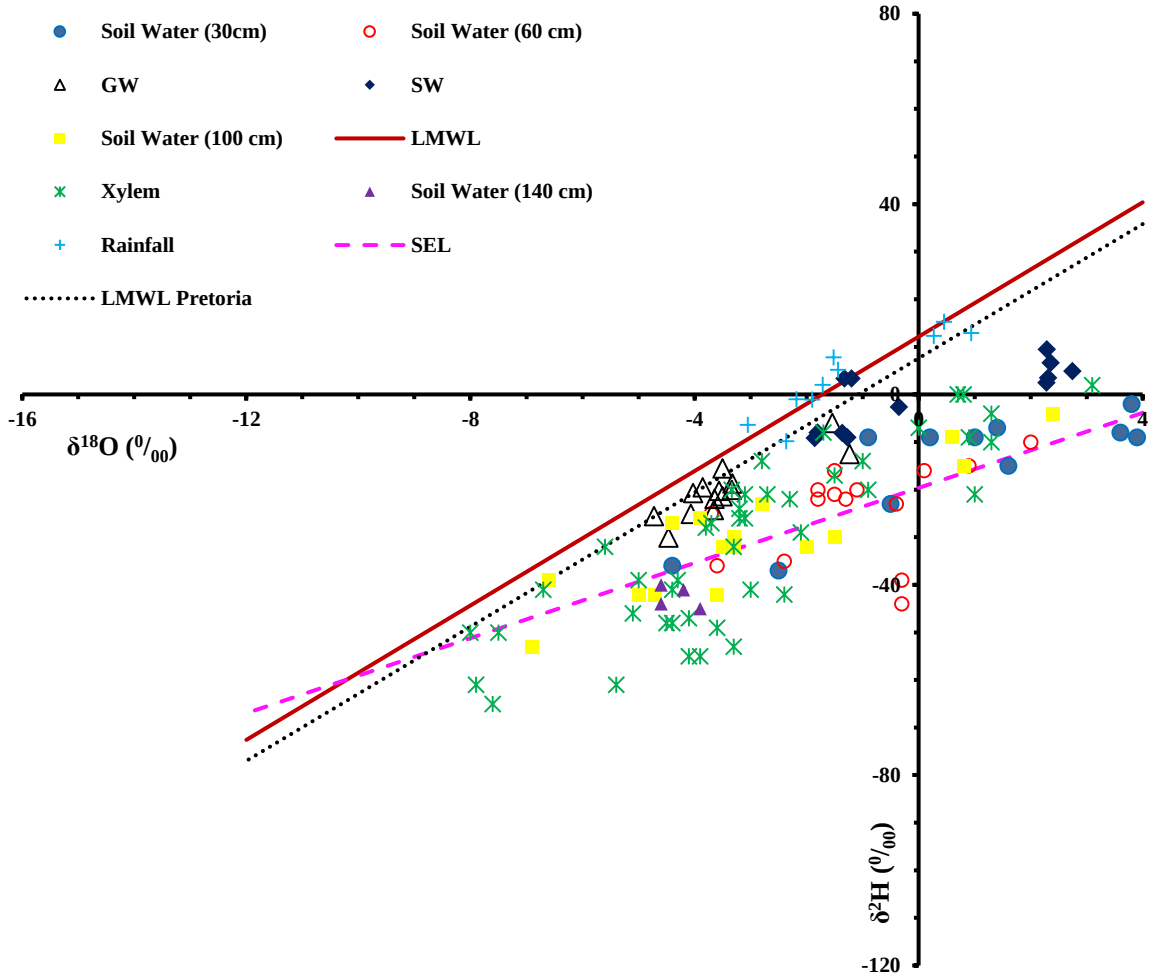

Figure 4.4 A plot of the relationship between δ^2H and $\delta^{18}O$ values for all water samples

δ^2H in xylem water ranged from -65.00 to 6.00 ‰, with a mean value of -29.56 ‰ (± 19.65 ‰). $\delta^{18}O$ in xylem water ranged from -8.00 to 6.20 ‰, with a mean value of -2.63 (± 3.19 ‰). The isotopic composition of δ^2H and $\delta^{18}O$ in the xylem water were shown to generally plot closest to the SEL (Figure 4.5), indicating that soil water is one of the main contributors to ET. δ^2H and $\delta^{18}O$ values of xylem water were generally concentrated around an uptake depth between 60 and 140 cm. This observation is reaffirmed by the results of the proportional contributions of sources to ET, shown in Table 4.2.

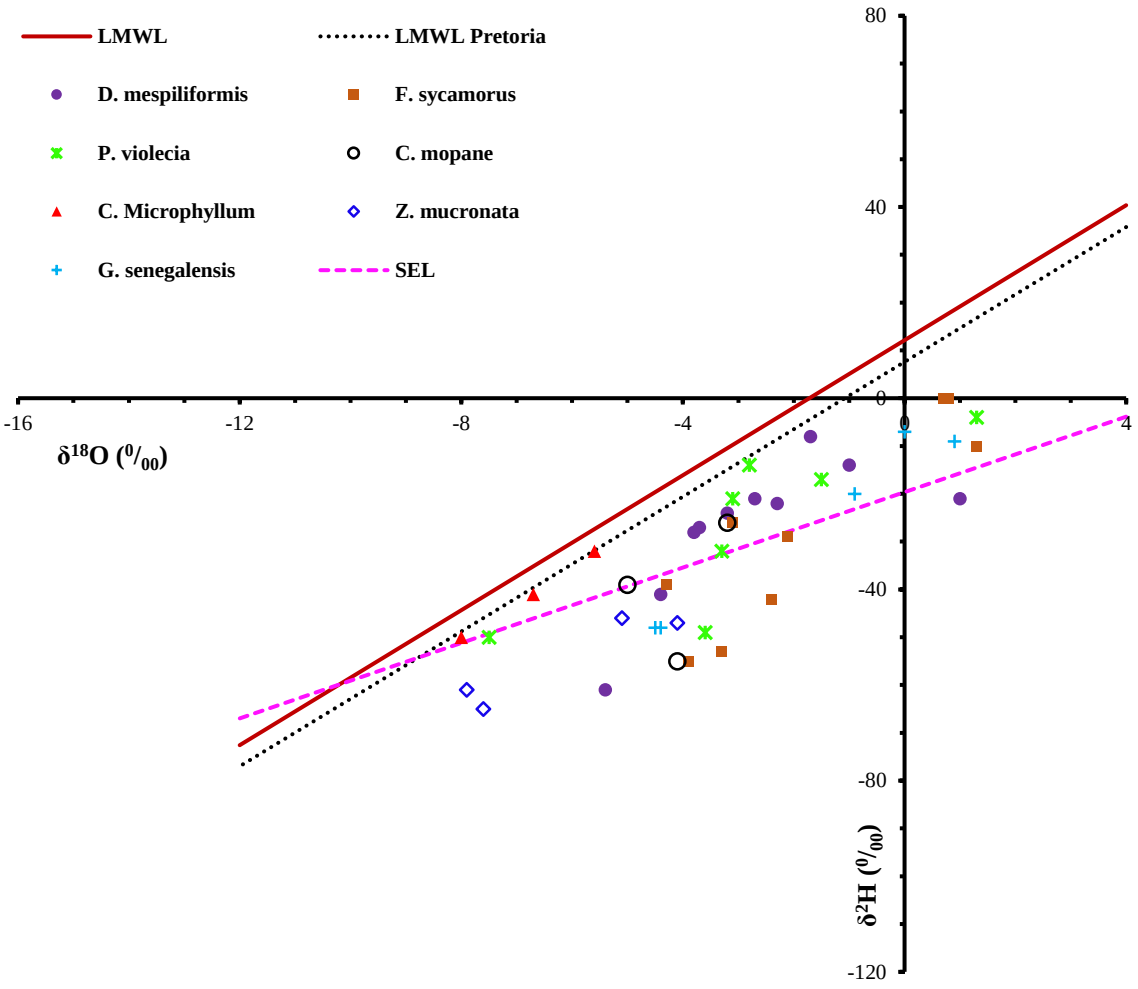

Figure 4.5 A plot of the relationship between δ^2H and $\delta^{18}O$ values for individual plant species

Table 4.2 Average proportional contribution of sources to individual plant species for the three sampling campaigns

Tree Species	Ground Water	Surface Water	Soil Water (30cm)	Soil Water (60cm)	Soil Water (100cm)	Soil Water (140cm)
F. sycamorus	1.50 %	1.70 %	1.60 %	1.70 %	72.40 %	20.20 %
P. violecia	4.40 %	3.50 %	4.90 %	5.60 %	73.60 %	5.40 %
D. mespiliformis	2.30 %	2.90 %	2.60 %	2.80 %	70.00 %	17.50 %
C. mopane	1.10 %	0.70 %	1.50 %	2.00 %	3.80 %	89.50 %
C. Microphyllum	1.20 %	0.90 %	1.50 %	1.90 %	16.10 %	77.50 %
G. senegalensis	1.50 %	1.70 %	1.60 %	1.80 %	67.00 %	25.40 %
Z. mucronata	1.10 %	0.60 %	1.50 %	2.00 %	3.30 %	90.00 %

4.4 Discussion

It has been shown that the water uptake patterns vary considerably amongst the trees that were sampled. However, these results could not be combined with the satellite-derived ET estimates to determine seasonal variations in ET_g for each plant species due to the mixed-pixel effect (Gibson et al., 2011). Due to this limitation, seasonal variations in ET_g at each location, as well as for the entire study area were quantified instead. Location specific δ^2H and $\delta^{18}O$ values of xylem and source waters were used as inputs to a mixing model (Simmr) to determine the proportional contribution of GW to ET during each month (Table 4.3). ET_g was then determined as the product of these values and the average daily ET for each month, as shown in Figure 4.6.

During the three sampling campaigns soil water was found to be the major contributing source to ET at each sampling location (approximately 88 %). Whereas GW contribution to ET was relatively low ranging from 0.20 to 10.00 %. The average daily ET_g during these periods ranged from 0.00 to 0.38 mm d^{-1}, with a mean value of 0.12 mm d^{-1}. Whereas average daily ET along the river reach ranged from 1.78 to 3.70 mm d^{-1}, with a mean value of 2.89 mm d^{-1}. Although GW contribution to ET was fairly low, it is evident that there are seasonal changes in water uptake patterns at each sampling location.

Table 4.3 Proportional contribution of sources to ET during the three sampling campaigns

	Location	Ground Water	Surface Water	Soil Water (30cm)	Soil Water (60cm)	Soil Water (100cm)	Soil Water (140cm)
May	1	1.40%	1.00%	2.00%	1.00%	1.20%	89.00%
	2	0.40%	17.50%	0.40%	0.40%	80.80%	0.30%
	3	0.20%	0.10%	0.60%	1.20%	0.10%	97.00%
	4	0.80%	41.00%	0.80%	0.90%	54.60%	1.70%
	5	1.30 %	1.70 %	1.40 %	1.50 %	56.70 %	36.40 %
	6	2.10%	0.70%	10.80%	22.20%	62.40%	1.10%
Aug	1	8.30%	8.50%	43.00%	6.20%	22.70%	8.50%
	2	10.20%	6.00%	11.30%	25.00%	17.00%	26.00%
	3	2.00%	3.00%	1.60%	1.80%	6.20%	85.00%
	4	6.00%	3.00%	14.00%	30.00%	42.00%	3.40%
	5	0.50%	0.50%	0.50%	0.70%	67.10%	30.40%
	6	6.10%	1.50%	32.60%	53.90%	2.90%	1.90%
Oct	1	6.10%	4.00%	8.00%	7.40%	9.00%	61.00%
	2	4.20%	2.20%	5.00%	6.00%	4.00%	76.00%
	3	0.90%	1.20%	0.90%	0.10%	43.00%	53.00%
	4	7.00%	14.00%	6.10%	6.10%	8.00%	56.00%
	5	0.30%	0.20%	0.40%	0.40%	40.20%	58.30%
	6	10.40%	6.00%	15.00%	20.00%	31.00%	12.00%

This occurrence can be largely attributed to the antecedent moisture conditions experienced at the study site (Chimner and Cooper, 2004; McLendon et al., 2008). Rainfall received in the study area from June 2015 till October 2016 was extremely low as shown in Figure 4.7, with approximately 180 mm received during this period. However, a significant proportion of this rainfall was received from a single high magnitude event during March 2016, with only 73 mm being received prior to this event.

The rainfall received from this high magnitude event and the minor contributions from subsequent events, would have significantly increased soil water availability during the initial stages of the dry season, compared to the rest of study period (Riddell et al., 2017). Consequently, during May there was minimal ET_g; however, as the dry season progressed and aridity increased, there was an increase in GW uptake to fulfil a portion of the daily transpiration demand.

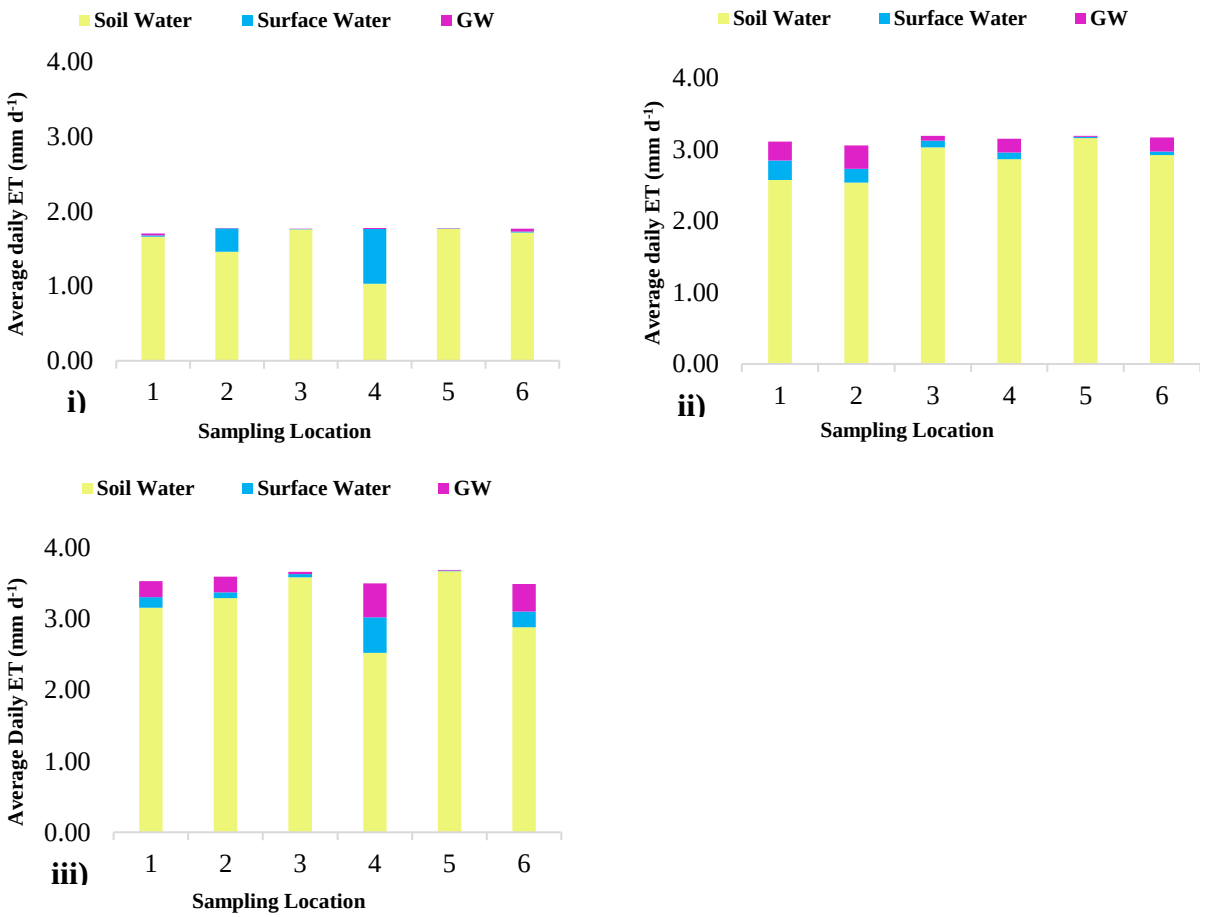

Figure 4.6 Contribution of sources to ET (mm d^{-1}) at each sampling location during; i) May, ii) August and iii) October 2016

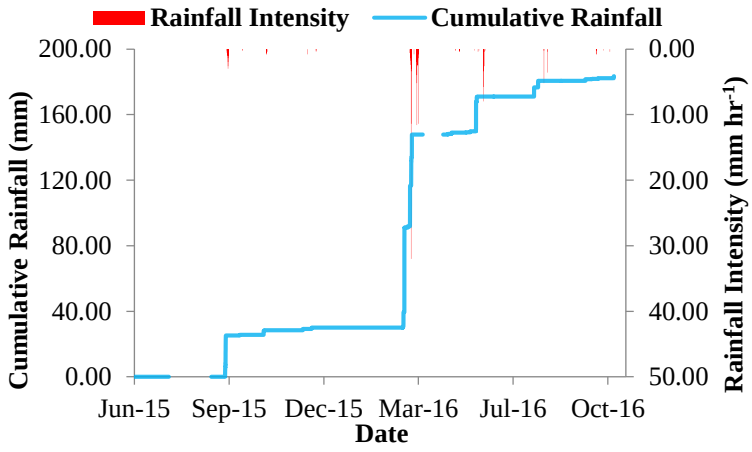

Figure 4.7 Rainfall measured at Phalaubeni for the 2015/2016 hydrological year

In addition to the seasonal changes in water uptake patterns, the species of riparian vegetation and their respective locations also showed variability in ET_g. Riparian vegetation situated along the southern bank of the study area generally used more GW to fulfil a portion of their transpiration demands, a trend which was consistent for each of the sampling campaigns. Whereas GW uptake by riparian vegetation situated within the river channel was consistently low.

Although GW represents a potential source to fulfil a portion of daily transpiration demands, especially as aridity increases, the accessibility of this resource for consumption and the amount used is largely controlled by the physiological characteristics of the plant/tree species (McLendon et al., 2008). In a similar environmental setting, February et al. (2007) showed that deep-rooted *P. violecia* were able to grow conservatively but consistently during conditions of water stress as they were able to access groundwater. However, the shallow rooted *C. mopane* predominantly relied upon available soil moisture and grew in rapid pulses in response to rainfall events.

These findings reaffirm our observations and provide further indication that individual tree species adopt alternative water use strategies to cope with conditions of water stress. Moreover, the depth to GW, as well as the physical properties of the soil and underlying aquifer may further influence the accessibility and use of this resource for plant water uptake (McLendon et al., 2008; Evaristo and McDonnell, 2017).

In order to quantify seasonal changes in GW use for the entire study area, all δ^2H and $\delta^{18}O$ values of xylem and source waters were respectively averaged for each sampling campaign. These values were then used as inputs to Simmr to determine source water contribution to transpiration. Spatial and seasonal variations in ET_g along the length of river reach studied was then determined as the product of these values (Table 4.4) and the satellite-derived ET pixel values covering the area of interest, as shown in Figure 4.8. During May, the average ET_g for the entire study area was extremely low (0.01 mm d^{-1}), accounting for only 0.10 % of daily ET. Whereas there was an increase in the average ET_g for August and October, with approximately 0.30 mm d^{-1} of GW being utilized during these months, as shown in Figure 4.9.

Table 4.4 Average proportional contribution of water sources to ET for the study site during each sampling campaign

Period (2016)	Ground Water	Surface Water	Soil Water (30cm)	Soil Water (60cm)	Soil Water (100cm)	Soil Water (140cm)
May (Late Autumn)	0.10 %	0.10 %	0.10 %	0.10 %	46.40 %	53.10 %
Aug (Mid-Winter)	10.00 %	6.00 %	12.00 %	17.00 %	38.40 %	13.00 %
Oct (Mid-Spring)	7.00 %	6.20 %	6.30 %	7.00 %	8.00 %	63.00 %

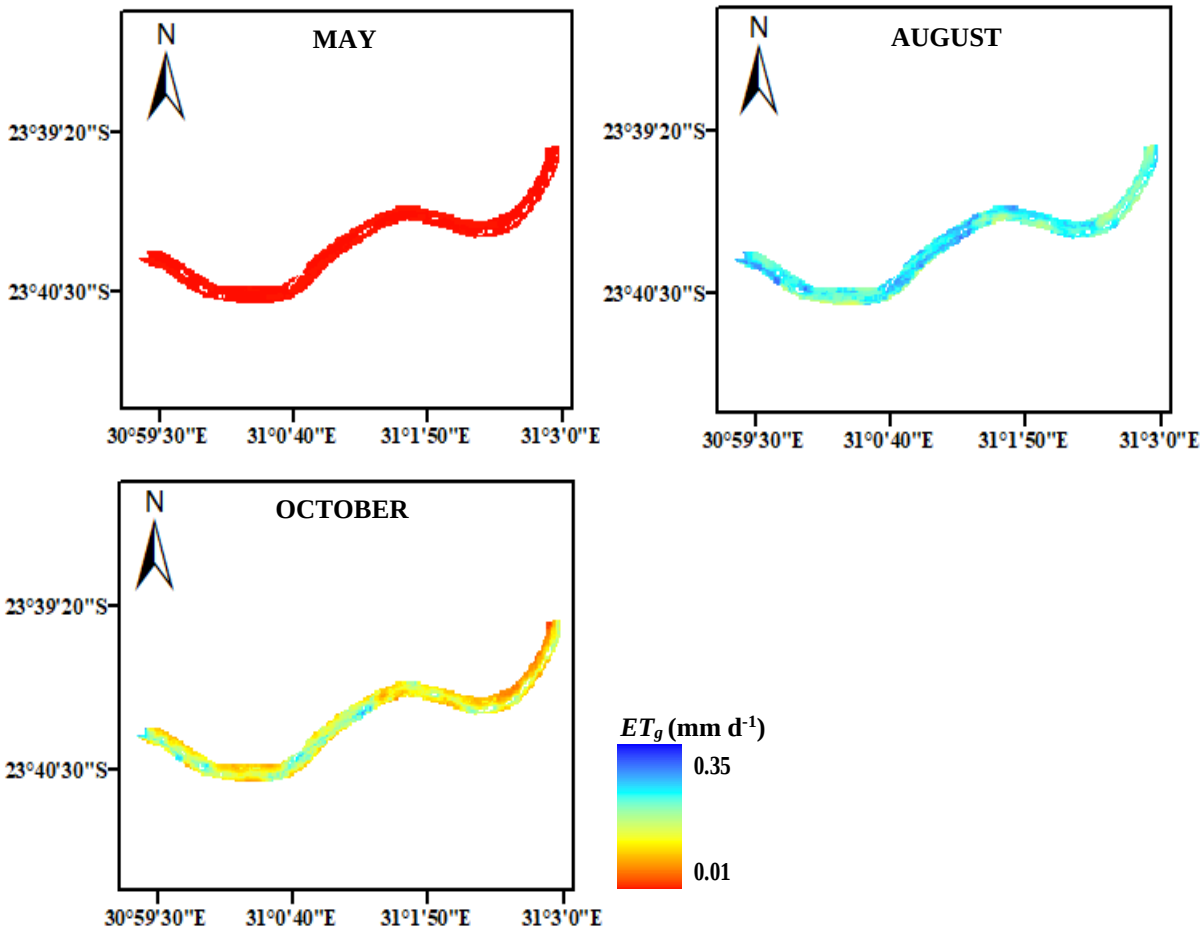

Figure 4.8 A comparison of seasonal and spatial variations in *ETg* (mm d^{-1}) along the length of river reach studied

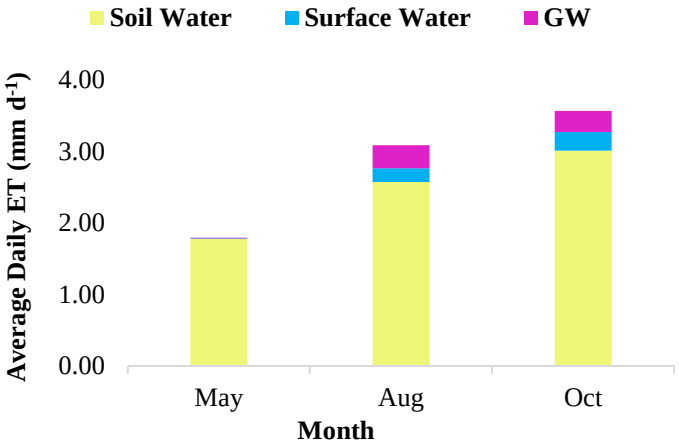

Figure 4.9 A comparison of seasonal variations in the contribution of sources to ET during the three sampling campaigns

Overall our results indicate that while GW use is prevalent and increases with aridity, the magnitude of ET_g is fairly minimal and lower than the global average (approximately 23 %) reported in Evaristo and McDonnell (2017). Furthermore the results of the stable isotope analysis presented in Figure 4.5 provides some evidence of ecohydrological separation (Evaristo et al., 2015) within our study site. δ^2H and $\delta^{18}O$ values for rainfall, stream water and GW from each of the sampling locations plot closely along the LMWL. However, δ^2H and $\delta^{18}O$ values for soil and xylem waters generally plot below these sources on the LMWL, signifying that the plant species within the study site are using soil water stores that are not contributing to streamflow or GW recharge (Evaristo et al., 2015).

Although the coupling of ET estimates from the satellite-based SEBS model with stable isotope analysis facilitated the quantification of seasonal and spatial variations in ET_g, the use of stable isotope analysis and a mixing model in this study may not necessarily provide an adequate insight on the actual plant water use dynamics within the study area, especially with regards to seasonal water use dynamics. This can be largely attributed to; i) the limited sampling frequency and number of samples collected for analysis and ii) general limitations and sources of uncertainty when using mixing models (Phillips et al., 2014). Furthermore, potentially significant differences in δ^2H composition between xylem and source waters due to isotopic fractionation during root water uptake may also lead to erroneous results, when using a single isotope ratio system (using δ^2H over $\delta^{18}O$) in a mixing model (Zhao et al., 2016; Evaristo et al., 2017). However, Evaristo et al. (2017) notes that a Bayesian mixing model approach (such as Simmr) may be insensitive to $^2H/^1H$ fractionation when using both δ^2H and $\delta^{18}O$.

While the aforementioned limitations may hinder the feasibility of applying the methodology described herein to estimate ET_g, this approach is neither site or model specific. Therefore, these constraints may be addressed by; increasing the water sampling frequency and the number of water samples collected during various seasons, adhering to recommended guidelines for best practices in the use of stable isotope mixing models or implementing a satellite-based ET model which is able to better capture ET and energy fluxes in this particular environment.

4.5 Conclusion

The relative importance of GW as a resource to sustain terrestrial vegetation, especially during conditions of water stress has been well documented. However, understanding and accurately quantifying GW dependency by riparian vegetation in data scarce regions may prove to be challenging. For this purpose, we employed the satellite-based SEBS model to estimate ET. These estimates were coupled with stable isotope analysis to determine spatial and seasonal variations in GW use during transpiration. The results of these investigations showed that soil water was the main contributing source to ET. In general, GW use was prevalent within the study area, however, the magnitude of its contribution to transpiration was fairly minimal and not as significant as generally reported in literature.

While the integration of satellite-based ET estimates and stable isotope analyses enabled us to acquire estimates of seasonal and spatial variations in ET_g, it is important to take cognisance of the various limitations associated with this approach, as addressing these constraints will ultimately influence the accuracy of quantifying spatial and seasonal dynamics in ET_g, using the methodology adopted in this study.

Nevertheless, the coupling of the satellite-derived ET estimates with stable isotope analysis provides a relatively simplistic and inexpensive means of quantifying and spatially extrapolating, not only the contribution of GW to transpiration but soil and stream water as well. Such information can prove to be extremely useful in deriving seasonal and spatially explicit water balances, which in turn can facilitate predicting how anthropogenic, climatic and environmental changes affect the rapport between plant growth and hydrological processes.

This may prove particularly beneficial to inform water resources management decisions in data scarce regions, as it can be used to provide baseline estimates of seasonal and spatial GW dependency by riparian vegetation, facilitating the improved allocation of this resource for human and environmental requirements.

Acknowledgements

The research presented in this paper emanates from a Water Research Commission (WRC) project entitled: Quantification of transmission losses along the Letaba River for improved delivery of environmental water requirements (ecological reserve), WRC Project No K5/2338. The authors would like to extend their gratitude to the Water Research Commission (WRC) and the South African Environmental Observation Network (SAEON) for the funding required to successfully complete this research. Furthermore, the authors would like to acknowledge Professor Simon Lorentz, Dr Goitom Adhanom, Mr Vivek Naiken and Miss Ntombiyenkosi Nxumalo for the various roles they played in preparation of the isotope samples and post-processing of the data. We would also like to acknowledge the anonymous reviewers who provided constructive feedback on the previous version of this manuscript.

REFERENCES

Allen, RG, Pereira LS, Raes D and Smith, M. 1998. Crop evaporation: Guidelines for computing crop water requirements, *FAO Irrigation and Drainage Paper no. 56*. Food and Agriculture Organization of the United Nations, Rome, Italy. ISBN 92-5-104219-5.

Chimner, RA and Cooper, DJ. 2004. Using stable oxygen isotopes to quantify the water source used for transpiration by native shrubs in the San Luis Valley, Colorado U.S.A. *Plant and Soil* 260 (1-2): 225-236.

Craig, H. 1961. Isotopic variations in meteoric waters. *Science* 133: 1702–1703.

Daly, RK, Tracy, RS, Crout, NMJ, Mairhofer, S, Pridmore, TP, Mooney, SJ and Roose, T. 2017. Quantification of root water uptake in soil using X-ray computed tomography and image-based modelling.

Dawson, TE, Mambelli, S, Plamboeck, AH, Templer, PH and Tu, KP. 2002. *Annu Rev Ecol Syst* 2002. 33:507–59.

Eamus, D, Zolfaghar, S, Villalobos-Vega, R, Cleverly, J and Huete, A. 2015. Groundwater-dependent ecosystems: recent insights from satellite and field-based studies. *Hydrol Earth Syst Sci* 19: 4229–4256.

Ellsworth, PZ and Williams, DG. 2007. Hydrogen isotope fractionation during water uptake by woody xerophytes. *Plant and Soil* 291, 93-107.

Evaristo, J and McDonnell, JJ. 2017. Prevalence and magnitude of groundwater use by vegetation: a global stable isotope meta-analysis. *Scientific Reports* 7: 44110.

Evaristo, J, McDonnell, JJ and Clemens, J. 2017. Plant source water apportionment using stable isotopes: A comparison of simple linear, two-compartment mixing model approaches. *Hydrological Processes* 31: 3750–3758.

Evaristo, J, Jasechko, S and McDonnell, JJ. 2015. Global separation of plant transpiration from groundwater and streamflow. *Nature* 525: 91–94.

February, EC, Higgins, SI, Netwon, R and West, AG. 2007. Tree distribution on a steep environmental gradient in an arid savanna. *Journal of Biogeography* 34: 270–278.

Fernández-Prieto, D., van Oevelen, P., Su, Z., Wagner, W., 2012. Advances in Earth observation for water cycle science. Hydrology and Earth System Science 16: 543–549.

Gibson, LA, M¨unch, Z and Engelbrecht, J. 2011. Particular uncertainties encountered in using a pre-packaged SEBS model to derive evapotranspiration in a heterogeneous study area in South Africa. *Hydrol Earth Syst Sci* 15: 295–310.

Gokool, S, Jarmain, C, Riddell, E, Swemmer, A, Lerm, R and Chetty KT. 2017a. Quantifying riparian total evaporation along the Groot Letaba River: A comparison between infilled and spatially downscaled satellite derived total evaporation estimates. *In Press*: *Journal of Arid Environments*. DOI: 10.1016/j.jaridenv.2017.07.014.

Heritage, GL, Moon, BP and Large, ARG. 2001. The February 2000 floods on the Letaba River, South Africa: an examination of magnitude and frequency. Koedoe 44 (2): 1-6.

Hong, S. Hendrickx. JMH and Borchers. B. 2011. Down-scaling of SEBAL derived evapotranspiration maps from MODIS (250 m) to Landsat (30 m) scales. *International Journal of Remote Sensing* 32(21): 6457–6477.

Jassas, H., Kanoua, W., Merkel., B., 2015. Actual evapotranspiration in the Al-Khazir Gomal Basin (Northern Iraq) using the Surface Energy Balance Algorithm for Land (SEBAL) and water balance. Geosciences 5: 141-159.

Katambara, Z and Ndiritu, JG. 2010. A hybrid conceptual-fuzzy inference streamflow modelling for the Letaba River system in South Africa. *Physics and Chemistry of the Earth* 35(13-14): 582-595.

Kogan, F., and Guo W., 2016. Strong 2015–2016 El Niño and implication to global ecosystems from space data. International Journal of Remote Sensing 38(1): 161-178.

Kumar, R, Shankar, V, and Jat, MK. 2014. Evaluation of root water uptake models–a review. *ISH Journal of Hydraulic Engineering* 21(2): 115-124, DOI: 10.1080/09715010.2014.981955.

Lange, J. 2005. Dynamics of transmission losses in a large arid stream channel. *Journal of Hydrology* 306: 112–126.

Lin, G and da Sternberg, LSL. 1993. Hydrogen isotopic fractionation by plant roots during water uptake in coastal wetland plants. In Ehleringer, JR, Hall AE and Farquhar GD (Eds.), Stable isotopes and plant carbon-water relations (pp. 497-510). New York: Academic Press Inc.

Lin, Z, Huili, Z, Xue, G, Yashu, QI, and Xing, X. 2016. Seasonal patterns in water uptake for Medicago sativa grown along an elevation gradient with shallow groundwater table in Yanchi county of Ningxia, Northwest China. *Journal of Arid Land* 8(6): 921–934.

Liu, JR, Song, XF, Yuan, GF, Sun, XM, Yang, LH. 2014. Stable isotopic compositions of precipitation in China. *Tellus B* 66, 22567.

Ma, Y and Song, X. 2016. Using stable isotopes to determine seasonal variations in water uptake of summer maize under different fertilization treatments. *Science of the Total Environment* 550: 471–483.

Mares R, Barnard HR, Mao D, Revil A and Singha K. 2016. Examining diel patterns of soil and xylem moisture using electrical resistivity imaging. *Journal of Hydrology* 536: 327-338.

Marwick, TR, Tamooh, F, Teodoru, CR, Borges, AV, Darchambeau, F and Bouillon, S. 2015. The age of river-transported carbon: A global perspective. *Global Biogeochem Cycles* 29: 122–137. doi:10.1002/ 2014GB004911.

McLendon, T, Hubbard, PJ and Martin, DW. 2008. Partitioning the use of precipitation-and groundwater-derived moisture by vegetation in an arid ecosystem in California. *J. Arid Environ* 72: 986–1001.

Mekiso, FA, Ochieng, GM and Snyman, J. 2015. Isotope Hydrology in the Middle Mohlapitsi Catchment, South Africa. *International Journal of Engineering Research and Development* 11 (01): 01-07.

Nippert, JB and Knapp, AK. 2007. Linking water uptake with rooting patterns in grassland species. Oecologia 153: 261-272.

Nourhi, H, Beecham, S, Kazemi, F, Hassanli, AM and Anderson, S. 2013. Remote sensing techniques for predicting evapotranspiration from mixed vegetated surfaces. *HESS Discuss* 10: 3897–3925.

Orrelana, F, Verma, P, Loheide II, SP and Daly, E. 2012. Monitoring and modeling water-vegetation interactions in groundwater-dependent ecosystems. *Reviews of Geophysics* 50 Paper number 2011RG000383.

Penna, D, Oliviero, O, Assendelft, R, Zuecco, G, van Meerveld, IHJ, Anfodillo T, Carraro, V, Borga, M and Fontana, GD. 2013. Tracing the water sources of trees and streams: isotopic analysis in a small pre-alpine catchment. *Procedia Environmental Sciences* 19: 106 – 112.

Pardo, N., Sanchez, L.M., Timmermans, J., Su, Z., Perez, I.A., and Garcia, M.A., 2014. SEBS validation in a Spanish rotating crop. *Agricultural and Forest Meteorology* 195-196: 132-142.

Parnell, A and Inger, R. 2016. Stable Isotope Mixing Models in R with Simmr. https://cran.r-project.org/web/packages/simmr/simmr.pdf, Accessed 27 November 2016.

Phillips DL, Inger, R, Bearhop, S, Jackson AL, Moore, JW, Parnell, AC, Semmens, BX and Ward EJ. 2014. Best practices for use of stable isotope mixing models in food-web studies. *Canadian journal of zoology* 92: 823-35.

Pollard, S and du Toit D. 2011. Towards Adaptive Integrated Water Resources Management in Southern Africa: The Role of Self-organisation and Multi-scale Feedbacks for Learning and Responsiveness in the Letaba and Crocodile Catchments. *Water resources management* 25 (15): 4019-4035.

Riddell, E.S., Nel, J.M., Gokool, S., Jarmain, C., Raubenheimer, R., Strydom, T., Swemmer, A., 2017. Quantification of transmission losses along the Letaba River for improved delivery of environmental water requirements (ecological reserve). *Water Research Commission Report*, Project Number K5/2338.

Riddell, ES, Kilian, W, Versfeld, W and Kosoana, M. 2016. Groundwater stable isotope profile of the Etosha National Park, Namibia. *Koedoe* 58(1), a1329, http:// dx.doi.org/10.4102/koedoev58i1.1329

Robinson JL, Slater LD and Schäfer VR. 2012. Evidence for spatial variability in hydraulic redistribution within an oak–pine forest from resistivity imaging. *Journal of Hydrology* 430: 69-79.

Savage, MJ, Everson, CS, Odhiambo, GO, Mengistu, MG and Jarmain, C. 2004. Theory and practice of evaporation measurement, with a special focus on SLS as an operational tool for the estimation of spatially-averaged evaporation. *Water Research Commission Report* 1335/1/04, Pretoria, South Africa. ISBN 1-77005-247-X.

Schulze, RE, Maharaj, M, Lynch, SD Howe, BJ and Melvil-Thomson, B. 1997. South African Atlas of Climatology and Agrohydrology. Water Research Commission, Pretoria, Report TT82/96.

Singh, RK, Senay, GB, Velpuri, NM, Bohms, S, Scott, RL and Verdin, JP. 2014. Actual Evapotranspiration (Water Use) Assessment of the Colorado River Basin at the Landsat Resolution Using the Operational Simplified Surface Energy Balance Model. *Remote Sensing* 6: 233-256.

Su, Z., 2002. The Surface Balance Energy System (SEBS) for estimating turbulent heat fluxes. *Hydrology and Earth System Sciences*. 6(1): 85-99.

Su, Z., and Wang, L., 2013. Earth Observation of Water Resources (SEBS). Practical Session Instructions (July 2013). ITC. University of Twente. The Netherlands.

Tanner, JL and Hughes, DA. 2015. Surface water–groundwater interactions in catchment scale water resources assessments: Understanding and hypothesis testing with a hydrological model. *Hydrological Sciences Journal* 60 (11). doi: 10.1080/02626667.2015.1052453.

Thaw, M, Visser, A, Deinhart, AL, Sharp, M, Everhart, A, Bibby, RK and Conklin, MH. 2016. Tracking water through the Southern Sierra Critical Zone Observatory using radioactive and stable isotopes. *Fall Meeting, American Geophysical Union, December 2016. Abstract H31K-07.*

United States Geological Survey (USGS). 2015. Landsat 8 (l8) Data Users Handbook. Version 1.0. June 2015.

Villarreyes CAR, Baroni G and Oswald SE. 2013. Calibration approaches of cosmic-ray neutron sensing for soil moisture measurement in cropped fields. *Hydrology and Earth System Sciences* 10: 4237-4274.

Walker C and Richardson, S. 1991. The use of stable isotopes of water in characterizing the source of water in vegetation. *Chemical Geology* 94(2): 145-158.

West, AG, Goldsmith, GR, Matimati, I and Dawson, TE. 2011. Spectral analysis software improves confidence in plant and soil water stable isotope analyses performed by isotope ratio infrared spectroscopy (IRIS). *Rapid Communication Mass Spectrom* 25: 2268-2274.

White, JWC, Cook, ER, Lawrence, JR and Broecker, WS. 1985. The D/H ratios of sap in trees: Implications for watersources and tree ring D/H ratios. *Geochim Cosmochim Acta* 49(1): 237–246.

Yang, Q, Xiao, HL, Zhao, LJ, Zhou, MX, Li, CZ and Cao, SK. 2010. Stable isotope techniques in plant water sources：a review. *Sciences in Cold and Arid Regions* 2(2): 0112–0122.

Zimmermann, U, Münnich, KO, Roether, W, Kreutz, W, Schubach, K and Siegel, O. 1966. Tracers determine movement of soil moisture and evapotranspiration. *Science* 152: 346-347.

Zhao, L, Wang, L, Cernusak, LA, Liu, X, Xiao, H, Zhou, M and Zhang, S. Significant difference in hydrogen isotope composition between xylem and tissue water in Populus euphratica. *Plant, Cell and Environment* 39(8): 1848–1857.

Zhang, ZQ, Evaristo, J, Li, Z, Si, BC and McDonnell, JJ. 2017. Tritium analysis shows apple trees may be transpiring water several decades old. *Hydrological Processes* 31: 1196–1201.

*****

Lead into chapter 5: With the ability of the SEO data sets and modified version of SEBS to more adequately represent ET within the study area confirmed (chapters 2 and 3), as well as an improved understanding of the seasonal and spatial variations in plant water use dynamics gained (chapter 4), chapter 5 addresses the overall objective of the thesis, which is to reduce the uncertainty associated with TL's by attempting to understand and quantify the hydrological processes which contribute to TL's along the Groot Letaba River. During these investigations, particular emphasis was placed upon establishing the influence of riparian total evaporation on TL's. Supplementary information and/or data which was used during the various analyses undertaken in this chapter but not presented herein, are provided in Appendices C and D.

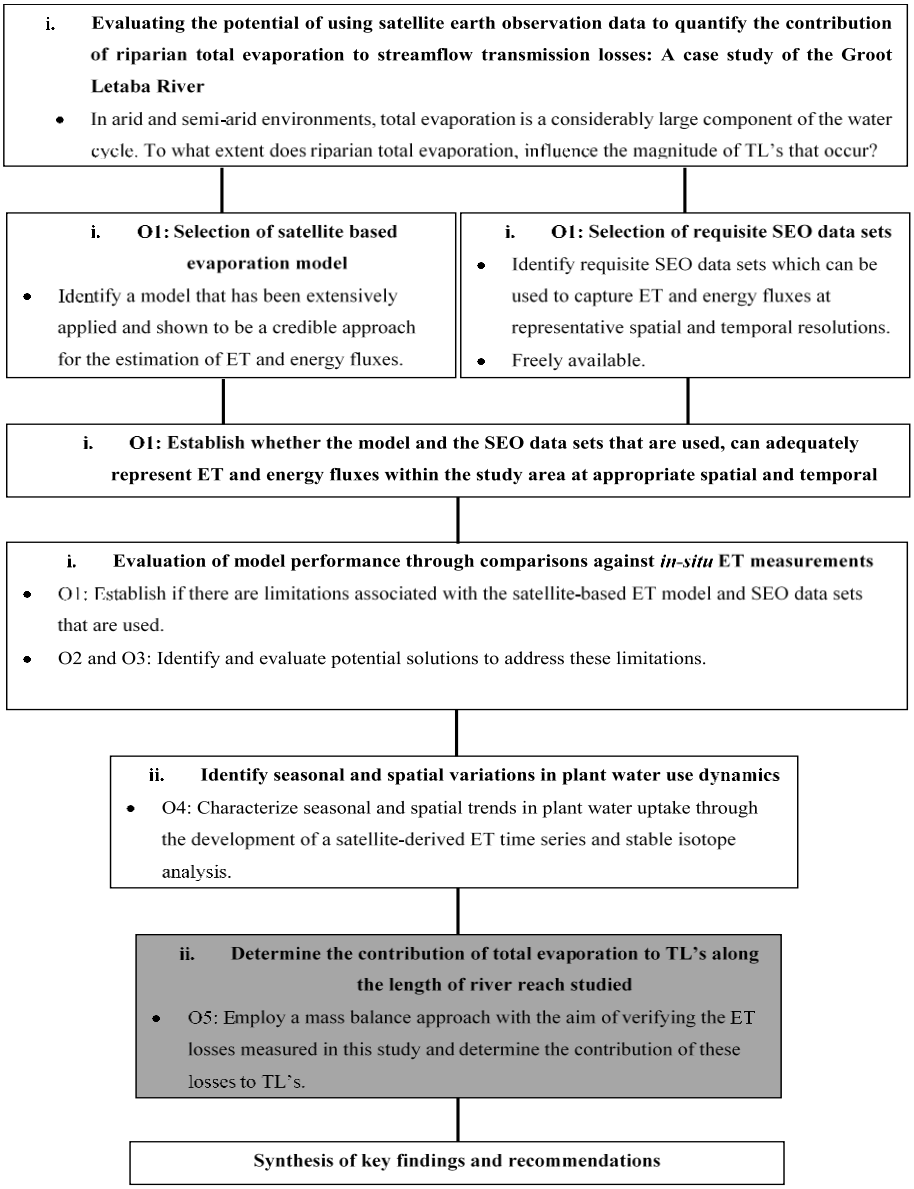

5. QUANTIFYING THE CONTRIBUTION OF RIPARIAN TOTAL EVAPORATION TO STREAMFLOW TRANSMISSION LOSSES: PRELIMINARY INVESTIGATIONS ALONG THE GROOT LETABA RIVER[4]

S Gokool[1], ES Riddell[1&2], JM Nel[3], R Raubenheimer[3], T Strydom[4], A Swemmer[5]and KT Chetty [1]

[1]*Centre for Water Resources Research, University of KwaZulu-Natal, Pietermaritzburg, South Africa*

[2]*Conservation Management, South African National Parks, Skukuza, South Africa*

[3]*GCS Consulting, Pretoria*

[4]*Scientific Services, South African National Parks, Skukuza, South Africa*

[5]*South African Environmental Observation Network (SAEON), Ndlovu Node, Phalaborwa, South Africa*

Corresponding Author: Shaeden Gokool, shaedengokool@gmail.com, University of KwaZulu-Natal, Pietermaritzburg, South Africa, 3201

ABSTRACT

The Groot Letaba River which is situated in the semi-arid north-eastern region of South Africa, is an example of a river system in which the uncertainty associated with transmission losses (TL's) has limited the effective management of environmental water requirement flows. For this purpose, we performed a detailed characterization of hydrological processes along the lower reaches of the river, which centred around the estimation of riparian total evaporation and quantifying the rapport between surface and subsurface water storage processes.

4S Gokool, ES Riddell, JM Nel, R Raubenheimer, T Strydom, A Swemmer, and KT Chetty. 2017. Quantifying the contribution of riparian total evaporation to streamflow transmission losses: Preliminary investigations along the lower reach of the Groot Letaba River. *Submitted to Journal of Hydrology: Regional Studies*

*Referencing conforms to format of Journal of Hydrology: Regional Studies

Riparian total evaporation losses were estimated using the satellite-based surface energy balance system (SEBS) model, soil water evaporation measurements and open water evaporation estimates. Losses from the river system to the adjacent aquifer were determined from the continuous monitoring of the groundwater phreatic surface and characterization of aquifer hydraulic properties. The results of these investigations indicated that total evaporation and losses from the river system to the adjacent aquifer accounted for approximately 5 to 15 % of the flow in the river system. Furthermore, it was shown that present flows within the system are likely to be insufficient to satisfy gazetted median and extreme low flow targets whilst simultaneously accounting for losses.

Keywords: Transmission loss, environmental water requirements, total evaporation, SEBS, subsurface water storage

5.1 Introduction

Globally, water scarcity has been exacerbated by the effects of increasing population growth, socio-economic development and climate change (Molle et al, 2010; Pittock and Lankford, 2010). As a result, the availability of water to sustain the natural functioning of riverine ecosystems and the provision of ecosystem goods and services has fallen under threat (Pittock and Lankford, 2010). In a South African context, numerous perennial river systems have become severely constrained, as water resources abstractions are close to exceeding or have exceeded the available supply and ecosystem resilience (Molle et al, 2010).

According to Pollard and Du Toit (2011a) during the latter periods of the 20th century, the environmental water requirements (EWR) in various catchments of the South African Lowveld have been on the decline. This has been attributed to the compounded effects of land-use change, as well as the improper management of water resources within these catchments (Pollard and Du Toit, 2011a). Consequently, the natural ecological functioning of the riverine ecosystems and surrounding environments have begun to steadily decline (Pollard and Du Toit, 2011a), despite the EWR's possessing the only 'right' to water, in addition to the Basic Human Needs reserve under South Africa's National Water Act (NWA, Act 36 of 1998).

Intensive management of the EWR flows is therefore required, to ensure that all water users receive an acceptable quantity and quality of water which can be supplied and sustained at an acceptable assurance level without impeding the ability to maintain the EWR (Riddell et al., 2017). Presently, knowledge regarding precipitation inputs to a river system, releases from dams and permitted water abstractions from river systems, are used to manage the flows for river operations within these environments (Riddell et al., 2017).

However, the lack of an adequate quantitative understanding with regards to the loss of water to streamflow transmission losses (TL's), remains a constraint to the effective management of flows especially in arid and semi-arid environments (Hughes, 2008; Costa et al., 2013). TL's are defined as a reduction in the volume of flow in a river system between upstream and downstream points, due to the loss of water through three natural processes i.e. (a) Riparian ET, (b) open-water evaporation or infiltration of flood waters stored in channel depressions or the flood plain and (c) the recharge of ground water as water infiltrates the stream channel or open-water evaporation directly from the stream channel (Cataldo et al., 2010).

The significance of TL's as a contributing process to the water balance of river systems particularly in arid and semi-arid environments has been well documented internationally (Hughes and Sami, 1992; Lange, 2005; Costelloe et al., 2003; Costa et al., 2013; Shanafield and Cook, 2014). However, there remains a paucity of studies of this process in southern Africa (Hughes, 2008; Tanner and Hughes, 2015). Whilst, TL's have not been adequately quantified through hydrological process definition for any South African river system (Riddell et al., 2017), the magnitude of these losses is estimated to be high, especially for perennial river systems flowing through arid and semi-arid environments (Everson et al., 2001; Boroto and Gorgens, 2003). Therefore, to ensure that EWR flows and water provisions are managed efficiently, it is essential that the hydrological processes contributing to this process in these environments are understood and quantified at various spatial and temporal scales. (Gu and Deutschman, 2001).

The use of conceptual models and time series analysis may perhaps allow for the reliable prediction of TL's for regions possessing long time series of streamflow data (Sharma and Murthy, 1994a; Costa et al., 2012). However, in arid and semi-arid environments the routine monitoring of streamflow is generally limited (Lange et al., 2005). In such circumstances, the use of process-orientated models, which are parameterized using representative measurements of hydrological parameters represent the most suitable tool to quantify TL (El-Hames and Richard, 1998; Gheith and Sultan, 2002).

For this purpose, we performed detailed characterizations of hydrological processes along a 14 km reach of the Groot Letaba River. In this study, particular emphasis was placed on accurately determining the contribution of riparian total evaporation to TL's, as it is often the case that this process is ignored or inadequately accounted for during the estimation of TL's (Hacker, 2005; Cataldo et al., 2010; Shanafield and Cook, 2014), even though it is generally the second largest component of the water balance in semi-arid and arid environments and has been shown to be a dominant contributing process to TL's (Everson et al., 2001).

These investigations were supplemented by a parallel study which focused on the continuous monitoring of the groundwater phreatic surface and hydraulic characterisation of aquifer properties using a multi-piezometer borehole network along the selected river reach (Riddell et al., 2017), to determine the hydraulic gradients between river and surrounding aquifer and thereby baseline estimates of losses and gains along the river.

5.2 Study area

5.2.1 Selection of the study area

The Letaba River is a typical example of a river system in which poor water governance and infrastructural development have resulted in flows within the river no longer resembling the natural flow regime (Vlok and Engelbrecht, 2000; Katambara and Ndiritu, 2010; Pollard and du Toit, 2011a). These circumstances have placed additional pressure on water resources managers in this region, as they attempt to balance the demands of various water users within the catchment, whilst attempting to maintain the mandated EWR flows.

This situation has improved to some extent, after the establishment of the river operating rules, whereby flows released from the Tzaneen Dam are monitored further downstream by the Kruger National Park and information is relayed back to dam operators through an adaptive feedback mechanism (Pollard and du Toit, 2011a; McLoughlin et al., 2011).

The Letaba operating rules were established in 2006 by the Department of Water Affairs and facilitated by a real time EWR implementation model (SPATSIM) (Hughes et al., 2008; Sawunyama and Hughes, 2010). However, one of the major challenges to the successful application of the model to date, has been the uncertainty regarding the magnitude and influence of TL's on flows within the river system (Riddell et al., 2017). TL's along the Groot Letaba are thought to significantly impact EWR flows, as it is often the case that specified EWR releases from the Tzaneen dam are not adequately met further downstream at the Letaba Ranch (B8H008) gauging weir close to the Kruger National Park (Sinha and Kumar, 2015). This therefore makes it challenging to operate the river, using downstream targets far from the source of operations.

5.2.2 Site description

The catchment generally experiences a semi-arid climate with hot and wet summer and mild and dry winter conditions. The mean annual precipitation within the catchment is approximately 612 mm, which predominantly occurs during the summer months (October to March). According to Katambara and Ndiritu (2010) 40 to 50 % of this rainfall is received during January and February, with the majority (60 %) of this rainfall being received in the mountainous western region (≈ 6 % of the total catchment area) (WRC, 2001).

In general, temperatures vary across the catchment with cooler conditions in the mountainous western region (≈ 18^0 C) to hotter conditions in the eastern region (≈ 28^0 C). Approximately three quarters of the catchment is underlain by granite and gneiss. The varied distribution of sediment along the Letaba River has resulted in the formation of varying channel types with distinctive vegetative compositions and morphological characteristics (Heritage et al., 2001). There are numerous land-use activities distributed throughout the Letaba catchment, amongst these the dominant land-uses include; intensive commercial afforestation and agriculture (predominantly citrus crops), densely-populated rural villages with informal dryland agriculture and conservation areas in the eastern regions of the catchment (Pollard and du Toit, 2011a).

The TL's study site is situated within the Letaba Catchment along the lower reach of the Groot Letaba river between the now defunct Mahale weir (B8H007) and the Letaba Ranch gauging weir (B8H008) situated approximately 14 km further downstream, as illustrated in Figure 5.1. The rationale for this site selection was to employ a mass balance approach (Costa et al., 2013) with the aim of; i) verifying the losses measured in this study and ii) determining the contribution of riparian total evaporation to these losses.

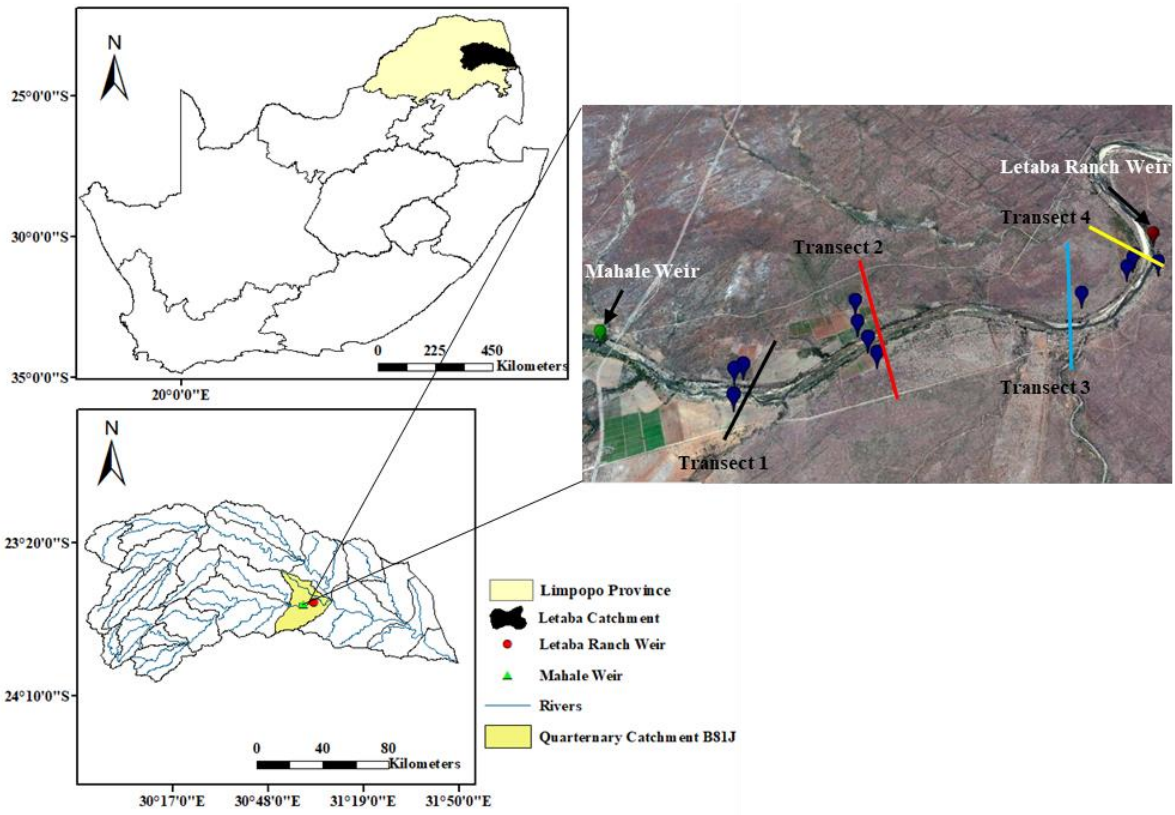

Figure 5.1 Location of the study area and distribution of borehole sampling points across the four geohydrological transects (Google Earth™ image), situated along the lower reach of the Groot Letaba River within the Quaternary catchment B81J (adapted from Riddell et al., 2017)

Between these two gauging weirs, there are no contributing tributaries. Agricultural areas are situated adjacent to the riparian zone in the west before the river traverses conservation areas further downstream (Riddell et al., 2017). The section of river studied between these weirs is largely dominated by riparian vegetation such as; *Ficus sycomorus*, *Philenoptera violacea* and *Diospyros mespiliformis*, with *Phragmites mauritianus* dominant in the river microchannel. Detailed descriptions of the soils, lithology, stream networks and topography are provided in Riddell et al. (2017).

TL's were estimated during the latter stages of the 2016 low flow period (August to October), which typically represents a critical period with regards to water scarcity. While TL's during higher flow periods are equally important for the estimation of EWR flows, during the dry season soil water availability is substantially lower. Consequently, riparian vegetation may access alternate water sources (stream and groundwater) if available to fulfil a portion of their daily transpiration demands (Gribovski et al., 2008; Cadol et al., 2012). Therefore, estimating riparian total evaporation during this period provides the ideal scenario to quantify the contribution of this process to TL's.

5.3 Methodology

5.3.1 Data Collection

Streamflow

Daily average flow data (m^3 s^{-1}) was acquired from B8H007 and B8H008, in order to verify the estimated losses along the length of river reach studied using a mass balance approach. Verified flow data for B8H008 was made available from the Department of Water and Sanitation (DWS) HYDSRTA data base (http://www.dwa.gov.za/Hydrology/). The now ungauged B8H007 weir was fitted with a Solinst™ Level Logger Junior to determine stage height, in a stilling pipe bolted to the upstream side of the weir in order to record the river stage at a 5-minute time step. A rating was then attempted for B8H007 to obtain the stage height discharge relationship. However, the unrefined structure of the weir wall prevented a full rating from being undertaken (Riddell et al., 2017). Therefore, when the level logger data showed a constant stage, it was assumed that there was no overtopping of the weir, but rather a continuous discharge through two low flow scour sluices located at the base of the structure.

This was determined as the product of the cross-sectional area of pipe and outflow rate measured using a Pasco^{TM} 2000 flow meter (Table 5.1).

Table 5.1 Low flow rating for Mahale weir

	Flow (m s^{-1})	**Pipe diameter (m)**	**Discharge (m^3 s^{-1})**	**Total Discharge (m^3 s^{-1})**
Sluice 1	3.4	0.3	0.24	0.50
Sluice 2	3.7	0.3	0.26	

Artificial abstractions

Artificial abstractions along the portion of river reach studied are relatively low (Riddell et al., 2017). However, these volumes needed to be determined in order to accurately quantify the losses between the two gauging weirs associated with natural processes. A hydro-census was undertaken within the surrounding areas of the study site, to determine the reliance of the local community on stream and ground water resources for domestic use and small scale-irrigation (Gokool et al., 2015). The results of this survey revealed that direct river abstractions were relatively low and estimated to be in the magnitude of 52 m^3 d^{-1} (Riddell et al., 2017).

Groundwater piezometric monitoring network

The rapport between stream water and groundwater interactions was established by performing a detailed hydraulic characterisation of the aquifer properties and through the continuous monitoring of groundwater levels. In order to continuously monitor stream water and groundwater interactions, a piezometric borehole network was drilled by the Department of Water and Sanitation Limpopo Drilling Division, along the northern and southern banks of the study site. This network consisted of paired piezometric boreholes which were drilled into shallow weathered material and deep fractured hard rock. The rationale for this was to determine gains/losses associated for both alluvial and hard rock material, as Hughes (2008) states that TL's from non-alluvial rivers can also be substantial due to the highly-fractured nature of the material of bed-rock channels. The groundwater piezometric network was divided into four geohydrological transects (Figure 5.1) and the river reach length represented by the adjacent aquifers was estimated.

Riparian total evaporation

In this study, riparian total evaporation was defined as the combined contribution of transpiration, soil water evaporation and open water evaporation. Open water losses were determined using the Priestley-Taylor method (Priestley and Taylor, 1972). Average daily soil water evaporation from August to October was measured as 0.15, 0.47 and 0.45 mm d^{-1}, respectively within the river channel. These measurements were obtained using from three to six micro-lysimeters, which were installed at various points within and adjacent to the active river channel.

The microlysimeters were made of 2 mm thick PVC pipe, were 100 mm deep and had an internal diameter of 50 mm. Each micro-lysimeter was equipped with one external cylinder made of 3 mm thick PVC pipe which was 80 mm in diameter and 145 mm deep. The external cylinders were placed at fixed positions, whilst the internal cylinders were filled with soil samples extracted from selected areas within the river channel.

Extraction of soil samples from the top soil layer was typically done at the start of the day, generally around 09:00 AM. The rate of soil water evaporation was calculated as;

$$E_s = \frac{\Delta Mass * 10^{-3}}{A} \quad (5.1)$$

Where ES is soil water evaporation in mm d^{-1}, $\Delta Mass$ is the mass difference between soil samples (g) and A is the surface area of the microlysimeter (0.0196 m^2).

We did not measure soil water evaporation along the banks of the riparian zone during this low flow period, as flow within the channel did not exceed bank full storage. Consequently, there would have been no enhanced loss of stream water due to soil water evaporation.

Transpiration was estimated indirectly by calculating the difference between soil water evaporation and daily evapotranspiration (ET) estimates acquired from a satellite-based evapotranspiration (ET) model. Satellite earth observation (SEO) data was used in this study, to obtain spatially representative estimates of ET within the study area.

The SEBS Model (Su, 2002) was applied in this study to estimate daily ET. SEBS computes all components of the shortened surface energy balance (Equation 5.2), as well as the evaporative fraction (*EF*), using land surface parameters which are derived from meteorological and satellite earth observation (SEO) sources, respectively.

$$R_n = Go + H + LE \quad (5.2)$$

Where R_n is net radiation (W m^{-2}), G_0 is the soil heat flux (W m^{-2}), H is the sensible heat flux (W m^{-2}) and LE is the latent heat flux (W m^{-2}).

SEBS has been extensively applied and shown to provide fairly accurate estimates of ET. A modified version of SEBS (Riddell et al., 2017) was applied to acquire daily ET estimates at the Landsat spatial resolution.

This was due to the inability of the original model formulation to adequately represent fluxes and ET within the study area (Gokool et al., 2017). These ET estimates were then used as inputs to the Kc_{act} infilling procedure as described by Gokool et al. (2017), to develop a moderate spatial resolution daily satellite-based ET time series. Comparisons between this data set and *in-situ* ET observations, were found to be in fairly good agreement, yielding correlation coefficient and Nash-Sutcliffe efficiency values of 0.79 and 0.60, respectively.

5.3.2 Estimation of transmission losses

It was initially envisaged that the losses estimated in this study would be verified using a mass balance approach. However, this was not possible as we were unable to obtain accurate inflow data from B8H007. It was assumed that when the data showed a constant stage height, there was no overtopping of the weir and a continuous discharge of 0.5 m^3 s^{-1} was experienced. However, this was seldom the case. Consequently, the abovementioned discharge could not be used to perform the mass balance calculation. Instead, we computed the inflow as a residual of the mass balance (Equation 5.3). It should be noted that while the magnitude of the estimated losses was compared relative to this estimated inflow, this inflow volume was not necessarily an accurate representation of the flow within the system.

$$Inflow = Outflow + TL \quad (5.3)$$

Following the groundwater hydraulic characterisation undertaken by Riddell et al. (2017), the interaction between the river and adjacent aquifers was quantified in terms of either gains or losses from the watercourse (Table 5.3). Further details regarding the borehole drilling information, fluid logging and derivation of undisturbed *in-situ* borehole parameters used to obtain these baseline estimates are provided in Riddell et al. (2017).

As shown in Table 5.3, there is a net loss from the river to the adjacent aquifer within the agricultural areas, with the highest loss occurring to the deep fractured hard rock aquifer. Whereas further downstream within the conservation areas, there is a net gain from the adjacent aquifer to the river, with the highest gains occurring from the shallow aquifer. In general, the length of river reach studied was shown to be a losing system, with a net loss of 253.98 $m^3\ d^{-1}$ to the adjacent aquifers within the riparian zone.

Table 5.2 Estimated gains and losses from the watercourse to the adjacent aquifers within the riparian zone during the dry season (adapted from Riddell et al., 2017)

		Borehole ID	Loss to Aquifer ($m^3\ d^{-1}$)
Deep Borehole Data (A)	**Letaba Farm**	**LF002**	-0.70
		LF003	2.18
		LF004	15.31
		LF005	-141.48
	Total		**-124.69**
	Letaba Reserve	**LR001**	5.17
		LR002	2.69
		LR004	-11.82
		LR005	26.96
	Total		**23.01**
Shallow Borehole Data (B)	**Letaba Farm**	**LF002**	-118.80
		LF003	-89.38
		LF004	26.46
		LF005	-4.05
	Total		**-185.76**
	Letaba Reserve	**LR001**	20.70
		LR002	3.67
		LR004	-51.57
		LR005	60.67
	Total		**33.47**

The daily transpiration estimated in this study represents the total water used by riparian vegetation from multiple sources such as; soil water, groundwater and streamflow. Although transpiration demands are generally met by available soil moisture (Gokool et al, 2017), in arid settings, riparian vegetation generally becomes increasingly reliant on groundwater and streamflow to fulfil a portion of their daily water requirements (Gribovski et al., 2008). The groundwater used during transpiration is typically replenished by subsurface flows further away from the stream channel or flow maybe redirected from the stream channel into the adjacent aquifer due to an inverse in the hydraulic gradient, ultimately resulting in a loss of streamflow (Gribovski et al., 2008; Tanner and Hughes, 2015).

Riparian ET of waters stored within the river banks may enhance TL's during high flow periods when flood waters exceed the bank full storage. During low flow periods, TL's may comprise the proportion of water consumed by riparian vegetation from stream and groundwater. Therefore, in order to estimate the contribution of transpiration to TL's, the proportional contribution from these sources needed to be quantified. For this purpose, Riddell et al. (2017) coupled stable isotope analysis of ^{2}H and ^{18}O contents of plant water, soil water, stream and groundwater with a Bayesian mixing model (Stable Isotope Mixing Model package available in R).

5.4 Results and Discussion

According to Cadol et al. (2012) the volume of water lost from stream and groundwater to transpiration, should equal the volume of water transpired over an area of influence within and adjacent to the stream. Therefore, the average proportion of surface and groundwater contributing to transpiration were used in conjunction with the satellite-derived daily ET estimates to determine the volume of water used from these sources. According to Riddell et al. (2017) the contribution of groundwater and stream water to transpiration during the latter stages of the 2016 dry season, was approximately 15%. However, this proportional contribution was only used to determine transpiration losses for vegetation situated on either side of the river channel (riparian forest). For riparian vegetation situated within the active river channel (*P. mauritianus*), it was assumed that daily transpiration demands are fulfilled by accessing water in the upper levels of the saturated zone (water table) and stream water (Everson et al., 2001), as *P. mauritianus* were predominantly located in areas in which the root zone was inundated by water.

Using the areas from Table 5.3, the volume of riparian total evaporation was determined as the combined contribution of transpiration, soil and open water evaporation. These losses were then combined with the baseline estimates of losses to the adjacent aquifer and artificial abstractions to determine the total volume lost in the system. The estimated reduction in flow for 2016 for the length of river reach that was investigated, is shown in Figure 5.2. The total volume of water loss 2016 ranged from 985.85 to 4066.06 $m^3 d^{-1}$, with a mean loss of 3209.26 $m^3 d^{-1}$.

Table 5.3 Distribution of riparian vegetation along a 14 km reach of the lower Groot Letaba River (adapted from Riddell et al., 2017)

	Land Cover Category				
	Riparian vegetation		Soils	Open Water	Total
	Riparian Forest	*P. mauritianus*			
Area (km^2)	1.09	0.41	0.25	0.16	1.91
Relative area (%)	57.00	21.00	13.00	9.00	100.00

In general, the inflow rate for August and September were fairly similar and the magnitude of flow reduction ranged between 5 and 10 %, as shown in Table 5.4. During these months, the average inflow (0.57 and 0.50 $m^3 s^{-1}$), was much higher than the loss of water due to natural processes ($\approx$ 0.04 $m^3 s^{-1}$). During this period, the flow would have been approximately 8.00 % higher, without the influence of these losses.

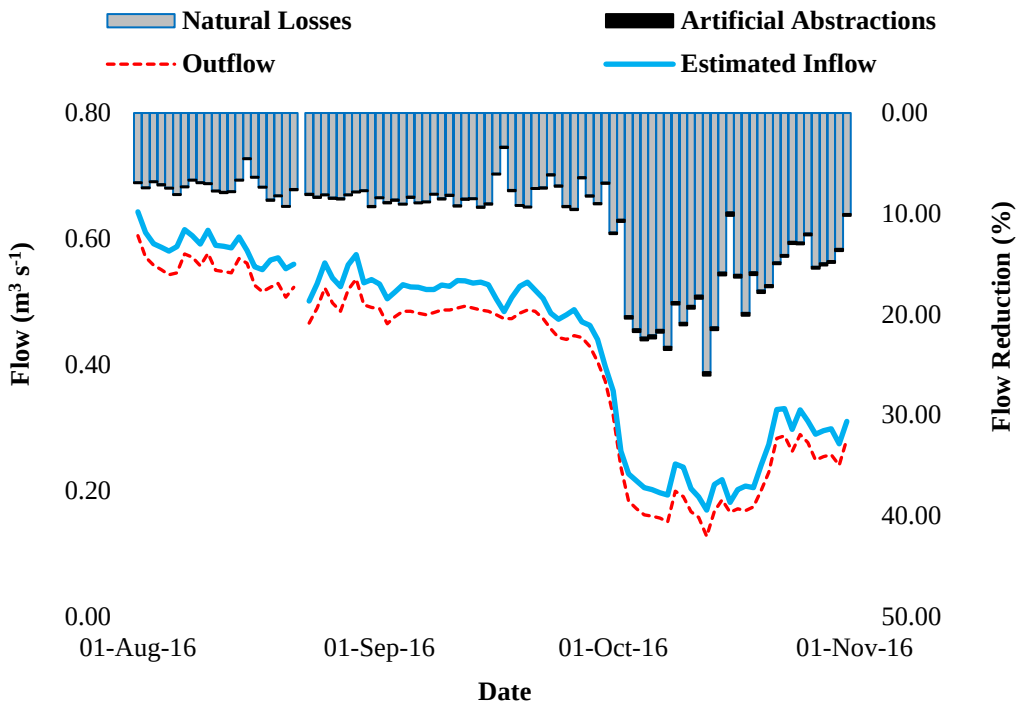

Figure 5.2 Daily TL's along a 14 km reach of the Groot Letaba River during the latter stages of the 2016 dry season

Table 5.4 Frequency range of TL's during the latter stages of the 2015 and 2016 dry season

Range	2016 Frequency (%)		
	Aug	Sep	Oct
0 %< TL< 5 %	3.33	3.33	
5 %< TL< 10 %	96.67	96.67	6.45
10 %< TL< 15 %			32.26
15 %< TL< 20 %			35.48
20 %< TL			25.81

However, during October there was an increase in the magnitude of streamflow reduction with losses generally ranging between 10 and 20 % and in a few instances exceeding 20 %. The inflow rates during this period were relatively lower (0.25 m^3 s^{-1}). Consequently, there is a greater influence of these natural losses on streamflow. The average reduction in flow during this period increased to approximately 17.00 %.

Comparisons of the different contributing processes to TL's, indicated that throughout the period of investigation, riparian total evaporation losses were found to be the chief contributing process to TL's along this portion of river reach, as shown in Figure 5.3. The average contribution of riparian total evaporation was approximately 2871.72 m^3 d^{-1} or approximately 90.00 % of daily TL's. Whereas the contribution of artificial abstractions and losses to the adjacent aquifer were only 2.00 and 8.00 %, respectively.

Riparian total evaporation losses were largely due to the proportion of water transpired from stream and groundwater, as shown in Figure 5.4. The average loss due to transpiration from the river banks and within the river channel was approximately 563.80 and 1263.64 m^3 d^{-1}, contributing a combined average of 56.00 % of TL's. Whereas the combined contribution of open water and soil water evaporation losses were approximately 34% of TL's.

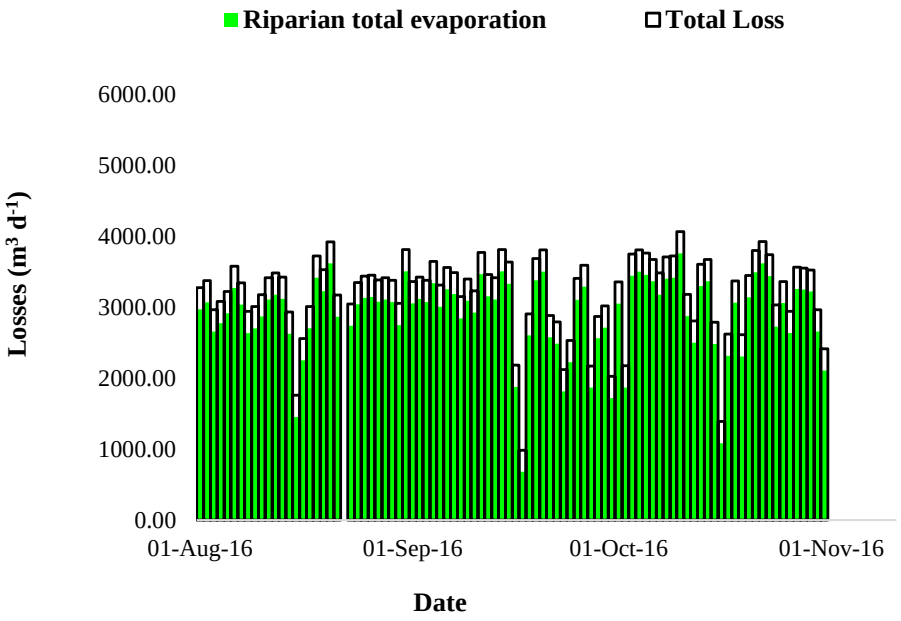

Figure 5.3 Contribution of riparian total evaporation to daily TL's during the latter stages of the 2016 dry season

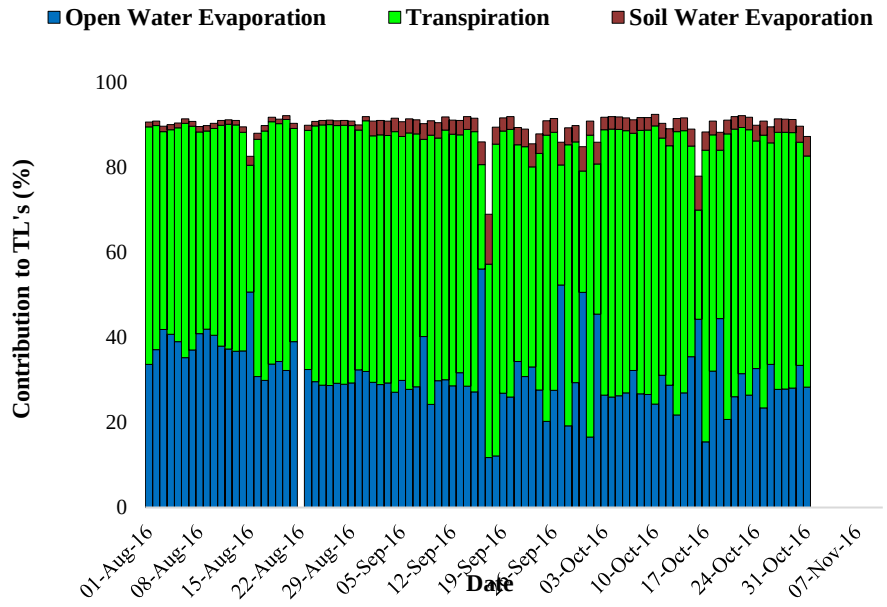

Figure 5.4 Percentage contribution of riparian total evaporation processes to TL's

In light of the recent gazetting of the Letaba Management Class and the mandatory implementation of EWR flows. The quantification of TL's takes on added significance to ensure that EWR flows are adequately managed and maintained so that the natural functioning of the riparian ecosystem is not compromised. Table 5 depicts the low flow assurance rules for the median (60th percentile) and ultra-low flows (90th percentile) at B8H008, respectively. These flow values have been gazetted for implementation prior to and proceeding the construction of the proposed Nwamitwa dam. Comparisons between the daily flows at B8H008 for 2016 against these target flows, indicates that the daily flows at B8H008 are currently unable to meet the mandated target flows, as shown in Figure 5.5.

Table 5.5 Low flow assurance rules for median (60th percentile) and extreme low flows (90th percentile)

	Median Target Flow at B8H008 ($m^3 s^{-1}$)			
	Prior to Construction		Post Construction	
Month	90%	60%	90%	60%
Aug	0.597	0.597	0.605	0.778
Sep	0.594	0.598	0.552	0.632
Oct	0.497	0.597	0.523	0.554

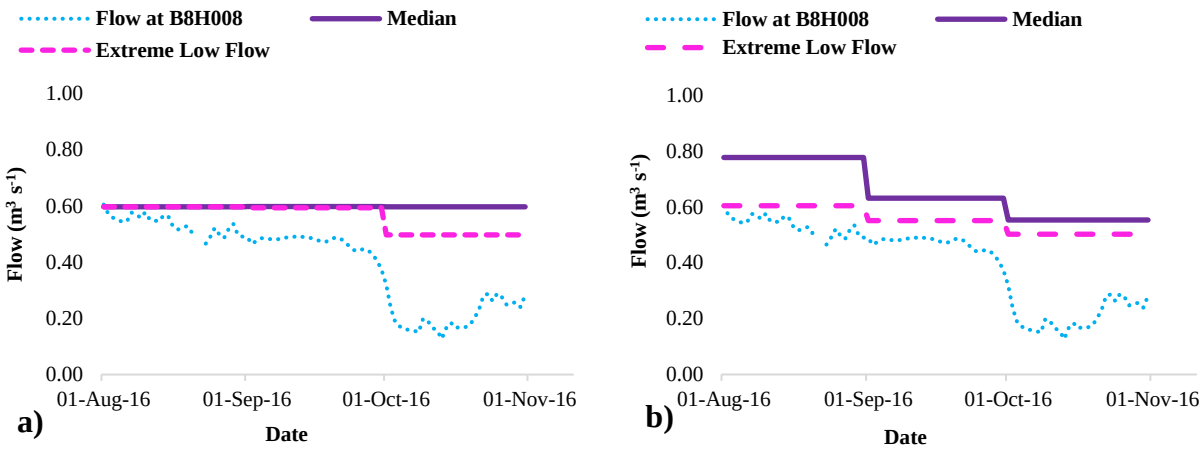

Figure 5.5 A comparison of the flow at B8H008 against gazetted flows for implementation prior to and subsequent to the construction of the proposed Nwamitwa dam.

Consequently, flows traversing B8H007 are required to be increased in order to satisfy both median and extreme low flow targets, whilst simultaneously accounting for TL's. To facilitate this process, baseline estimates of the required increases to the flow emanating from B8H007 were determined (Table 5.6), using monthly averages of the estimated TL's and inflow volumes. The magnitude of this increase in flow for B8H007for 2016 ranges from; 0.069 (11.99 %) to 0.449 (181.22 %) m^3 s^{-1} prior to the construction of the dam. Whereas post dam construction the magnitude of flow increase for B8H007 ranges from; 0.077 (13.49 %) to 0.399 (160.96 %) m^3 s^{-1}.

The proposed increases in flow required to meet the gazetted target flows should be considered preliminary findings, as it was not possible to quantify the uncertainty in our estimated TL's. due to the lack of accurate inflow data. Nevertheless, the temporal progression and magnitude of these losses in relation to streamflow are analogous to the losses reported by DWAF (2006a) (between 8 and 50%) and Everson et al. (2001) (approximately 15 %) in similar environmental settings, lending some credibility to the TL's estimated in this study.

Based on the estimated current inflows from B8H007 and TL's within this portion of river reach, the gazetted target flows will not be reached without further increases to the flow emanating from B8H007 (Table 5.6). While this situation is particularly concerning, it may be further compounded by the effects of anthropogenic driven land use changes.

Table 5.6 Baseline estimates of the required increases to the flow emanating from B8H007 to meet the gazetted low flow assurance rules for the median and extreme low flows at B8H008

			Target Flow ($m^3 s^{-1}$)	B8H007 average Inflow ($m^3 s^{-1}$)	TL's (%)	Required increase to inflow ($m^3 s^{-1}$)	Required increase to inflow (%)
2016	Prior to Construction (90 %)	Aug	0.597	0.573	7.00	0.069	11.99
		Sep	0.594	0.504	8.00	0.137	27.22
		Oct	0.497	0.248	17.00	0.333	134.11
	Prior to Construction (60 %)	Aug	0.597	0.573	7.00	0.069	11.99
		Sep	0.598	0.504	8.00	0.141	28.07
		Oct	0.597	0.248	17.00	0.449	181.22
	Post Construction (90 %)	Aug	0.605	0.573	7.00	0.077	13.49
		Sep	0.552	0.504	8.00	0.092	18.22
		Oct	0.523	0.248	17.00	0.363	146.36
	Post Construction (60 %)	Aug	0.778	0.573	7.00	0.263	49.95
		Sep	0.632	0.504	8.00	0.178	35.35
		Oct	0.554	0.248	17.00	0.399	160.96

Everson et al. (2001) noted that the degradation of the riparian forests and increased sedimentation may result in a shift towards more reed-based communities within the riparian zone. Consequently, this may significantly alter the magnitude and temporal progression of TL's within the system.

For this purpose, Everson et al. (2001) simulated evapotranspiration losses that would occur if riparian forests were completely replaced with reed communities and Consequently determined how this would influence TL's along the Sabie River. Following this approach (Everson et al., 2001), we attempted to quantify how such a change in land use would affect the estimated TL's in this study, as well as the implementation of the gazetted target flows. This scenario was simulated by assuming that there are no further changes in the losses of stream water to the aquifer or to artificial abstractions and the riparian zone consisted entirely of *P.mauritianus* with the root zone being inundated by stream water.

Using the estimated inflows from B8H007, the estimated TL's and the proposed increase to the flow are presented in Figure 5.6 and Table 5.7, respectively. These results show that there would be a substantial increase in the magnitude of TL's within this portion of river, with TL's in the range of 10 to 25 % occurring most frequently, if the aforementioned change in land use were to occur.

The magnitude of this increase in flow for B8H007for the land use change scenario ranges from; 0.101 (17.63%) to 0.546 (222.87 %) $m^3 s^{-1}$ prior to the construction of the dam. Whereas post dam construction the magnitude of flow increase for B8H007 ranges from; 0.110 (14.66 %) to 0.489 (164.50 %) $m^3 s^{-1}$.

Although this is a rudimentary approach at modelling the effect that the proposed land use change would have on TL's. It clearly demonstrates how such changes can alter the flow dynamics within the river system and constrain the successful implementation of EWR flow targets if these changes are unaccounted for. While this scenario was used to provide further insights on the effects of land use changes on TL's. This approach can be easily adapted to assess the effects that changing water uptake patterns (stream and groundwater uptake) during varying climatic conditions has on the magnitude of TL's.

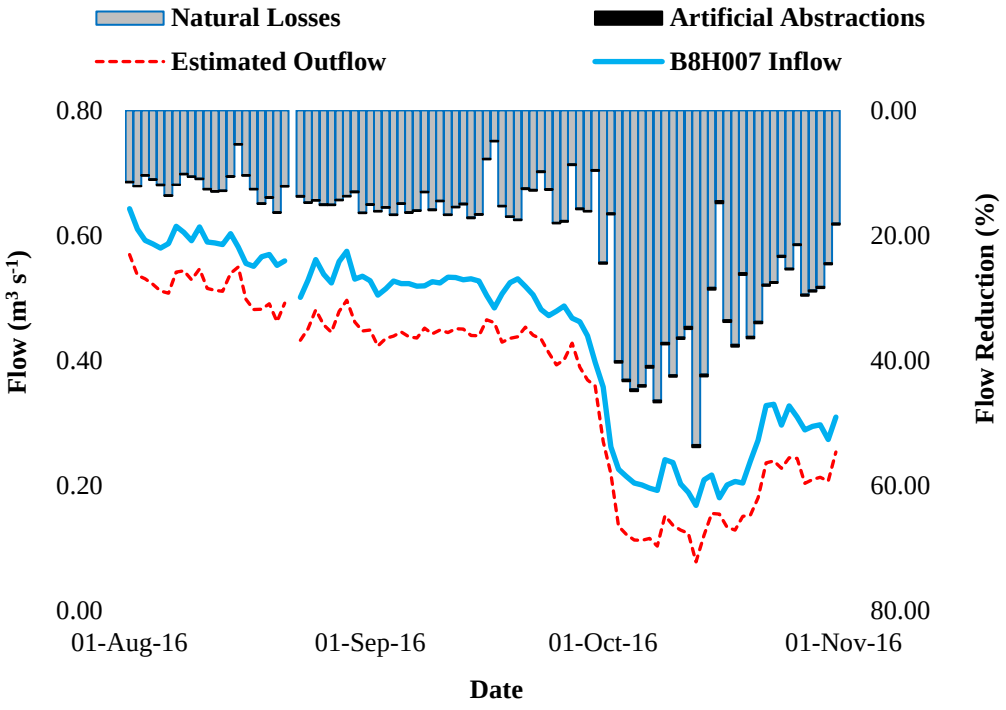

Figure 5.6 Daily TL's along a 14 km reach of the Groot Letaba River during the latter stages of the 2016 dry season for the land use change scenario

Table 5.7 Baseline estimates of the required increases to the flow emanating from B8H007 to meet the gazetted low flow assurance rules for the median and extreme low flows at B8H008 for the land use change scenario

			Target Flow ($m^3 s^{-1}$)	B8H007 average Inflow ($m^3 s^{-1}$)	TL's (%)	Required increase to inflow ($m^3 s^{-1}$)	Required increase to inflow (%)
2016	Prior to Construction (90 %)	Aug	0.597	0.573	0.13	0.099	17.23
		Sep	0.594	0.504	0.14	0.174	34.55
		Oct	0.497	0.248	0.33	0.411	165.67
	Prior to Construction (60 %)	Aug	0.597	0.573	0.13	0.099	17.23
		Sep	0.598	0.504	0.14	0.179	35.45
		Oct	0.597	0.248	0.33	0.543	219.13
	Post Construction (90 %)	Aug	0.605	0.573	0.13	0.099	17.23
		Sep	0.552	0.504	0.14	0.126	25.03
		Oct	0.523	0.248	0.33	0.445	179.57
	Post Construction (60 %)	Aug	0.778	0.573	0.13	0.302	52.78
		Sep	0.632	0.504	0.14	0.217	43.15
		Oct	0.554	0.248	0.33	0.486	196.14

5.5 Conclusion

In order to, reduce the uncertainty associated with TL's along the Groot Letaba River system, detailed characterization of hydrological processes along the lower reaches of the river, which was centred around the estimation of riparian total evaporation and quantifying the rapport between surface and subsurface water storage processes, was undertaken. The results of these investigations showed that there is a net loss from the river to the adjacent aquifer within the agricultural areas. While further downstream within the conservation areas, there is a net gain from the adjacent aquifer to the river. However, over the length of river reach studied, the river was shown to be a losing system.

A modified version of the satellite-based SEBS model was used to estimate ET along the length of river reach studied. These estimates were then coupled with soil water evaporation measurements and open water evaporation estimates to determine the riparian total evaporation. The riparian total evaporation estimates and losses from the river system to the adjacent aquifer were then used to determine TL's. The findings presented in this study indicated that TL's generally accounted for 5 to 15 % of the flow in the river system.

Riparian total evaporation and transpiration in particular were found to be the most significant contributing processes to these losses. This finding is of particular relevance, as riparian total evaporation has generally been considered to be a minor contributing process to TL's and is often inadequately represented or excluded from TL estimation procedures.

In general, it was shown that flows within the river system are unable to meet the gazetted low flow targets and are required to be increased in order to fulfil this requirement, whilst simultaneously accounting for TL's. Furthermore, the results of the land use change scenario reaffirmed the importance of understanding and quantifying riparian water use requirements, as it can assist in providing a more accurate estimate of the flows required to meet EWR flow targets under changing land use conditions.

Overall the study has detailed key hydrological processes influencing TL's along the Groot Letaba River. However, it should be noted that while the study site was extensively gauged, these observations only provide an understanding of the system for a limited period in time. Therefore, it would prove to be advantageous to continue longer term monitoring at the site, which may facilitate an improved understanding of the system under changing environmental conditions, as well as allowing for a reduction in the assumptions and related uncertainties that had to be factored into the analysis.

Moreover, these preliminary investigations only enabled the localized estimation of TL's. Recent studies have demonstrated how satellite earth observation data can be used to quantify losses or gains to the adjacent aquifer. Although it was not within the scope of this study, the coupling of these methodologies with the use of satellite-derived ET estimates provides an opportunity to obtain spatially explicit estimates of TL's at catchment and field scales. This in turn can prove to be extremely beneficial to the future effective management of EWR flows in the system.

Acknowledgements

The research presented in this paper emanates from a non-solicited Water Research Commission (WRC) project entitled: Quantification of transmission losses along the Letaba River for improved delivery of environmental water requirements (ecological reserve), WRC Project No K5/2338.

The authors would like to extend their gratitude to the Water Research Commission (WRC), the South African Environmental Observation Network (SAEON) and Department of Water and Sanitation Limpopo drilling division for the funding required to successfully complete this research. Furthermore, the authors would like to acknowledge the Council for Scientific and Industrial Research (CSIR) for the loaning of field equipment during the Eddy covariance campaign, as well as Engineering and Exploration Geophysical Services during the geophysics campaign.

References

Boroto J and Gorgens AHM. 2003. Limpopo River: an overview of alternative methods for estimating transmission losses. Hydrology of Mediterranean and Semiarid regions. *Proc. Montpellier Conference* IAHS Publ 278.

Cadol D, Kampf S and Wohl E. 2012. Effects of evapotranspiration on baseflow in a tropical headwater catchment. *Journal of Hydrology* 462–463: 4–14.

Cataldo J, Behr C, Montalto F and Pierce RJ. 2010. Prediction of Transmission Losses in Ephemeral Streams, Western U.S.A. *The Open Hydrology Journal* 4: 19-34.

Costa AC, Bronstert A and de Araujo JC. 2012. A channel transmission losses model for different dryland rivers. *Hydrology Earth System Science* 16: 1111–1135.

Costa AC, Foerster S, de Araujo JC and Bronstert A. 2013. Analysis of channel transmission losses in a dryland river reach in north-eastern Brazil using streamflow series, groundwater level series and multi-temporal satellite data. *Hydrological Process*es 27: 1046–1060.

Costelloe JF, Grayson RB, Argent RM and McMahon TA. 2003. Modelling the flow regime of an arid zone floodplain river, Diamantina River, Australia. *Environmental Modelling and Software* 18: 693–703.

Department of Water Affairs and Forestry. 2006a. Letaba River System Annual Operating Analysis. DWAF Report No: WMA 02/000/00/0406.

El-Hames AS and Richards SK. 1998. An integrated, physically based model for arid region flash flood prediction capable of simulating dynamic transmission loss. *Hydrol Process* 12: 1219-1233.

Everson CS, Burger C, Olbrich, BW and Gush, MB. 2001. Verification of estimates of water use from riverine vegetation on the Sabie river in the Kruger National Park. Water Research Commission Report, Project Number 877/1/01.

Falkenmark M and Molden D. 2008. Wake up to the realities of river basin closure. *Water Resour Dev* 24(2): 201–215.

Gheith H and Sulta, M. 2002. Construction of a hydrology model for estimating wadi runoff and groundwater recharge in the Eastern Desert, Egypt. *Journal of Hydrology* 263: 36-55.

Gokool, S, Riddell, ES, Strydom, T, Jarmain, C, Nel, JM and Swemmer A. 2015. Quantification of transmission processes along the Letaba River for improved delivery of environmental water requirements (Ecological Reserve). WRC Report, Deliverable No. 3: Project K5/2338/1.

Gokool, S, Jarmain, C, Riddell, E, Swemmer, A, Lerm, R and Chetty KT. 2017. Quantifying riparian total evaporation along the Groot Letaba River: A comparison between infilled and spatially downscaled satellite derived total evaporation estimates. Journal of Arid Environments 147: 114-124. http://dx.doi.org/10.1016/j.jaridenv.2017.07.014 0140-1963/© 2017.

Gribovski Z, Kalicz P, Szilagyi J and Kucsara, M. 2007. Riparian zone evapotranspiration estimation from diurnal groundwater level fluctuations. *Journal of Hydrology* 349: 6.

Gu R and Deutschman, M. 2001. Hydrologic Assessment of Water Losses in River. *Journal of Water Resources Planning and Management* 127 (1): 6-12.

Hacker, F. 2005. Model for Water Availability in Semi-Arid Environments (WASA): Estimation of transmission losses by infiltration at rivers in the semi-arid Federal State of Ceara (Brazil). MSc Thesis, University of Potsdam, Germany.

Heritage GL, Moon BP and Large ARG. 2001. The February 2000 floods on the Letaba River, South Africa: an examination of magnitude and frequency. *Koedoe* 44 2: 1-6.

Hughes DA and Sami K. 1992. Transmission losses to alluvium and associated moisture dynamics in a semi-arid ephemeral channel system in southern Africa. *Hydrological Processes* 6: 45-53.

Hughes DA. 2008. Modelling semi-arid and arid hydrology and water resources the Southern African experience. gwadi.org/sites/gwadi.org/files/hughes_L5.pdfand#8206; Hughes DA, Mallory SJL and Louw D (2008) Methods and software for the real-time implementation of the ecological reserve-explanations and user manual. *WRC Report 1582/1/08*.

Katambara Z and Ndiritu JG. 2010. A hybrid conceptual-fuzzy inference streamflow modelling for the Letaba River system in South Africa. *Physics and Chemistry of the Earth* 3513-14: 582-595.

Lange, J. 2005. Dynamics of transmission losses in a large arid stream channel. *Journal of Hydrology* 306: 112–126.

McLoughlin C, Deacon A Sithole, H and Gyedu-Ababio T. 2011. History, rationale, and lessons learned: Thresholds of potential concern in Kruger National Park river adaptive management. *Koedoe* 53(2): 1-27

Molle F, Wester, P and Hirsch, P. 2010. River basin closure: Processes, implications and responses. *Agricultural Water Management* 97: 569-577.

Pittock J and Lankford BJ. 2010. Environmental water requirements: demand management in an era of water scarcity. *Journal of Integrative Environmental Sciences* 7(1): 75–93.

Pollard S and du Toit D. 2011a. Towards Adaptive Integrated Water Resources Management in Southern Africa: The Role of Self-organisation and Multi-scale Feedbacks for Learning and Responsiveness in the Letaba and Crocodile Catchments. *Water resources management* 25 15: 4019-4035.

Priestley CHB and Taylor RJ. 1972. On the assessment of surface heat flux and evaporation using large-scale parameters. *Monthly Weather Review* 100: 81–92.

Riddell ES, Nel, JM, Gokool S, Jarmain, C, Raubenheimer R, Strydom T and Swemmer A. 2017. Quantification of transmission losses along the Letaba River for improved delivery of environmental water requirements (ecological reserve). Water Research Commission Report, Project Number K5/2338.

Sawunyama T and Hughes DA. 2010. Using satellite-based rainfall data to support the implementation of environmental water requirements in South Africa. *Water SA* 364.

Shanafield M and Cook PG. 2014. Transmission losses, infiltration and groundwater recharge through ephemeral and intermittent streambeds: A review of applied methods. *Journal of Hydrology* 511: 518–529.

Sharma KD and Murthy JSR. 1994a. Estimating transmission losses in an arid region. Journal of Arid Environments 26: 209-219.

Sinha PJ and Kumar R. 2015. Statistical Analysis to Investigate the Possible Impact of Climate Change on Water Availability in Letaba River of South Africa. *International Journal of Recent Technology and Engineering (IJRTE)* 3(6): 2277-3878.

The National Water Act (NWA). 1998. Act No. 36 of 1998. Republic of South Africa. *Government Gazette No. 19182*. Government Printers. Pretoria.

Tanner, JL and Hughes, DA. 2015a. Understanding and modelling surface water-groundwater interactions. WRC Report No. 2056/2/14. ISBN 978-1-4312-0630-8.

Vlok W and Engelbrecht JS. 2000. Some aspects of the ecology of the Groot Letaba River in the Northern Province, South Africa. *African Journal of Aquatic Science* 25 (1): 76-83.

Water Research Commission (WRC). 2001. State of the Rivers Report: Letaba and Luvuvhu Rivers Systems. WRC Report No TT 165/01, Water Research Commission, Pretoria, RSA.

With the overall objective of the study to understand and quantify the hydrological processes which contribute to TL's along the Letaba River, particularly focusing upon establishing the influence of riparian total evaporation on TL's, being addressed in chapter 5, chapter 6 details key findings of the research and proposes recommendations for future investigations.

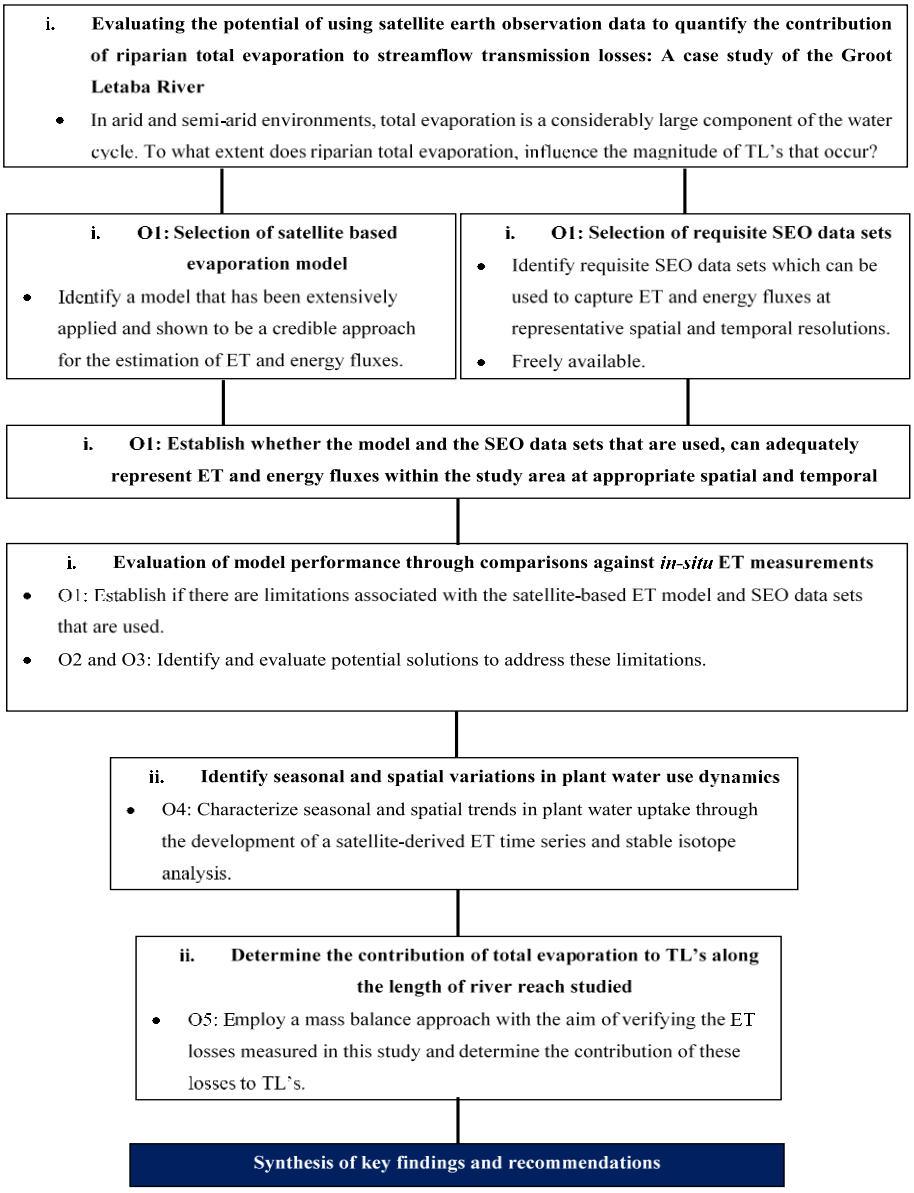

6. SYNTHESIS: KEY FINDINGS AND RECOMMENDATIONS FOR FUTURE INVESTIGATIONS

6.1 Introduction

During the latter stages of the 20th century the implementation and preservation of EWR flows in various catchments of the South African Lowveld has become increasingly difficult, due to the compounded effects of climate and land-use changes, as well as the improper management of water resources within these catchments. The efficient management of limited water resources in these environments is therefore dependent on comprehensively quantifying all hydrological processes, to understand and account for how these processes impact the flows within these river systems.

To date, the limited hydrological process understanding associated with system losses via TL's remains a constraint to the effective planning and management of water resources in arid and semi-arid climatic regimes and particularly the implementation of EWR flows. The Letaba River is an archetypal example of a river system in which EWR flow management has been adversely impacted by the lack of a quantitative understanding of TL's

In order to improve water provisions and proficiently manage EWR flows in this environment, it is imperative that hydrological processes contributing to TL's are understood and accurately quantified at various spatial and temporal scales. For this purpose, the research presented in this thesis progressively documents approaches which can be used to obtain spatially explicit estimates of evapotranspiration (ET), which is a major contributing process to the water balance of arid and semi-arid environments, yet has seldom been incorporated or adequately represented into TL's estimation procedures.

This research was centred around evaluating the potential of using a satellite-based approach to estimate ET along the length of river reach studied, to determine the most suitable and pragmatic approach which can be adopted for operational water resources management. To achieve this; existing and innovative approaches were employed and evaluated against *in-situ* observations, providing further insights into their application.

Furthermore, these investigations were supplemented by a parallel study focusing on quantifying surface and subsurface water storage processes. The coupling of this information with that acquired from the ET investigations, provided invaluable insights on the natural drivers of TL's in this river system.

6.2 Revisiting the objectives of the study and summary of key findings

The overall objective of this thesis was to reduce the uncertainty associated with TL's by attempting to understand and accurately quantify the hydrological processes which contribute to TL's along the Groot Letaba River, with particular emphasis being placed upon improving the estimation of riparian total evaporation and establishing the influence of this process on TL's. Considering the significant role that riparian ET plays in the water balance of river systems flowing through arid and semi-arid environments, it is essential to develop techniques or approaches which can be used to accurately quantify riparian ET at varying spatial and temporal scales, to better understand and quantify how this process influences the magnitude of TL's in these environments.

The use of satellite-based ET models and SEO data provide an opportunity to acquire such information. However, chapter 2 showed that limitations such as the trade-off between the spatial and temporal resolution of available imagery and the ability of the associated models to accurately estimate fluxes and ET in different environmental settings, may limit the feasibility of employing these approaches for operational water resources management.

The SEBS model, as well as Landsat and MODIS data were selected to estimate ET within a portion of the Groot Letaba River. While SEBS and these data sets have been extensively applied for the estimation of ET, limitations associated with the spatial and temporal resolution of these images presented challenges to the estimation of daily ET at the required spatial scale. Procedures detailed in Hong et al. (2011) (Output Downscaling with Linear Regression or ODLR) and Gokool et al. (2016) (Kc_{act}) were identified as suitable approaches to address these limitations. However, to establish confidence in the implementation of these approaches comparisons against *in-situ* ET observations were essential.

The results of these investigations showed that comparisons against daily EC_{ET} measurements were less than satisfactory. This poor correlation was largely attributed to the inability of SEBS to explicitly account for the influence of soil moisture and biophysical parameters during the derivation of surface fluxes.

Consequently, SEBS overestimated ET for this water stressed environment with the degree of overestimation of the evaporative fraction (*EF*) and (*LE*) being markedly higher for drier soils lacking vegetation coverage. Recent studies have identified potential solutions to address this limitation through the integration of a scaling factor into the original model formulation ($SEBS_0$) to correct for the overestimation of the evaporative fraction (*EF*) and the latent heat flux (*LE*) within the model.

After conducting a detailed review of the available literature with regards to approaches that could be implemented to address this particular limitation associated with $SEBS_0$, the integration of an evaporative calibration factor (*ESF*) into $SEBS_0$ was proposed in chapter 3, as the most pragmatic approach to address this limitation. This factor was derived from SEO and *in-situ* data which had been collected in this study, thereby limiting the time required for further data acquisition and processing. The integration of the *ESF* into $SEBS_0$ was shown to significantly improve the correlation between EC_{ET} and modelled ET estimates, as well as increasing the percentage of modelled ET estimates within an acceptable accuracy range.

Through the application of this modified version of SEBS ($SEBS_{ESF}$), the ability of the ODLR and Kc_{act} approaches to develop a time-series of daily moderate spatial resolution ET estimates could now be demonstrated (chapter 4). The use of the $SEBS_{ESF}$ derived ET estimates as inputs to the aforementioned approaches improved the estimation of the daily ET at a MSR when compared against *in-situ* observations, the Kc_{act} approach was shown to compare most favourably to EC_{ET}, yielding correlation coefficient and Nash-Sutcliffe efficiency values of 0.79 and 0.60, respectively.

With the ability of this satellite-based approach to adequately represent ET within this environment now confirmed. Stable isotope analysis (of ^{18}O and ^{2}H) and a Bayesian mixing model were coupled with the Kc_{act} derived ET estimates, to further investigate spatial and seasonal variations in plant water uptake dynamics. The results of these investigations showed that soil water was the main contributing source to ET (approximately 88%), with soil water at depths between 60 and 140 cm being the dominant contributing source during plant water uptake, throughout the period of investigation.

Stream and groundwater use during transpiration was also prevalent within the study area (approximately 15 %) and increased with aridity, however, the magnitude of its contribution to transpiration was fairly minimal and not as significant as generally reported in literature. However, it should be noted that in other environmental settings the contribution of groundwater to riparian ET may be somewhat different depending on the riparian plant species present and their respective locations.

The insights acquired from chapter 4 on the spatial and seasonal variations in plant water use dynamics, assisted in deriving baseline estimates of TL's the during the latter stages of the 2016 low flow period (August to October), which typically represents a critical period with regards to water shortages. This involved using the satellite-derived daily ET time series in conjunction with data obtained from a parallel investigation (Riddell et al., 2017), which focused on quantifying the rapport between surface and sub-surface water storage processes.

The results presented in chapter 5, showed that TL's during this period generally accounted for between 5 and 15 % of streamflow. Riparian total evaporation and transpiration in particular were found to be the dominant contributing processes to these losses. This finding was considered particularly relevant, as riparian total evaporation has generally been considered to be a minor contributing process to TL's and is often inadequately represented or excluded from TL's estimation procedures. In general, it was shown that flows within the river system were unable to meet gazetted low flow targets and are required to be increased in order to fulfil this requirement, whilst simultaneously accounting for TL's. Furthermore, the results of the land use change scenario reaffirmed the importance of understanding and quantifying riparian water use requirements, as it can assist in providing a more accurate estimate of the flows required to meet EWR flow targets under changing land use conditions.

The aforementioned findings relate to the specific objectives described within chapters 2 to 5. In general, there was an important observation which continuously re-emerged during these various investigations, which essentially relates to the need for accurate long-term *in-situ* data records. The use of SEO data and satellite-based evaporation models allows for the spatially explicit estimation of ET which generally can't be attained by conventional approaches. Furthermore, these techniques are inexpensive and can be used to provide detailed hydrological process information in data scarce regions. Consequently, in recent times there has been an increase in the use of these data sets and models for various applications, *inter alia*; irrigation scheduling, water resources management and as data source for hydrological modelling.

While satellite-earth observation provides an alternative approach to obtain hydrological process information, these approaches are generally evaluated against conventional approaches before they are applied with any degree of confidence. Furthermore, these *in-situ* observations are required to understand inherent limitations associated with the model or data sets, so that existing approaches can be improved upon or new approaches can be developed. Using the investigations and results of this study as an example, the importance of accurate data acquired from conventional approaches can be emphasized as follows;

i) Uncertainties associated with the modelled ET estimates, especially the inability of $SEBS_0$ to adequately capture energy fluxes and ET during water stressed conditions would have not been identified without comparisons against *in-situ* ET observations.

ii) Evaluation of the $SEBS_{ESF}$ approach as a potential solution to address this limitation would have not been possible without *in-situ* ET observations.

iii) The uncertainty associated with flux tower estimates acquired from the EC system in the Malopeni study area could have led to a false perception in the performance of the $SEBS_{ESF}$ approach.

iv) Uncertainties associated with the TL's estimated in this study could not be quantified due to a lack of accurate streamflow data.

These observations clearly demonstrate that while the use of satellite-earth observation approaches is utilized more frequently and are being advocated as an alternative to obtain hydrological process information, the successful application of these approaches for present and future studies will to some degree be dependent on data collected from conventional *in-situ* approaches. Therefore, it is imperative that; these conventional approaches continue to be used for the provision of hydrological process information, existing *in-situ* networks are adequately maintained and additional networks are established in the future.

6.3 Contributions of this research to new knowledge

Overall the study has detailed key hydrological processes influencing TL's along the Groot Letaba River. It is envisaged that this will enable the establishment of an improved conceptual model of the system, which may prove to be beneficial for future hydrological modelling applications in this region.

Specific contributions of this research to new knowledge and how these contributions met the objectives described within each chapter (chapters 2 to 5) are summarised as follows:

i) The implementation of the Kc_{act} and ODLR approaches assisted in overcoming the spatial and temporal resolution issues associated with the SEO data sets used in this study, enabling the development of a daily satellite-derived ET time-series suitable for field scale applications within the study area (chapters 2 and 4).

ii) Prior to the investigations discussed in chapters 2 and 4, the ODLR procedure had not yet been applied to obtain seasonal continuous moderate spatial resolution (MSR) ET estimates. Consequently, the suitability of applying this approach to generate daily ET at a MSR was relatively unknown (Bhattarai et al., 2015). The results presented in these chapters have to a large extent, addressed this knowledge gap by providing invaluable insights on the suitability of this approach for the estimation of daily ET at a MSR.

iii) From a South African perspective, chapters 2 and 3 have facilitated an improved hydrological process understanding of the factors which influence the performance of satellite-based ET estimation approaches for different climatic conditions. Thus, providing further insights on the factors to consider before selecting and implementing a satellite-based ET model.

iv) The $SEBS_{ESF}$ approach was proposed and evaluated as an alternative approach to address the shortcomings of implementing $SEBS_0$ during conditions of water stress (chapter 3). The results of these investigations showed that the integration of the *ESF* into $SEBS_0$ significantly improved the estimation of energy fluxes and ET during conditions of water stress within the study area. This approach has merits to improve the localized mapping of energy fluxes and ET in arid and semi-arid climatic regimes. Furthermore, the *ESF* can be derived from data which had been previously collected for the implementation of $SEBS_0$, therefore limiting the time required for further data acquisition and processing.

v) The use of SEBS and stable isotope analysis are well established and frequently applied approaches to estimate ET and investigate the sources of plant water uptake, respectively. The coupling of the data emanating from these independent approaches (chapter 4) provides an innovative means of quantifying spatial and seasonal variations in source contribution to ET.

vi) Bayesian mixing models have seldom been applied to determine the proportional contribution of sources to plant water uptake and to the author's knowledge Simmr has not yet been applied for hydrological applications. Therefore, the results discussed in chapter 4 provide valuable insights as to how Simmr can be used to investigate plant water use dynamics.

vii) Previous TL's estimation procedures have seldom included or adequately incorporated the influence of riparian total evaporation. The investigations and results presented in chapter 5, have shown that this process can play a significant role in the water balance of river systems flowing through arid and semi-arid environments. Furthermore, the use of satellite-derived ET estimates has enabled the spatially explicit quantification of the contribution of ET to TL's in this environment, which was previously unattainable using conventional ET estimation procedures. This can prove to be particularly advantageous for the future effective management of EWR flows in the system at both catchment and regional levels.

viii) The results presented in chapter 5 provided new insights, as to how gazetted target flows within this portion of river reach can be achieved through the improved estimation of TL's under present or changing environmental conditions (Overall objective).

ix) The timing of this study coincided with a large El-Nino induced drought period (Kogan and Guo, 2016). Consequently, the results of the various investigations have provided invaluable insights on the dynamics of hydrological processes within this region, during extreme drought conditions.

6.4 Challenges experienced during the duration of this study

Due to capacity constraints, such as finances, human resources and duration of the study *inter alia,* there were various limitations experienced throughout the investigation period. These are summarized as follows;

i) In order to apply a SEO approach to obtain hydrological process information with any degree of confidence, the data emanating from these approaches were compared against *in-situ* observations. Therefore, investigations were limited to the periods in which adequate observed data were available.

ii) Due to the nature of the investigations and the methodology applied herein, a large volume of satellite-imagery was required. These images were manually collected and processed to derive the requisite data sets used in this study. While automated bulk-processing of this imagery is an option, the necessary software and training required to implement such an approach was not available within the time frames of this project. Consequently, we were only able to perform analysis for a limited number of sites over a 2-year period.

iii) Comparisons between the satellite derived ET estimates against observed ET data, allows for the quantification of errors and uncertainties associated with the modelled estimate. However, uncertainties associated with the observed data, such as the Malopeni flux data may have led to a false perception of the model performance or the data sets that were used, if these inaccuracies remained unaccounted for. Furthermore, while the $SEBS_{ESF}$ was shown to improve the estimation of ET in the Malopeni study site, the degree to which this approach improved ET estimation could not be truly gauged.

iv) the implementation of the $SEBS_{ESF}$ approach negates the advantage that SEBS has over other satellite-based ET estimation models, *viz*. that it is a purely physical process of the model and consequently provides credible results irrespective of season or location.

v) Due to the remote locality of the study site, collection of samples for stable isotope analysis was undertaken during three window periods. Consequently, these observations may not adequately represent the seasonal variations in plant water use dynamics.

vi) Uncertainties in the estimated TL's could not be verified using a mass balance approach, due to the lack of accurate observed streamflow data. Consequently, these estimates as well as the proposed increases in flow required to meet the gazetted target flows should be considered preliminary findings.

vii) Although the study site was extensively gauged during the period of investigation, these observations only provide an understanding of the system for a limited period in time.

6.5 Future research opportunities

Throughout the duration of this thesis; detailed analysis of available literature was undertaken to guide the various approaches which were eventually implemented and tested, in order to fulfil the objectives of this study. However, considering the additional knowledge that has been acquired with regards to the research subject, the following are proposed as opportunities for possible future investigations:

i) While MODIS and Landsat data, as well as the SEBS model were selected for implementation in this study, largely due to their extensive use in research and operational studies. Alternate data sets and satellite-based ET models which meet these criteria, were not considered as they were not freely available. Depending on the resources available and the objectives of the study; the use of data acquired from higher resolution imagery, the application of alternate satellite-based ET models such as the Surface Energy Balance Algorithm for Land (SEBAL; Bastiaanssen et al., 1998) and Mapping Evapotranspiration with High Resolution and Internalized Calibration (METRIC; Allen et al., 2007) or satellite-based ET products (MOD-16) can be used to obtain spatially explicit estimates of ET. Furthermore, recent advances in google earth engine and the SEBS Global Land ET product (Chen, 2017) offers new and exciting research opportunities.

ii) The use of the ODLR and Kc_{act} approaches were selected for application in this study due to their relative ease of application and minimal data requirements, which may prove to be appealing for operational water resources management. However, there are additional downscaling and image fusion based approaches such as those detailed in; Ha et al. (2011), Singh et al. (2014), Alidoost et al. (2015) and Bhattarai et al. (2015), which may enable the more accurate estimation of daily ET at a MSR but were not considered due to the aforementioned criteria.

iii) While the proposed integration of *ESF* into $SEBS_0$ was shown to be a credible approach for estimating ET during conditions of water stress, future investigations regarding the application of the $SEBS_{ESF}$ approach should also be compared against other modified versions of SEBS (Gokmen et al., 2012; Pardo et al., 2014; Hueng et al., 2015), to truly gauge if the proposed method offers any significant improvement to the mapping of ET in arid and semi-arid environments. Additionally, future research efforts could be focused on improving the modelling of the kB^{-1} parameter or extra (stomatal) resistance terms when deriving *H*, during conditions of water stress.

iv) Increasing the sampling frequency and number of water samples collected during stable isotope analyses would facilitate an improved representation of source contributions to ET, which in turn may allow for invaluable time-series comparisons of seasonal and spatial variations in plant water uptake dynamics.

v) The preliminary estimates of TL's and proposed increases the in flow required to meet the gazetted target flows, could not be verified in this study. The methodology used to obtain this information was neither site or model specific and therefore has the potential to be applied in other environmental settings.

vi) The preliminary investigations in this study only enabled the localized estimation of TL's. Recent studies (Walter et al., 2011; Costa et al., 2013) have demonstrated how satellite earth observation data can be used to quantify losses or gains to the adjacent aquifer. The coupling of these methodologies with the use of satellite-derived ET estimates provides an opportunity to obtain spatially explicit estimates of TL's at both catchment and regional scales. This in turn can prove to be extremely beneficial to the future effective management of EWR flows in the system.

vii) The study site was extensively gauged and detailed investigations of hydrological processes contributing to TL's were undertaken during the low flow period, which typically represents a critical period with regards to water shortages. However, these observations only provide an understanding of the system for a limited period in time. Therefore, it would prove to be advantageous to continue longer term monitoring at the site, which may facilitate an improved understanding of the system during higher flow periods and under changing environmental conditions. Furthermore, this may allow for a reduction in the assumptions and related uncertainties that had to be factored into the analysis.

References

Alidoost, F., Sharifi, M.A., Stein, A., 2015. Region and pixel-based image fusion for disaggregation of actual evapotranspiration. International Journal of Image and Data Fusion. DOI: 10.1080/19479832.2015.1055834.

Allen, R, Tasumi, M, Morse, A, Trezza, R, Wright, J, Bastiaanssen, W, Kramber, W, Lorite, I and Robison, C. 2007. Satellite-Based Energy Balance for Mapping Evapotranspiration with Internalized Calibration (METRIC)—Applications. Journal of Irrigation and Drainage Engineering 133(4): 395–406.

Bhattarai, N., Quackenbush, L.J., Dougherty, M., Marzen, L.J., 2015. A simple Landsat–MODIS fusion approach for monitoring seasonal evapotranspiration at 30 m spatial resolution. International Journal of Remote Sensing 36(1): 115-143.

Chen, X. 2017. Personal communication. University of Twente, Department of Water Resources, Faculty of Geo-Information Science and Earth Observation (ITC). 16th October 2017.

Costa, AC, Foerster, S, de Araujo, JC and Bronstert, A. 2013. Analysis of channel transmission losses in a dryland river reach in north-eastern Brazil using streamflow series, groundwater level series and multi-temporal satellite data. *Hydrological Process*es 27: 1046–1060.

Gokmen, M., Vekerdy, Z., Verhoef, A., Verhoef, W., Batelaan, O., Tol, C., 2012. Integration of soil moisture in SEBS for improving evapotranspiration estimation under water stress conditions. Remote Sens Environ 121: 261–274. DOI: 10.1016/j.rse.2012.02.003

Gokool, S, Chetty, KT, Jewitt, GPW and Heeralal, A. 2016. Estimating total evaporation at the field scale using the SEBS model and data infilling procedures. *Water SA* 42(4): 673-683.

Ha, W., Gowda, P.H., Howell, T.A., 2013. A review of downscaling methods for remote sensing-based irrigation management: Part I. Irrigation Science 31: 831–850.

Hong, S., Hendrickx, J.M.H., Borchers. B., 2011. Down-scaling of SEBAL derived evapotranspiration maps from MODIS (250 m) to Landsat (30 m) scales. International Journal of Remote Sensing 32(21): 6457–6477.

Hueng, C., Li, Y., Gu, J., Lu, J., Li, X., 2015. Improving Estimation of Evapotranspiration under Water-Limited Conditions Based on SEBS and MODIS Data in Arid Regions. Remote Sens 7:16795–16814. DOI:10.3390/rs71215854.

Kogan, F., and Guo W., 2016. Strong 2015–2016 El Niño and implication to global ecosystems from space data. International Journal of Remote Sensing 38(1): 161-178.

Pardo, N., Sanchez, L.M., Timmermans, J., Su, Z., Perez, I.A., and Garcia, M.A., 2014. SEBS validation in a Spanish rotating crop. Agricultural and Forest Meteorology 195-196: 132-142.

Singh, R.K., Senay, G.B., Velpuri, N.M., Bohms, S., and Verdin, J.P., 2014b. On the Downscaling of Actual Evapotranspiration Maps Based on Combination of MODIS and Landsat-Based Actual Evapotranspiration Estimates. Remote Sensing 6: 10483-10509.

Walter, G.R., Necsoiu, M., McGinnis, R., 2011. Estimating aquifer channel recharge using optical data interpretation. Ground Water 50 (1): 68–76.

APPENDIX A: IMAGE PROCESSING AND METEOROLOGICAL DATA

The procedures outlined in Su and Wang (2013), Singh et al. (2014a) and USGS (2015), used to derive the necessary land surface parameters required as inputs to SEBS for the estimation of ET are detailed as follows.

Pre-processing of Landsat 7 Level 1 Geotiff data products

The data provided in Landsat 7 bands, are represented as digital numbers (DN) and therefore need to be converted into at-sensor radiance and top of the atmosphere (TOA) reflectance. Radiometric rescaling coefficients provided in the meta-data file are used to perform this conversion.

Conversion to at-sensor radiance

The conversion to at-sensor radiance is given as:

$$L = \frac{(L_{max} - L_{min})(DN - Q_{calmin})}{(Q_{calmax} - Q_{calmin})} + L_{min} \quad \text{(A1)}$$

Where L is the spectral radiance (W m^{-2} sr^{-1} μm^{-1}), L_{max} is the maximum rescaling factor (W m^{-2} sr^{-1} μm^{-1}), L_{min} is the minimum rescaling factor (W m^{-2} sr^{-1} μm^{-1}), DN is the quantized calibrated pixel value, Q_{calmax} is the quantized calibrated pixel value related to L_{max} and Q_{calmin} is the quantized calibrated pixel value related to L_{min}.

Conversion to planetary TOA reflectance

$$\rho = \frac{\pi \text{ x } L}{(E_{sun} \text{ x } Cos\theta \text{ x } d_r)} \quad \text{(A2)}$$

Where ρ is the planetary TOA reflectance, d_r is the earth sun distance parameter, E_{sun} is the mean exoatmospheric solar irradiance (W m^{-2} μm^{-1}) and θ is the solar zenith angle (^{0}). E_{sun} can be obtained from the LPSO (2006).

Computation of SEBS input maps (albedo, NDVI, emissivity and land surface temperature)

The TOA albedo can be calculated as:

$$\alpha_{toa} = \sum(\rho \text{ x } w\lambda) \quad \text{(A3)}$$

Where α_{toa} is the top of the atmosphere albedo and $w\lambda$ is a weighting coefficient given as:

$$w\lambda = \frac{E_{sun}}{\sum E_{sun}} \quad \text{(A4)}$$

The surface albedo can then be computed as:

$$\alpha = \frac{(\alpha_{toa} - \alpha_{path})}{\tau_{sw}^2} \quad \text{(A5)}$$

Where α is the surface albedo, α_{path} is the albedo path radiance ranging between 0.025 and 0.04 (Singh *et al*., 2014a) and τ_{sw} is the transmittance, which is calculated as:

$$\tau_{sw} = (0.75 + 2\text{x}10^{-5}) \text{ x } Z \quad \text{(A6)}$$

Where Z is the altitude above mean sea level (m).

The NDVI can be calculated as:

$$NDVI = \frac{(NIR - Red)}{(NIR + Red} \quad \text{(A7)}$$

Where *NIR* is the Near-Infra Red band (W m^{-2} μm^{-1}) and Red is the red band (W m^{-2} μm^{-1}).

The surface emissivity is computed as:

$$\varepsilon_o = (1.009 + 0.047)\text{x } \ln(NDVI) \quad \text{(A8)}$$

The land surface temperature (LST) is computed as:

$$Ts = \frac{T_{bb}}{\varepsilon_o^{0.25}} \quad \text{(A9)}$$

Where Ts is the LST (K) and T_{bb} is the at-satellite brightness temperature (K).

T_{bb} is estimated as:

$$T_{bb} = \frac{K_2}{\ln\left(\frac{K_1}{L\lambda}\right)+1} \quad \text{(A10)}$$

Where K2 and K1 are calibration constants, respectively (1282.71 K and 666.09 W m^{-2} sr^{-1} μm^{-1}) and $L\lambda$ is the band 6 spectral radiance (W m^{-2} sr^{-1} μm^{-1}).

Pre-processing of Landsat 8 Level 1 Geotiff data products

Conversion to at-sensor radiance

The conversion to at-sensor radiance is given as:

$$L\lambda = M_L \text{x } Q_{cal} + A_L \quad \text{(A11)}$$

Where $L\lambda$ is the spectral radiance (W m^{-2} sr^{-1} μm^{-1}), M_L is the radiance multiplicative scaling factor for the band (RADIANCE_MULT_BAND acquired from the MTL file), A_L is the radiance additive scaling factor for the band (RADIANCE_ADD_BAND acquired from the MTL file) and Q_{cal} is the Level 1 pixel value in DN (USGS, 2015).

Conversion to OLI TOA reflectance

$$\rho\lambda' = M_\rho \text{x } Q_{cal} + A_\rho \quad \text{(A12)}$$

Where $\rho\lambda'$ is the TOA planetary spectral reflectance, without correction for solar angle, $M\rho$ is the reflectance multiplicative scaling factor for the band (REFLECTANCE_MULT_BAND acquired from the MTL file) and $A\rho$ is the radiance additive scaling factor for the band (REFLECTANCE _ADD_BAND acquired from the MTL file) (USGS, 2015). The $\rho\lambda'$ is not a true TOA reflectance, as it has not been corrected for the solar elevation angle. The solar elevation angle can either be calculated or acquired from the MTL file. Once this value has been ascertained, the true TOA reflectance can be calculated (USGS, 2015) as:

$$\rho\lambda = \frac{\rho\lambda\prime}{\sin\theta} \quad \text{(A13)}$$

Where $\rho\lambda$ is the TOA planetary reflectance and $sin\ \theta$ is the solar angle (calculated or acquired from the MTL file).

Computation of SEBS input maps (albedo, NDVI, emissivity and LST)

Equations A3 to A6 can be applied to derive the surface albedo. However, E_{sun} values are not provided for Landsat 8 Level 1 Geotiff data products, as they are not required for the conversion of DN to reflectances. Consequently, these values have to be calculated.

E_{sun} values for Landsat 8 Level 1, bands 2 to 5 and 7 are determined as:

$$E_{sun} = (\pi \text{ x } d^2)(\frac{RAD\_MAX}{REF\_MAX}) \quad \text{(A14)}$$

Where *d* is the earth sun distance, *RAD_MAX* is the maximum radiance for the respective band and *REF_MAX* is the maximum reflectance for the respective band (acquired from the MTL file). Equations A7 and A8 can be applied to determine the *NDVI* and ε_o, respectively. Equation A9 is used to convert the radiance values of bands 10 and 11 to at-satellite brightness temperature. The thermal conversion constants K_1 and K_2 can be obtained from the MTL file (K1_CONSTANT_BAND and K2_CONSTANT_BAND) (USGS, 2015). Band 10 and 11, represent low and high gain conditions, respectively. Therefore, one band may be better suited to estimate the LST for a particular surface. For example, a high gain is suited for grassland environments. However due to the heterogeneity of the study area it was decided that the at-satellite brightness temperature for bands 10 and 11 would be the averaged and then applied in Equation A10, to determine the LST.

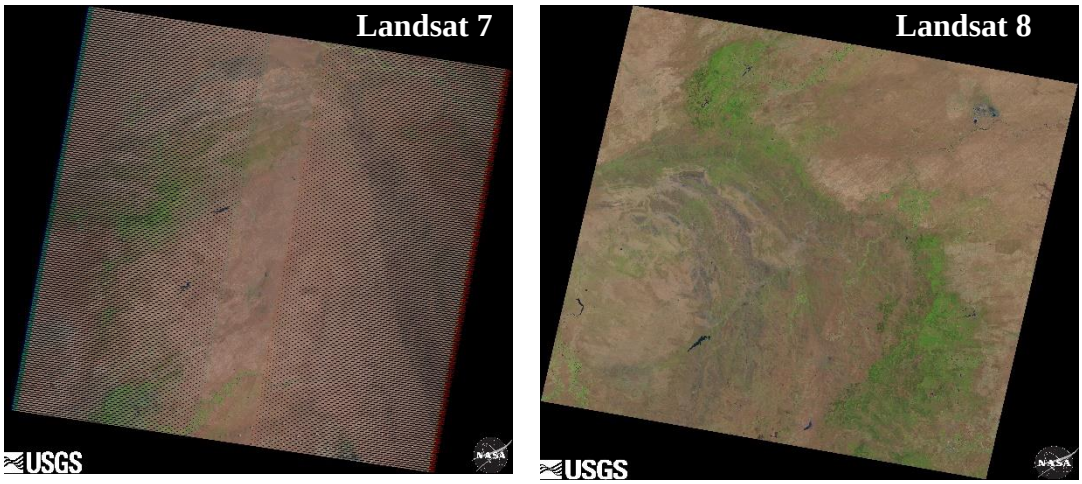

Figure A1 An axample of a Landsat 7 and 8 Level 1 natural colour composite covering the location of the study area

Pre-processing of MODIS Level 1_B data products

MODIS Level 1_B calibrated radiances and geolocation files are given in an orbit based format. These files therefore need to be projected into a standard format and projection, in order to be compatible with Geographic Information System (GIS) software. The aforementioned files can be converted into geographic projection and GeotTiff format, using the MODIS reprojection Swath Tool. MODIS provides multispectral data for 36 bands, however; only 13 bands were utilized to derive the inputs necessary for the application of the SEBS Model. These bands are presented in Table 1.

Table A1 MODIS bands used to derive the inputs necessary for the application of the SEBS Model (adapted from Su and Wang, 2013)

MODIS band GeoTiff Filename	File name in ILWIS
EV 250 Aggr1km RefSB bo.tif	Band1_dn
EV 250 Aggr1km RefSB b1.tif	Band2_dn
EV 500 Aggr1km RefSB b0.tif	Band3_dn
EV 500 Aggr1km RefSB b1.tif	Band4_dn
EV 500 Aggr1km RefSB b2.tif	Band5_dn
EV 500 Aggr1km RefSB b4.tif	Band7_dn
EV 1KM Emissive RefSB b10.tif	Band31_dn
EV 1KM Emissive RefSB b11.tif	Band32_dn
Solar Zenith.tif	Sza_dn
Solar Azimuth.tif	Saa_dn
Sensor Zenith.tif	Vza_dn
Sensor Azimuth.tif	Vaa_dn
Height.tif	Height

Conversion to radiance and reflectance

The data provided in the 13 MODIS Level 1_B bands, are represented as digital numbers (DN) and therefore need to be converted into radiance and reflectance values. The HDF View 2.9 Software Tool can be used to view the metadata associated with the MODIS Level 1_B data, in order to obtain the calibration coefficients required to perform the abovementioned conversion. The reflectance and radiance calibration coefficients were applied to convert band 1_dn to band 5_dn, as well as band 7_dn into reflectance values and band 31_dn and band 32_dn into radiance values. Additionally, a scaling factor (0.01) was applied to the Sza_dn, Saa_dn, Vza_dn, and Saa_dn.

Application of a simplified method for the atmospheric correction of satellite measurements (SMAC)

It is essential to correct for atmospheric absorption and scattering effects in the visible channels, when dealing with approaches which are predicated on the shortened surface energy balance. The SMAC algorithm is available as a tool within ILWIS to perform atmospheric calibrations for the visible channels. The SMAC algorithm is applied to Band 1_dn to Band 7_dn, to obtain atmospherically corrected bands which can be used for albedo, NDVI and emissivity computations.

Computation of SEBS input maps (albedo, NDVI, emissivity and LST)

The atmospherically corrected MODIS reflectance bands are used to compute the surface albedo, which is computed as:

$$\alpha = (0.16B_1) + (0.291B_2) + (0.243B_3) + (0.116B_4) + (0.112B_5) + (0.018B_7) - 0.0015 \quad \text{(A15)}$$

Where B_1, B_2, B_3, B_4, B_5 and B_7 are the atmospherically corrected surface reflectance bands derived from MODIS bands 1, 2, 3, 4, 5 and 7, respectively. The *NDVI* can be determined by using the atmospherically corrected Red and Near Infra-Red bands in Equation A7. The NDVI values are then used to compute the land surface emissivity. The NDVI value is used to differentiate between different types of pixels i.e. bare soil, vegetation and mixed pixels. Contingent, to these values the surface emissivity can be estimated using the atmospherically corrected Red and Near Infra-Red bands. During the computation of the land surface emissivity in ILWIS, optional parameters can be generated, these include the spectral emissivity difference and the f_c. Furthermore, Su (2002) state that the NDVI can also be used as a surrogate when detailed vegetation information is unavailable. Internal routines and models available within SEBS can be used to provide this information using NDVI as a basis for these estimation procedures. Due, to the lack of detailed vegetation information in this study, the aforementioned approach was adopted when implementing SEBS.

The following formula is used for the LST computation:

$$LST = b_{tm31} + 1.02 + 1.79(b_{tm31} - b_{tm32}) + 1.2(b_{tm31} - b_{tm32})^2 + (34.83 - 0.68W) \text{ x } (1 - \varepsilon_o) + (-73.27 - 5.19W) \text{ x } d\varepsilon_o \quad \text{(A16)}$$

Where b_{tm31} is the brightness temperature obtained from MODIS band 31, b_{tm32} is the brightness temperature obtained from MODIS band 32, W is the water vapour content and $d\varepsilon_o$ is the emissivity difference. In the absence of a water vapour data set, a simplified form of the Equation 16 can be used to estimate *LST*, which is given as:

$$LST = b_{tm31} + 1.02 + 1.79(b_{tm31} - b_{tm32}) + 1.2(b_{tm31} - b_{tm32})^2 \quad \text{(A17)}$$

The brightness temperature can be derived by converting MODIS bands 31 and 32 from radiances to blackbody temperatures, using the Planck equation, which is given as:

$$T_c = \frac{C_2}{\lambda_c \log\left(\frac{C_1}{\lambda^5 \pi L_s}\right)+1} \quad \text{(A18)}$$

Where T_c is the brightness temperature from a central wavelength, λ_c is the sensor's central wavelength, C_1 and C_2 are the blackbody constants and L_s is the radiance for the respective band.

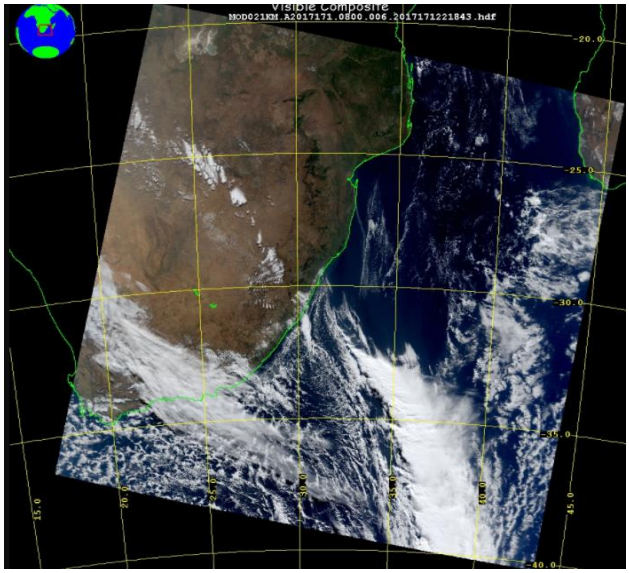

Figure A2 An example of a MOD21 Level1 B visible composite covering the location of the study area

Meteorological and Energy Balance Data

Observations of meteorological variables were made every 10 seconds and the appropriate statistical outputs were stored on a data logger at 10-minute intervals, as shown in Figure A3. Whereas, the EC system was equipped with a CSAT 3-D sonic anemometer that was connected to a CR3000 datalogger and measurements of the sonic air temperature, wind speed and direction were taken with a sampling frequency of 10 Hz. The averages of these high frequency measurements (from instantaneous data) were then used to compute a half-hourly sensible heat flux (Figure A4). The aforementioned data is displayed using the View Pro 4.2 utility available in Loggernet 4.2.1.

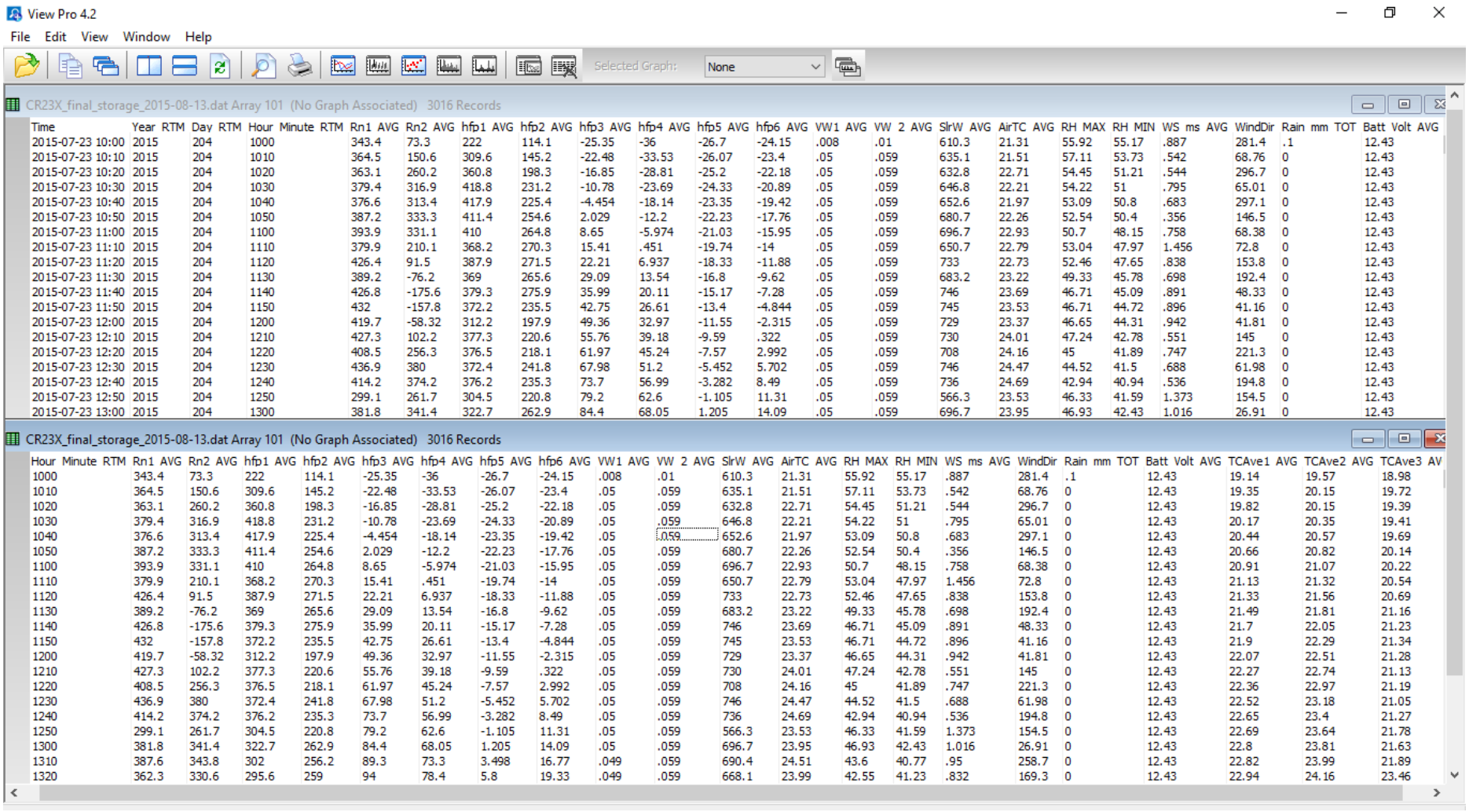

Figure A3 An example of the meteorological and energy balance data captured by the various sensors and stored on the CR23X logger output file

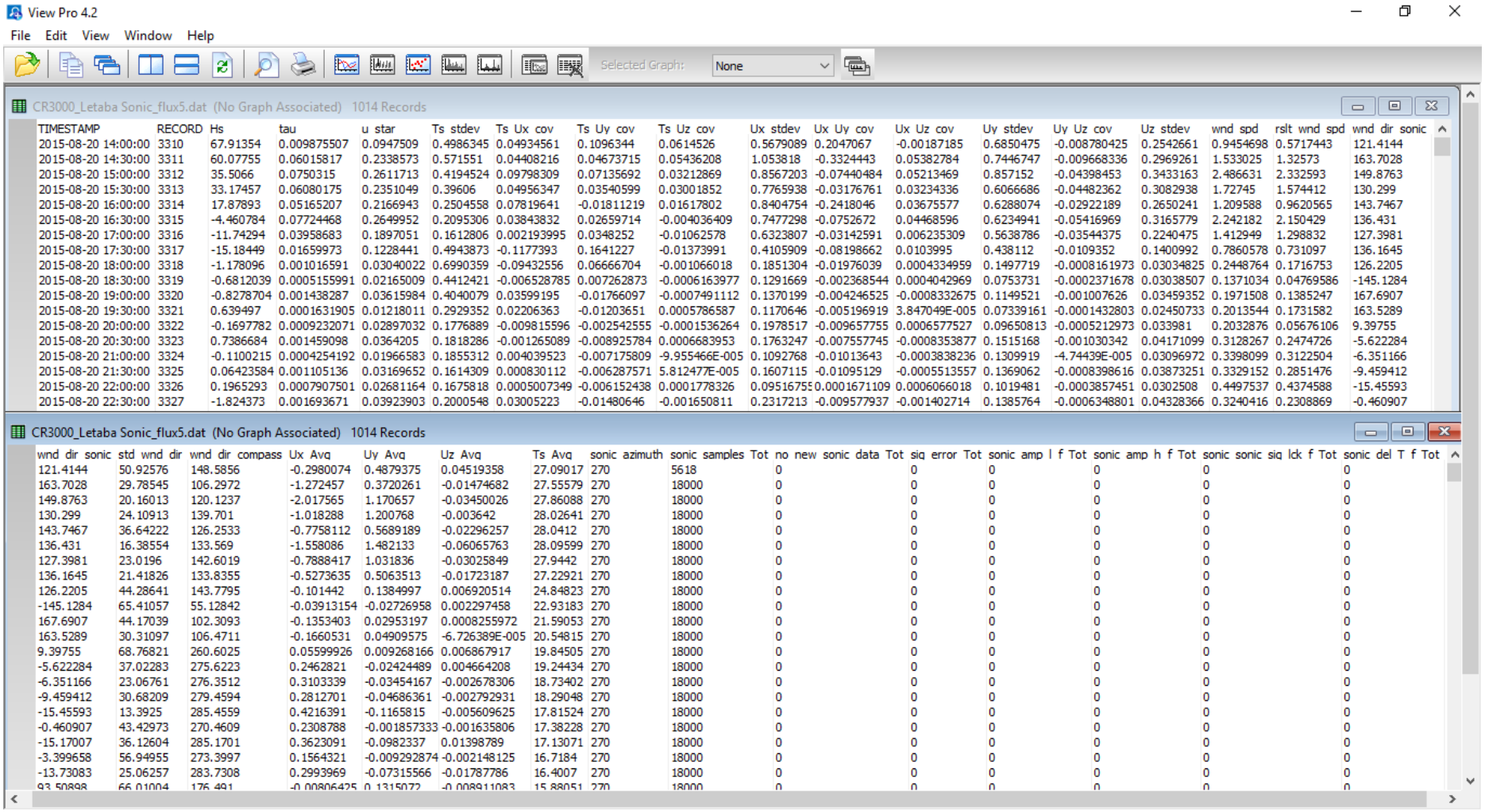

Figure A4 An example of the data captured by the CSAT 3-D sonic anemometer and stored on the CR3000 logger output file

APPENDIX B: STABLE ISOTOPE SAMPLING AND ANALYSES

The samples collected for stable isotope analysis are presented in Tables B1. The measured δ^2H and $\delta^{18}O$ for each of the potential sources were then used as inputs to Simmr to determine the proportional contribution of sources to ET (Figure B1). In this particular study, the potential sources of water used by the vegetation was considered to be soil water (assumed to have mixed proportionally with older soil moisture) at the different sampling depths, GW and stream water. The isotopic composition of these samples was generally distinguishable, therefore the source input data used in Simmr was the measured δ^2H and $\delta^{18}O$ for plant stem water, soil water (30, 60, 100 and 1400 cm), GW and SW.

As previously mentioned, the package implements a Markov Chain Monte Carlo (MCMC) function to repeatedly estimate the proportions of the various sources in the mixture and determine the values which best fit the mixture data. It should be noted that the isotopic composition of δ^2H and $\delta^{18}O$ in the xylem water must fall between those of the potential water source EM, in order to be explained as a mixture of them (Figure B2).

While the model is able to compute a mathematical solution of the proportion of sources that sum to 1, if the aforementioned condition is not met, the proportion of one of the sources will be negative, while the proportion of one of the remaining sources will be greater than one, neither of which is hydrologically possible.

The initial estimates are usually poor and are discarded as part of the burn-in phase (initial phase). The subsequent iterations are then used to determine the best estimates of the source proportions. Convergence diagnostics can then be used to check if the model has run correctly (Figure B3), as it can take thousands of iterations to depart from the initial guesses. Once the model has run correctly the contribution of each source to ET at various percentiles is provided in tabular and graphical form (Figure B3).

Table B1 Stable isotope samples collected during the three window period sampling campaigns

Sample ID	Location (South)	Location (East)	Source	Description	$\delta^{2}H$ (‰)	$\delta^{2}H$ std (‰)	$\delta^{18}O$ (‰)	$\delta^{18}O$ std (‰)
mthimkulu (r1)-Avg	23.66	31.05	Rainfall	Rainfall sample at Letaba Ranch	7.81	1.10	-1.52	0.16
mahale farm (r2)-Avg	23.67	31.02	Rainfall	Rainfall Sample at Malisa's farm	2.03	0.70	-1.71	0.08
mahale farm (r3)-Avg	23.67	31.02	Rainfall	Rainfall Sample at Malisa's farm	12.92	0.68	0.94	0.11
mahale farm (r4)-Avg	23.67	31.02	Rainfall	Rainfall Sample at Malisa's farm	12.31	0.40	0.27	0.18
mthimkulu (r12)-Avg	23.66	31.05	Rainfall	Rainfall sample at Letaba Ranch	-9.79	0.21	-2.36	0.30
mahale farm (r14)-Avg	23.67	31.02	Rainfall	Rainfall Sample at Malisa's farm	-1.08	0.32	-1.90	0.13
mthimkulu (r16)-Avg	23.66	31.05	Rainfall	Rainfall sample at Letaba Ranch	-1.00	2.17	-2.18	0.03
mthimkulu (r18)-Avg	23.66	31.05	Rainfall	Rainfall sample at Letaba Ranch	15.26	0.69	0.45	0.03
mthimkulu (r19)-Avg	23.66	31.05	Rainfall	Rainfall sample at Letaba Ranch	5.20	0.32	-1.44	0.20
mthimkulu (r20)-Avg	23.66	31.05	Rainfall	Rainfall sample at Letaba Ranch	-6.38	1.43	-3.05	0.07
mthimkulu (r1)-Avg	23.66	31.05	Rainfall	Rainfall sample at Letaba Ranch	7.81	1.10	-1.52	0.16
mahale farm (r2)-Avg	23.67	31.02	Rainfall	Rainfall Sample at Malisa's farm	2.03	0.70	-1.71	0.08
id7 may	23.67	31.02	Stream	Stream sample at Malisa's Farm	-9.20	0.40	-1.90	0.10
id11a may	23.67	31.02	Stream	Stream sample at Malisa's Farm	-8.10	1.10	-1.40	0.20
id20a may	23.66	31.05	Stream	Stream sample in Letaba Ranch	-9.00	2.40	-1.30	0.20
id24a may	23.66	31.05	Stream	Letaba Ranch weir stream sample	-7.60	0.50	-1.20	0.10
id24a may	23.66	31.05	Stream	Letaba Ranch weir stream sample	-8.00	1.30	-1.30	0.20
cstream aug	23.67	31.02	Stream	Stream sample at Malisa's Farm	3.40	1.30	-0.40	0.20
estream aug	-23.68	31.00	Stream	Stream sample (LF near stream NB)	3.40	2.70	0.00	0.10
13	23.67	31.02	Stream	stream sample near malisa's farm	2.50	1.00	2.30	0.20
15	-23.68	31.00	Stream	stream sample (LF near stream NB)	3.50	0.70	2.30	0.20
11	23.66	31.05	Stream	stream sample letaba ranch nb (Northern Bank)	9.50	0.60	2.30	0.10
2	-23.66	31.05	Stream	stream sample from letaba ranch weir	6.70	0.30	2.40	0.10
17	-23.66	31.05	Stream	stream sample letaba ranch (Southern Bank)	5.00	0.70	2.70	0.20
id7 may	23.67	31.02	Stream	Stream sample at Malisa's Farm	-9.20	0.40	-1.90	0.10

	23.67	31.02	Stream	Stream sample at Malisa's Farm	-8.10	1.10	-1.40	0.20
id1b may	23.67	31.02	Groundwater	Shallow borehole in Malisa's Farm (Northern Bank)	-20.20	0.60	-3.60	0.10
id4 may	23.67	31.00	Groundwater	Borehole near Mahale weir (Northern Bank)	-21.90	0.60	-3.60	0.10
5.2	23.67	31.02	Groundwater	Borehole in Letaba Ranch (Northern Bank)	-19.50	1.60	-3.90	0.20
id23a may	23.66	31.05	Groundwater	Borehole within river channel near Letaba Ranch	-20.00	1.10	-3.30	0.10
cbore aug	-23.67	31.02	Groundwater	Borehole in Malisa's Farm (Northern Bank)	-18.70	0.90	-3.30	0.20
ebore aug	-23.67	31.00	Groundwater	Borehole near Mahale weir (LF near stream NB)	-6.00	1.50	-1.50	0.20
bbore aug	-23.66	31.05	Groundwater	Borehole in Letaba Ranch (Northern Bank)	-20.70	1.50	-4.00	0.10
abore aug	-23.66	31.05	Groundwater	Borehole within river channel (Letaba Ranch near weir)	-15.50	1.60	-3.50	0.10
gbore aug	-23.66	31.05	Groundwater	Borehole in Letaba Ranch (Southern Bank)	-21.40	1.70	-3.50	0.10
gbore aug	-23.66	31.05	Groundwater	Borehole in Letaba Ranch (Southern Bank)	-20.90	1.60	-3.30	0.10
gbore aug	-23.66	31.05	Groundwater	Borehole in Letaba Ranch (Southern Bank)	-21.20	1.70	-3.40	0.00
12	-23.67	31.02	Groundwater	borehole at malisa's farm (Northern Bank)	-25.10	1.60	-4.10	0.30
14	-23.67	31.00	Groundwater	borehole sample near mahale weir (LF near stream NB)	-12.50	0.10	-1.20	0.30
10	-23.66	31.05	Groundwater	borehole letaba ranch nb (Northern Bank)	-25.50	0.60	-4.70	0.20
1	-23.66	31.05	Groundwater	borehole within river letaba ranch (Letaba Ranch near weir)	-24.30	0.70	-3.70	0.30
16	-23.66	31.05	Groundwater	borehole sample letaba ranch sb (Southern Bank)	-30.00	0.50	-4.50	0.20
6	-23.66	31.05	Soil	Soil at 30 cm depth (LR within river channel and near stream NB)	-12.0	0.3	4.1	0.0
23	-23.66	31.05	Soil	Soil at 30 cm depth (LR near stream NB)	-2.0	0.1	3.8	0.0
31	-23.67	31.02	Soil	Soil at 30 cm depth (LF near stream NB)	-8.0	0.9	3.6	0.1
35	-23.68	31.00	Soil	Soil at 30 cm depth (LF near stream NB)	7.0	0.7	7.9	0.3
42	-23.66	31.05	Soil	Soil at 30 cm depth (LR near stream SB)	-9.0	1.8	3.9	0.2
A30	-23.66	31.05	Soil	Soil at 30 cm depth (LR within river channel and near stream NB)	-15.0	0.2	1.6	0.0
C30	-23.67	31.02	Soil	Soil at 30 cm depth (LF near stream NB)	-9.0	0.5	1.0	0.1
D30	-23.67	31.02	Soil	Soil at 30 cm depth (LF near stream SB)	-6.0	5.9	4.1	0.3
E30	-23.68	31.00	Soil	Soil at 30 cm depth (LF near stream NB)	-7.0	1.1	1.4	0.2
G30	-23.66	31.05	Soil	Soil at 30 cm depth (LR near stream SB)	6.0	0.0	5.6	0.1
A	23.67	31.02	Soil	Soil samples (30 cm) on Northern Bank, near Mahale weir	-9.0	0.3	-0.9	0.0

D	23.67	31.02	Soil	Soil samples (30 cm) on Southern Bank, near Malisa's Farm	-36.0	0.2	-4.4	0.1
J	23.68	31.00	Soil	Soil samples (30 cm) on Northern Bank, near Mahale weir	-37.0	0.2	-2.5	0.0
N	23.66	31.05	Soil	Soil samples (30 cm) on Southern Bank, near Letaba Ranch weir	-9.0	0.4	0.2	0.1
O	23.66	31.05	Soil	Soil (30 cm) on Northern Bank, near Letaba Ranch weir	-23.0	0.1	-0.5	0.1
7	-23.66	31.05	Soil	Soil at 60 cm depth (LR within river channel and near stream NB)	-16.0	0.6	-1.5	0.1
24	-23.66	31.05	Soil	Soil at 60 cm depth (LR near stream NB)	-20.0	0.2	-1.8	0.1
32	-23.67	31.02	Soil	Soil at 60 cm depth (LF near stream NB)	-10.0	0.5	2.0	1.0
36	-23.68	31.00	Soil	Soil at 60 cm depth (LF near stream NB)	-35.0	0.8	-2.4	0.1
43	-23.66	31.05	Soil	Soil at 60 cm depth (LR near stream SB)	-20.0	0.8	-1.1	0.1
A60	-23.66	31.05	Soil	Soil at 60 cm depth (LR within river channel and near stream NB)	-15.0	0.9	0.9	0.2
B60	-23.66	31.05	Soil	Soil at 60 cm depth (LR near stream NB)	-23.0	2.4	-0.4	0.2
C60	-23.67	31.02	Soil	Soil at 60 cm depth (LF near stream NB)	-39.0	0.3	-0.3	0.0
D60	-23.67	31.02	Soil	Soil at 60 cm depth (LF near stream SB)	-44.0	0.7	-0.3	0.2
E60	-23.68	31.00	Soil	Soil at 60 cm depth (LF near stream NB)	-36.0	1.3	-3.6	0.2
G60	-23.66	31.05	Soil	Soil at 60 cm depth (LR near stream SB)	-16.0	0.7	0.1	0.1
F	23.68	31.00	Soil	Soil samples (60 cm) on Northern Bank, near Mahale weir	-22.0	0.1	-1.8	0.0
G	23.67	31.02	Soil	Soil samples (60 cm) on Southern Bank, near Malisa's Farm	-25.0	0.3	-3.7	0.1
P	23.66	31.05	Soil	Soil samples (60 cm) on Southern Bank, near Letaba Ranch weir	-22.0	0.3	-1.3	0.1
R	23.66	31.05	Soil	Soil (60 cm) on Northern Bank, near Letaba Ranch weir	-21.0	0.1	-1.5	0.0
8	-23.66	31.05	Soil	Soil at 100 cm depth (LR within river channel and near stream NB)	-4.0	1.2	2.4	0.2
25	-23.66	31.05	Soil	Soil at 100 cm depth (LR near stream NB)	-42.0	0.1	-5.0	0.1
33	-23.67	31.02	Soil	Soil at 100 cm depth (LF near stream NB)	-32.0	0.2	-3.3	0.0
37	-23.68	31.00	Soil	Soil at 100 cm depth (LF near stream NB)	-23.0	1.6	-2.8	0.1
44	-23.66	31.05	Soil	Soil at 100 cm depth (LR near stream SB)	-30.0	0.3	-3.3	0.1
A120	-23.66	31.05	Soil	Soil at 100 cm depth (LR within river channel and near stream NB)	-32.0	0.1	-2.0	0.1
B80	-23.66	31.05	Soil	Soil at 100 cm depth (LR near stream NB)	-15.0	0.4	0.8	0.1
C120	-23.67	31.02	Soil	Soil at 100 cm depth (LF near stream NB)	-30.0	0.5	-1.5	0.1
D120	-23.67	31.02	Soil	Soil at 100 cm depth (LF near stream SB)	-9.0	0.7	0.6	0.3
E120	-23.68	31.00	Soil	Soil at 100 cm depth (LF near stream NB)	-26.0	0.4	-3.9	0.1
G120	-23.66	31.05	Soil	Soil at 100 cm depth (LR near stream SB)	-42.0	0.2	-3.6	0.1

L	23.66	31.05	Soil	Soil samples (100 cm) on Southern Bank, near Letaba Ranch weir	-32.0	0.3	-3.5	0.1
C	23.67	31.02	Soil	Soil samples (100 cm) on Northern Bank, near Mahale weir	-27.0	0.2	-4.4	0.1
E	23.67	31.02	Soil	Soil samples (100 cm) on Southern Bank, near Malisa's Farm	-53.0	0.2	-6.9	0.1
I	23.68	31.00	Soil	Soil samples (100 cm) on Northern Bank, near Mahale weir	-42.0	0.1	-4.7	0.0
M	23.66	31.05	Soil	Soil (100 cm), Northern Bank, near Letaba Ranch weir	-39.0	0.1	-6.6	0.1
9	-23.66	31.05	Soil	Soil at 140 cm depth (LR within river channel and near stream NB)	-42.5	0.4	-4.3	0.0
26	-23.66	31.05	Soil	Soil at 140 cm depth (LR near stream NB)	-40.0	0.5	-4.6	0.0
34	-23.67	31.02	Soil	Soil at 140 cm depth (LF near stream NB)	-45.0	0.4	-3.9	0.0
38	-23.68	31.00	Soil	Soil at 140 cm depth (LF near stream NB)	-44.0	0.1	-4.6	0.1
45	-23.66	31.05	Soil	Soil at 140 cm depth (LR near stream SB)	-41.0	0.5	-4.2	0.0
C2	-23.67	31.02	Stem	*P. violacea* (LF near stream NB)	-14.00	0.10	-2.80	0.10
E4	-23.68	31.00	Stem	*P. violacea* (LF near stream NB)	-21.00	0.30	-3.10	0.00
27	-23.67	31.01	Stem	*P. violacea* (LF near stream NB)	-32.00	0.10	-3.30	0.10
B2	-23.66	31.05	Stem	*P. violacea* (LR near stream NB)	-4.00	0.80	1.30	0.20
F1	-23.66	31.05	Stem	*P. violacea* (LR near stream SB)	5.00	0.60	6.20	0.20
A4	-23.66	31.05	Stem	*P. violacea* (LR within river channel and near stream NB)	-17.00	0.20	-1.50	0.00
5	-23.66	31.05	Stem	*P. violacea* (LR within river channel and near stream NB)	-50.00	1.30	-7.50	0.00
17	23.66	31.05	Stem	*P. violacea* on Northern Bank, near Letaba Ranch weir	-49.00	0.50	-3.60	0.00
B1	-23.66	31.05	Stem	*Z. mucronata*	6.00	1.20	5.70	0.40
E2	-23.68	31.00	Stem	*Z. mucronata* (LF near stream NB)	-65.00	0.60	-7.60	0.10
A1	-23.66	31.05	Stem	*Z. mucronata* (LR within river channel and near stream NB)	-46.00	0.30	-5.10	0.00
28	23.66	31.05	Stem	*Z. mucronata* on Southern Bank, near Letaba Ranch weir	-61.00	0.30	-7.90	0.00
25	23.66	31.05	Stem	*Z. mucronata* within River Channel, near Letaba Ranch weir	-47.00	0.30	-4.10	0.00
30	-23.67	31.00	Stem	*C. microphyllum* (LF near stream NB)	-50.00	0.30	-8.00	0.10
40	-23.68	31.01	Stem	*C. microphyllum* (LF near stream SB)	-32.00	0.10	-5.60	0.00
D2	-23.67	31.02	Stem	*C. microphyllum* (LF near stream SB)	-41.00	1.20	-6.70	0.10
29	-23.67	31.00	Stem	*F. sycamorous* (LF near stream NB)	-39.00	0.20	-4.30	0.00
E1	-23.68	31.00	Stem	*F. sycamorous* (LF near stream NB)	-53.00	0.10	-3.30	0.20
D1	-23.67	31.02	Stem	*F. sycamorous* (LF near stream SB)	0.00	0.20	0.70	0.10
39	-23.67	31.01	Stem	*F. sycamorous* (LF near stream SB)	-42.00	0.60	-2.40	0.20

G2	23.66	31.05	Stem	*F. sycamorous* (LR near stream SB)	0.00	0.20	0.80	0.10
46	-23.66	31.05	Stem	*F. sycamorous* (LR near stream SB)	-26.00	0.40	-3.10	0.00
48	-23.66	31.05	Stem	*F. sycamorous* (LR near stream SB)	-10.00	0.10	1.30	0.10
26	23.66	31.05	Stem	*F. sycamorous* on Southern Bank, near Letaba Ranch weir	-29.00	0.10	-2.10	0.10
9	23.67	31.02	Stem	*F. sycamorous* on Southern Bank, near Malisa's Farm	-55.00	0.30	-3.90	0.00
47	-23.66	31.05	Stem	*G. senegalensis* (LR near stream SB)	-7.00	3.00	0.00	0.10
14 B	23.68	31.00	Stem	*G. senegalensis* on Northern Bank, near Mahale weir	-48.00	0.30	-4.50	0.00
4	-23.66	31.05	Stem	*G. senegalensis* (LR within river channel and near stream NB)	-48.00	0.50	-4.40	0.00
G1	-23.66	31.05	Stem	*G. senegalensis* (LR near stream SB)	-9.00	0.10	0.90	0.00
A2	-23.66	31.05	Stem	*G. senegalensis* (LR within river channel and near stream NB)	-20.00	0.20	-0.90	0.00
3	23.67	31.02	Stem	*D. mespiliformis* on Northern Bank, near Malisa's Farm	-41.00	0.10	-4.40	0.00
C1	-23.67	31.02	Stem	*D. mespiliformis* (LF near stream NB)	-8.00	0.70	-1.70	0.10
E3	-23.68	31.00	Stem	*D. mespiliformis* (LF near stream NB)	-24.00	0.20	-3.20	0.10
28	-23.67	31.02	Stem	*D. mespiliformis* (LF near stream NB)	-28.00	3.20	-3.80	0.10
B4	-23.66	31.05	Stem	*D. mespiliformis* (LR near stream NB)	-27.00	0.10	-3.70	0.10
20	-23.66	31.05	Stem	*D. mespiliformis* (LR near stream NB)	-22.00	2.70	-2.30	0.10
F3	-23.66	31.05	Stem	*D. mespiliformis* (LR near stream SB)	-21.00	0.00	1.00	0.10
A3	-23.66	31.05	Stem	*D. mespiliformis* (LR within river channel and near stream NB)	-21.00	0.60	-2.70	0.10
3	-23.66	31.05	Stem	*D. mespiliformis* (LR within river channel and near stream NB)	-14.00	0.30	-1.00	0.10
21	23.66	31.05	Stem	*D. mespiliformis* on Northern Bank, near Letaba Ranch weir	-61.00	0.20	-5.40	0.00
B3	-23.66	31.05	Stem	*C. mopane* (LR near stream NB)	-26.00	0.10	-3.20	0.10
19	-23.66	31.05	Stem	*C. mopane* (LR near stream NB)	-39.00	0.40	-5.00	0.10
18	23.66	31.05	Stem	*C. mopane* on Northern Bank, near Letaba Ranch weir	-55.00	0.40	-4.10	0.10

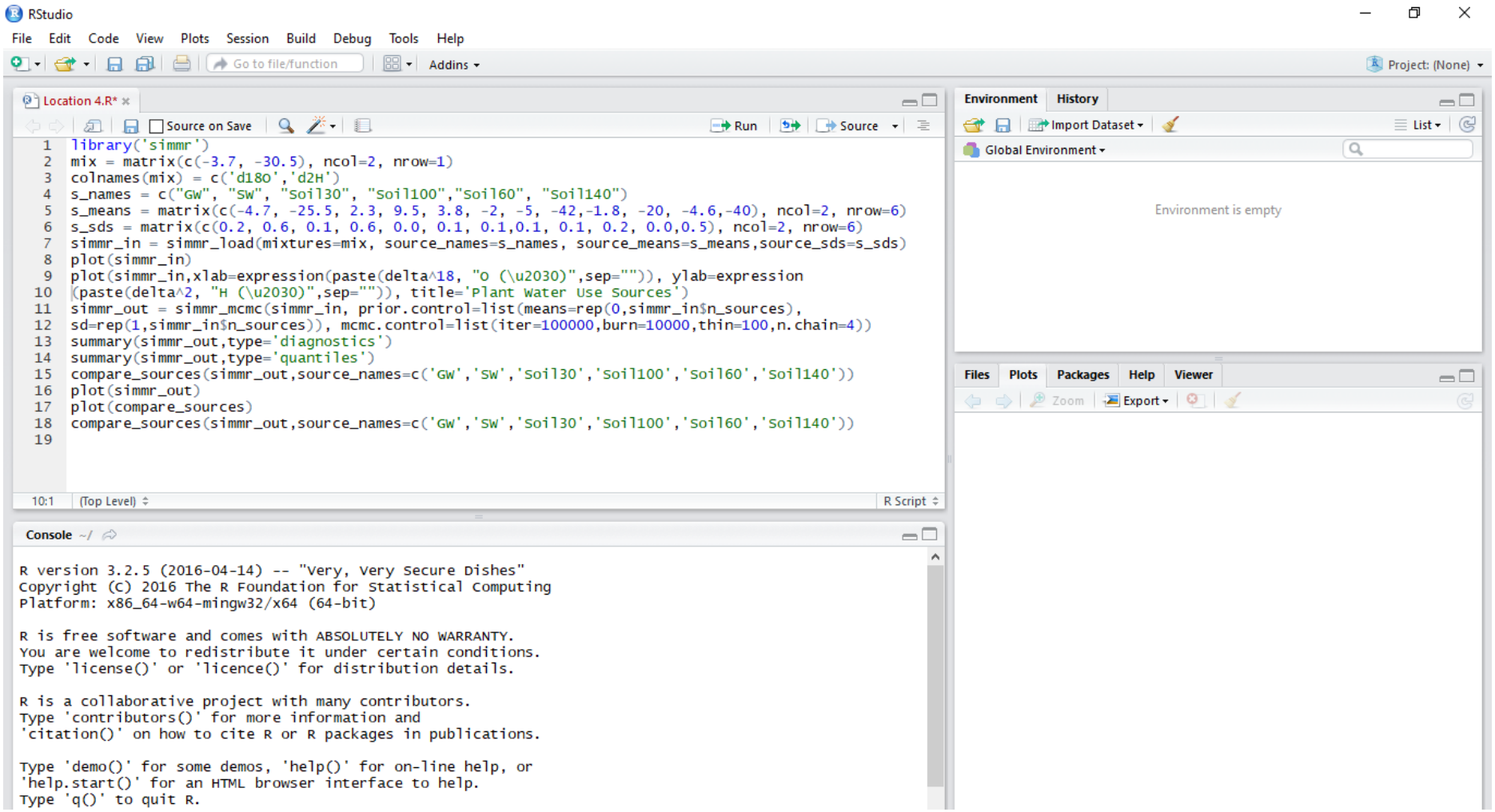

Figure B1 An example of the script (adapted from https://cran.r-project.org/web/packages/simmr/vignettes/simmr.html) used in the R studio statistical software package to estimate the proportional contribution of sources to ET

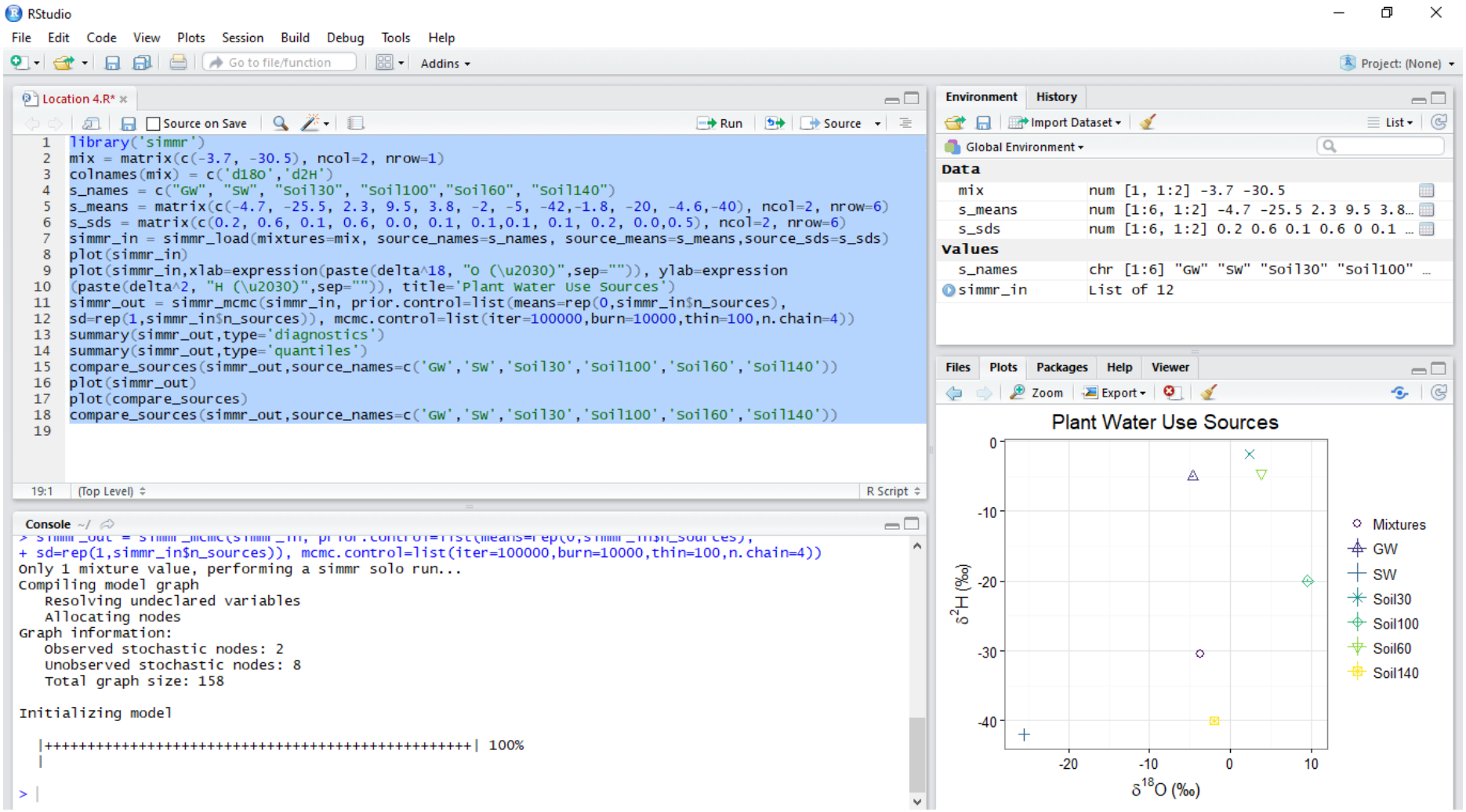

Figure B2 An example of the different water sources plotted within the dual stable isotope space

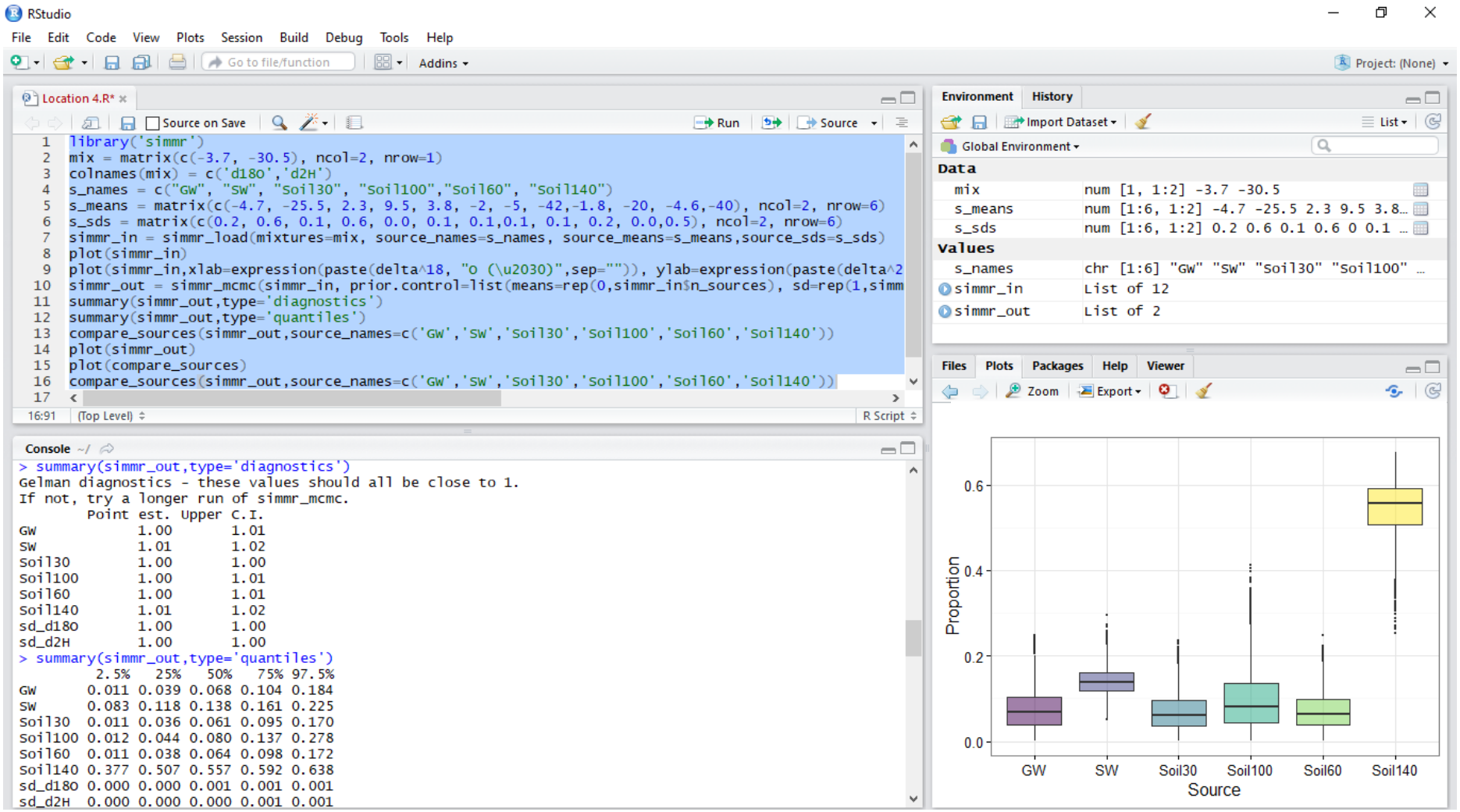

Figure B3 An example of a successful model run in Simmr

APPENDIX C: LYSIMETER AND GROUNDWATER PIEZOMETRIC DATA

Measurements of soil water evaporation during August, September and October were derived from data collected *in-situ*, using micro-lysimeters. *Information relating to these measurements are provided in Tables C1 and C2. Borehole drilling information and hydraulic characteristics relating to the paired piezometric borehole network drilled into the deep fractured hard rock and shallow weathered material is provided in Tables C3 and C4.

Table C1 Micro-Lysimeter dimensions

	Outer Sleeve	**Inner Sleeve**
Thickness	2 mm	2 mm
Internal Diameter	80 mm	50 mm
Depth	145 mm	50 mm

Table C2 An example of micro-lysimeter measurements collected during a field sampling campaign

	Mass of Samples (g)					
	Bank nearest Letaba Farm		**Inner Channel**		**Far end of Channel**	
Time	**Lys 1**	**Lys 2**	**Lys 3**	**Lys 4**	**Lys 5**	**Lys 6**
08:00 AM	340.28	347.52	398.64			
09:00 AM	340.010	347.300	398.480	387.420	395.310	420.010
10:00 AM	338.980	346.430	397.540	386.750	394.720	419.050
11:00 AM	337.140	344.980	396.120	385.680	393.820	418.020
12:00 PM	335.360	343.480	394.720	384.570	392.870	417.090
01:00 PM	333.190	341.710	393.060	383.220	391.810	415.800
02:00 PM	331.540	340.320	391.680	381.830	390.800	414.600
03:00 PM	329.940	339.040	390.420	380.430	390.000	413.350
04:00 PM	328.680	338.030	389.440	379.140	389.220	412.110

* Lysimeter measurements were generally conducted from 8:00 am to 4:00pm due to the remote locality of the study area and the requirement of a game-guard during sampling. Consequently, this limited the amount of time that could be spent in the field to obtain measurements.

Table C3 *Borehole drilling information.

	Site Name	Site Description	Latitude	Longitude	Altitude (m)	Depth (m)	Solid Casing Depth (m)	Casing height (m)	Date completed	Initial Water Level (m)	Strike (m)	Blow Out yield (l/s)	EC (uS/cm)
Farms	LF002A	Mabunda/Baloi	-23.674299259	31.005508751	332.816	60	6	0.51	08/10/2015	11.51	11	1	
	LF002 B	Mabunda/Baloi	-23.674297937	31.005498881	332.966	15	6	0.58	10/09/2015	11.78	11	0.4	864
	LF0021	Mabunda/Baloi in river	-23.674764519	31.004662622	329.940	24	6	0.63	01/11/2015	8.26			
	LF003 A	Maliesa's Farm	-23.669515034	31.016633354	332.840	72	36	0.7	25/05/2015	10.97	15	0.3	1740
	LF003 B	Maliesa's Farm	-23.669519698	31.016568496	328.683	20	14	0.8	01/06/2015	10.76	12	<0.5	1446
	LF003C	Maliesa's Farm	-23.669494574	31.016672592	333.985			Dry					
	LF0031 A	Maliesa's Farm	-23.667002914	31.016215720	333.183	60	24	0.22	25/05/2015	12.95	21	3	1518
	LF0031 B	Maliesa's Farm	-23.667069700	31.016260718	335.904	20	6	0.255	26/06/2015	12.68	19	1	2535
	LF004 A	Abram's Farm	-23.677412130	31.005063317	337.243	72	24	0.43	22/10/2015	13.385	25	0.5	3413
	LF004 B	Abram's Farm	-23.677413088	31.005053265	338.883	15	10	0.46	23/10/2015	13.39	12	0.5	3996.00
	LF005 A	Bongele,s Farm	-23.671245070	31.017841574	328.391	72	30	0.29	04/06/2015	12.33	32	0.5	2800
	LF005 B	Bongele,s Farm	-23.671308501	31.017884338	330.151	42	6	0.305	09/06/2015	12.15	13	<0.5	3354
	LF005 C	Bongele,s Farm	-23.671222963	31.017831282	332.179	18	6	0.345	14/07/2015	10.97	13	0.5	3074
	LF0051 A	Bongele,s Farm	-23.673002919	31.018831950	328.978	54	36	0.54	11/06/2015	14.29	25/40	1.5	1446
	LF0051 B	Bongele,s Farm	-23.673047435	31.018857310	327.363	30	6	0.36	25/06/2015	14.26	16	1	1393
reserves	LR001 A	Mthimkhulu	-23.661769123	31.046823055	328.039	60	30	0.46	03/09/2015	10.35	10	0.5	5600 - 7000
	LR001 B	Mthimkhulu	-23.661764275	31.046805745	330.826	12	6	0.355	08/09/2015	11.93	10		>10 000
	LR0011 A	Mthimkhulu	-23.662934730	31.045922747	324.700	72	24	0.3	14/09/2015	10.3	10	0.1	>10 200
	LR0011 B	Mthimkhulu	-23.662913645	31.045961774	331.089	10	6	0.315	15/09/2015	10.15	10		11 100
	LR002 A	Mthimkhulu	-23.666323042	31.040506466	330.907	42	24	0.43	28/09/2015	10.59	25	0.5	2478.00
	LR002 B	Mthimkhulu	-23.666330049	31.040511463	329.536	10	6	DRY	01/10/2015				
	LR003	Mthimkhulu. Tercias BH	-23.661232653	31.047126602	326.855	10	4	0.355	26/09/2015	Initially dry	0	0	5595
	LR004 A	Letaba Ranch	-23.669463099	31.042411630	327.109	54	30	0.57	02/12/2015				
	LR004 B	Letaba Ranch	-23.669447874	31.042414074	326.388	24	0	0.505	03/12/2015				
	LR005 A	Letaba Ranch	-23.662268314	31.049551881	327.444	60	42	0.265	09/07/2015	8.95	25/38/50	5.7	1740
	LR005 B	Letaba Ranch	-23.662269810	31.049502905	328.971	24	6	0.56	13/07/2015	8.94	19	1.8	1580
	LRW001	Mthimkhulu in river	-23.659273246	31.048663193	316.063	12	0	0.35	26/11/2015	1.23	5	0.2	
	LRW002	Mthimkhulu in river	-23.659964290	31.048604409	317.902	6	0	0.52	30/11/2015	1	4	0.2	
	LR006	Mthimkhulu Near camp				75	0		24/11/2015				

*The naming convention for these boreholes are given as follows; Letaba Farms (LF), Letaba Ranch (LR) and Letaba River Water (within active river channel, LRW). These names are then followed by a number (eg. 01 or 001), where more than two numerals imply that the borehole was drilled away from the riparian zone and an alphabet (A or B) is used to identify deep and shallow boreholes, respectively (Riddell et al., 2017).

Table C4 Hydraulic characteristics of the boreholes within the study site (adapted from Riddell et al., 2017)

			Section Length (m)	T (m^2 d^{-1})	Hydraulic Gradient	Loss to Aquifer (m^3 d^{-1})
Deep Borehole Data (A)	**Farms**	**LF002**	2200.00	0.08	0.00	-0.70
		LF003	2180.00	0.05	0.02	2.18
		LF004	2200.00	0.87	0.01	15.31
		LF005	2180.00	1.18	-0.06	-141.48
	Total					**-124.69**
	Reserves	**LR001**	880.00	0.98	0.01	5.17
		LR002	1580.00	0.16	0.01	2.69
		LR004	1580.00	0.68	-0.01	-11.82
		LR005	880.00	3.83	0.01	26.96
	Total					**23.01**
Shallow Borehole Data (B)	**Farms**	**LF002**	2200.00	18.00	0.00	-118.80
		LF003	2180.00	1.00	-0.04	-89.38
		LF004	2200.00	0.67	0.02	26.46
		LF005	2180.00	0.06	-0.03	-4.05
	Total					**-185.76**
	Reserves	**LR001**	880.00	0.98	0.02	20.70
		LR002	1580.00	0.16	0.02	3.67
		LR004	1580.00	2.04	-0.02	-51.57
		LR005	880.00	3.83	0.02	60.67
	Total					**33.47**
					Net Gain/Loss	**-253.98**

APPENDIX D: MAHALE AND LETABA RANCH WEIRS

Figure D1 An illustration of the gauging weirs used in this study, with Mahale weir on the left and Letaba Ranch weir on the right (Riddell et al., 2017)

Figure D2 An illustration of the Solinst Level Logger installed at the Mahale weir to record streamflow head, which was installed on 22 April 2015 (Riddell et al., 2017)